Discrete symmetry breaking beyond the standard model

Dekens, Wouter Gerard

Discrete symmetry breaking beyond the Standard Model

rijksuniversiteit
groningen

PRINTED BY: Ipskamp Drukkers, Enschede, September 2015

ISBN: 978-90-367-8118-3 Printed version
ISBN: 978-90-367-8117-6 Electronic version

rijksuniversiteit
groningen

Discrete symmetry breaking beyond the Standard Model

Proefschrift

ter verkrijging van de graad van doctor aan de
Rijksuniversiteit Groningen
op gezag van de
rector magnificus prof. dr. E. Sterken,
en volgens besluit van het College voor Promoties.

De openbare verdediging zal plaatsvinden op

16 oktober 2015 om 14:30 uur

door

Wouter Gerard Dekens

geboren op 3 september 1987
te Aduard

Promoteres
Prof. dr. D. Boer
Prof. dr. R.G.E. Timmermans

Beoordelingscommissie
Prof. dr. R. Fleischer
Prof. dr. J.M. Frère
Prof. dr. D. Roest

List of Publications

The work in this thesis is based to a large extent on the following publications and preprints:

Published:

1. W. Dekens and J. de Vries, *Renormalization Group Running of Dimension-Six Sources of Parity and Time-Reversal Violation*, JHEP **1305**, 149 (2013).

2. W. Dekens, J. de Vries, J. Bsaisou, W. Bernreuther, C. Hanhart, U. -G. Meißner, A. Nogga and A. Wirzba, *Unraveling models of CP violation through electric dipole moments of light nuclei*, JHEP **1407**, 069 (2014).

3. W. Dekens, D. Boer, *CP violation in left-right symmetric models*, Nucl. Phys. B **889**, 727 (2014).

Preprints:

- W. Dekens and K. K. Vos, *T violation in radiative β decay and electric dipole moments*, arXiv:1502.04629.

Contents

Chapter 1

Introduction

The Universe has been explored over a wide range of scales, from the very large size of the observable Universe, roughly 10^{26} meters, to the small distances $\sim 10^{-18}$ m now being probed at the Large Hadron Collider (LHC). This has led to the observation of a myriad of phenomena occurring across the broad range of length scales probed so far. At first sight it may seem impossible to construct a theory describing this wide variety of phenomena occurring at these vastly different scales. Fortunately, it is often possible to describe a number of phenomena in isolation without having to understand everything else at the same time. This possibility relies on the fact that, in physics, phenomena at very different scales can often be separated from one another. For instance, when considering phenomena at large distances, or equivalently low energies, the details of the physics at small distances, or high energy scales, can usually be neglected. In fact, much of the progress in our understanding of the Universe is due to the possibility to separate physics at very different scales.

An example of this principle is the description of muon (μ) decay. This subatomic particle is a heavier version of the electron, about 200 times as massive, with the same spin and charge. Like the electron, the muon is a lepton (a matter particle which does not feel the strong nuclear force) together with the neutral, extremely light, and weakly interacting neutrinos. As the muon is heavy compared to the electron and neutrinos it is energetically allowed to decay to an electron and two neutrinos. This decay is mediated by one of the force carrier particles of the weak interaction, namely, the W boson, which is roughly 800 times as heavy as a muon. In this process the muon transforms into a muon-neutrino and a W boson, which subsequently decays to an electron-antineutrino and an electron, as depicted in Fig. 1.1a.

Although the above description of this process, through the mediation of the W boson, leads to well-tested predictions, it is also possible to accurately describe this decay by a theory which does not incorporate the W boson. This simpler theory, called Fermi theory, instead describes this process by an effective interaction between the four fermions, as shown in Fig. 1.1b, and does not require knowledge of the W boson. Such a description is possible because the W has a mass far above the energy scale where muon decay takes place. This heavy mass means that knowledge of the properties of the W boson only becomes important when probing energies much higher than those where muon decay occurs. Thus, in the description without the W boson, we have essentially divided up the

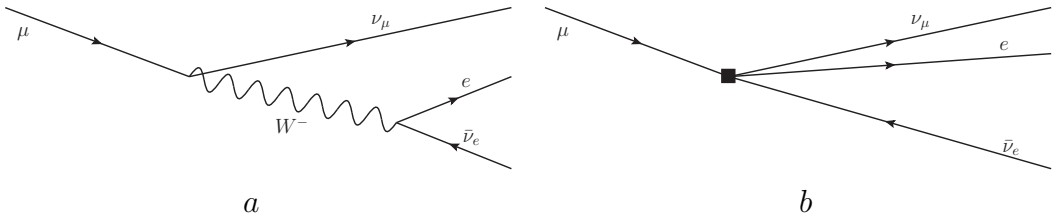

Figure 1.1: Figure (a) depicts muon decay in the full theory, which includes the W boson. Figure (b) shows the same decay in the simpler *effective* theory which does not include the W. Here the black square indicates the effective interaction between the fermions.

particles (more technically, the *degrees of freedom*), into those which are not important at low energies (the W boson) and those which are (the leptons).

Separating phenomena at very different scales in this way is useful as it allows one to study a few phenomena at a time without having to understand everything else simultaneously. In addition, this division often allows for a simplified theory, with less degrees of freedom. However, this also means that such theories are essentially *effective theories*; they have a limited regime of validity. For example, in case of the W boson, once energies comparable to the mass of the W are probed knowledge of the particle itself becomes important for an accurate description, and it can no longer be left out of the theory. Thus, the effective Fermi theory is only valid in a certain energy range. Beyond this other theories are needed, which could again be effective theories themselves.

This approach leads to a picture of our understanding of nature as a hierarchy of effective theories, all with a limited, possibly overlapping, range of validity. A schematic visualization of this is depicted in Fig. 1.2. The largest scales, from the sizes of galaxies to the observable Universe, are the domain of cosmology and astronomy where most phenomena are well described by Einstein's general relativity. Physics at the opposite end of the spectrum can be described by quantum physics which studies particles at the smallest length scales. At present the model that offers the best description of high-energy physics, and subatomic particles at the highest energies (smallest distances) probed so far, is a quantum field theory called the Standard Model (SM).

In this thesis we will mainly be concerned with models which propose physics at even smaller scales, outside of the range of validity of the SM. We will try to constrain such beyond the SM (BSM) physics using experimental results in order to get some idea of what may or may not lie beyond the SM. In doing so we will make extensive use of effective theories. First, however, we will discuss the SM and how we know it should be viewed as an effective theory, which presumably derives from a BSM theory, before discussing attempts to go beyond it.

1.1 The Standard Model

The SM is based on a few principles that have been very successful. The most important of these are gauge symmetries, renormalizability, and Lorentz invariance. All of these principles restrict the interactions and behaviour of particles in the theory in some way. For example, the gauge symmetries determine the way in which the forces act on the

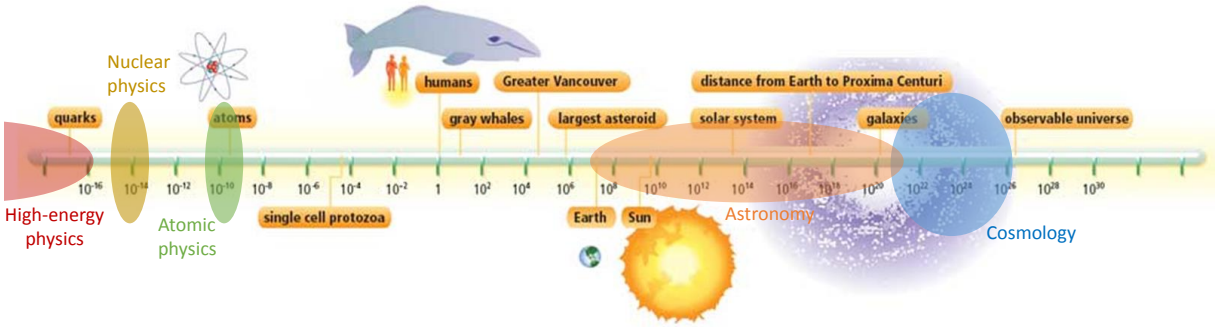

Figure 1.2: The figure depicts a number of examples of fields in science and the length scales on which the phenomena they cover occur.
Figure adapted from http://hendrix2.uoregon.edu/.

matter particles. The gauge symmetries of the SM are $SU(3) \times SU(2) \times U(1)$. Of these the $SU(3)$ group describes the strong nuclear force, mediated by the gluons, while the $SU(2) \times U(1)$ group describes the electromagnetic force, mediated by the photon, and weak force mediated by the W and Z bosons. Once the gauge symmetries and the way these act on the fields, i.e. the representations, are specified only very specific interactions are allowed.

The second principle, renormalizability is often assumed so that the theory may be predictive. In a general field theory, quantum corrections can introduce additional interactions and parameters to the theory. In non-renormalizable theories this effect results in an infinite number of parameters. In this case, one would expect an infinite number of measurements to be required to determine all parameters before any predictions can be made. Instead, a renormalizable theory does not require an infinite number of parameters and can allow for predictions after a finite number of measurements. A quantum field theory (in four dimensions) is renormalizable if it is gauge invariant and includes no interactions described by operators of dimension higher than four. As a consequence, demanding renormalizability also greatly restricts the interactions allowed in a theory.

Thus, after specifying the gauge symmetries, the way they act on the fields and demanding the theory to be renormalizable and Lorentz invariant one ends up with the SM. This theory has been tested to high precision, both in high-energy collider experiments as well as in low-energy precision measurements. Up to now the SM seems to be passing all these tests. Furthermore, in 2012 the discovery of a Higgs-like particle was announced [1]. This discovery would make the Higgs the last particle contained in the SM to be experimentally verified, after being proposed more than forty years previously by Brout, Englert, and Higgs[1] [2, 3, 4]. Further tests are still necessary to establish with certainty whether or not the discovered particle behaves like the SM Higgs boson in all respects. Nonetheless, so far no significant deviations from the SM have been found, and the SM seems to provide an accurate description of the Higgs boson as well.

Given its success one might wonder whether the SM could be valid at all energy scales.

[1] As mentioned, multiple authors were involved in the development of the theoretical framework behind this scalar particle and the associated symmetry breaking mechanism. Nevertheless, as has become common practice, we will refer to such scalar particles as 'Higgs bosons' in the remainder of this thesis.

However, there are several reasons to believe that there should be BSM physics. Two such reasons are the evidence for dark matter and the matter-antimatter asymmetry of the Universe. The first remains unexplained in the SM, as it does not contain particles that could constitute dark matter. Secondly, the matter-antimatter asymmetry, named the baryon asymmetry of the Universe (BAU), can only be generated if the Sakharov conditions are satisfied. One of these conditions requires CP violation. This transformation, CP, is the combination of a parity transformation (P), which is the inversion of space $\vec{x} \to -\vec{x}$, and charge conjugation (C), which interchanges particles with their antiparticles. Nature was assumed to be symmetric under these transformations, until the 1950's and '60's when it was discovered that they are violated; both C and P separately [5, 6] as well as their combination CP [7]. Although the SM explains the CP violation measured so far, it does not offer a viable mechanism to generate the BAU [8, 9]. One of the reasons the SM does not provide such a mechanism is that it does not seem to contain enough CP violation [10]. Thus, an explanation of either of these two questions calls for BSM physics.

1.2 Beyond the Standard Model

The problems mentioned above have led to the search for a theory of BSM physics. During this search many models have been proposed, most of which come with additional particles and/or interactions. As experimentally possible deviations from the SM must be small to have gone unnoticed so far, any BSM effects cannot be very large. Thus, experimental tests of the SM constrain the strengths of the additional interactions and masses of the new particles in the BSM theories. In order to quantify these constraints, some description of the BSM theory is necessary. In a top-down approach, one studies the constraints in one of the many BSM theories. Another possibility, which is not confined to a single BSM model, is the bottom-up approach. In this thesis we will use both approaches in order to constrain BSM physics.

The latter approach, the bottom-up approach, depends on the same idea that is behind the effective theories discussed previously, namely, that the physics at low energies should not depend on the details of the physics at high energies. In a quantum field theory, this principle implies that the physics at SM energy-scales should not be dependent on dynamics of the new heavy particles which appear in a BSM theory. At energies far below the mass of such particles they can be removed from the theory, analogous to the way the W boson was removed in Fermi theory, leaving behind effective interactions (as in Fig. 1.1). These particles are then 'integrated out', which reduces the theory to one involving the well-known SM particles only. However, the process of 'integrating out' the heavy new particles does introduce new effective interactions, again analogous to Fermi theory. Another example of an effective interaction generated when heavy particles are integrated out is depicted in Fig. 1.3. Theories containing such effective interactions are *effective field theories* (EFT). The idea of an EFT is to simply add all possible interactions to the SM, such that any model of BSM physics can be described by this EFT at low energies[2]. Different BSM theories are then described by the same EFT, but different BSM

[2]Here, one assumes that there are no new *light* interacting particles.

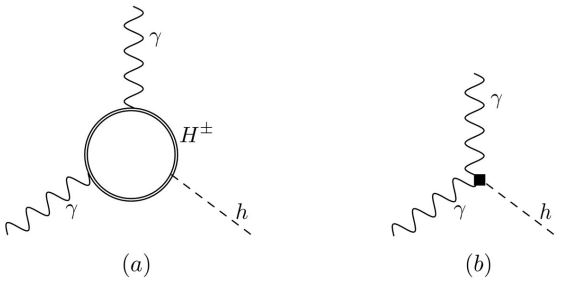

Figure 1.3: Figure (a) depicts a loop diagram involving a heavy BSM scalar particle, H. At low energies the effect of H can be described by an effective interaction shown in Figure (b).

theories will generally give rise to different strengths of the effective interactions. Thus, any specific BSM model relates to this EFT through an expression for the strengths of the effective interactions in terms of the parameters of the BSM model.

A feature of EFTs is that they are not renormalizable as the process of integrating out heavy particles introduces interactions described by operators of dimension higher than four. As mentioned before, such operators introduce an infinite number of interactions to the theory, which would then seem to be unable to make predictions. However, although there are infinitely many operators in an EFT, there is a finite number of operators of a given dimension. These operators, which arise through integrating out heavy new particles, are suppressed by powers of masses of these particles; the higher the dimension of the operator the more it is suppressed. This mechanism ensures that in measurable quantities the contribution of higher-dimensional operators is suppressed with respect to those of lower-dimensional operators. Thus, although such quantities depend on an infinite number of parameters in an EFT, if a finite precision is required only operators up to a certain dimension need to be included. As a result the measurable quantity depends on a finite number of relevant parameters. Nonetheless, when we probe higher and higher energies, operators of higher and higher dimension must be included to reach the same precision. Therefore, there is an energy scale, comparable to masses of the new particles, where an infinite number of operators must be included. At this point the EFT breaks down, so that the EFT has a limited range of validity, as one would expect from an *effective* theory. Nevertheless, if we assume the new particles arising in BSM theories to be heavy, BSM models at low energies are well described by such an EFT.

In this thesis we will apply these EFT techniques to describe CP-violating BSM physics, and subsequently constrain it using low-energy CP-violating observables. In particular, we will be interested in the effects of BSM physics on electric dipole moments (EDMs). An EDM is the $\not{T}$ interaction of the spin of a particle with a static external electric field. In systems with a spherically symmetric charge distribution such an EDM must vanish unless CP is violated. The SM prediction for EDMs of particles like the proton, neutron, and electron (which have spherically symmetric charge distributions) is very small[3]. This small SM background, in combination with the fact that the EDMs of

[3]This prediction no longer necessarily holds when one includes a nonzero QCD $\bar{\theta}$ term, see section 2.4.2 for more details.

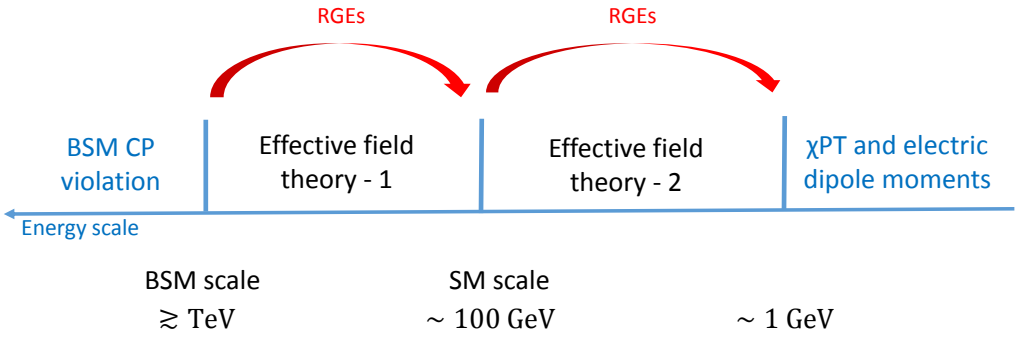

Figure 1.4: The necessary steps to bridge the energy gap between the BSM physics arising at high energies and the low-energy EDM measurements. First the EFT, describing BSM physics, is evolved to the SM scale, where the heavy SM particles are integrated out. This results in a second EFT which can be evolved to down to $\sim 1\,\text{GeV}$. To go to even lower energies, and finally connect the BSM physics to EDMs, χPT is needed in the final step.

these particles can be measured to high precision, make the EDMs promising probes of BSM physics.

In general, a BSM source of CP violation is expected to contribute to EDMs. However, in order to assess the contribution of BSM CP violation to EDMs the gap between the high energy scale where the BSM physics appears and the low energies where EDMs are measured should be bridged. This requires several steps, schematically depicted in Fig. 1.4. The first step requires the calculation of the renormalization group equations (RGEs), which work naturally in combination with the EFT techniques. These equations describe the energy dependence of the coupling constants, which determine the strengths of the effective interactions. In this first step, the RGEs allow us to move from the scale of BSM physics down to that of the SM. At this point the heavy SM particles, like the W boson, are integrated out, before moving to even lower energies using the RGEs. However, when we arrive at the scale of $\sim 1\,\text{GeV}$, the SM becomes non-perturbative and RGE calculations are no longer reliable. To reach even lower energies, we will employ another EFT, namely, chiral perturbation theory (χPT). In this EFT it is finally possible to calculate the contributions of the BSM CP-violating sources to EDMs. At this point the stringent EDM limits can be used to set strong bounds on the BSM CP-violating sources.

In the second part of this thesis we will take the second approach, the top-down approach, in order to study a specific model of BSM physics. Although an attractive feature of the EFT approach is that it is, in principle, able to capture any model of new physics, its generality also means that it can be less predictive. In specific BSM models, usually only a subset of all the possible interactions appear, whose couplings will tend to be related. Therefore, constraints can be far more stringent when considering a specific BSM model. In this thesis, we will consider left-right models (LRMs). These models were first proposed in order to explain the violation of parity in the SM [11, 12, 13]. As such, they offer a way to restore either P or C symmetry at high energies. Apart from being theoretically attractive, LRMs with either of these symmetries are rather predictive. For

instance, these symmetries in part determine the predictions for a range of observables, from low-energy precision measurements such as EDMs to meson mixing observables and LHC phenomenology. In addition, these symmetries impact the Higgs sector of the LRM, which determines how the symmetries of the model are broken. In both the Higgs sector as well as the experimental observables that will be considered, CP violation again plays an important role.

1.3 Outline of this thesis

We begin by reviewing the SM, paying particular attention to its CP-violating parts, in chapter 2. Chapters 3, 4 and 5 are devoted to the study of BSM CP-violating sources in a model-independent EFT approach. We introduce the EFT formalism, construct the EFT containing BSM CP-violating sources, and briefly review the necessary χPT techniques in chapter 3. In chapter 4, we calculate the necessary RGEs in this EFT, thereby linking the BSM physics at high energies to the EDM experiments at low energies. The actual bounds, giving insight in what kind of BSM physics is still allowed, that can derived from the stringent EDM limits by using this analysis are discussed in chapter 5.

The LRM is discussed in chapters 6, 7, and 8. In chapter 6 we introduce the LRM and most of its general features, while in chapter 7 we consider the possible LRMs with a C and/or P symmetry. Here we discuss the bounds coming from collider physics, meson-mixing, as well as those coming from low-energy observables such as EDMs and β decay. In addition, we discuss the Higgs sectors of these models, in particular, the amount of fine-tuning they require. As we will see, both the experimental constraints and the Higgs sectors will depend on which of the symmetries are enforced and how they are implemented.

In chapter 8, we focus on the prediction of the LRM with regards to EDMs. In particular, we derive the pattern it predicts for the EDMs of light nuclei. In chapter 9 we investigate whether such patterns in these EDMs can be used to distinguish between different BSM models. To answer this question we consider two additional BSM scenarios; the aligned two Higgs-doublet model (A2HDM) and a scenario in which the SM QCD θ term gives the dominant contribution. In order to connect these specific models to EDMs, we match them to the CP-violating EFT after which the usual EFT techniques are applied. Therefore, this last chapter contains a mix of the top-down and bottom-up approaches, and serves as an illustration of how such an analysis can be done for other BSM models. We summarize and conclude in chapter 10, while several appendices are devoted to technical details.

Chapter 2

The Standard Model and its discrete symmetries

Although eventually we will be interested in theories going beyond the SM, we will first briefly review the SM itself. In doing so, we will mainly be concerned with the way parity (P), charge conjugation (C) and their combination, CP, are broken in the SM. Violation of CP invariance in the SM gives rise to a background to the CP-violating BSM sources we will be considering in later chapters (3, 4 and 5). It is therefore useful to have an estimate of the size of this background. On the other hand, the violation of P and C in the weak interaction give a motivation for left-right models which will be discussed in chapters 6 and 7. In this chapter we will recall these and other features of the SM that will be relied upon in later chapters. Furthermore, the upcoming discussion should make clear most of the definitions and conventions used in this thesis.

2.1 The SM Lagrangian

As already mentioned in the introduction the standard model (SM) is based on a few underlying principles, namely, gauge and Lorentz invariance. Thus, an important part of the SM are its gauge groups and the way in which the fields transform under them, i.e. their representations. The gauge group of the SM is given by $SU(3)_c \times SU(2)_L \times U(1)_Y$, under which the quark fields transform as follows,

$$\begin{aligned} Q_L = & \begin{pmatrix} U_L \\ D_L \end{pmatrix} = \{ \begin{pmatrix} u_L \\ d_L \end{pmatrix}, \begin{pmatrix} c_L \\ s_L \end{pmatrix}, \begin{pmatrix} t_L \\ b_L \end{pmatrix} \} & \in (3,\, 2,\, 1/6), \\ U_R = & \{u_R,\, c_R,\, t_R\} & \in (3,\, 1,\, 2/3), \\ D_R = & \{d_R,\, s_R,\, b_R\} & \in (3,\, 1,\, -1/3). \end{aligned} \tag{2.1}$$

All the quark fields are triplets under $SU(3)_c$ and the left-handed quarks form doublets under $SU(2)_L$, while the right-handed fields are singlets. In the lepton sector the left-handed fields form doublets under $SU(2)_L$ while the right-handed fields are again singlets,

$$\begin{aligned} L_L = & \begin{pmatrix} \nu_L \\ l_L \end{pmatrix} = \{ \begin{pmatrix} \nu_{eL} \\ e_L \end{pmatrix}, \begin{pmatrix} \nu_{\mu L} \\ \mu_L \end{pmatrix}, \begin{pmatrix} \nu_{\tau L} \\ \tau_L \end{pmatrix} \} & \in (1,\, 2,\, -1/2), \\ l_R = & \{e_R,\, \mu_R,\, \tau_R\} & \in (1,\, 1,\, -1). \end{aligned} \tag{2.2}$$

For both the quarks and the leptons the three generations are equivalent as far as their representations are concerned.

The interaction between fermions is mediated by the gauge bosons. These fields are automatically introduced when demanding that the theory is also invariant under space-time dependent $SU(3)_c \times SU(2)_L \times U(1)_Y$ transformations. We will denote the gauge fields of $SU(3)_c$, $SU(2)_L$ and $U(1)_Y$ by G^a_μ, W^i_μ, and B_μ respectively.

The final field left to introduce is the only scalar field in the SM, the Higgs field, which transforms as,

$$\varphi = \begin{pmatrix} \varphi^+ \\ \varphi^0 \end{pmatrix} \in (1, 2, 1/2). \tag{2.3}$$

Now that we have introduced the fields of the SM, and the way they transform under the gauge symmetries, we can start to build up the gauge-invariant terms of the SM Lagrangian. These can be constructed from gauge-covariant building blocks using the fields themselves, the covariant derivative, and the field strengths. The covariant derivative is defined as

$$D_\mu \equiv \partial_\mu - i g_s \, G^a_\mu t^a - i \frac{g}{2} \, W^i_\mu \tau^i - i g' Y B_\mu, \tag{2.4}$$

where g_s, g, and g' are the $SU_c(3)$, $SU_L(2)$, and $U_Y(1)$ coupling constants. Furthermore, t^a and $\tau^i/2$ are $SU(3)$ and $SU(2)_L$ generators, in the representation of the field on which the derivative acts, and Y is the hypercharge given in Eqs. (2.1) and (2.2). The field strengths are given by

$$\begin{aligned} G^a_{\mu\nu} &\equiv \partial_\mu G^a_\nu - \partial_\mu G^a_\mu + g_s f^{abc} G^b_\mu G^c_\nu, & (2.5)\\ W^i_{\mu\nu} &\equiv \partial_\mu W^i_\nu - \partial_\nu W^i_\mu + g \varepsilon^{ijk} W^j_\mu W^k_\nu, & (2.6)\\ B_{\mu\nu} &\equiv \partial_\mu B_\nu - \partial_\nu B_\mu, & (2.7) \end{aligned}$$

where f^{abc} and ε^{ijk} denote the $SU(3)$ and $SU(2)_L$ structure constants, respectively.

As mentioned, the complete SM Lagrangian can now be assembled by combining the fields, covariant derivatives, and field strengths in a gauge- and Lorentz-invariant way. In principle, if one views the SM as an effective field theory, one could consider terms obeying the above symmetries which are of higher dimensions than four. There is an infinite number of such terms, although more and more suppressed as their dimension increases. This is the approach we will be taking in the next chapter, where the additional terms will be interpreted as arising from BSM physics. For now, however, we will consider only the terms of dimension up to four, which are the terms usually described as the SM. These terms are given by

$$\begin{aligned} \mathcal{L}_{SM} &= -\frac{1}{4} G^a_{\mu\nu} G^{a\,\mu\nu} - \frac{1}{4} W^i_{\mu\nu} W^{i\,\mu\nu} - \frac{1}{4} B_{\mu\nu} B^{\mu\nu} & (2.8)\\ &\quad + \overline{Q}_L i \not{D} Q_L + \overline{U}_R i \not{D} U_R + \overline{D}_R i \not{D} D_R + \overline{L}_L i \not{D} L_L + \overline{l}_R i \not{D} l_R & (2.9)\\ &\quad - \left[\overline{Q}_L \varphi Y_d D_R + \overline{Q}_L \tilde{\varphi} Y_u U_R + \overline{L}_L \varphi Y_l l_R + \text{h.c.} \right] & (2.10)\\ &\quad + (D_\mu \varphi)^\dagger D^\mu \varphi + \mu^2 \varphi^\dagger \varphi - \lambda (\varphi^\dagger \varphi)^2 & (2.11)\\ &\quad - \theta \frac{g_s^2}{32\pi^2} G^a_{\mu\nu} \tilde{G}^{a\,\mu\nu} - \theta_W \frac{g^2}{32\pi^2} W^i_{\mu\nu} \tilde{W}^{i\,\mu\nu} - \theta_B \frac{g'^2}{32\pi^2} B_{\mu\nu} \tilde{B}^{\mu\nu}, & (2.12) \end{aligned}$$

where $Y_{u,d,l}$ are 3×3 matrices, $\tilde{X}^{\mu\nu} = \frac{1}{2}\varepsilon^{\mu\nu\alpha\beta}X_{\alpha\beta}$ is the dual of the field strength $X_{\mu\nu} = \{G^a_{\mu\nu}, W^i_{\mu\nu}, B_{\mu\nu}\}$, and $\tilde{\varphi} = \varepsilon_{ij}\varphi^*_j$. Here $\varepsilon^{\mu\nu\alpha\beta}$ and ε_{ij} are the totally antisymmetric tensors, in four and two dimensions respectively, with $\varepsilon^{0123} = \varepsilon_{12} = +1$.

This Lagrangian can be summarized as follows. The first line, (2.8), contains the kinetic terms for the gauge fields, which describe the free gauge fields, and their self interactions. In turn, the seccond line, (2.9), incorporates the kinetic terms for the fermions and their interactions with the gauge fields. The third line, (2.10), represents the interactions of the Higgs field with the fermions, which, after electroweak symmetry breaking (EWSB), generate masses for the fermions. The terms in the fourth line, (2.11), include the kinetic term and gauge- and self-interactions of the Higgs field. The interactions of the Higgs field with the gauge fields give rise to masses for the weak bosons after EWSB. Instead, the μ^2 and λ terms determine the mass of the Higgs and its vacuum expectation value (vev), the latter of which gives rise to EWSB. The final line of the SM Lagrangian, (2.12), involves topological terms. We will return to these terms, especially the θ term, later on. First, however, we will discuss EWSB and how this affects Eqs. (2.9), (2.10), and (2.11).

2.2 Electroweak symmetry breaking

As was mentioned above, the fermions and the weak gauge bosons acquire masses after EWSB, in the SM this occurs when the Higgs field acquires a nonzero vauum expectation value (vev). By minimizing the Higgs potential one finds, for positive values of μ^2, that the Higgs field indeed obtains a nonzero vev. In the unitarity gauge of $SU(2)_L$, which we will adopt throughout this thesis, we have

$$\varphi = \frac{1}{\sqrt{2}}\begin{pmatrix} 0 \\ v + h \end{pmatrix}, \qquad v = \sqrt{\mu^2/\lambda}, \tag{2.13}$$

where v is the vev of the Higgs field and h represents perturbations around this minimum[1], *i.e.* the Higgs particle. However, it is the vev of φ that gives rise to the mass terms for the electroweak gauge bosons and fermions. Through the Higgs-gauge interactions of Eq. (2.11) v gives rise to masses for certain combinations of the gauge fields, the weak Z and $W^\pm$ bosons obtain a mass while the photon and gluons remain massless,

$$m_W^2 = \frac{g^2v^2}{4}, \qquad m_Z^2 = \frac{(g'^2 + g^2)v^2}{4}, \qquad m_{A,G} = 0, \tag{2.14}$$

where $W^\pm_\mu = \sqrt{1/2}(W^1_\mu \mp i\, W^2_\mu)$. The Z and A mass eigenstates are related to the gauge eigenstates, W^3 and B, by

$$\begin{pmatrix} W^3_\mu \\ B_\mu \end{pmatrix} = \begin{pmatrix} c_w & s_w \\ -s_w & c_w \end{pmatrix}\begin{pmatrix} Z_\mu \\ A_\mu \end{pmatrix}, \tag{2.15}$$

where $c_w = \cos\theta_w$, $s_w = \sin\theta_w$, and $\tan\theta_w = g'/g$. Defining the electromagnetic coupling to be positive, $e > 0$, we have $e = -g\, s_w$ and the electric charge of a fermion, f, can be

[1]These perturbations corresponding to the Higgs particle are in a specific direction, namely, in the radial direction. The perturbations in the remaining directions correspond to the would-be-Goldstone bosons.

expressed as $Q_f = T_f^3 + Y_F$. Here, T_f^3 is the third component of weak isospin, for example, for the leptons one has, $T_{e_L}^3 = -T_{\nu_L}^3 = -1/2$, while $T_{e_R}^3 = 0$.

Apart from the masses of the weak bosons the vev of φ also gives rise to mass terms for the fermions. In fact, the Yukawa terms of Eq. (2.10) lead to,

$$\mathcal{L}_Y = -\overline{U}_L M_u U_R - \overline{D}_L M_d D_R - \overline{L}_L M_l l_R + \text{h.c.}, \tag{2.16}$$

where $M_{u,d,l} = \frac{v}{\sqrt{2}} Y_{u,d,l}$, which in general is not diagonal. It is always possible to bring the fermions to their mass eigenstates by use of a basis transformation,

$$\begin{aligned} U_{L,R} \to V_{L,R}^u U_{L,R}, \quad D_{L,R} \to V_{L,R}^d D_{L,R}, \\ L_L \to V_L^l L_L, \qquad l_R \to V_R^l l_R, \end{aligned} \tag{2.17}$$

such that the mass matrices become positive, real, and diagonal,

$$D_u = V_L^{u\dagger} M_u V_R^u, \qquad D_d = V_L^{d\dagger} M_d V_R^d, \qquad D_l = V_L^{l\dagger} M_l V_R^l. \tag{2.18}$$

This transformation leaves the rest of the Lagrangian invariant apart from the charged-current interaction[2], which now becomes

$$\mathcal{L}_{cc} = \frac{g}{\sqrt{2}} \overline{U}_L \gamma^\mu V D_L W_\mu^+ + \text{h.c.}, \tag{2.19}$$

where $V = V_L^{u\dagger} V_L^d$ is the Cabibbo-Kobayashi-Maskawa (CKM) mixing matrix. Note that the charged-lepton current remains unchanged by the transformation of Eq. (2.17). This is due to the fact that there was no neutrino mass matrix to diagonalize, such that the ν_L fields did not need to be rotated separately. Throughout this thesis we will leave the inclusion of neutrino masses aside, and focus on the quark sector instead.

The CKM matrix appearing in Eq. (2.19) is a unitary $N \times N$ matrix, where N is the number of generation, and therefore has N^2 free parameters. These parameters consist of $N(N-1)/2$ angles and $N(N+1)/2$ phases. However, $2N-1$ of the phases in this matrix can be eliminated by a redefinition of the quark fields, which leaves $(N-2)(N-1)/2$ phases and $(N-1)^2$ free parameters in total. Note that this counting implies that three generations are required in order to have a physical phase. This is realized in the SM where we have three generations and thus three mixing angles and one phase. This remaining phase is responsible for explicit CP violation in the weak interaction. Before going on to discuss this source of CP violation, we will briefly recount P, C, and CP transformations.

2.3 P and C violation

Under parity and charge conjugation the Higgs (φ) and fermion fields, ψ, transform as follows,

$$\begin{aligned} P: &\qquad \psi(t,\mathbf{x}) \to \gamma_0\, \psi(t,-\mathbf{x}), &&\qquad \varphi(t,\mathbf{x}) \to \varphi(t,-\mathbf{x}), \\ C: &\qquad \psi \to C\overline{\psi}^T, &&\qquad \varphi \to \varphi^*, \end{aligned} \tag{2.20}$$

[2]Due to the chiral anomaly this is not quite true, see section 2.4.

where $C = i\gamma^2\gamma^0$ in the Weyl representation of the gamma matrices, see appendix 2.A for more details. In order to ensure the interactions of photons and gluons with fermions are invariant under P and C, the gauge fields should transform as follows,

$$\begin{aligned} P : V_\mu(t, \mathbf{x}) &\to (-1)^\mu V_\mu(t, -\mathbf{x}), \\ C : \qquad V_\mu &\to -(V_\mu)^T, \end{aligned} \tag{2.21}$$

where $V_\mu = (t^a G^a_\mu,\, \tau^i W^i_\mu,\, B_\mu)$ and $(-1)^\mu$ is $+1$ for $\mu = 0$ and -1 otherwise. As the electric and magnetic fields can be identified with $E_i = F^{i0}$ and $B_i = -\frac{1}{2}\epsilon_{ijk}F^{jk}$, it can be seen that these transformations reproduce the familiar transformations of the E and B fields,

$$\begin{aligned} P : &\quad \mathbf{E} \to -\mathbf{E}, \quad \mathbf{B} \to \mathbf{B}, \\ C : &\quad \mathbf{E} \to -\mathbf{E}, \quad \mathbf{B} \to -\mathbf{B}. \end{aligned} \tag{2.22}$$

With these transformation rules Eqs. (2.20), (2.21), it can be seen that, although the kinetic terms for the gauge fields and fermions are invariant under P and C, this is not the case for chiral interactions between fermions and the gauge fields. In the SM, both the $SU(2)_L$ and $U(1)_Y$ groups are chiral, as they treat the left- and right-handed fermions differently, as can be seen from Eqs. (2.1) and (2.2). Therefore, these interactions break P and C. In fact, as the $W^\pm$ bosons only couple to the left-handed fermions, P and C are said to be maximally broken in the weak interaction. This violation of parity and charge conjugation has been well tested experimentally. Nonetheless, it remains unclear why only the left-handed fermions are charged under the $SU(2)_L$ gauge group, leading to maximal C and P violation. Left-right symmetric models, to be discussed later on, would offer a possible explanation for this problem.

2.4 CP violation in the SM

Although the SM contains a number of P- and C-violating terms, most of the SM Lagrangian is invariant under their combination, CP. In fact, using the transformation rules, Eqs. (2.20), (2.21), one can show that only the Yukawa couplings in Eq. (2.10) and the θ terms of Eq. (2.12) are sources of CP violation. We will start by discussing the former.

2.4.1 Yukawa sector

Simply applying the combination of the P and C transformations of Eq. (2.20), one would come to the conclusion that any imaginary part of the Yukawa couplings would violate CP. However, this is not quite true, as we should consider the most general CP transformations which leave the kinetic terms invariant. The transformations of Eq. (2.20) can be generalized to include a flavor rotation, we then have for their combination

$$\begin{aligned} CP : \quad Q_L \to V_Q C Q_L^*, \quad U_R \to V_U C U_R^*, \quad D_R \to V_D C D_R^*, \\ L_L \to V_L C L_L^*, \quad l_R \to V_l C l_R^*, \end{aligned} \tag{2.23}$$

where $V_{Q,U,D,L,l}$ are unitary 3×3 matrices. Apart from the Yukawa terms, all of the SM Lagrangian is invariant under the added flavor rotation. Thus, all of the SM Lagrangian is invariant under Eq. (2.23) apart from the Yukawa and θ terms. For the Yukawa interactions, demanding invariance under Eq. (2.23) gives the following conditions,

$$Y_U = V_Q^T Y_U^* V_U^*, \qquad Y_D = V_Q^T Y_D^* V_D^*, \qquad Y_l = V_L^T Y_l^* V_l^*. \tag{2.24}$$

As long as matrices $V_{Q,U,D,L,l}$ exist such that the above equations are satisfied, CP is conserved. Note that one can always find matrices $V_{L,l}$ such that the condition for Y_l is satisfied. This is due to the fact that we have only one condition in the lepton sector, this changes once one includes neutrino masses.

The conditions for the quarks cannot generally be satisfied. In fact, Eq. (2.24) allows one to derive a measure of CP violation, which is non-zero if and only if CP is broken. In order to do so, consider the commutator [14]

$$C_J = \left[Y_U Y_U^\dagger,\, Y_D Y_D^\dagger\right]. \tag{2.25}$$

This commutator is anti-hermitian, so that, $\mathrm{Det}\, C_J = -\mathrm{Det}\, C_J^*$. On the other hand Eq. (2.24) implies $\mathrm{Det}\, C_J = \mathrm{Det}\, C_J^*$, thus, in the CP-symmetric case we must have $\mathrm{Det}\, C_J = 0$. Clearly, the vanishing of this determinant is a necessary condition for CP conservation. Within the Yukawa sector of the SM it can also be shown that this is a sufficient condition. Therefore, $\mathrm{Det}\, C_J$ is a measure of CP violation. After EWSB and by using Eq. (2.18) this can be written in terms of the quark masses and CKM elements,

$$\begin{aligned} \frac{v^{12}}{64}\mathrm{Det}\, C_J &= \mathrm{Det}\left(\left[D_u^2,\, V D_d^2 V^\dagger\right]\right) \\ &= 2i(m_b^2 - m_s^2)(m_b^2 - m_d^2)(m_d^2 - m_s^2)(m_t^2 - m_c^2)(m_t^2 - m_u^2)(m_u^2 - m_c^2) J, \end{aligned} \tag{2.26}$$

where $J \equiv \mathrm{Im}\, V_{11} V_{22} V_{12}^* V_{21}^*$ is the Jarlskog invariant [15]. Any CKM-induced CP violation will be proportional to the basis-independent J. As all the quark masses are different, a nonzero value for J is a sufficient condition for CP violation. Experimentally it is determined to be $J \approx 3 \cdot 10^{-5}$ [16].

This source of CP violation contributes only weakly to EDMs. This is in part due to the fact that the CP violating phase requires all three generations to play a role while the EDM is a flavor-diagonal interaction. For instance, the CKM contribution to the neutron EDM is $d_n \sim 10^{-32}\, e\,\mathrm{cm}$ [17], roughly six orders of magnitude below the current experimental precision [18]. The EDM of the electron is even smaller in the SM, because it appears only at the four-loop level and should be below $d_e \leq 10^{-38} e\,\mathrm{cm}$ [19, 20][3], which is more than 9 orders of magnitude below the current experimental precision.

So far we have discussed explicit CP violation. However, it is in principle also possible for CP to be broken spontaneously. In the SM this could occur through the vev of the Higgs field. In this case it is easy to show there is no spontaneous CP violation. The requirement for CP invariance is, $\langle 0|\varphi|0\rangle = \langle 0|\varphi^*|0\rangle$ and thus $v = v^*$. As we can always

[3]This is the case in the SM without CP violation in the neutrino sector. For instance, if neutrinos are Majorana particles additional contributions to d_e already appear at the two-loop level and $d_e \sim 10^{-33} e\,\mathrm{cm}$ could be possible [21, 22].

find a basis where v is real, this condition is always satisfied. However, in models involving additional Higgs fields this condition can not always be satisfied, as we will see in later chapters.

Having discussed CP violation in the Yukawa sector, this leaves one source of CP violation in the SM, namely, the θ terms.

2.4.2 The θ term

Using the transformation rules of Eq. (2.21) it is clear that the terms in Eq. (2.12) are P odd and C even and thus violate CP. These terms are of the form

$$\mathcal{L} \propto F^a_{\mu\nu}\tilde{F}^{a\,\mu\nu}, \tag{2.27}$$

for a gauge field $X = \{B_\mu, W^a_\mu, G^a_\mu\}$ with field strength $X^a_{\mu\nu} = \{B_{\mu\nu}, W^a_{\mu\nu}, G^a_{\mu\nu}\}$. Such terms are topological in nature, and contribute to the action solely through non-perturbative effects, see *e.g.* [23]. This is due to the fact that Eq. (2.27) can be written as a total derivative,

$$X^a_{\mu\nu}\tilde{X}^{a\,\mu\nu} = \partial_\mu K^\mu, \qquad K^\mu = \varepsilon^{\mu\nu\alpha\beta}X^a_\nu(X^a_{\alpha\beta} - \frac{g}{3}f_{abc}X^b_\alpha X^c_\beta), \tag{2.28}$$

which means Eq. (2.27) contributes a surface integral to the action. Such an integral usually vanishes. This is because the field strength should go to zero faster than $1/|x|^2$, as $|x| \to \infty$, in order for the kinetic terms, Eq. (2.8), to give a finite contribution to the action. This can be arranged by letting the gauge fields decrease faster than $1/|x|$, in this case the surface integral that Eq. (2.27) contributes to the action will indeed vanish. Another possibility is that the gauge fields approach zero up to a gauge transformation as $|x| \to \infty$, this is a so-called "pure gauge" configuration,

$$it^a A^a_\mu \xrightarrow{|x|\to\infty} \frac{1}{g}g(x)^{-1}\partial_\mu g(x), \tag{2.29}$$

where $g(x)$ is an element of the gauge group and g the gauge coupling. These pure gauge configurations can contribute to the action while keeping the kinetic terms finite. Thus, the term in Eq. (2.27) can contribute to the action through the so-called *instanton* solutions of Eq. (2.29) [24, 25, 26].

In the limit $|x| \to \infty$, the points x lie on the three-sphere S^3. As a result, the configurations in Eq. (2.29) provide mappings from S^3 to elements of the gauge group. In particular, these configurations map to the elements forming $SU(2)$, contained in both the $SU(2)_L$ and $SU(3)_c$ gauge groups. These mappings can be divided up into equivalence classes, which together form a homotopy group, $\pi_3(SU(2)) = Z$. This homotopy group gives rise to the *winding number*, which characterizes the different equivalence classes, and is related to the term in Eq. (2.27) through

$$\int dx^4 \partial_\mu K^\mu = \frac{32i\pi^2}{g^2}|\nu|, \tag{2.30}$$

where ν is the winding number, explicitly showing that the term in Eq. (2.27) does contribute to the action. However, this is only the case for the non-Abelian groups of the

SM, for the Abelian group, $U(1)_Y$ one has $\pi_3(U(1)) = 0$ and the integral over the term in Eq. (2.27) does vanish.

Thus, it would appear that the θ and θ_W of Eq. (2.12) are both sources of CP violation, however, these constants are not by themselves observable. Due to the chiral anomaly a chiral transformation effectively induces a contribution to the θ, $\theta_{W,B}$ terms in Eq. (2.12) [27, 28]. For instance, focussing on θ, a chiral $U(1)_A$ transformation of the quark fields $q_f \to e^{i\alpha_f\gamma_5/2}q_f$ has the following effect,

$$\theta\,\frac{g_s^2}{32\pi^2}G^a_{\mu\nu}\tilde{G}^{a\,\mu\nu} \to \left(\theta + \sum_f \alpha_f\right)\frac{g_s^2}{32\pi^2}G^a_{\mu\nu}\tilde{G}^{a\,\mu\nu}. \tag{2.31}$$

Note that we needed to perform a chiral basis transformation, Eq. (2.17), in order to bring the mass matrices to their real and diagonal form. The overall phase of this transformation is a chiral transformation like Eq. (2.31) with $\alpha_f = \frac{1}{n_f}\text{Arg Det}\, M_u M_d$ and n_f the number of quark flavors. Thus, this transformation shifts θ, making only the combination $\bar{\theta} = \theta + \text{Arg Det}\, M_u M_d$ observable in the SM.

Unlike the CP violation in the CKM matrix, the $\bar{\theta}$ term is flavor-diagonal and can give a significant contribution to the neutron EDM. The current experimental upper bound [18] limits $|\bar{\theta}| \lesssim 10^{-10}$ [29]. This is an unnaturally small value for a parameter which one would naively expect to be of $\mathcal{O}(1)$. This issue is referred to as the strong CP problem. There is no experimentally verified solution to this problem, although some, like the Peccei-Quinn mechanism [30], have been proposed.

No such problem exists for the weak θ_W term as the contribution of the instantons to the action is proportional to e^{-1/g^2}, which for the $SU(2)_L$ gauge coupling results in an extreme suppression at low energies. In fact, in the SM, θ_W can even be removed from the theory by a field transformation [31, 32, 33]. One can rotate the left- and right-handed fermion fields by a phase such that the mass matrices remain unaltered. Such a rotation is a vector transformation, however, as only the left-handed fields are charged under $SU(2)_L$ this still induces a contribution to θ_W, and can therefore be used to cancel θ_W. Both these arguments do not hold for the θ term. The first is spoiled by the fact that the $SU(3)_c$ gauge coupling becomes large at low energies, the second does not hold because the left- and right-handed quarks have the same $SU(3)_c$ charges.

2.5 Summary

In summary, both parity and charge conjugation are violated in the SM. In the weak interaction these symmetries are maximally violated. Although the P and C violation of the SM has been verified experimentally, it remains unclear why only the left-handed fermions are charged under the $SU(2)_L$ gauge group. For an answer to this question, if any exists, one should presumably look to BSM physics. We will come back to this issue in chapter 6.

The combination of P and C, CP, is conserved by a larger part of the SM Lagrangian. Nonetheless, there are two CP-violating sources in the SM, namely, the phase in the CKM matrix and the QCD θ angle. These two sources will in general contribute to EDMs. As

we will discuss EDMs as probes for BSM CP violation in later chapters, it is important to consider the SM background generated by these sources. Although the CP-violating phase in the CKM matrix is not small, for it to give rise to CP violation in any given process requires the participation of all three quark generations. As EDMs are flavor-diagonal observables, the CKM phase only contributes through loops. As a result, the contribution of CKM CP-violation to EDMs is exceedingly small and can be neglected. In contrast, the QCD θ term contributes significantly to the hadronic EDMs. As a result the upper bound on the neutron EDM strongly limits $|\bar{\theta}| \lesssim 10^{-10}$. However, a very small, but nonzero, θ term could still form a SM background to BSM CP-violating physics.

The reason to study BSM physics is of course, that the SM as discussed in this chapter does not offer an explanation for all phenomena that have been observed so far. For instance, the SM does not tell us what dark matter is or whether neutrinos are Dirac or Majorana particles. Another problem of the SM is that it is unable to account for the baryon asymmetry of the universe [8, 9]. This asymmetry can only be generated in processes which satisfy the three Sakharov conditions [34]. Such a process should violate C and CP, be out of equilibrium, and violate baryon number. As we have seen in this chapter, the SM breaks C and CP, thereby satisfying the first condition. In order to satisfy the last condition, however, the electroweak phase transition of the SM should be a first-order transition. Unfortunately, for the measured value of the Higgs boson mass, the SM phase transition is second order [10], such that the SM cannot explain the BAU. Furthermore, even in the case of an unrealistically light Higgs boson, which would allow for a first-order phase transition, the amount of CP violation in the SM is too small to produce the BAU [10].

This last point leads one to suspect there should be physics beyond the SM, and, in particular, new sources of CP violation. The investigation of this possibility constitutes a large part of the remainder of this thesis. We will investigate BSM sources of CP violation in both a model-independent and a model-dependent way. In the next chapter we will start with the former. Here, we will describe CP-violating BSM physics by effective interactions in an EFT framework. In particular, we will consider CP-violating effective interactions of dimension-six, which are invariant under the SM gauge symmetries, and focus on those most important for hadronic EDMs[4]. In the upcoming chapter we will construct the Lagrangian describing these effective interactions with the aim to see how these are constrained by EDM limits in later chapters.

Appendix 2.A C, P, and T transformations

In this appendix we will briefly discuss the parity, charge-conjugation, and time-reversal transformations and their most general forms for the case of multiple fermion flavors. We will start with parity transformations.

[4]We will consider interactions which do not involve leptons, and do not involve quarks of the second and third generations.

2.A.1 Parity

Under parity one inverts the spatial coordinates, $\vec{x} \to \vec{x}$. For a single fermion field, ψ the parity transformation should then be of the form

$$\psi(t, \vec{x}) \to U_P \psi(t, -\vec{x}), \tag{2.32}$$

with U_P a unitary matrix which can be determined by demanding that the Dirac equation is invariant under parity. This requirement leads to

$$P: \qquad \psi(t, \vec{x}) \to \eta_P \gamma_0 \psi(t, -\vec{x}), \tag{2.33}$$

with $|\eta_P|^2 = 1$.

2.A.2 Charge conjugation

Charge conjugation transforms particles into their antiparticles. The transformation itself can be written as

$$C: \qquad \psi(t, \vec{x}) \to \eta_C C \bar{\psi}(t, \vec{x})^T, \tag{2.34}$$

with C a unitary matrix. Since this transformation transforms particles into antiparticles, the charge-conjugated field should have the opposite charge from the original field. This implies that the Dirac equation,

$$0 = \left(i\partial\!\!\!/ - eQ_f A\!\!\!/\right)\psi(t, \vec{x}), \tag{2.35}$$

should have a different sign for the gauge interaction term when being applied to the charge-conjugated field

$$0 = \left(i\partial\!\!\!/ + eQ_f A\!\!\!/\right)\psi^C(t, \vec{x}), \qquad \psi^C(t, \vec{x}) = \eta_C C \bar{\psi}(t, \vec{x})^T. \tag{2.36}$$

From this requirement, the unitarity of C, and the fact that applying charge conjugation twice should leave ψ invariant, one can deduce the following properties of C,

$$C\gamma_\mu^T C^{-1} = -\gamma_\mu, \qquad C^\dagger = C^{-1}, \qquad C^T = -C, \qquad |\eta_c|^2 = 1. \tag{2.37}$$

The matrix explicit form of C depends on the representation of the gamma matrices. In the Weyl representation, used in section 2.3, it is given by

$$C = i\gamma_2\gamma_0. \tag{2.38}$$

2.A.3 Time reversal

Finally, the time-reversal transformation can be written as

$$T: \qquad \psi(t, \vec{x}) \to \eta_T T \psi(-t, \vec{x}), \tag{2.39}$$

with the additional property that the application of time reversal conjugates all complex numbers. If we again demand that the Dirac equation is invariant under time reversal, and that two successive applications leave ψ unaltered, we obtain

$$T\gamma_0^* T^{-1} = \gamma_0, \qquad T\gamma_i^* T^{-1} = -\gamma_i, \qquad |\eta_T|^2 = 1, \tag{2.40}$$

where $i = 1, 2, 3$. Like the charge conjugation matrix C, the matrix T depends on the representation of the gamma matrices. In the Weyl representation, we have $T = \gamma_1\gamma_3$.

The combination of C, P, and T, called CPT, has special status within quantum field theory. In fact, Lorentz-invariant local quantum field theories with a hermitian Hamiltonian, e.g. the theories that will be considered in this thesis, conserve CPT [35, 36].

2.A.4 C, P, and T with flavor rotations

So far we have only considered the application of these transformations on a single fermion field. Nonetheless, in each case the P, C and T transformations came with an additional, unknown phase $\eta_{P,C,T}$. The reason for this is that the kinetic term of a fermion field ψ is invariant under a global phase transformation. Therefore, the most general C, P, and T transformation should involve such a phase rotation to be completely general. The appearance of this rotation addresses the possibility that we may not be in the basis in which these transformations take their simplest form, i.e. with $\eta_{P,C,T} = 1$.

In the case that we have multiple fermion fields, these phases above generalize to matrices. For example, in the case where we have N fermion fields, ψ_i, the kinetic terms will be left invariant by the following transformation,

$$\psi_i \to U_{ij}\psi_j, \qquad UU^\dagger = U^\dagger U = \mathbf{1}. \tag{2.41}$$

Therefore, similar to the above phase transformation, this rotation between fermion fields should be included in the P, C, and T transformations in order to be completely general. Within the SM, these transformations are rotations between fermion fields which differ only by their flavor since rotations between fermions with different quantum numbers will not leave the gauge interactions invariant.

For the discussion about the parity and charge conjugation properties of the SM Lagrangian in section 2.3, however, such rotations were neglected. Nonetheless, in this particular case, these flavor rotations would not change the conclusion that both C and P are broken in the SM. This is due to the fact that the P and C transformations change the weak current from being purely left-handed to purely right-handed. As flavor rotations preserve chirality, they will alter this conclusion. In contrast, the case of CP transformations, discussed in section 2.4, is not so clear-cut, and the the most general CP transformations are needed. Within the SM these are given by

$$\begin{aligned} CP: \quad & Q_L \to V_Q C Q_L^*, \quad U_R \to V_U C U_R^*, \quad D_R \to V_D C D_R^*, \\ & L_L \to V_L C L_L^*, \quad l_R \to V_l C l_R^*, \end{aligned} \tag{2.42}$$

where $V_{Q,U,D,L,l}$ are 3×3 unitary matrices. In fact, as mentioned in section 2.4, using the simpler transformations without flavor rotations would result in the conclusion that any phase of the Yukawa couplings violates CP, while in reality, there is only one physical CP-violating phase in the CKM matrix.

Chapter 3

The effective field theory of CP-violating new physics

As discussed in the previous chapters, the CP-violating terms of the SM cannot account for the current matter-antimatter asymmetry of the Universe [8, 9]. As such, new sources of CP violation are expected to appear when going beyond the SM. In chapter 5 we will consider constraints on such sources from low-energy precision-experiments. In order to derive these constraints, several steps are required. First, a description of the sources of BSM CP violation is needed. We will employ a model-independent EFT approach, in which we will describe the CP-violating BSM physics in terms of higher-dimensional operators [37, 38, 39, 40, 41]. In this chapter we will construct these operators and add them to the SM Lagrangian. Secondly, as we will consider bounds from low-energy experiments, while BSM physics is expected to appear at high energies, the BSM operators have to be evolved to low energies. This process involves the calculation of the renormalization group equations (RGEs). However, at and below the QCD scale $M_{\rm QCD} \sim 1\,\text{GeV}$, g_s becomes large and consequently perturbation theory and the RGEs break down. Therefore, in order to describe physics at energies below $M_{\rm QCD}$, we will employ the QCD EFT for pions and nucleons, namely, chiral perturbation theory (χPT). In the final step, χPT will allow for the calculation of low-energy observables, thereby providing the link to experiment.

The low-energy observables we will consider are the EDMs of nucleons, nuclei, atoms and molecules. Theories of BSM physics generally contain additional sources of CP violation, which induce new contributions to these EDMs. These contributions, in combination with the impressive experimental accuracy of EDM measurements, and the fact that the CKM phase contributes negligibly to EDMs [42], make EDMs good probes of BSM physics. At the current precision a nonzero measurement would imply a small but finite $\bar{\theta}$ term or BSM CP violation. In chapters 8 and 9 we will consider both possibilities in regard to the EDMs of light nuclei. However, for our present goal to constrain BSM sources of CP violation, we will focus on the latter possibility, by setting $\bar{\theta}$ to zero, and consider mainly hadronic EDMs, in particular the neutron EDM. This choice of observables will, in part, determine the set of CP-violating operators we will consider.

This chapter covers the EFT aspects needed to describe the BSM CP violation at high and low energies, as depicted in Fig. 3.1. We will construct the set of CP-violating operators, which are expected to be the most important ones for hadronic EDMs, and add them

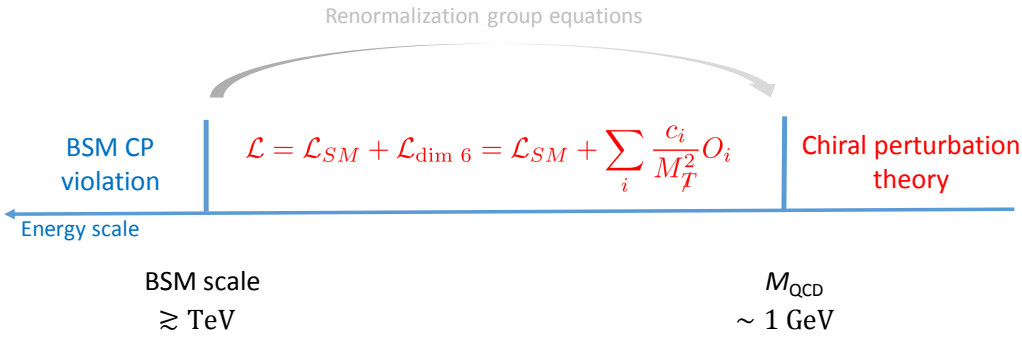

Figure 3.1: The necessary steps to bridge the energy gap between the BSM physics arising at high energies and the low-energies, $< M_{\rm QCD}$, where EDM measurements take place. In this chapter we will focus on the required effective-field-theory techniques. In particular, we will consider the EFT describing the BSM sources at high energies in terms of dimension-six operators, and the EFT describing the CP violation at low energies, namely chiral perturbation theory. Both EFTs are shown in red. The evolution of the first EFT from high to low energies, shown in gray, will be left to the next chapter.

to the SM Lagrangian. In addition, we will briefly review the necessary χPT techniques and the interactions in the chiral Lagrangian which give the dominant contributions to hadronic EDMs. Finally, we will discuss the matching between the CP-violating operators at $M_{\rm QCD}$ in terms of SM fields and the interactions they induce in the chiral Lagrangian in terms of hadronic degrees of freedom. This leaves one final step of the process described above, namely, the evolution of the CP-violating operators from high energies to $M_{\rm QCD}$. We leave this topic to chapter 4, while finally combining all the steps and calculating the constraints on the CP-violating operators in chapter 5.

3.1 Dimension-six operators

The model-independent approach we will be considering relies heavily on EFT techniques, for reviews see *e.g.* [43, 44, 45, 46]. In turn, the EFT we will construct in this chapter relies on the assumption that the CP-violating BSM physics appears at a scale, $M_{\not T}$, considerably higher than the electroweak scale, $M_{\rm EW} \sim 100\,\text{GeV}$. This assumption implies no new particles exist with masses below $M_{\rm EW}$. Considering the success of the SM, this seems like a reasonable assumption.

Starting just below $M_{\not T}$, the effects of new physics can be described by effective higher-dimensional interactions consisting of SM fields only, *i.e.*

$$\mathcal{L} = \mathcal{L}_{\rm SM} + \sum_{i,d} \frac{c_d^i}{M_{\not T}^{d-4}} O_i^d, \tag{3.1}$$

where O_i^d and $c_d^i \lesssim \mathcal{O}(1)$ stand for operators of dimension $d > 4$ and their couplings, respectively. These interactions can be thought of as resulting from integrating out the heavy particles of a BSM theory. As mentioned in chapter 1, there is an infinite number of these operators. However, although the theory is non-renormalizable, it can

be renormalized order-by-order in an expansion of $1/M_{\not T}$. Furthermore, the effects of higher-dimensional operators are suppressed with respect to those of lower dimensions. In particular, when calculating physical quantities, the contribution of higher-dimensional operators will be proportional to $\sim c_d^i \left(\frac{E}{M_{\not T}}\right)^d$, where E stands for an energy scale in the EFT (for instance, particle masses or the energy scale of a given process) [43]. This argument shows that the EFT breaks down when probing high energies, $E \sim M_{\not T}$. At this point the contributions from all the operators become equally important. However, as long as $E \ll M_{\not T}$, the operators can be ordered by their dimension, and we can consider the lowest-dimensional operators only.

There are several requirements the non-renormalizable operators we are interested in should meet. Firstly, these operators should be CP-violating. Secondly, since the SM and its gauge structure have been tested to high precision in numerous experiments, we assume the SM gauge symmetries to be valid at and beyond the SM scale. In particular, since it would hard to understand why explicit symmetry-breaking terms would only appear at dimension-six and not in the $d \leq 4$ Lagrangian [39], we will assume the dimensions-six operators to be gauge invariant. Since $SU(2) \times U(1)$ is spontaneously broken at around M_{EW} one may be tempted to start the analysis at lower energies by constructing all operators that obey $SU_c(3) \times U(1)$ invariance. However, the latter strategy does not exploit all available information, as the breaking of $SU_L(2) \times U_Y(1)$ is dictated by the Higgs mechanism and does not happen in a general way. For example, it turns out that only a subset of the set of $SU_c(3) \times U(1)$ invariant $\not P \not T$ (and CP-violating) four-quark interactions [47, 48] generally needs to be taken into account. The remaining operators are suppressed due to their particular gauge-symmetry breaking properties. A third requirement is that the operators do not contain lepton fields, as we will focus on hadronic EDMs. Finally, since the number of operators is large, we focus on those containing the up and down quarks, which should give the dominant contributions to the hadronic EDMs, leaving the second and third generation aside.

It should be mentioned that these requirements lead to a set of dimension-six operators that is far from complete, because it does not include operators involving heavier quarks. Allowing such fields would increase the number of operators significantly, especially if one allows for generation-changing operators, in this case the number of CP-violating operators is 1149 [49]. Most importantly, this set does not include operators involving strange quarks which are still present in the EFT at $M_{\rm QCD}$ and could have important consequences for hadronic and nuclear EDMs. We leave a study of operators involving strangeness to future work. In general, operators involving heavier quarks than up, down, and strange are expected to give suppressed contributions to operators around $M_{\rm QCD}$ due to the need of integrating out the heavier quarks. However, exceptions to this argument exist, see, for example, discussions in Refs. [42, 48].

The non-renormalizable operators start at dimension five, where a single operator appears, which gives rise to Majorana masses for the neutrinos [50]. However, as it is a leptonic operator we discard it. At dimension six there are 59 operators[1] which were constructed in Refs. [37, 41]. We now turn to this list of gauge-invariant dimension-six

[1]Barring flavor structure and hermitian conjugates the number of operators is 59, otherwise the number is to 2499 [49].

operators, taking into account the requirements described above. We start by considering various interactions between a quark, a scalar boson, and a gauge boson

$$\begin{aligned}\mathcal{L}_{6,qq\varphi X} &= -\frac{1}{\sqrt{2}}\bar{q}_L\sigma^{\mu\nu}\tilde{\Gamma}^u t^a\frac{\tilde{\varphi}}{v}u_R G^a_{\mu\nu} - \frac{1}{\sqrt{2}}\bar{q}_L\sigma^{\mu\nu}\tilde{\Gamma}^d t^a\frac{\varphi}{v}d_R G^a_{\mu\nu}\\ &\quad -\frac{1}{\sqrt{2}}\bar{q}_L\sigma^{\mu\nu}(\Gamma^u_B B_{\mu\nu} + \Gamma^u_W\boldsymbol{\tau}\cdot\boldsymbol{W}_{\mu\nu})\frac{\tilde{\varphi}}{v}u_R\\ &\quad -\frac{1}{\sqrt{2}}\bar{q}_L\sigma^{\mu\nu}(\Gamma^d_B B_{\mu\nu} + \Gamma^d_W\boldsymbol{\tau}\cdot\boldsymbol{W}_{\mu\nu})\frac{\varphi}{v}d_R + \text{h.c.},\end{aligned} \tag{3.2}$$

where $\tilde{\Gamma}^{u,d}$ and $\Gamma^{u,d}_{B,W}$ are complex coupling constants, $q = (u,\, d)^T$, and an explicit factor v was taken out for later convenience. All the introduced coupling constants are proportional to $M_{\not T}^{-2}$. As the couplings in Eq. (3.2) flip the chirality of the quark field we assume them to be proportional to the SM Yukawa couplings. However, the coupling constants can simply be rescaled if this assumption breaks down in a particular high-energy model. Combined with the Higgs vev, the Yukawa couplings can be traded for the light-quark mass. It is convenient to write Eq. (3.2) in terms of the physical gauge-boson fields. Focusing on the $\not P\not T$ terms only, we find the following interactions containing massless gauge bosons

$$\begin{aligned}\mathcal{L}_{6,\text{q(C)EDM}} &= -\frac{1}{2}\big[m_u Q_u d_u(\bar{u}i\sigma^{\mu\nu}\gamma_5 u)\, eF_{\mu\nu} + m_d Q_d d_d(\bar{d}i\sigma^{\mu\nu}\gamma_5 d)\, eF_{\mu\nu}\\ &\qquad + m_u\tilde{d}_u(\bar{u}i\sigma^{\mu\nu}\gamma_5 t^a u)\, G^a_{\mu\nu} + m_d\tilde{d}_d(\bar{d}i\sigma^{\mu\nu}\gamma_5 t^a d)\, G^a_{\mu\nu}\big]\left(1+\frac{h}{v}\right).\end{aligned} \tag{3.3}$$

The terms without the Higgs boson in the first and second line of Eq. (3.3) can be interpreted as respectively, the quark electric and chromo-electric dipole moment (quark EDM and CEDM) with coupling constants

$$d_u \equiv \frac{c_w\text{Im}\,\Gamma^u_B + s_w\text{Im}\,\Gamma^u_W}{em_u Q_u}, \qquad d_d \equiv \frac{c_w\text{Im}\,\Gamma^d_B - s_w\text{Im}\,\Gamma^d_W}{em_d Q_d}, \qquad \tilde{d}_q \equiv \frac{\text{Im}\,\tilde{\Gamma}^q}{m_q}. \tag{3.4}$$

After electroweak symmetry breaking Eq. (3.2) also contributes to interactions involving heavy gauge-boson fields. Interactions involving the Z boson, in particular its "abelian" field strength $Z_{\mu\nu} \equiv \partial_\mu Z_\nu - \partial_\nu Z_\mu$, are given by

$$\mathcal{L}_{6,\text{qZEDM}} = -\frac{g}{2}\big[z_u m_u(\bar{u}i\sigma^{\mu\nu}\gamma_5 u)\, Z_{\mu\nu} + z_d m_d(\bar{d}i\sigma^{\mu\nu}\gamma_5 d)\, Z_{\mu\nu}\big]\left(1+\frac{h}{v}\right), \tag{3.5}$$

with coupling constants

$$z_u \equiv \frac{c_w\text{Im}\,\Gamma^u_W - s_w\text{Im}\,\Gamma^u_B}{gm_u}, \qquad z_d \equiv -\frac{c_w\text{Im}\,\Gamma^d_W + s_w\text{Im}\,\Gamma^d_B}{gm_d}. \tag{3.6}$$

Finally, there are terms involving the charged gauge bosons $W^\pm_\mu$ and their field strengths

$W^{\pm}_{\mu\nu} \equiv (W^1_{\mu\nu} \mp iW^2_{\mu\nu})/\sqrt{2}$, which are of the form

$$\begin{aligned}\mathcal{L}_{6,\mathrm{qWEDM}} &= -\frac{g}{\sqrt{2}} m_u w_u \left[(\bar{d}_L i\sigma^{\mu\nu} u_R)\, W^-_{\mu\nu} - i\frac{g}{\sqrt{2}} (\bar{u} i\sigma^{\mu\nu}\gamma_5 u)\, W^+_\mu W^-_\nu + \mathrm{h.c.} \right] \left(1 + \frac{h}{v}\right), \\ &\quad -\frac{g}{\sqrt{2}} m_d w_d \left[(\bar{u}_L i\sigma^{\mu\nu} d_R)\, W^+_{\mu\nu} + i\frac{g}{\sqrt{2}} (\bar{d} i\sigma^{\mu\nu}\gamma_5 d)\, W^+_\mu W^-_\nu + \mathrm{h.c.} \right] \left(1 + \frac{h}{v}\right),\end{aligned} \tag{3.7}$$

where

$$w_u \equiv \frac{\mathrm{Im}\,\Gamma^u_W}{g m_u}, \qquad w_d \equiv \frac{\mathrm{Im}\,\Gamma^d_W}{g m_d}. \tag{3.8}$$

The quark EDMs and weak EDMs are related by gauge symmetry as can be seen from Eqs. (3.4), (3.6), and (3.8).

The next dimension-six operator is the Weinberg operator [38] which contains only gluons

$$\mathcal{L}_{6,GGG} = \frac{d_W}{6} f^{abc} \varepsilon^{\mu\nu\alpha\beta} G^a_{\alpha\beta} G^b_{\mu\rho} G^{c\,\rho}_{\nu}. \tag{3.9}$$

This operator can be interpreted as the CEDM of the gluon [51].

Next we consider $\not{P}\not{T}$ interactions among quarks [40]

$$\mathcal{L}_{6,qqqq} = \Sigma_1 (\bar{q}^i_L u_R) \varepsilon_{ij} (\bar{q}^j_L d_R) + \Sigma_8 (\bar{q}^i_L t_a u_R) \varepsilon_{ij} (\bar{q}^j_L t_a d_R) + \mathrm{h.c.} \tag{3.10}$$

The $\not{P}\not{T}$ terms can be rewritten as

$$\begin{aligned}\mathcal{L}_{6,qqqq} &= i\frac{\mathrm{Im}\,\Sigma_1}{2} (\bar{u}u\,\bar{d}\gamma_5 d + \bar{u}\gamma_5 u\,\bar{d}d - \bar{d}u\,\bar{u}\gamma_5 d - \bar{d}\gamma_5 u\,\bar{u}d) \\ &\quad + i\frac{\mathrm{Im}\,\Sigma_8}{2} (\bar{u}t^a u\,\bar{d}\gamma_5 t^a d + \bar{u}\gamma_5 t^a u\,\bar{d}t^a d - \bar{d}t^a u\,\bar{u}\gamma_5 t^a d - \bar{d}\gamma_5 t^a u\,\bar{u}t^a d) + \ldots,\end{aligned} \tag{3.11}$$

where the dots stand for PT-symmetric terms. These are the only $\not{P}\not{T}$ dimension-six four-quark interactions among the first generation of quarks that are allowed by the SM gauge symmetries. These four-quark operators are not necessarily suppressed by light-quark masses. We denote the operators in Eq. (3.11) by FQPS because of their pseudoscalar-scalar form. Based on their color structure we name the operators in the first and second lines of Eq. (3.11), respectively, the color-singlet and color-octet FQPS operator even though, of course, both operators are scalars under $SU(3)_c$.

At lower energies additional four-quark interactions will appear when the Higgs and heavy gauge bosons that appear in various dimension-six operators are integrated out. An operator responsible for such four-quark interactions is [52]

$$\mathcal{L}_{6,qq\varphi\varphi} = \Xi\, \bar{u}_R \gamma^\mu d_R (\tilde{\varphi}^\dagger i D_\mu \varphi) + \mathrm{h.c.}, \tag{3.12}$$

which after electroweak-symmetry breaking becomes

$$\mathcal{L}_{6,qq\varphi\varphi} = \frac{v^2 g}{2\sqrt{2}} \left[\Xi\, \bar{u}_R \gamma^\mu d_R\, W^+_\mu + \mathrm{h.c.} \right] \left(1 + \frac{h}{v}\right)^2. \tag{3.13}$$

Below the electroweak scale, the W boson is integrated out and the terms proportional to $\mathrm{Im}\,\Xi$ will contribute to $\not{P}\not{T}$ four-quark interactions with different structure than Eq. (3.11) [52]. The associated factor $G_F = 1/\sqrt{2}v^2$ is compensated by the factor v^2 in Eq. (3.13). Because these four-quark interactions only appear at the scale M_W, we will discuss them in more detail when moving to lower energies in chapter 4.

At the level of dimension-six operators additional interactions among quarks and Higgs bosons appear

$$\mathcal{L}_{6,qq\varphi\varphi\varphi} = \sqrt{2}\varphi^\dagger\varphi\left(\bar{q}_L Y'^u\tilde{\varphi}u_R + \bar{q}_L Y'^d\varphi d_R\right) + \text{h.c.}\,. \tag{3.14}$$

The terms proportional to $(v+h)$ can be absorbed into the Yukawa couplings appearing in the SM. The $\not{P}\not{T}$ terms that remain are

$$\mathcal{L}_{6,qq\varphi\varphi\varphi} = h\,(v+h)\left(v+\frac{h}{2}\right)\left(i\,\mathrm{Im}\,Y'^u\,\bar{u}\gamma^5 u + i\,\mathrm{Im}\,Y'^d\,\bar{d}\gamma^5 d\right). \tag{3.15}$$

Finally, there are operators consisting purely of gauge and scalar bosons. Analogous to Eq. (3.9) one can write an interaction among $SU(2)_L$ gauge bosons

$$\mathcal{L}_{6,WWW} = \frac{d_w}{6}\varepsilon^{ijk}\varepsilon^{\mu\nu\alpha\beta}W^i_{\alpha\beta}W^j_{\mu\rho}W^{k\,\rho}_{\nu}, \tag{3.16}$$

which can be written in terms of physical gauge bosons as [39]

$$-id_w\varepsilon^{\mu\nu\alpha\beta}W^{+\,\rho}_{\beta}W^-_{\rho\alpha}\left(s_w F_{\mu\nu} + c_w Z_{\mu\nu} - 2igW^+_\mu W^-_\nu\right). \tag{3.17}$$

Other operators involve the Higgs field

$$\begin{aligned}\mathcal{L}_{6,XX\varphi\varphi} &= \varepsilon^{\mu\nu\alpha\beta}\left(\theta' g_s^2 G^a_{\mu\nu}G^a_{\alpha\beta} + \theta'_W g^2 W^i_{\mu\nu}W^i_{\alpha\beta} + \theta'_B g'^2 B_{\mu\nu}B_{\alpha\beta}\right)\varphi^\dagger\varphi \\ &\quad -\varepsilon^{\mu\nu\alpha\beta}gg'\theta'_{WB}W^i_{\mu\nu}B_{\alpha\beta}\left(\varphi^\dagger\tau^i\varphi\right).\end{aligned} \tag{3.18}$$

Without any Higgs field, *i.e.* using $\varphi^\dagger\varphi/v^2 = 1/2$, the first three operators in Eq. (3.18) can be absorbed into the $SU_c(3)$, $SU_L(2)$, and $U_Y(1)$ topological theta terms described in chapter 2. This is not the case for terms which contain at least one explicit Higgs field. These are given by

$$\begin{aligned}\mathcal{L}_{6,XXh\varphi} &= \varepsilon^{\mu\nu\alpha\beta}\Big[\theta' g_s^2 G^a_{\mu\nu}G^a_{\alpha\beta} + (c_w^2 g'^2\theta'_B + s_w^2 g^2\theta'_W)F_{\mu\nu}F_{\alpha\beta} \\ &\quad +(s_w^2 g'^2\theta'_B + c_w^2 g^2\theta'_W)Z_{\mu\nu}Z_{\alpha\beta} - 2s_w c_w(g'^2\theta'_B - g^2\theta'_W)F_{\mu\nu}Z_{\alpha\beta} \\ &\quad +2g^2\theta'_W\,W^+_{\mu\nu}W^-_{\alpha\beta}\Big]h(v+\frac{h}{2}) + \ldots,\end{aligned} \tag{3.19}$$

where the dots stand for terms involving three weak gauge bosons. We will not be considering these terms further on, as they will necessarily require at least two electroweak loops to contribute to hadronic EDMs. The fourth term in Eq. (3.18) contains non-topological terms both with and without an explicit Higgs boson [39]

$$\begin{aligned}\mathcal{L}_{6,\theta_{WB}} &= \varepsilon^{\mu\nu\alpha\beta}gg'\theta'_{WB}\Big[(s_w F_{\mu\nu} + c_w Z_{\mu\nu})(c_w F_{\alpha\beta} - s_w Z_{\alpha\beta})h(v+\frac{h}{2}) \\ &\quad -ig(W^+_\mu W^-_\nu)(c_w F_{\alpha\beta} - s_w Z_{\alpha\beta})(v+h)^2\Big].\end{aligned} \tag{3.20}$$

Linear combinations of the operators without Higgs fields in Eqs. (3.17) and (3.20) can be interpreted as the electric dipole and magnetic quadrupole moment of the $W^\pm$ boson [53].

The total Lagrangian can be written as

$$\mathcal{L}_6 = \mathcal{L}_{SM} + \mathcal{L}_{6,qq\varphi X} + \mathcal{L}_{6,GGG} + \mathcal{L}_{6,qqqq} + \mathcal{L}_{6,qq\varphi\varphi} + \mathcal{L}_{6,qq\varphi\varphi\varphi} + \mathcal{L}_{6,WWW} + \mathcal{L}_{6,XX\varphi\varphi} \quad (3.21)$$

The goal is now to bring operators in Eq. (3.21) to the QCD scale $\sim 1\,\text{GeV}$. Along the way, the heavy SM particles should be integrated out. At the electroweak scale, $\sim 100\,\text{GeV}$, the top quark, the Higgs boson and the $W^\pm$ and Z bosons should be integrated out, while the same should be done for the bottom and charm quarks at m_b and m_c,[2] respectively. At the QCD scale we then end up with a theory involving only the up and down quarks, gluons, and photons. To describe the effects of BSM CP violation at even lower energies we will employ χPT. Thus, in order to connect this low-energy scale to the scale of BSM physics, we will have to match Eq. (3.21) onto the chiral Lagrangian. We will discuss the relevant chiral Lagrangian and how the EFT of Eq. (3.21) can be matched onto it, while leaving the evolution of the dimension-six operators to chapter 4.

3.2 The chiral Lagrangian

In two-flavor chiral perturbation theory the degrees of freedom are the nucleons $N = (p,\, n)^T$, pions $\boldsymbol{\pi}$, and the photon A_μ. χPT is based on the fact that the two-flavor, massless QCD Lagrangian is globally invariant under $SU(2)_L \times SU(2)_R \sim SO(4)$. However, the spectrum of baryons and mesons exhibits only the isospin diagonal subgroup[3], which suggests that $SU(2)_L \times SU(2)_R$ is be spontaneously broken to $SU(2)_V$. The spontaneous breaking of this $SO(4)$ symmetry results in three massless Goldstone bosons which can be identified as the pions. In reality, the up and down quarks do have, relatively small, masses which explicitly break $SU(2)_L \times SU(2)_R$, and lead to small masses for the pions.

One can write down a Lagrangian, in terms of pions and nucleons, which satisfies the above symmetry considerations. However, naively this Lagrangian will involve large pion-nucleon couplings which do not allow for the usual perturbative expansion. Nonetheless, instead of an expansion in a small coupling, it is possible to obtain a different expansion parameter. This can be achieved by rotating the $SO(4)$ vectors in the theory by the following matrix

$$R = \begin{pmatrix} \delta_{ij} - \frac{1}{D}\frac{\pi_i \pi_j}{2F_\pi^2} & \frac{1}{D}\frac{\pi_i}{F_\pi} \\ -\frac{1}{D}\frac{\pi_j}{F_\pi} & \frac{1}{D}\left(1 - \frac{\boldsymbol{\pi}^2}{4F_\pi^2}\right) \end{pmatrix}, \quad (3.22)$$

where $D \equiv 1 + \frac{\boldsymbol{\pi}^2}{4F_\pi^2}$. Here, and in the remainder of this chapter, we follow the parametrization of Refs. [54, 23], which is not based on an $SU(2)_L \times SU(2)_R$ but $SO(4)$ representation. Due to the chiral symmetry of the Lagrangrian, this field redefinition would have the effect

[2] Although we do not consider operators which involve heavy quarks explicitly, they do appear in several relevant loop diagrams and affect the running of the QCD coupling and are taken into account.

[3] Neglecting the small explicit breaking of $SO(4)$ by the electromagnetic interaction and the quark mass difference.

of almost removing the pion fields from the Lagrangian. This can be seen from the fact that, in the parametrization of Refs. [54, 23], the pion fields are collected in the following $SO(4)$ vector

$$\phi = \begin{pmatrix} \phi^i \\ \phi^4 \end{pmatrix}, \qquad \phi^i = \frac{\sigma}{D}\pi^i, \qquad \phi^4 = \frac{1 - \boldsymbol{\pi}^2/4F_\pi^2}{D}\sigma, \tag{3.23}$$

where ϕ^4 is a scalar field whose vev is responsible for spontaneous symmetry breaking. It can be seen from Eqs. (3.22) and (3.23) that we now have $R^T\phi = (\vec{0},\, \sigma)^T$, so that the rotation R seems to remove the pion fields from the theory. This would indeed be the case, if not for the fact that R is a spacetime-dependent transformation, while the Lagrangian is only invariant under spacetime-independent chiral $SO(4)$ transformations. Thus, the pion fields do not disappear from the theory completely. However, as the only pion dependence must be the result of the spacetime dependence of R, the only terms involving pions R can introduce necessarily involve derivatives acting on the pion fields.

After performing this chiral $SO(4)$ rotation, each pion vertex will involve derivatives of the pion fields. Diagrams containing these vertices will thereby be accompanied by additional factors of the pion momentum. This allows for an expansion in $Q/M_{\rm QCD}$, where Q is the energy scale of a given process, such that at low energies an EFT framework can again be applied [54, 23, 55].

The explicit breaking, caused by the quark masses, the $\bar{\theta}$ term, electroweak interactions, and the dimension-six operators, induces interactions which are not necessarily accompanied by additional derivatives, however, these are proportional to powers of small symmetry-breaking parameters, such as $\bar{m}/M_{\rm QCD}$, $\bar{\theta}$, α_{em}/π, and $M_{\rm QCD}^2 C_{\text{dim-6}}$, respectively. Thus, χPT allows to incorporate both $SU(2)_L \times SU(2)_R$-conserving as well as $SU(2)_L \times SU(2)_R$-violating terms, while ensuring small expansion parameters. These small parameters are $Q/M_{\rm QCD}$ for the interactions originating from $SO(4)$-invariant terms and small symmetry-breaking parameters, such as the quark masses or $\bar{\theta}$, for the interactions originating from those that do. We will use results obtained in this formalism to estimate the contributions of the dimension-six operators to the neutron EDM.

For our purposes, the most important CP-odd interactions that the dimension-six operators give rise to can be written as

$$\begin{aligned} \mathcal{L} \;=\; & -2\,\bar{N}\left(\bar{d}_0 + \bar{d}_1\tau_3\right) S^\mu N\, v^\nu F_{\mu\nu} \\ & + \bar{g}_0 \bar{N}\boldsymbol{\pi}\cdot\boldsymbol{\tau}N + \bar{g}_1\bar{N}\pi_3 N - \bar{\Delta}\frac{\pi_3\boldsymbol{\pi}^2}{2F_\pi}. \end{aligned} \tag{3.24}$$

in terms of the nucleon spin $S^\mu = (0\,,\, \vec{\sigma}/2)^T$ and the velocity $v^\mu = (1\,,\, \vec{0})^T$ in the nucleon rest-frame, and $F_\pi \approx 92.2\,\text{MeV}$ is the pion decay constant. Here, we follow the notation of [56], and $\bar{d}_{0,1}$, $\bar{g}_{0,1}$ and $\bar{\Delta}$ are low-energy constants (LECs).

At tree-level the $\bar{d}_{0,1}$ terms give rise to the neutron and proton EDMs, $d_{p,n} = \bar{d}_0 \pm \bar{d}_1$. However, the remaining interactions contribute to $\bar{d}_{0,1}$ through loop diagrams. At next-to-leading order we have [57, 58, 59],

$$\begin{aligned} d_n \;&=\; \bar{d}_0 - \bar{d}_1 + \frac{e g_A \bar{g}_0}{8\pi^2 F_\pi}\left(\ln\frac{m_\pi^2}{m_N^2} - \frac{\pi m_\pi}{2m_N}\right), \\ d_p \;&=\; \bar{d}_0 + \bar{d}_1 - \frac{e g_A}{8\pi^2 F_\pi}\left[\bar{g}_0\left(\ln\frac{m_\pi^2}{m_N^2} - \frac{2\pi m_\pi}{m_N}\right) - \bar{g}_1\frac{\pi m_\pi}{2m_N}\right], \end{aligned} \tag{3.25}$$

where $g_A \approx 1.27$ is the axial charge and m_π (m_N) is the pion (nucleon) mass. The loop divergences have been absorbed in the counterterms of $\bar{d}_{0,1}$. Contributions from the three-pion vertex $\bar{\Delta}$ to the nucleon EDM vanish up to next-to-leading order [56], however, it will play a role when considering the EDMs of light nuclei in chapter 8. Since we will first focus on the limits that can be derived from the upper bound on the neutron EDM, only $\bar{d}_{0,1}$ and $\bar{g}_0$ will play role.

Which of the interactions in Eq. (3.24) is generated by a specific dimension-six operator, is determined by its chiral and isospin properties. In order to derive the interactions generated by $SU(2)_L \times SU(2)_R$ breaking operators we will follow the framework developed in Refs. [23, 60, 61, 62]. The generated interactions can be constructed from non-Goldstone operators, denoted by $\mathcal{O}[0,\psi]$, made up of nucleon and photon fields and covariant derivatives. Starting from such operators, one arrives at the induced operators, denoted by $\mathcal{O}[\pi,\psi]$, by performing the $SO(4)$ rotation mentioned above,

$$\mathcal{O}_{ab\ldots z}[\pi,\psi] = R_{a\alpha}R_{b\beta}\ldots R_{z\zeta}\mathcal{O}_{\alpha\beta\ldots\zeta}[0,\psi]. \tag{3.26}$$

The operators $\mathcal{O}_{ab\ldots,z}[\pi,\psi]$ and $\mathcal{O}_{\alpha\beta\ldots,\zeta}[0,\psi]$ are generally $SO(4)$ tensors, while $a,b,\ldots z$ and $\alpha,\beta,\ldots\zeta$ stand for their $SO(4)$ indices, respectively.

To clarify this procedure, consider, for instance, the QCD Lagrangian, which, including the $\bar{\theta}$ term, can be written as

$$\mathcal{L}_{\text{QCD}} = -\frac{1}{4}G^a_{\mu\nu}G^{a\,\mu\nu} + \bar{q}i\not{D}q - \bar{m}\bar{q}q - \varepsilon\bar{m}\bar{q}\tau_3 q + m_*\bar{\theta}\,\bar{q}i\gamma_5 q, \tag{3.27}$$

after using a chiral $U(1)_A$ transformation similar to Eq. (2.31) to rotate the θ term into the quark mass matrix. Here $\bar{m} = (m_u + m_d)/2$, $\varepsilon = (m_u - m_d)/(m_u + m_d)$, and $m_* = m_u m_d/(m_u + m_d)$. In the last term, m_* ensures that the mass matrices of the up and down quarks satisfy, $\text{Arg}\,\text{Det}\,M_u M_d = \bar{\theta}$ (for $\bar{\theta} \ll 1$). The last term transforms as the fourth component of the $SO(4)$ vector,

$$P = \begin{pmatrix} \bar{q}\boldsymbol{\tau}q \\ \bar{q}i\gamma_5 q \end{pmatrix}. \tag{3.28}$$

Taking for the non-Goldstone operator, $\mathcal{O}_\alpha[0,\psi] = v_0 m_*\bar{\theta}\left(\bar{N}\boldsymbol{\tau}N, \quad 0\right)^T$, where v_0 is a constant determined by the spontaneous breaking of the chiral $SU(2)_L \times SU(2)_R$ symmetry, this generates,

$$\mathcal{O}_4[\pi,\psi] = R_{4\alpha}\mathcal{O}_\alpha[0,\psi] = -\frac{v_0 m_*\bar{\theta}}{F_\pi D}\bar{N}\boldsymbol{\tau}\cdot\boldsymbol{\pi}N, \tag{3.29}$$

where we are interested in the fourth component of $\mathcal{O}_a[\pi,\psi]$ as $\bar{\theta}$ transform like the fourth component of an $SO(4)$ vector. In this manner the $\bar{\theta}$ term contributes to the isospin conserving pion-nucleon interaction, $\bar{g}_0$.

Although such symmetry arguments give information on which CP-violating source generates which LECs, in general they do not tell us how large the induced LECs are. In the previous example this lack of knowledge was due to the unknown constant v_0. However, in this particular case, when $\bar{\theta}$ is the only CP-violating source, one can make more

precise statements about the contribution of $\bar{\theta}$ to $\bar{g}_0$. This is made possible by the fact that the quark-mass difference transforms like the third component of the same $SO(4)$ vector $\bar{\theta}$ belongs to. Analogous to the above example, the quark-mass difference induces a difference between the neutron and proton masses. Taking $\mathcal{O}_\alpha[0,\psi] = -v_0\varepsilon\bar{m}\left(\bar{N}\boldsymbol{\tau}N,\quad 0\right)^T$, the following term is generated

$$\mathcal{O}_3[\pi,\psi] = R_{3\alpha}\mathcal{O}_\alpha[0,\psi] = v_0\varepsilon\bar{m}\bar{N}\left(\tau_3 - \frac{1}{D}\frac{\boldsymbol{\pi}^2\pi_3}{2F_\pi^2}\right)N. \tag{3.30}$$

This includes a contribution to the strong nucleon mass difference, $(m_n - m_p)^{strong} = 2v_0\varepsilon\bar{m}$, which allows one to relate v_0 to $(m_n - m_p)^{strong} \simeq 2.6\,\text{MeV}$ [63, 64]. For the $\bar{\theta}$ contribution to $\bar{g}_0$ we then have,

$$\bar{g}_0 = (m_n - m_p)^{strong}\frac{(1-\varepsilon^2)}{4\varepsilon F_\pi}\bar{\theta}. \tag{3.31}$$

As both $(m_n - m_p)^{strong}$ and ε are known [63, 64, 65], Eq. (3.31) allows one to estimate the size of the $\bar{\theta}$-term contribution to $\bar{g}_0$.

Unfortunately, such a determination of the contributions to the LECs is not possible for the dimension-six operators. For some of the dimension-six operators we consider, the contributions to the neutron EDM have been calculated using other techniques. Some of these results will be used in chapters 8 and 9. However, in order to be able to treat the bounds on all the dimension-six operators in a single framework we will use naive dimensional analysis (NDA) to determine their contributions to the LECs of Eq. (3.24). We will briefly introduce NDA in the next section.

3.3 Naive dimensional analysis

NDA allows one to estimate the contributions of the dimension-six operators to the interactions in the chiral Lagrangian they induce. NDA is based on dimensional arguments. In particular, it relies on the observation that if interactions made up out of pions, nucleons, photons, and derivatives have *reduced couplings* of order one, the loop corrections are of the same order as the tree-level couplings. In this case the theory describing these interactions can be said to satisfy a certain sense of naturalness [66]. This reduced coupling, for an operator with a coupling g, is defined as [66, 38, 62],

$$g^R = g(4\pi)^{2-N}M_{\text{QCD}}^{D-4}, \tag{3.32}$$

where N is the number of fermion and boson fields contained in the operator and D is its dimension. To see the ideas behind the arguments that lead to this reduced coupling, let us look at an example.

In general, we can schematically write any interaction involving pions and nucleons in the following way,

$$\mathcal{L} \sim g\left(\boldsymbol{\pi}\right)^A\left(\psi\right)^B\left(\partial_\mu\right)^C, \tag{3.33}$$

where π, ψ, and ∂_μ stand for general pion fields, nucleon fields, and derivatives. The integers, A, B, and C are the number of pion fields, nucleon fields, and derivatives appearing, respectively, and $D = A + 3/2B + C$ and $N = A + B$. As an example we will consider the Lagrangian involving two interactions, one four-pion interaction with four derivatives ($A_1 = 4$, $B_1 = 0$, $C_1 = 2$) and a second four-pion interaction with four derivatives ($A_2 = 4$, $B_2 = 0$, $C_2 = 4$). We then, schematically, have

$$\mathcal{L} = g_1 \big(\partial_\mu\big)^2 \big(\boldsymbol{\pi}\big)^4 + g_2 \big(\partial_\mu\big)^4 \big(\boldsymbol{\pi}\big)^4. \tag{3.34}$$

To see how naturalness comes into this, we have to consider this 'theory' at loop level. In this case the first interaction (g_1) will contribute to the second (g_2) through a one-loop bubble diagram. The piece of this diagram with all the derivatives working on the external pion fields, gives the following contribution

$$g_1^2 p^4 \int \left(\frac{dk}{2\pi}\right)^4 \left(\frac{1}{k^2}\right)^2 \sim g_1^2 p^4 \frac{1}{(4\pi)^2} \ln(M_{\rm QCD}^2/\mu^2), \tag{3.35}$$

where we have used a cut-off, $M_{\rm QCD}$, to estimate the loop, p the pion momentum, and μ is the renormalization scale. This renormalization scale dependence will have to be absorbed by a counterterm in the chiral Lagrangian, in this case the second term in Eq. (3.34). Thus, the bubble diagram makes the following contribution to g_2,

$$\delta g_2 \sim \frac{g_1^2}{(4\pi)^2} \ln(M_{\rm QCD}^2/\mu^2). \tag{3.36}$$

According to NDA the theory can be said to be natural if this contribution to g_2 is of similar size as δg_2, when setting the log to one. As a result, for a natural theory, we have

$$g_2 \sim \frac{g_1^2}{(4\pi)^2}. \tag{3.37}$$

The NDA estimates that can be derived from Eq. (3.32), give

$$g_1 = g_1^R \frac{(4\pi)^2}{M_{\rm QCD}^2}, \qquad g_2 = g_2^R \frac{(4\pi)^2}{M_{\rm QCD}^4}, \tag{3.38}$$

which is in agreement with Eq. (3.37) for a natural theory, i.e. if the reduced couplings are of order one. Thus, in this example, if we set the couplings equal to their NDA estimates Eq. (3.32), the theory is indeed natural, i.e. the loop effects are no larger than the tree-level couplings. This sense of naturalness can be shown to hold for a general theory with interactions of the form of Eq. (3.33), as long as their couplings follow Eq. (3.32) [66].

Thus, in case $g^R = \mathcal{O}(1)$ for all the interactions in the theory, the quantum corrections to these operators will maximally be of the same order as the tree-level couplings [66] and no fine-tuning between counterterms and loop contributions is necessary. A similar argument holds for interactions involving gluons, quarks, and photons, which allows one to calculate reduced couplings in both χPT and the theory above $M_{\rm QCD}$ by the same rule, Eq. (3.32).

The NDA procedure to estimate the contributions of operators to the interactions they induce in the chiral Lagrangian is to set the respective reduced couplings of the operators and the interactions they induce equal to one another. Of course, one is only allowed to link couplings of operators to interactions they can induce in the chiral Lagrangian, by the mechanism explained in section 3.2. In addition, we will require the NDA procedure in the case that several operators in the theory above $M_{\rm QCD}$ are required to generate an interaction in the chiral Lagrangian. In such a case it should be clear that when one of the operators in the theory above $M_{\rm QCD}$ vanishes, the induced interaction in the chiral Lagrangian should vanish as well. Therefore, in this situation, the reduced couplings of these operators are multiplied and set equal to the reduced coupling of the respective interaction.

In order to clarify this procedure, let us consider an example. If we were to estimate the contribution of the $\bar{\theta}$ term of the previous section to $\bar{g}_0$, for instance, we would obtain

$$(m_*\bar{\theta})^R = \frac{m_*}{M_{\rm QCD}}\bar{\theta}, \qquad \bar{g}_0^R = \frac{\bar{g}_0}{4\pi}. \tag{3.39}$$

We cannot assume that both reduced couplings should be $\mathcal{O}(1)$, as this would imply a far too large $\bar{\theta}$ term. Nevertheless, the NDA procedure is to set the two reduced couplings equal to one another, $\bar{g}_0^R = (m_*\bar{\theta})^R$. Because a departure of reduced couplings from $\mathcal{O}(1)$ signifies the theory is no longer natural, setting the reduced couplings equal can be justified by the assumption that the couplings are equally unnatural. Taking these reduced couplings to be equal we have

$$\bar{g}_0 = \frac{4\pi m_*}{M_{\rm QCD}}\bar{\theta}, \tag{3.40}$$

and one can check this agrees numerically quite well with Eq. (3.31). However, this agreement is not immediately apparent from the two equations themselves. In order to see the two are indeed similar, we first require the following relation, $M_{\rm QCD} = 4\pi F_\pi \simeq 1.2\,\text{GeV}$, which can be derived as an NDA estimate [66]. Secondly, we will need an NDA estimate for the contribution of the quark mass difference to $(m_n - m_p)^{strong}$,

$$(\varepsilon\bar{m})^R = \frac{\varepsilon\bar{m}}{M_{\rm QCD}}, \qquad \left(\frac{(m_n - m_p)^{strong}}{2}\right)^R = \frac{(m_n - m_p)^{strong}}{2M_{\rm QCD}}. \tag{3.41}$$

the factor of two in the second equality appears as the term in the Lagrangian describing the nucleon mass difference is given by $\mathcal{L}_{\delta m_N} = -(m_n - m_p)/2\,\bar{N}\tau_3 N$. Again taking the reduced couplings to be equal, we have

$$(m_n - m_p)^{strong} = 2\varepsilon\bar{m} \approx 3.4\,\text{MeV}. \tag{3.42}$$

Plugging this and $M_{\rm QCD} = 4\pi F_\pi$ into Eq. (3.40) we again obtain Eq. (3.31), thus, NDA turns out to be in very good agreement in this case.

NDA estimates such as these rely on dimensional estimates, like the one in Eq. (3.35), and the idea that the reduced couplings in the theory above $M_{\rm QCD}$ should be equally (un)natural as those in the chiral Lagrangian. As such, these estimates are generally

only expected to hold within a factor of < 10. Nonetheless, NDA works well when reproducing the sizes of known coupling constants. For instance, NDA results such as $g_A = \mathcal{O}(1)$ and $m_\pi^2 = \bar{m} M_{\rm QCD}$ agree well with their experimental values, and our estimate for $(m_n - m_p)^{strong}$ in Eq. (3.42), is in good agreement with its actual value, $(m_n - m_p)^{strong} = (2.6 \pm 0.85)\,\text{MeV}$ [63, 64]. In addition, whenever the NDA estimates for the dimension-six CP-violating operators can be compared to other techniques the results tend to be in good agreement. We will come back to such comparisons in the upcoming chapters.

3.4 Summary

In this chapter we have constructed the model-independent Lagrangian parametrizing BSM sources of CP violation. Due to the success of the SM we assume the BSM physics to appear at an energy scale well above the electroweak scale and for the SM gauge symmetries to be valid beyond the SM. Given these assumptions, the leading effects of CP-violating BSM physics can be described by gauge-invariant dimension-six operators. In section 3.1 we constructed the relevant operators of which we will consider the contributions to electric dipole moments (EDMs) in upcoming chapters. As we will be focusing on hadronic EDMs, we have considered only non-leptonic operators. In addition, as the operators involving the lightest quarks should be most important for hadronic EDMs we did not take into account those involving the second or third generations of quarks.

After the construction of the Lagrangian describing the BSM sources at high energies, we turned to the EFT needed to describe the same CP violation at low energies, namely chiral perturbation χPT. This second EFT is necessary because, although the CP violation is assumed to arise at high energies, the EDM measurements take place at energies below $M_{\rm QCD} \sim 1\,\text{GeV}$. At these low energies the usual expansion in small couplings breaks down and we will employ χPT. In this EFT the degrees of freedom are pions, nucleons, and photons instead of the quarks and gluons in the theory above $M_{\rm QCD}$. Furthermore, χPT does not rely on an expansion in a small coupling, but uses an expansion in the small parameter, $Q/M_{\rm QCD}$, where Q is the energy scale of the process under consideration. Therefore, for processes at low energies, $Q \ll M_{\rm QCD}$, χPT allows for a description of the interactions between pions, nucleons and photons.

We introduced chiral perturbation theory in section 3.2, where we also discussed ways in which the EFT in terms and quarks, gluons, and photons can be related to the χPT Lagrangian. Although the two EFTs involve completely different degrees of freedom, it is possible to determine which interactions in the chiral Lagrangian can be induced by a particular operator in the theory above $M_{\rm QCD}$. This determination relies on the chiral $SU(2)_L \times SU(2)_R$ symmetry properties of the interactions in both theories. Specifically, one demands these properties of the operator in the theory above $M_{\rm QCD}$ to be the same as those of the interactions it induces in the χPT Lagrangian.

Thus, these symmetry arguments dictate which interactions below $M_{\rm QCD}$ can be induced by a specific operator above it. Unfortunately, such arguments cannot tell us the sizes of the low-energy constants (LECs), describing the strengths of the interactions, that are induced. As the sizes of the LECs are determined by non-perturbative physics

this is a difficult problem. In fact, for the relation of the LECs to the couplings of the dimension-six operators, we can often do no better than order of magnitude estimates. In section 3.3 we briefly reviewed naive dimensional analysis (NDA), which we will employ for these kinds of estimates in the upcoming chapters. In this section we discussed the dimensional analysis and the naturalness arguments on which NDA estimates rely. In addition, we considered the procedure to relate a given coupling in the Lagrangian above $M_{\rm QCD}$ to the interactions it induces in the χPT Lagrangian.

In summary, this chapter covered the EFT describing the CP-violating BSM sources at high energies, the χPT techniques necessary to describe them at low energies, and the way to relate the two EFTs. Nonetheless, there is still one step needed to relate the high-energy couplings of the dimension-six operators to the neutron EDM, namely, the evolution of the effective Lagrangian discussed in section 3.1 from $M_{\not T}$ to a scale around $M_{\rm QCD}$. After considering this evolution in the next chapter, we will be in a position to put all the pieces together. Starting with the dimension-six operators of section 3.1 and evolving them to $M_{\rm QCD}$, the techniques discussed in sections 3.2 and 3.3 of this chapter can be used to relate their couplings at $M_{\not T}$ to the neutron EDM. In the next chapter we will consider the necessary RGE techniques and evolve the dimension-six operators to $M_{\rm QCD}$. After arriving at $M_{\rm QCD}$ we will employ results obtained by the techniques of sections 3.2 and 3.3 to determine the contributions the operators make to the neutron EDM.

Chapter 4

Evolution of CP-violating new physics

Sources of BSM CP violation can be described in terms of dimension-six operators above $M_{\rm QCD}$ and interactions in the chiral Lagrangian at low energies. After the discussion of the previous chapter on these topics, one final step is needed to connect these sources of CP violation to EDMs, namely, the evolution from the scale of BSM physics $M_{\not T}$ down to the QCD scale, $M_{\rm QCD}$, depicted schematically in Fig. 4.1. This last step is described by the renormalization group equations (RGEs), which is the topic of the current chapter.

At tree level the evolution from $M_{\not T}$ to $M_{\rm QCD}$ is trivial: the operators do not evolve at all, and their couplings at the low scale simply equal those at high energies, $C_i(M_{\rm QCD}) = C_i(M_{\not T})$. However, once one includes higher-order loop effects the operators will 'run' with changing energy scale. The dominant contributions to this running effect are due to QCD renormalization, i.e. effects which are higher order in g_s resulting from loop diagrams. The reason QCD renormalization gives the dominant contribution to the running is because the QCD coupling constant is the largest of the gauge couplings (at the energies we consider), making it more sensitive to the renormalization scale. Therefore, we will focus on the running due to QCD renormalization here, considering electroweak running only when there are no QCD contributions.

Since this evolution is a higher-order effect, one might wonder if it is necessary to include it, or whether the relevant physics is captured well enough by tree-level expressions. There are several reasons to include the running of the dimension-six operators. Firstly, these effects are not necessarily small; it is not uncommon for the evolution due to QCD renormalization to change couplings by factors of a few when changing the scale to $M_{\rm QCD}$. However, such running factors are not the main reason for taking the RGEs into account. In fact, the uncertainties related to the matching between the Lagrangian at $M_{\rm QCD}$ and the χPT Lagrangian tend to be of $\mathcal{O}(1)$ or larger, making exact knowledge for most of the RGE factors less of a priority. However, also this effect should become increasingly important once determinations of the nucleon EDM in terms of dimension-six sources become more precise (for instance through lattice calculations). In addition, there is a qualitatively new effect induced by the RGEs, namely, the mixing between different operators. The result of this mixing is that operators can induce other operators under RGE evolution. In other words, even if one starts with a single operator at high energies, multiple operators might

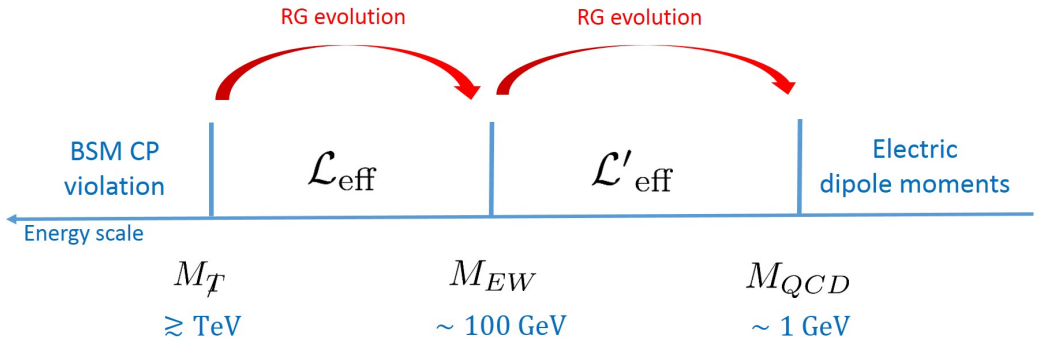

Figure 4.1: Figure depicting the relevant energy scales, with the highest energies on the left. Additional sources of CP violation arise at high scales, M_T, while EDM measurements take place at low energies. In order to connect the two the renormalization group (RG) evolution, shown in red, has the be taken into account. We will first move down to the electroweak scale (M_{EW}), where the heavy SM fields will have to be integrated out, before evolving further down to M_{QCD}.

appear at low energies. This implies that the relations between the couplings at low and high energies is not one-to-one; those at low energies are generally a linear combination of those at high energies. This is an important effect when constraining the couplings at high energies, because the bounds derived at low energy cannot be simply translated to those at high energies. Thus, by incorporating the RGE evolution of the dimension-six operators, one obtains more precise values for their low-energy coefficients and, perhaps more importantly, determines the relations between the couplings at different scales.

We will start by briefly reviewing RGEs, an explicit example of which is worked out in appendix 4.A, before moving on to apply these techniques to the dimension-six operators discussed in chapter 3.

4.1 The evolution of coupling constants

Although the Lagrangian and observables should be independent of the renormalization scale, μ, renormalized operators and their couplings in the EFT,

$$\mathcal{L} = \sum_i C_i(\mu) O_i(\mu), \tag{4.1}$$

do generally depend on it. This μ dependence appears due to divergent loop diagrams. The way to calculate this μ dependence has been the topic of numerous reviews [43, 44, 45, 46], here we will briefly recount the important points.

The renormalized operators in Eq. (4.1), can be related to the bare, unrenormalized, operators O_B as follows,

$$\langle O_i(\mu) \rangle = Z_{ij}(\mu) \langle O_j \rangle_B, \tag{4.2}$$

where $\langle O_i \rangle$ stands for the matrix element of O_i between asymptotic states of the theory, and the off-diagonal elements of Z_{ij} allow for mixing to occur between different operators.

For explicit calculations it will be useful to divide the renormalization factor Z into parts due to field renormalization and renormalization specific to O. Since we will consider mainly QCD renormalization effects, for our purposes the only important field renormalization factors are those of the quark and gluon fields. The renormalization of these fields can be written as

$$q = Z_q^{-1/2} q_B, \qquad G_\mu = Z_G^{-1/2} (G_\mu)_B. \tag{4.3}$$

Assuming the operator O_i to contain n_i quark and m_i gluon fields, the renormalization factor, Z can be written as

$$Z_{ij} = Z_q^{-n_i/2} Z_G^{-m_i/2} Z_O^{ij}, \tag{4.4}$$

where Z_O^{ij} is the renormalization associated with the divergences specific to the corresponding operators, O_i and O_j. The above equation can be combined with Eq. (4.2) to give

$$\begin{aligned} \frac{\partial \langle O(\mu)_i \rangle}{\partial \ln \mu} &= \left[-\frac{n_i}{2} Z_q^{-1} \frac{\partial Z_q}{\partial \ln \mu} - \frac{m_i}{2} Z_G^{-1} \frac{\partial Z_G}{\partial \ln \mu} + \left(Z_O^{ij}\right)^{-1} \frac{\partial Z_O^{ij}}{\partial \ln \mu} \right] \langle O_j(\mu) \rangle \\ &\equiv -\gamma_{ji} \langle O_j(\mu) \rangle. \end{aligned} \tag{4.5}$$

This is the Callan-Symanzik equation for the operators O_i. The term between brackets is the *anomalous-dimension matrix*[1], γ, and determines the scale evolution of the operator through Eq. (4.5). The anomalous dimension can be related to the counterterms through $Z_{q,G} = 1 + \delta_{q,G}$, and $Z_O^{ij} = \mathbf{1}^{ij} + \delta_O^{ij}$, where δ_O^{ij} is the counterterm needed to cancel the divergence from a diagram involving an insertion of O_i, producing a contribution proportional to O_j. To one-loop order this leads to

$$\gamma_{ij} = \frac{\partial}{\partial \ln \mu} \left[\mathbf{1}_{ij} \left(\frac{n_i}{2} \delta_q + \frac{m_i}{2} \delta_G \right) - \delta_O^{ji} \right], \tag{4.6}$$

with no sum over repeated indices. As the field strength renormalization of the quark and gluon fields are well known, this only leaves the δ_O term to be determined. After this calculation the evolution of the operators O_i can be determined by solving Eq. (4.5). Throughout this thesis, however, we will mainly be interested in the evolution of the coupling C, instead of that of the operator. Because the combination $C_i(\mu)\langle O_i(\mu)\rangle$ should be μ independent, these two are related,

$$\frac{\partial C_i(\mu)}{\partial \ln \mu} \langle O_i(\mu) \rangle = -\frac{\partial \langle O_j(\mu) \rangle}{\partial \ln \mu} C_j(\mu), \tag{4.7}$$

which allows us to write

$$\frac{\partial C_i(\mu)}{\partial \ln \mu} = \gamma_{ij}\, C_j(\mu). \tag{4.8}$$

[1]The slightly awkward definition of γ in Eq. (4.5), involving a minus sign and transposition of indices, is such that the related equation for the couplings will have a simpler form.

This is the type of RGE we will need to solve in the remainder of this chapter, in order to relate the coupling at high energy to that at low energies.

For our purposes, however, Eqs. (4.6) and (4.8) will need to be extended somewhat. So far we have been assuming the O_i were defined without any factors of the strong coupling constant or the quark masses, g_s and m_q. These quantities also obtain a μ dependence after renormalization, which has to be taken into account if they appear in an operator O_i. Allowing for these factors to appear in the operators comes down to a simple redefinition, $O_i' = g_s^{k_i} m_q^{l_i} O_i$, $C_i' = g_s^{-k_i} m_q^{-l_i} C_i$. Such a redefinition effectively changes the expression for the anomalous dimension to

$$\gamma_{ij} = \frac{\partial}{\partial \ln \mu}\left[\mathbf{1}_{ij}\big(\frac{n_i}{2}\delta_q + \frac{m_i}{2}\delta_G\big) - \delta_O^{ji}\right] - \mathbf{1}_{ij}\big(k_i\frac{\beta}{g_s} + l_i\gamma_m\big), \tag{4.9}$$

with no sum over repeated indices and where we employed the definition of the β function, $\beta = \frac{\partial g_s}{\partial \ln \mu}$, and the mass anomalous dimension, $\gamma_m = \frac{\partial \ln m_q}{\partial \ln \mu}$. It is this expression that will be used for the calculation of anomalous dimensions throughout this thesis. An example of an explicit calculation is given in appendix 4.A.

Once the anomalous-dimension matrix γ_{ij} is calculated through Eq. (4.9), the evolution of the couplings requires one to solve Eq. (4.8). At the one-loop level, the anomalous dimensions can be expressed as $\gamma_{ij} = \frac{\alpha_s}{4\pi}\gamma_{ij}^0$, where the γ_{ij}^0 are μ independent quantities. The RGEs can then be solved by first diagonalizing the equations through a basis transformation, $\tilde{C}_i = U_{ij}C_j$ which gives

$$\frac{\partial \tilde{C}_i(\mu)}{\partial \ln \mu} = \tilde{\gamma}_i\, \tilde{C}_i(\mu) = \frac{\alpha_s}{4\pi}\tilde{\gamma}_i^0\, \tilde{C}_i(\mu), \qquad U_{ik}\gamma_{kl}(U^{-1})_{lj} = \mathbf{1}_{ij}\tilde{\gamma}_i. \tag{4.10}$$

This equation can then be solved by

$$\begin{aligned}\tilde{C}_i(\mu_1) &= \exp\left[\int_{\mu_2}^{\mu_1} \frac{\alpha_s(\mu)}{4\pi}\tilde{\gamma}_i^0 d\ln\mu\right]\tilde{C}_i(\mu_2) \\ &= \exp\left[\int_{g_s(\mu_2)}^{g_s(\mu_1)} \frac{\alpha_s(\mu)}{4\pi\beta}\tilde{\gamma}_i^0 dg_s\right]\tilde{C}_i(\mu_2) = \left(\frac{\alpha_s(\mu_2)}{\alpha_s(\mu_1)}\right)^{\tilde{\gamma}_i^0/2\beta_0}\tilde{C}_i(\mu_2)\end{aligned} \tag{4.11}$$

or in terms of the couplings C_i,

$$C_i(\mu_1) = (U^{-1})_{ij}\left(\frac{\alpha_s(\mu_2)}{\alpha_s(\mu_1)}\right)^{\tilde{\gamma}_j^0/2\beta_0} U_{jk}C_k(\mu_2), \tag{4.12}$$

where we used the one-loop expression for $\beta = -\frac{g_s^3}{(4\pi)^2}\beta_0$, and $\beta_0 = \frac{11}{3}N - \frac{2}{3}n_f$, with N (n_f) the number of colors (flavors). Clearly, the evaluation of Eq. (4.12) requires the μ dependence of α. To one-loop order the definition of the β function can be used to obtain,

$$\alpha(\mu) = \frac{2\pi}{\beta_0 \ln(\mu/\Lambda_{QCD})}, \qquad \Lambda_{QCD} = \mu\, e^{-\frac{2\pi}{\beta_0\alpha(\mu)}}, \tag{4.13}$$

where $\Lambda_{\rm QCD}$ is the scale where the one-loop expression for α_s goes to infinity. Thus, the one-loop approximation breaks down when considering scales close to $\Lambda_{\rm QCD}$. Furthermore, $\Lambda_{\rm QCD}$ depends on the number of active flavors, i.e. the number of quarks with masses below the renormalization scale under consideration, $m_q < \mu$. Numerically, for three active flavors ($m_s < \mu < m_b$) we have $\Lambda_{\rm QCD}(n_f = 3) \simeq 140\,\text{MeV}$, which implies that QCD does indeed become non-perturbative around $M_{\rm QCD} \sim 1\,\text{GeV}$.

4.1.1 The $\overline{MS}$ scheme

The above covers nearly all the tools we will require to evaluate the running of the couplings from high to low energies. However, the calculation of the counterterms still remains. Since this is a loop calculation the counterterms will necessarily depend on the subtraction scheme that is employed. A particularly convenient scheme for the calculation of anomalous dimensions is the $\overline{MS}$ scheme. This scheme uses the fact that in dimensional regularization the divergent part of a diagram takes the form

$$a\left(\frac{2}{4-d} - \gamma_E + \ln 4\pi - \ln \Delta\right), \tag{4.14}$$

where a is a coefficient determined by the loop diagram, d is the dimensionality of space-time, γ_E is Euler's constant and $\Delta = \Delta(p_i \cdot p_j,\, m_i^2)$ is a dimensionfull function of masses and external momenta. In the $\overline{MS}$ scheme one subtracts the divergence plus the constants that always appear alongside it, such that the counterterm becomes,

$$\delta = -a\left(\frac{2}{d-4} - \gamma_E + \ln 4\pi - \ln \mu^2\right), \tag{4.15}$$

where the renormalization scale μ is introduced in order to ensure the argument of the logarithm in the renormalized quantity is dimensionless. Thus, in this scheme, the μ dependence always appears logarithmically, $\sim \ln \mu$. As a result the RGEs can be seen as a way of dealing with corrections of higher order in the coupling constant, but enhanced by, possibly large, logarithms, $\sim \frac{g^2}{(4\pi)^2} \ln \mu_1^2/\mu_2^2$. In the $\overline{MS}$ scheme the contribution of such loop corrections to the anomalous dimension, appearing in Eq. (4.9), can simply be read off from the coefficient of the pole, i.e. $\frac{\partial \delta}{\partial \ln \mu} = 2a$. It is this feature that makes the $\overline{MS}$ scheme particularly convenient for the calculation of anomalous dimensions.

There is one drawback, however, because this scheme is mass-independent, heavy particles do not decouple. This can be seen, for instance, by looking at the QCD β function, $\beta = -\frac{g_s^3}{(4\pi)^2}(\frac{11}{3}N - \frac{2}{3}n_f)$. It is clear from the n_f term that all flavors contribute equally at all scales. Thus, even at a scale $\mu \ll m_t$ the top-quark will contribute as much to the running of g_s as the much lighter up- and down- quarks. This is a problematic and unphysical feature of the $\overline{MS}$ scheme when considering scales below a mass threshold. In order to overcome this non-decoupling of particles, the $\overline{MS}$ scheme can be applied within an EFT framework, in which one integrates out the heavy particles at their mass thresholds [67, 68, 69, 70]. For example, when moving through the top-quark threshold, we move from a theory including the top-quark, where it contributes to β, so that we have $n_f = 6$, to one without the top-quark where $n_f = 5$. In order for the two theories to give the same predictions at $\mu = m_t$, one has to match the two theories at this scale. At the one-loop RGE level one then has $g_s^{(n_f=6)}(m_t) = g_s^{(n_f=5)}(m_t)$. The effect of the quark mass thresholds is depicted in Fig. 4.2, see appendix 4.A for how these thresholds affect on the couplings of several CP-violating dimension-six operators. In this framework, we move from one effective theory to the next when lowering the scale, integrating out the corresponding particle at its threshold in the process. In between the mass thresholds, the RGEs, calculated in the $\overline{MS}$ scheme, are used to determine the scale dependence. In

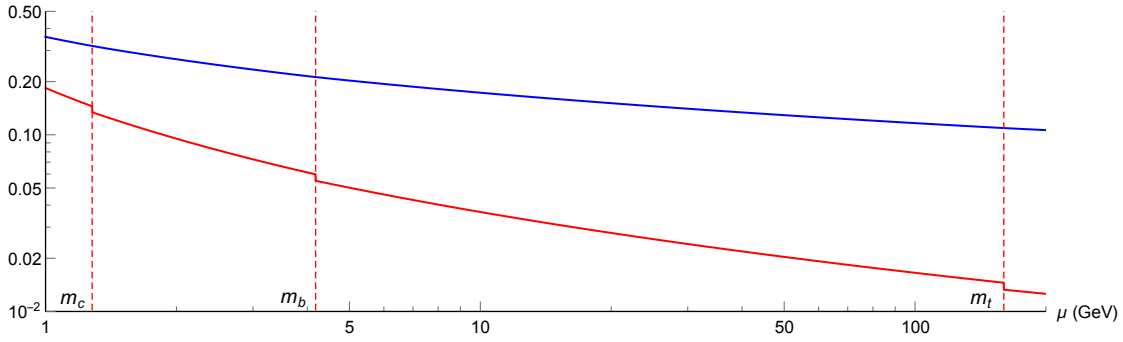

Figure 4.2: Figure depicting the one-loop running of α_s in blue and its derivative $\frac{d\alpha_s}{d\ln\mu}$ in red, while the mass thresholds of the charm, bottom, and top quarks, are marked by the red dashed lines. In the $\overline{MS}$ scheme the mass thresholds introduce discontinuities in the slope of α_s, when we move from $\beta(n_f)$ to $\beta(n_f+1)$ at these points. These effects are hardly visible in the running of α_s, but can easily be seen in the the red line, depicting $\frac{d\alpha_s}{d\ln\mu}$.

this way one can still take advantage of the simple evaluation of anomalous dimensions, while retaining the correct decoupling behaviour of heavy particles.

Having reviewed the necessary techniques for the calculation of anomalous dimensions and RGE evolution, we will now move on to apply these techniques to the CP-violating dimension-six operators introduced in the previous chapter.

4.2 Evolution of unsuppressed dimension-six operators

The goal is now to evolve the operators in Eq. (3.21) from the scale of new physics, $M_{\mathcal{T}}$, to the electroweak scale $\sim M_W$ and subsequently to $M_{\rm QCD}$, as shown in Fig. 4.1. In the process we will integrate out the heavy fields at M_W and include the effects of QCD and, in some cases, electroweak renormalization-group running. Although all these operators are proportional to two inverse powers of $M_{\mathcal{T}}$ not all operators will be equally important at low energies. Due to the need to integrate out the heavy gauge and Higgs bosons, certain operators induce low-energy interactions which are, apart from the $M_{\mathcal{T}}^{-2}$ suppression, additionally suppressed by small SM quantities such as electroweak gauge couplings or the ratio of light-quark masses to the electroweak scale. It is therefore convenient to divide the operators into two sets. The first set contains the operators that induce low-energy interactions without suppression other than the usual $1/M_{\mathcal{T}}^2$. After studying this set in the current section, we will turn in section 4.3 to the remaining operators which do suffer from additional suppression.

We begin just below the scale $M_{\mathcal{T}}$ where all SM fields are still present in the effective field theory. At this scale, the operators in the first set are given by the quark EDMs and color EDMs (CEDMs) in Eq. (3.3), the gluon CEDM in Eq. (3.9), the four-quark operators in Eq. (3.11), the right-handed weak current in Eq. (3.13), and finally the quark-Higgs and gluon-Higgs interactions of Eqs. (3.15) and (3.19). The first goal is to evolve these

operators down to the electroweak scale $M_{\rm EW} \sim M_W$, where M_W is the mass of the W boson. At this scale we integrate out the Higgs and heavy gauge bosons. In principle it would be better to integrate out each field at its particular threshold, however, the running of α_s is slow at these energy scales, so that $\alpha_s(m_H) \simeq \alpha_s(M_W)$. Therefore, this would complicate matters without gaining much. Somewhat above $M_{\rm EW}$ we pass $\mu = m_t$, where we integrate out the top quark, which has important consequences for certain operators.

From $M_{\not T}$ to $M_{\rm EW}$

To calculate the QCD running of the operators it is convenient to write the Lagrangian as

$$\mathcal{L}_6 \;=\; \sum_i C_i(\mu) O_i(\mu), \tag{4.16}$$

with μ the renormalization scale and $O_i(\mu)$ the set of operators

$$\begin{aligned}
O_q &= -\frac{i}{2} e m_q Q_q \bar{q} \sigma^{\mu\nu} \gamma_5 q \, F_{\mu\nu}, \\
\tilde{O}_q &= -\frac{i}{2} g_s m_q \, \bar{q} \sigma^{\mu\nu} \gamma_5 t_a q \, G^a_{\mu\nu}, \\
O_W &= \frac{1}{6} g_s f_{abc} \varepsilon^{\mu\nu\alpha\beta} G^a_{\alpha\beta} G^b_{\mu\rho} G^{c\,\rho}_{\nu}, \\
O_{PS_1} &= \frac{i g_s^2}{2} (\bar{u}u \, \bar{d}\gamma_5 d + \bar{u}\gamma_5 u \, \bar{d}d - \bar{d}u \, \bar{u}\gamma_5 d - \bar{d}\gamma_5 u \, \bar{u}d), \\
O_{PS_8} &= \frac{i g_s^2}{2} (\bar{u}t^a u \, \bar{d}\gamma_5 t^a d + \bar{u}\gamma_5 t^a u \, \bar{d}t^a d - \bar{d}t^a u \, \bar{u}\gamma_5 t^a d - \bar{d}\gamma_5 t^a u \, \bar{u}t^a d), \\
O_{W_R} &= \frac{g v^2}{2\sqrt{2}} (i \bar{u}_R \gamma^\mu d_R W^+_\mu - i \bar{d}_R \gamma^\mu u_R W^-_\mu), \\
O_{qH} &= v^2 \, h \, \bar{q} i \gamma^5 q, \\
O_{gH} &= g_s^2 \varepsilon^{\mu\nu\alpha\beta} G^a_{\mu\nu} G^a_{\alpha\beta} \, v h,
\end{aligned} \tag{4.17}$$

where $q \in \{u, d\}$. By comparison with section 3.1 the coupling constants at $M_{\not T}$ are found to be

$$\begin{aligned}
C_q(M_{\not T}) &= d_q(M_{\not T}), & \tilde{C}_q(M_{\not T}) &= \frac{\tilde{d}_q(M_{\not T})}{g_s(M_{\not T})}, \\
C_W(M_{\not T}) &= \frac{d_W(M_{\not T})}{g_s(M_{\not T})}, & C_{\rm PS_{1,8}}(M_{\not T}) &= \frac{\mathrm{Im}\,\Sigma_{1,8}(M_{\not T})}{g_s^2(M_{\not T})}, \\
C_{W_R}(M_{\not T}) &= \mathrm{Im}\,\Xi(M_{\not T}), & C_{qH}(M_{\not T}) &= \mathrm{Im}\,Y'^q(M_{\not T}), \\
C_{gH}(M_{\not T}) &= \theta'(M_{\not T}), & &
\end{aligned} \tag{4.18}$$

which are all proportional to $M_{\not T}^{-2}$. We use the following operator basis

$$\vec{C}(\mu) = (C_q(\mu), \tilde{C}_q(\mu), C_W(\mu), C_{PS_1}(\mu), C_{PS_8}(\mu), C_{W_R}(\mu), C_{qH}(\mu), C_{gH}(\mu))^T. \tag{4.19}$$

Figure 4.3: One-loop diagrams contributing to the quark electric and chromo-electric dipole moments. Solid, wavy, and curly lines represent the propagation of quarks, photons, and gluons respectively. The square denotes a $\not{P}\not{T}$ four-quark interaction, other vertices representing T interactions from the Standard Model.

The RGE can again be expressed as

$$\frac{d\vec{C}(\mu)}{d\ln\mu} = \gamma\vec{C}(\mu), \tag{4.20}$$

where γ is the anomalous-dimension matrix which is expanded in powers of $g_s^2/(4\pi)^2 = \alpha_s/(4\pi)$. Up to one-loop order γ can be written as

$$\gamma = \frac{\alpha_s}{4\pi}\begin{pmatrix} \gamma_{\text{dipole}} & \gamma_{\text{mix}} & 0 & 0 & \gamma_{\text{mix}\,gH} \\ 0 & \gamma_{PS} & 0 & 0 & 0 \\ 0 & 0 & \gamma_{W_R} & 0 & 0 \\ 0 & 0 & 0 & \gamma_{qH} & 0 \\ 0 & 0 & 0 & 0 & \gamma_{gH} \end{pmatrix}. \tag{4.21}$$

The submatrices appearing in Eq. (4.21) have been calculated in the literature, here we rederive and confirm these results. Furthermore, we employ a different basis for the four-quark operators, which gives rise to a simplified anomalous-dimension matrix.

Starting with the running and mixing of the quark and gluon dipole operators, which were calculated in Refs. [38, 71, 72, 73], we have

$$\gamma_{\text{dipole}} = \begin{pmatrix} 8C_2(N) & -8C_2(N) & 0 \\ 0 & 16C_2(N) - 4N & 2N \\ 0 & 0 & N + 2n_f + \beta_0 \end{pmatrix}, \tag{4.22}$$

where $C_2(N) = (N^2-1)/2N$.

The submatrix γ_{PS} describes the running and mixing of the $\not{P}\not{T}$ four-quark operators. In Refs. [47, 48] these matrices were calculated for a different basis of operators consisting of the most general flavor-diagonal $\not{P}\not{T}$ four-quark operators containing up, down, and strange quarks. In the limiting case of only two flavors, that set contains ten different operators whereas our set, based on gauge invariance, consists of two interactions only. As we will see, below M_{EW} two additional four-quark operators will be induced by O_{W_R}, while the remaining six operators are in general suppressed by small Yukawa couplings. The suppressed terms are discussed in section 4.3. In the basis of Eq. (4.19) the anomalous-dimension matrix of the FQPS operators is

$$\gamma_{PS} \;=\; -2\begin{pmatrix} \frac{(3N+4)(N^2-1)}{N^2} - \beta_0 & \frac{(N+1)^2(N-2)(N-1)}{N^3} \\ -4\frac{N+2}{N} & 2\frac{N^2+2}{N^2} - 2C_2(N) - \beta_0 \end{pmatrix}. \tag{4.23}$$

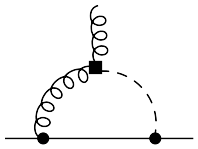

Figure 4.4: One-loop diagram contributing to a quark chromo-electric dipole moment. The dashed line denotes the propagation of a Higgs boson. The square denotes the $\not{P}\not{T}$ gluon-Higgs interaction from Eq. (4.17). Other notation is as in Fig. 4.3. For simplicity only one possible ordering is shown here.

This is in agreement with the results obtained in Refs. [47, 48] after a suitable basis transformation.

It is necessary to consider mixing of the four-quark interactions with the dipole operators. This is described by the submatrix $\gamma_{\rm mix}$. The diagrams responsible for this mixing are shown in Fig. 4.3. The FQPS operators are invariant under chiral symmetry (*i.e.* under global $SU(2)_L \times SU(2)_R$ rotations) [74, 56] such that they can only contribute to (C)EDMs, which break chiral symmetry, through a mass insertion. For this reason, the qCEDMs do not induce the four-quark operators and the mixing is one way only. To $\mathcal{O}(\alpha_s)$, the FQPS operators and the gluon CEDM do not mix although they are both chiral invariant. With these considerations we find

$$\gamma_{\rm mix} \;=\; 2\frac{m_{q'}}{m_q}\begin{pmatrix} \frac{Q_{q'}}{Q_q} & \frac{Q_{q'}}{Q_q}C_2(N) \\ -1 & \frac{N}{2} - C_2(N) \\ 0 & 0 \end{pmatrix}, \tag{4.24}$$

where q' denotes the quark flavor which is different from the flavor of the induced quark (C)EDM (the FQPS operators contain both the up and down quarks such that $q \neq q'$). For example, for the mixing between the up quark EDM and O_{PS_1} the relevant entry is $(\gamma_{\rm mix})_{11} = 2(m_d/m_u)(-1/3)/(2/3) = -m_d/m_u$. Again, after a basis transformation, Eq. (4.24) is in agreement with results in Ref. [48].

The next operator is the right-handed weak current. This operator will obviously not mix with the other operators via QCD corrections due to the presence of the W boson. At the level of one-loop electroweak diagrams it will induce corrections to the quark (C)EDM, but these corrections are smaller than tree-level diagrams contributing to four-quark operators [52]. These tree-level diagrams will be considered in the next section. At $\mathcal{O}(\alpha_s)$ the operator O_{W_R} does not run and its anomalous dimension is zero,

$$\gamma_{W_R} = 0. \tag{4.25}$$

Then there are the $\not{P}\not{T}$ Higgs-quark interactions with anomalous dimension

$$\gamma_{q_H} = -6C_2(N). \tag{4.26}$$

At tree- and one-loop level these interactions induce four-quark operators and the quark (C)EDM, but such contributions are suppressed by a factor m_q/v. At the two-loop level it is possible to circumvent this suppression via a top-quark loop shown in Fig. 4.5 which

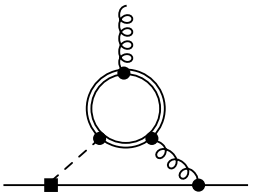

Figure 4.5: Two-loop diagram contributing to the quark chromo-electric dipole moment. The double solid line denotes a top-quark propagator. The square denotes the $\not{P}\not{T}$ quark-Higgs interaction from Eq. (4.17). Other notation is as in Figs. 4.3 and 4.4. For simplicity only one possible ordering is shown here.

contributes to the qCEDM. We will come to the contribution of this diagram after discussing the final operator the first set.

Finally, we consider the gluon-Higgs interaction. In order to calculate its anomalous dimension and its mixing with the dipoles it is useful to rewrite

$$\frac{1}{2}\varepsilon^{\mu\nu\alpha\beta}G^a_{\mu\nu}G^a_{\alpha\beta} = \varepsilon^{\mu\nu\alpha\beta}\partial_\mu\left[G^a_\nu\left(G^a_{\alpha\beta} - \frac{g_s}{3}f_{abc}G^b_\alpha G^c_\beta\right)\right], \tag{4.27}$$

which makes it easier to obtain

$$\gamma_{gH} = 0, \qquad \gamma_{\text{mix}\,gH} = \begin{pmatrix}0 & 16 & 0\end{pmatrix}^T, \tag{4.28}$$

where the mixing with the quark CEDM is due to the loop diagram in Fig. 4.4. The vanishing of γ_{gH} at the one-loop level is in agreement with Refs. [75, 76].

Having calculated the anomalous dimensions of the operators, it is possible to solve the RGE and run the operators down to the electroweak scale M_{EW}. During this process we pass the threshold of the top quark. Here, the top quark is integrated out and we match the EFT with six flavors to the EFT with five flavors, through the same process as described in section 4.1.1 and appendix 4.A. As none of the operators contain the top quark the operator basis remains unchanged as we move from one EFT to the next. The matching conditions are

$$\vec{C}^6(m_t^+) = \vec{C}^5(m_t^-), \tag{4.29}$$

where $\vec{C}^6$ are the coupling constants belonging to the EFT incorporating the top quark and $\vec{C}^5$ to the EFT without it and m_t^+ (m_t^-) denotes the energy scale just above (below) the mass of the top quark. The running is somewhat different for the various EFTs as the anomalous-dimension matrix depends on n_f explicitly as well as implicitly through $\alpha_s(\mu)$. We employ the one-loop running of α_s for the sake of consistency. The above treatment works for all operators except for the $\not{P}\not{T}$ Higgs-quark interactions for which, as mentioned above, the passing of the top-quark threshold does have important consequences. The two-loop diagram in Fig. 4.5 gives a large contribution to the qCEDM

$$\tilde{C}_q(m_t^-)|_{qq\varphi} = -\frac{\alpha_s(m_t)}{32\pi^3}\frac{v}{m_q(m_t)}f(\frac{m_t^2}{m_H^2})\,C_{qH}(m_t^+), \tag{4.30}$$

Table 4.1: The size of the quark electric and quark and gluon chromo-electric dipole moments at M_W in terms of various dimension-six operators at 1 and 10 TeV. A "−" indicates that there is no contribution at this order.

	$C_q(1\,\text{TeV})$	$\tilde{C}_q(1\,\text{TeV})$	$C_W(1\,\text{TeV})$	$C_{qH}(1\,\text{TeV})$	$C_{gH}(1\,\text{TeV})$
$C_q\,(M_W)$	0.80	0.18	−0.010	$-1.4\times10^{-5}\frac{v}{m_q}$	−0.032
$\tilde{C}_q\,(M_W)$	–	0.82	−0.090	$-2.1\cdot10^{-4}\frac{v}{m_q}$	−0.30
$C_W\,(M_W)$	–	–	0.64	–	–
	$C_q(10\,\text{TeV})$	$\tilde{C}_q(10\,\text{TeV})$	$C_W(10\,\text{TeV})$	$C_{\text{qH}}(10\,\text{TeV})$	$C_{gH}(10\,\text{TeV})$
$C_q\,(M_W)$	0.69	0.26	−0.025	$-1.6\times10^{-5}\frac{v}{m_q}$	−0.085
$\tilde{C}_q\,(M_W)$	–	0.72	−0.12	$-2.4\cdot10^{-4}\frac{v}{m_q}$	−0.48
$C_W\,(M_W)$	–	–	0.46	–	–

where $f(\frac{m_t^2}{m_H^2}) \simeq 1$ [77] is a function of the top-quark and Higgs mass. Here the light quark mass should be evaluated at the scale m_t, however, we prefer to present results in terms of quark masses evaluated at the scale M_{QCD}. The one-loop running of the quark masses gives

$$m_q(m_t) \simeq 0.55\, m_q(M_{\text{QCD}}). \tag{4.31}$$

Similar diagrams as Fig. 4.5 but with gluons replaced by electroweak gauge bosons contribute to the quark EDM, but these contributions are smaller by approximately an order of magnitude due to the smallness of $\alpha_w(m_t)$ compared to $\alpha_s(m_t)$ and we neglect them. Because the two-loop diagram gives by far the most important contribution to low-energy P and T violation coming from Eq. (3.15), below m_t the quark-Higgs interactions can be neglected. Their effects are well approximated by the qCEDM contribution in Eq. (4.30).

We can now express the dimension-six coupling constants at the electroweak scale ($M_{\text{EW}} = M_W$) as function of those at the scale of new physics ($M_{\not T}$). Here we consider numerical solutions for two specific values of $M_{\not T}$ ($M_{\not T} = 1\,\text{TeV}$ and $M_{\not T} = 10\,\text{TeV}$) because the analytical solution of the RGE, while easy to obtain once the anomalous dimensions are known, is very lengthy and not insightful. The following masses are used as input [65]

$$M_Z = 91.2\,\text{GeV}, \qquad M_W = 80.4\,\text{GeV}, \qquad m_t(m_t) = 160\,\text{GeV}. \tag{4.32}$$

Note that the $\overline{MS}$ top quark mass differs significantly from the usual pole mass $m_t^{\text{Pole}} \simeq 173$. For the value of α_s we use [65]

$$\alpha_s^{n_f=5}(M_Z) = 0.118. \tag{4.33}$$

The one-loop running then gives

$$\alpha_s^{n_f=6}(1\,\text{TeV}) = 0.089, \qquad \alpha_s^{n_f=6}(10\,\text{TeV}) = 0.073. \tag{4.34}$$

We will suppress the n_f dependence of α_s from here on as the number of flavors should always be clear from the context. The results are shown in Tables 4.1 and 4.2. The operator O_{W_R} is not shown because it does not run and gives the trivial result $C_{W_R}(M_{\not T}) = C_{W_R}(M_W)$. The results are not very dependent on the choice of $M_{\not T}$, because α_s runs slowly at high energies.

Table 4.2: The size of the coupling constants of various dimensions-six operators at M_W in terms of the four-quark operators $O_{PS_{1,8}}$ at 1 and 10 TeV. A "$-$" indicates that there is no contribution at this order. The notation q' appearing in the first two rows denotes the quark flavor, which is different from the flavor of the induced quark (C)EDM.

	$C_{PS_1}(1\,\text{TeV})$	$C_{PS_8}(1\,\text{TeV})$
$C_q(M_W)$	$\left(0.0043 - 0.034\frac{Q_{q'}}{Q_q}\right)\frac{m_{q'}}{m_q}$	$-\left(0.00053 + 0.043\frac{Q_{q'}}{Q_q}\right)\frac{m_{q'}}{m_q}$
$\tilde{C}_q(M_W)$	$0.042\frac{m_{q'}}{m_q}$	$-0.0045\frac{m_{q'}}{m_q}$
$C_W(M_W)$	$-$	$-$
$C_{PS_1}(M_W)$	1.2	0.046
$C_{PS_8}(M_W)$	-0.26	0.73
	$C_{\text{PS}_1}(10\,\text{TeV})$	$C_{\text{PS}_8}(10\,\text{TeV})$
$C_q(M_W)$	$\left(0.012 - 0.051\frac{Q_{q'}}{Q_q}\right)\frac{m_{q'}}{m_q}$	$-\left(0.0012 + 0.063\frac{Q_{q'}}{Q_q}\right)\frac{m_{q'}}{m_q}$
$\tilde{C}_q(M_W)$	$0.074\frac{m_{q'}}{m_q}$	$-0.0052\frac{m_{q'}}{m_q}$
$C_W(M_W)$	$-$	$-$
$C_{PS_1}(M_W)$	1.3	0.077
$C_{PS_8}(M_W)$	-0.44	0.58

4.2.1 From M_{EW} to M_{QCD}

Having evolved the operators from $M_{\not T}$ to M_W, the next step is to cross the electroweak scale at which we integrate out the Higgs and heavy gauge bosons. Because the Higgs-quark $\not P\not T$ interactions have effectively disappeared from the operator basis around the top-quark threshold, the only operators involving heavy fields are the right-handed weak current and the gluon-Higgs operators. The W boson in the right-handed weak current in Eq. (3.13) can be integrated out via a tree-level diagram among light quarks [52]. Since the SM couples the W boson to left-handed quarks only, the appearing effective operator is of the form

$$\begin{aligned}\mathcal{L}_{6,\text{FQLR}} &= ig_s^2 C_{LR_1}\left(\bar{u}_R\gamma^\mu d_R\,\bar{d}_L\gamma_\mu u_L - \bar{d}_R\gamma^\mu u_R\,\bar{u}_L\gamma_\mu d_L\right) + \ldots \\ &= \frac{ig_s^2}{2} C_{LR_1}\left(\bar{u}\gamma^\mu\gamma^5 d\,\bar{d}\gamma_\mu u - \bar{d}\gamma^\mu\gamma^5 u\,\bar{u}\gamma_\mu d\right) + \ldots,\end{aligned} \tag{4.35}$$

where the dots stand for higher-dimensional terms appearing from expanding the W-boson propagator. The factor g_s^2 is introduced for later convenience. The coupling constant right below the electroweak scale is given by

$$C_{LR_1}(M_W^-) = -\frac{V_{ud}}{g_s^2(M_W)} C_{W_R}(M_W^+) = -\frac{V_{ud}}{g_s^2(M_W)}\,\text{Im}\,\Xi(M_{\not T}), \tag{4.36}$$

where $V_{ud} \simeq 0.97$ is the up-down CKM matrix element and M_W^+ (M_W^-) denotes the scale just above (below) the W-boson mass.

After integrating out the heavy fields the operator basis has changed. The right-handed weak current, the Higgs-quark, and the Higgs-gluon interactions are removed and two new

Table 4.3: The size of the coupling constants of various dimension-six operators at $M_{\rm QCD}$ in terms of those of at M_W. A "−" indicates that there is no contribution at this order.

	$C_q\,(M_W)$	$\tilde{C}_q\,(M_W)$	$C_W\,(M_W)$	$C_{PS_1}\,(M_W)$	$C_{PS_8}\,(M_W)$
C_q	0.48	0.37	−0.060	$\left(0.040-0.071\frac{Q_{q'}}{Q_q}\right)\frac{m_{q'}}{m_q}$	$-\left(0.0019+0.078\frac{Q_{q'}}{Q_q}\right)\frac{m_{q'}}{m_q}$
$\tilde{C}_q$	–	0.53	−0.15	$0.14\frac{m_{q'}}{m_q}$	$-0.0017\frac{m_{q'}}{m_q}$
C_W	–	–	0.26	–	–
C_{PS_1}	–	–	–	1.5	0.13
C_{PS_8}	–	–	–	−0.71	0.28

four-quark operators are added

$$\begin{aligned} O_{LR_1} &= i\,g_s^2\,(\bar{u}_R\gamma^\mu d_R\,\bar{d}_L\gamma_\mu u_L - \bar{d}_R\gamma^\mu u_R\,\bar{u}_L\gamma_\mu d_L), \\ O_{LR_8} &= i\,g_s^2\,(\bar{u}_R\gamma^\mu t_a d_R\,\bar{d}_L\gamma_\mu t_a u_L - \bar{d}_R\gamma^\mu t_a u_R\,\bar{u}_L\gamma_\mu t_a d_L). \end{aligned} \tag{4.37}$$

The coupling constant of O_{LR_1} is given in Eq. (4.36), while $C_{LR_8}(M_W) = 0$. The first operator in Eq. (4.37) is produced by integrating out the W boson as discussed above, while the second arises when O_{LR_1} is evolved to lower energies. Because these four-quark interactions couple left-handed to right-handed quarks they are denoted by FQLR. The new operator basis becomes

$$\vec{C}(\mu) = (C_q(\mu), \tilde{C}_q(\mu), C_W(\mu), C_{PS_1}(\mu), C_{PS_8}(\mu), C_{LR_1}(\mu), C_{LR_8}(\mu))^T. \tag{4.38}$$

Apart from the appearance of the FQLR operators and the disappearance of the gluon-Higgs interaction, the basis has not changed by moving through the M_W threshold, thus for the remaining couplings we have $C_i(M_W^-) = C_i(M_W^+)$, $i \neq LR_{1,8}$. Below the scale M_W the running of the couplings in Eq. (4.38) is determined by the anomalous-dimension matrix

$$\gamma = \frac{\alpha_s}{4\pi}\begin{pmatrix} \gamma_{\rm dipole} & \gamma_{\rm mix} & 0 \\ 0 & \gamma_{PS} & 0 \\ 0 & 0 & \gamma_{LR} \end{pmatrix}, \tag{4.39}$$

where, apart from γ_{LR}, all entries can be found in the previous section. The diagrams in Fig. 4.3 vanish for the FQLR operators such that they do not induce the quark (C)EDM. Furthermore, the FQPS and FQLR operators do not mix because of their different chiral properties [56], justifying the form of Eq. (4.39). The submatrix γ_{LR}, describing the running and mixing of O_{LR_1} and O_{LR_8}, also considered in a different basis in Refs. [47, 48, 78], is given by

$$\gamma_{LR} = -2\begin{pmatrix} -\beta_0 & \frac{3C_2(N)}{N} \\ 6 & 3\frac{N^2-2}{N} - \beta_0 \end{pmatrix}. \tag{4.40}$$

We can now solve the RGEs described by Eq. (4.39) and run the operators down to the energy scale $M_{\rm QCD}$. During this process we pass the thresholds of the bottom and

Table 4.4: The size of the coupling constants of the FQLR operators at $M_{\rm QCD}$ in terms of those at M_W.

	$C_{LR_1}(M_W)$	$C_{LR_8}(M_W)$
$C_{LR_1}(M_{\rm QCD})$	0.37	0.10
$C_{LR_8}(M_{\rm QCD})$	0.47	0.92

charm quarks which are handled in the same way as the top-quark threshold. None of the $\not{P}\not{T}$ operators involve these quarks explicitly, such that the operator basis does not change between thresholds. We use [65]

$$m_b(m_b) = 4.18\,\text{GeV}, \qquad m_c(m_c) = 1.28\,\text{GeV}, \tag{4.41}$$

and run the operators down to $M_{\rm QCD} = 1\,\text{GeV}$. At this scale the strong coupling constant is

$$\alpha_s(M_{\rm QCD}) = 0.36. \tag{4.42}$$

The results are collected in Tables 4.3 and 4.4.

This completes the running for this set of operators, since it is now possible to read off the size the coupling constants at $M_{\rm QCD}$ in terms of those at $M_{\not{T}}$ by combining Tables 4.1-4.4. We will now give a summary of the results so far and examine the relations between the low- and high-energy couplings.

4.2.2 Summary

Although the bases in Eqs. (4.19) and (4.38) are useful to calculate the anomalous dimensions, the explicit appearance of factors of g_s in the operators is unconventional. We therefore mention the results for the operators without these factors. The couplings used below can be related to the C_i used above through

$$\begin{aligned}
C_q(\mu) &= d_q(\mu), & \tilde{C}_q(\mu) &= \frac{\tilde{d}_q(\mu)}{g_s(\mu)},\\
C_W(\mu) &= \frac{d_W(\mu)}{g_s(\mu)}, & C_{\rm PS_{1,8}}(\mu) &= \frac{\text{Im}\,\Sigma_{1,8}(\mu)}{g_s^2(\mu)},\\
C_{LR_{1,8}}(\mu) &= \frac{\text{Im}\,\Xi_{LR_{1,8}}(\mu)}{g_s^2(\mu)}, & C_{qH}(\mu) &= \text{Im}\,Y'^q(\mu),\\
C_{gH}(\mu) &= \theta'(\mu).
\end{aligned} \tag{4.43}$$

In summary, the main result of this section is the $\not{P}\not{T}$ Lagrangian at the scale $M_{\rm QCD}$,

which can be written as

$$\begin{aligned}
\mathcal{L}_{6,\text{set 1}} &= -\frac{1}{2}\Big(d_u e m_u Q_u\, \bar{u} i\sigma^{\mu\nu}\gamma_5 u\, F_{\mu\nu} + d_d e m_d Q_d\, \bar{d} i\sigma^{\mu\nu}\gamma_5 d\, F_{\mu\nu} \\
&\quad + \tilde{d}_u m_u\, \bar{u} i\sigma^{\mu\nu}\gamma_5 t^a u\, G^a_{\mu\nu} + \tilde{d}_d m_d\, \bar{d} i\sigma^{\mu\nu}\gamma_5 t^a d\, G^a_{\mu\nu} \Big) \\
&\quad + \frac{d_W}{6} f^{abc} \varepsilon^{\mu\nu\alpha\beta} G^a_{\alpha\beta} G^b_{\mu\rho} G^{c\,\rho}_{\nu} \\
&\quad + i\frac{\text{Im}\,\Sigma_1}{2}(\bar{u}u\,\bar{d}\gamma_5 d + \bar{u}\gamma_5 u\,\bar{d}d - \bar{d}u\,\bar{u}\gamma_5 d - \bar{d}\gamma_5 u\,\bar{u}d) \\
&\quad + i\frac{\text{Im}\,\Sigma_8}{2}(\bar{u}t^a u\,\bar{d}\gamma_5 t^a d + \bar{u}\gamma_5 t^a u\,\bar{d}t^a d - \bar{d}t^a u\,\bar{u}\gamma_5 t^a d - \bar{d}\gamma_5 t^a u\,\bar{u}t^a d) \\
&\quad + i\,\text{Im}\,\Xi_{LR_1}\left(\bar{u}_R\gamma^\mu d_R\,\bar{d}_L\gamma_\mu u_L - \bar{d}_R\gamma^\mu u_R\,\bar{u}_L\gamma_\mu d_L\right) \\
&\quad + i\,\text{Im}\,\Xi_{LR_8}\left(\bar{u}_R\gamma^\mu t^a d_R\,\bar{d}_L\gamma_\mu t^a u_L - \bar{d}_R\gamma^\mu t^a u_R\,\bar{u}_L\gamma_\mu t^a d_L\right), \qquad (4.44)
\end{aligned}$$

where the coupling constants are all evaluated at M_{QCD}. We expect the above Lagrangian to capture the most important contributions from physics beyond the SM to first generation $\not{P}\not{T}$ observables. For example, the coupling constants appearing in Eq. (4.44) should account for the dominant contributions to the EDMs of the nucleon and light nuclei.

We will now discuss the values of the couplings in Eq. (4.44) in terms of the coupling constants at the high-energy, starting with the quark (C)EDMs. We obtain for $M_{\not{T}} = 1\,\text{TeV}$

$$\begin{aligned}
d_q\,(M_{\text{QCD}}) &= 0.39\,d_q(1\,\text{TeV}) + 0.37\,\tilde{d}_q(1\,\text{TeV}) - 0.13\,\theta'\,(1\,\text{TeV}) \\
&\quad -0.072\,d_W(1\,\text{TeV}) - (8.4\cdot 10^{-5})\frac{v}{m_q}\text{Im}\,Y'^q(1\,\text{TeV}) \\
&\quad + \{0.20,\,0.097\}\,\text{Im}\,\Sigma_1(1\,\text{TeV}) + \{0.073,\,0.069\}\,\text{Im}\,\Sigma_8(1\,\text{TeV}), \\
\tilde{d}_q\,(M_{\text{QCD}}) &= 0.88\,\tilde{d}_q(1\,\text{TeV}) - 0.34\,\theta'\,(1\,\text{TeV}) \\
&\quad -0.29\,d_W(1\,\text{TeV}) - (2.4\cdot 10^{-4})\frac{v}{m_q}\text{Im}\,Y'^q(1\,\text{TeV}) \\
&\quad + \{0.74,\,0.17\}\,\text{Im}\,\Sigma_1(1\,\text{TeV}) + \{0.011,\,0.0025\}\,\text{Im}\,\Sigma_8(1\,\text{TeV}), \qquad (4.45)
\end{aligned}$$

where the first (second) term in brackets in front of $\text{Im}\,\Sigma_{1.8}$ corresponds to the up (down) quark. For $M_{\not{T}} = 10\,\text{TeV}$ we find slightly different values

$$\begin{aligned}
d_q\,(M_{\text{QCD}}) &= 0.33\,d_q(10\,\text{TeV}) + 0.41\,\tilde{d}_q(10\,\text{TeV}) - 0.22\,\theta'(10\,\text{TeV}) \\
&\quad -0.089\,d_W(10\,\text{TeV}) - (9.5\cdot 10^{-5})\frac{v}{m_q}\text{Im}\,Y'^q(10\,\text{TeV}) \\
&\quad + \{0.30,\,0.14\}\,\text{Im}\,\Sigma_1(10\,\text{TeV}) + \{0.092,\,0.085\}\,\text{Im}\,\Sigma_8(10\,\text{TeV}), \\
\tilde{d}_q\,(M_{\text{QCD}}) &= 0.85\,\tilde{d}_q(10\,\text{TeV}) - 0.54\,\theta'(10\,\text{TeV}) \\
&\quad -0.30\,d_W(10\,\text{TeV}) - (2.7\cdot 10^{-4})\frac{v}{m_q}\text{Im}\,Y'^q(10\,\text{TeV}) \\
&\quad + \{1.1,\,0.25\}\,\text{Im}\,\Sigma_1(10\,\text{TeV}) + \{0.034,\,0.0078\}\,\text{Im}\,\Sigma_8(10\,\text{TeV}). \qquad (4.46)
\end{aligned}$$

It remains difficult to draw conclusions from Eqs. (4.45) and (4.46) without looking at specific models of new physics. Indeed without knowledge of the couplings at $M_{\not{T}}$, it

is difficult to compare the various contributions to the low-energy quark (C)EDMs. If we simply assume the various coupling constants to be of equal size at $M_{\not T}$ and using $v/m_q \sim \mathcal{O}(10^5)$ one would conclude that the low-energy quark (C)EDMs are dominated by the $\not P\not T$ Higgs-quark interactions. However, in models of new physics, such as those in Refs. [79, 80, 81], the Yukawa-like couplings $Y'^{u,d}$ tend scale with the quark mass and are thus $\mathcal{O}(m_q/vM_{\not T}^2)$ instead of $\mathcal{O}(1/M_{\not T}^2)$ as assumed in section 3.1. In this case the resulting suppression makes the contributions proportional to $Y'^{u,d}$ negligible with respect to those from other operators. In such a scenario, the low-energy quark EDM gets contributions of roughly equal size from all other dimension-six operators at $M_{\not T}$, although the dependence on the gluon CEDM and color-octet FQPS is somewhat smaller. The low-energy quark CEDMs are mainly determined by the high-energy CEDMs and, depending on the quark flavor, the color-singlet FQPS. The contributions from the gluon CEDM and the gluon-Higgs interaction are also significant, while the influence of the color-octet FQPS can be neglected. We stress again that these statements are very model dependent, since the coupling constants at the high-energy scale might, depending on the model of physics beyond the SM, possess a large hierarchy. Some may even be zero. In any case, it is unlikely that all coupling constants at $M_{\not T}$ are of similar size.

The next relation between couplings at low and high energies are those for the gluon CEDM, which is defined without g_s as in Eq. (3.9). At this order, the gluon CEDM does not depend on other sources such that

$$d_W\left(M_{\rm QCD}\right) = 0.33\, d_W\left(1\,\text{TeV}\right), \qquad d_W\left(M_{\rm QCD}\right) = 0.27\, d_W\left(10\,\text{TeV}\right). \tag{4.47}$$

The gluon CEDM is somewhat suppressed at low energies in agreement with Refs. [39, 72, 73].

Moving on to the FQPS operators, we find a rather simple solution of the RGEs as these operators do not mix with other four-quark operators. For $M_{\not T} = 1\,\text{TeV}$,

$$\begin{aligned} \operatorname{Im}\Sigma_1\left(M_{\rm QCD}\right) &= 7.2\operatorname{Im}\Sigma_1\left(1\,\text{TeV}\right) + 0.66\operatorname{Im}\Sigma_8\left(1\,\text{TeV}\right), \\ \operatorname{Im}\Sigma_8\left(M_{\rm QCD}\right) &= -3.7\operatorname{Im}\Sigma_1\left(1\,\text{TeV}\right) + 0.69\operatorname{Im}\Sigma_8\left(1\,\text{TeV}\right), \end{aligned} \tag{4.48}$$

and for $M_{\not T} = 10\,\text{TeV}$,

$$\begin{aligned} \operatorname{Im}\Sigma_1\left(M_{\rm QCD}\right) &= 10\operatorname{Im}\Sigma_1\left(10\,\text{TeV}\right) + 0.95\operatorname{Im}\Sigma_8\left(10\,\text{TeV}\right), \\ \operatorname{Im}\Sigma_8\left(M_{\rm QCD}\right) &= -5.3\operatorname{Im}\Sigma_1\left(10\,\text{TeV}\right) + 0.53\operatorname{Im}\Sigma_8\left(10\,\text{TeV}\right). \end{aligned} \tag{4.49}$$

Again assuming that the coupling constants are of the same order at the high-energy scale, the FQPS operators at $M_{\rm QCD}$ are dominated by $\operatorname{Im}\Sigma_1(M_{\not T})$. Barring unexpected fine-tuning, $\operatorname{Im}\Sigma_1\left(M_{\rm QCD}\right)$ and $\operatorname{Im}\Sigma_8\left(M_{\rm QCD}\right)$ are of approximately the same size and both operators should be taken into account at low energies. It is interesting that the coefficient of the color-singlet operator grows significantly when evolved to lower energies.

Finally, we look at the FQLR operators. Because the operator O_{W_R}, from which the FQLR operators originate, does not run between $M_{\not T}$ and $M_{\rm EW}$ the results do not depend on the particular value of $M_{\not T}$ (of course, this is true only as far as the running is concerned. The size of the couplings is proportional to $M_{\not T}^{-2}$),

$$\begin{aligned} \operatorname{Im}\Xi_{LR_1}\left(M_{\rm QCD}\right) &= -1.1\, V_{ud}\operatorname{Im}\Xi\left(M_{\not T}\right), \\ \operatorname{Im}\Xi_{LR_8}\left(M_{\rm QCD}\right) &= -1.4\, V_{ud}\operatorname{Im}\Xi\left(M_{\not T}\right). \end{aligned} \tag{4.50}$$

The conclusion is that both four-quark operators are of approximately the same magnitude at low energies even though O_{LR_8} does not get a direct contribution at the electroweak scale. Clearly, the coupling constants of the two FQLR operators are not independent. Both depend on the same fundamental parameter $\Xi(M_T)$.

An important result of this section is the form of the $\not{P}\not{T}$ four-quark operators. Although they look complicated, their form is very intuitive if one insists on gauge invariance at the scale where the dimension-six operators are generated. This is also indicated by the simple block-diagonal form (apart from mixing with the quark dipoles) of the anomalous-dimension matrix. From Eq. (4.44), we can conclude that around a scale $M_{\mathrm{QCD}} \sim 1\,\mathrm{GeV}$ there are four $\not{P}\not{T}$ four-quark operators that need to be taken into account with three independent couplings. This conclusion implies that the remaining six four-quark operators, allowed by $SU(3)_c \times U(1)_{EM}$ gauge invariance, should be suppressed. Indeed, these four-quark interactions belong to the set of suppressed operators mentioned earlier. It is this set of operators that will be discussed in the next section.

4.3 Evolution of additionally suppressed dimension-six operators

As argued above, one would expect the operators in Eq. (4.44) (which descend from Eq. (4.17)) to describe the dominant part of P and T violation due to physics beyond the SM in first-generation hadronic and nuclear systems. In particular, this is the case when the couplings of the unsuppressed dimension-six operators are of similar size or larger than those with additional suppression. Although generally unexpected, the couplings of the unsuppressed operators could be smaller, or even zero, in specific models of new physics, due to additional symmetry considerations or unexpected cancellations. In such models the most important operators might be operators such as the remaining dimension-six operators mentioned in section 3.1, which were neglected so far and obtain additional suppression at low energies. Higher-dimensional operators might also become relevant, but we limit the discussion to the dimension-six operators. In this section we assume that for some reason the operators of the previous section are suppressed, thereby leaving room for the remaining dimension-six operators. In order to keep the discussion organized, we first discuss the $\not{P}\not{T}$ quark-Higgs operators in section 4.3.1. These operators give rise to a rich set of $\not{P}\not{T}$ four-quark operators at low energies. In section 4.3.2 we discuss the remaining $\not{P}\not{T}$ operators which involve heavy gauge bosons.

4.3.1 Yukawa-suppressed four-quark interactions

We begin the analysis with Eq. (3.15) which describes interactions between light quarks and Higgs bosons

$$\begin{aligned}\mathcal{L}_{6,qq\varphi\varphi\varphi} &= h\,(v+h)\left(v+\frac{h}{2}\right)\left(i\,\mathrm{Im}\,Y'^{u}\,\bar{u}\gamma^5 u + i\,\mathrm{Im}\,Y'^{d}\,\bar{d}\gamma^5 d\right)\\ &= \sum_{q=u,d} C_{qH}\,O_{qH} + \ldots,\end{aligned} \tag{4.51}$$

where the dots denote terms with more than one Higgs boson and Eqs. (4.17) and (4.18) were applied. These interactions have already been considered in the previous section, where they induced relatively large corrections to the quark CEDMs via two-loop diagrams involving top quarks [77]. Here we assume that these corrections, together with the other contributions to the quark (C)EDMs, are suppressed. This requires fine-tuning between different coupling constants which is not expected on general grounds but might occur in specific models of new physics.

Starting at the high-energy scale $M_{\not T}$, the Higgs-quark interactions are first evolved down to $M_{\rm EW} = M_W$. The anomalous dimension is given in Eq. (4.26) and the solution of the RGE is

$$C_{qH}(M_W) = \left(\frac{\alpha_s(M_W)}{\alpha_s(m_t)}\right)^{12/23} \left(\frac{\alpha_s(m_t)}{\alpha_s(M_{\not T})}\right)^{4/7} C_{qH}(M_{\not T}). \tag{4.52}$$

Numerically this becomes for two explicit values of $M_{\not T}$

$$C_{qH}(M_W) = 1.2\, C_{qH}(1\,\text{TeV}), \qquad C_{qH}(M_W) = 1.3\, C_{qH}(10\,\text{TeV}). \tag{4.53}$$

Below M_W the Higgs boson is integrated out which at tree-level generates $\not P\not T$ four-quark operators among light quarks of the form

$$\begin{aligned} \mathcal{L}_{6,\,qqqq} &= -\frac{iv}{M_H^2}\Big(m_u C_{uH}(M_W)\, \bar u\gamma^5 u\, \bar u u + m_d C_{dH}(M_W)\, \bar d\gamma^5 d\, \bar d d \\ &\quad + m_d C_{uH}(M_W)\, \bar u\gamma^5 u\, \bar d d + m_u C_{dH}(M_W)\, \bar u u\, \bar d\gamma^5 d \Big). \end{aligned} \tag{4.54}$$

Since $C_{qH} = \mathcal{O}(1/M_{\not T}^2)$, these interactions scale as $\mathcal{O}(v m_q/M_H^2 M_{\not T}^2) \simeq \mathcal{O}(m_q/v M_{\not T}^2)$ such that they are not only suppressed by two powers of $M_{\not T}$, but also by the ratio of the light-quark mass to the Higgs vev, $v \simeq 246\,\text{GeV}$. The structure of the four-quark operators appearing in Eq. (4.54) is different from that in the previous section. It turns out that this requires an extension of the operator basis in Eqs. (4.17) and (4.37) with six additional four-quark operators,

$$\begin{aligned} \tilde O_{PS_1} &= \frac{ig_s^2}{2}(\bar u u\, \bar d\gamma_5 d + \bar u\gamma_5 u\, \bar d d + \bar d u\, \bar u\gamma_5 d + \bar d\gamma_5 u\, \bar u d), \\ \tilde O_{PS_8} &= \frac{ig_s^2}{2}(\bar u t^a u\, \bar d\gamma_5 t^a d + \bar u\gamma_5 t^a u\, \bar d t^a d + \bar d t^a u\, \bar u\gamma_5 t^a d + \bar d\gamma_5 t^a u\, \bar u t^a d), \\ O_{4q_1} &= i\, g_s^2\, (\bar q\gamma^5 q\, \bar q q), \\ O_{4q_8} &= i\, g_s^2\, (\bar q\gamma^5 t^a q\, \bar q t^a q), \end{aligned} \tag{4.55}$$

where again $q \in \{u, d\}$. Using the Fierz identities

$$\begin{aligned} ig_s^2\, \bar u\gamma^5 u\, \bar d d &= \frac{1}{2}(O_{PS_1} + \tilde O_{PS_1}) + \frac{1}{6} O_{LR_1} + O_{LR_8}, \\ ig_s^2\, \bar u u\, \bar d\gamma^5 d &= \frac{1}{2}(O_{PS_1} + \tilde O_{PS_1}) - \frac{1}{6} O_{LR_1} - O_{LR_8}, \end{aligned} \tag{4.56}$$

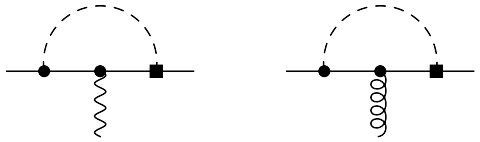

Figure 4.6: One-loop diagrams contributing to the quark electric and chromo-electric dipole moments. A square marks a $\not{P}\not{T}$ interaction from Eq. (4.51). Other notation is as in Figs. 4.3 and 4.4. For simplicity only one possible ordering is shown here.

the coupling constants $C_i(\mu)$ at the scale M_W^- are found to be

$$\begin{aligned}
C_{PS_1}(M_W^-) &= \tilde{C}_{PS_1}(M_W^-) = -\frac{1}{2}\frac{1}{g_s^2(M_W^+)}\left(\frac{m_d v}{M_H^2}C_{uH}(M_W^+) + \frac{m_u v}{M_H^2}C_{dH}(M_W^+)\right), \\
C_{LR_1}(M_W^-) &= \frac{1}{6}C_{LR_8}(M_W^-) = -\frac{1}{6}\frac{1}{g_s^2(M_W^+)}\left(\frac{m_d v}{M_H^2}C_{uH}(M_W^+) - \frac{m_u v}{M_H^2}C_{dH}(M_W^+)\right), \\
C_{4q_1}(M_W^-) &= -\frac{1}{g_s^2(M_W^+)}\frac{m_q v}{M_H^2}C_{qH}(M_W^+), \\
C_{PS_8}(M_W^-) &= \tilde{C}_{PS_8}(M_W^-) = C_{4q_8}(M_W^-) = 0.
\end{aligned} \tag{4.57}$$

In addition to the four-quark operators described above, the $\not{P}\not{T}$ quark-Higgs interactions also induce the quark EDM and CEDM through one-loop diagrams shown in Fig. 4.6. These diagrams are finite and give the following contributions [48]

$$C_q(M_W^-) = -\tilde{C}_q(M_W^-) = \frac{1}{(2\pi)^2}\frac{m_q v}{M_H^2}\left(\frac{3}{4} + \ln\frac{m_q}{m_H}\right)C_{qH}(M_W^+), \tag{4.58}$$

which are smaller by a factor $\mathcal{O}(10^{-5})$ compared to Eq. (4.30). This is approximately the level of fine-tuning needed in order to make the four-quark operators in Eq. (4.54) significant at low energies. Eqs. (4.57) and (4.58) represent matching conditions at $\mu = M_W$, meaning that the quark masses appearing there should be evaluated at this scale as well. The one-loop QCD running gives $m_q(M_W) \simeq 0.58\, m_q(M_{\rm QCD})$. In the results below we will use m_q to denote the quark mass at $M_{\rm QCD}$.

The next step is to evolve the operators down to $M_{\rm QCD}$. We choose the basis

$$\begin{aligned}
\vec{C}(\mu) = {} & (C_q(\mu), \tilde{C}_q(\mu), C_W(\mu), C_{PS_1}(\mu), C_{PS_8}(\mu), C_{LR_1}(\mu), C_{LR_8}(\mu), \\
& \tilde{C}_{PS_1}(\mu), \tilde{C}_{PS_8}(\mu), C_{4q_1}(\mu), C_{4q_8}(\mu))^T.
\end{aligned} \tag{4.59}$$

Up to first order in α_s, the corresponding γ can be written as

$$\gamma = \frac{\alpha_s}{4\pi}\begin{pmatrix}
\gamma_{\rm dipole} & \gamma_{\rm mix} & 0 & \tilde{\gamma}_{\rm mix} & \gamma_{4q,\rm mix} \\
0 & \gamma_{PS} & 0 & 0 & 0 \\
0 & 0 & \gamma_{LR} & 0 & 0 \\
0 & 0 & 0 & \tilde{\gamma}_{PS} & 0 \\
0 & 0 & 0 & 0 & \gamma_{4q}
\end{pmatrix}. \tag{4.60}$$

Table 4.5: Dependence of the quark electric and chromo-electric dipole moments and four-quark operators at $M_{\rm QCD}$ on the same four-quark operators at M_W.

	$\tilde{C}_{PS_1}(M_W)$	$\tilde{C}_{PS_8}(M_W)$	$C_{4q_1}(M_W)$	$C_{4q_8}(M_W)$
$C_q(M_{\rm QCD})$	$\left(0.070\frac{Q_{q'}}{Q_q} - 0.027\right)\frac{m_{q'}}{m_q}$	$\left(0.045\frac{Q_{q'}}{Q_q} + 0.0058\right)\frac{m_{q'}}{m_q}$	0.085	0.10
$\tilde{C}_q(M_{\rm QCD})$	$-0.080\frac{m_{q'}}{m_q}$	$0.018\frac{m_{q'}}{m_q}$	-0.16	0.037
$\tilde{C}_{PS_1}(M_{\rm QCD})$	0.63	-0.14	–	–
$\tilde{C}_{PS_8}(M_{\rm QCD})$	-0.063	0.18	–	–
$C_{4q_1}(M_{\rm QCD})$	–	–	0.63	-0.14
$C_{4q_8}(M_{\rm QCD})$	–	–	-0.063	0.18

The top-left entries of this matrix are given in Eqs. (4.22), (4.23), (4.24), and (4.40). The other entries denote the running and mixing of the four-quark operators in Eq. (4.55). As is already clear from the form of γ, these additional four-quark operators do not mix with the FQPS and FQLR operators. Furthermore, $\tilde{O}_{PS,1,8}$ do not mix with $O_{4q,1,8}$ at the one-loop level. These considerations justify the block-diagonal form of γ, apart from $\gamma_{\rm mix}$, $\tilde{\gamma}_{\rm mix}$, and $\gamma_{4q,\rm mix}$ which give rise to contributions to the quark (C)EDMs from the various four-quark interactions. Explicit calculation shows that $\tilde{\gamma}_{PS}$ is identical to γ_{4q},

$$\tilde{\gamma}_{PS} = \gamma_{4q} = 2\begin{pmatrix} \frac{(4-3N)(N^2-1)}{N^2} + \beta_0 & \frac{(N-1)^2(1+N)(2+N)}{N^3} \\ 4\frac{N-2}{N} & 2C_2(N) + 2\frac{N^2+2}{N^2} + \beta_0 \end{pmatrix}. \tag{4.61}$$

Apart from a sign $\tilde{O}_{PS,1,8}$ mixes into the quark (C)EDMs the same way as $O_{PS,1,8}$ such that $\tilde{\gamma}_{\rm mix} = -\gamma_{\rm mix}$. The four-quark operators containing a single flavor contribute to the dipoles via

$$\gamma_{4q,\rm mix} = 4\begin{pmatrix} -1 & -C_2(N) \\ 1 & C_2(N) - \frac{N}{2} \\ 0 & 0 \end{pmatrix}, \tag{4.62}$$

where it is implied that the operator containing only up (down) quarks induces only the up (down) quark (C)EDM. This result for the anomalous-dimension matrix takes a simpler form than those in Refs. [47, 48], nevertheless the matrices agree with one another after a basis transformation.

Following the same procedure as in section 4.2.1 we now find, apart from Table 4.3, additional contributions, shown in Table 4.5, to the quark (C)EDMs. The results for the gluon CEDM, the FQPS, and the FQLR operators are unchanged.

The following results for the quark (C)EDMs are obtained for $M_{\mathcal{T}} = 1\,\text{TeV}$:

$$\begin{aligned}
d_q(M_{\text{QCD}}) &= \left[0.0020\left(0.21 + \ln\frac{m_q}{M_H}\right) - 0.038\right]\frac{m_q v}{M_H^2}\text{Im}\,Y'^q(1\,\text{TeV}) \\
&\quad + \frac{m_{q'}}{m_q}\left[0.00035\frac{Q_{q'}}{Q_q} - 0.0028\right]\left(\frac{m_u v}{M_H^2}\text{Im}\,Y'^d(1\,\text{TeV}) + \frac{m_d v}{M_H^2}\text{Im}\,Y'^u(1\,\text{TeV})\right), \\
\tilde{d}_q(M_{\text{QCD}}) &= \left[0.15 - 0.020\left(0.21 + \ln\frac{m_q}{M_H}\right)\right]\frac{m_q v}{M_H^2}\text{Im}\,Y'^q(1\,\text{TeV}) \\
&\quad - 0.028\frac{m_{q'}}{m_q}\left(\frac{m_u v}{M_H^2}\text{Im}\,Y'^d(1\,\text{TeV}) + \frac{m_d v}{M_H^2}\text{Im}\,Y'^u(1\,\text{TeV})\right),
\end{aligned} \tag{4.63}$$

while for $M_{\mathcal{T}} = 10\,\text{TeV}$ the results are trivially obtained from Eq. (4.53), which corresponds to a rescaling of the couplings Y'^q by a factor $1.3/1.2 \simeq 1.1$. Because the logarithm is rather large, $\ln m_q/M_H \simeq -10$, the one-loop diagrams contribute at the same order as the mixing of the four-quark operators into the dipoles. However, all terms receive a suppression of m_q/v compared to Eqs. (4.45) and (4.46).

The contributions to the various four-quark operators are suppressed by m_q/v as well. For the four-quark operators appearing in section 4.2, we find

$$\begin{aligned}
\begin{pmatrix}\text{Im}\,\Sigma_1(M_{\text{QCD}})\\ \text{Im}\,\Sigma_8(M_{\text{QCD}})\end{pmatrix} &= \begin{pmatrix}-1.6\\ 0.73\end{pmatrix}\times\left[\frac{m_d v}{M_H^2}\text{Im}\,Y'^u(1\,\text{TeV}) + \frac{m_u v}{M_H^2}\text{Im}\,Y'^d(1\,\text{TeV})\right], \\
\begin{pmatrix}\text{Im}\,\Xi_{LR_1}(M_{\text{QCD}})\\ \text{Im}\,\Xi_{LR_8}(M_{\text{QCD}})\end{pmatrix} &= -\begin{pmatrix}0.34\\ 2.0\end{pmatrix}\times\left[\frac{m_d v}{M_H^2}\text{Im}\,Y'^u(1\,\text{TeV}) - \frac{m_u v}{M_H^2}\text{Im}\,Y'^d(1\,\text{TeV})\right].
\end{aligned} \tag{4.64}$$

A comparison of Eqs. (4.63) and (4.64) makes it clear that the four-quark operators are larger by one to two orders of magnitude than the quark (C)EDMs. In the specific scenario discussed here, it seems safe to neglect the latter.

Finally, there are the remaining six four-quark operators in Eq. (4.55). In order to compare with Eq. (4.64) it is useful to redefine these operators without the factor g_s^2 and define new coupling constants

$$\begin{aligned}
\tilde{\Sigma}_{1,8}(\mu) &\equiv g_s^2(\mu)\,\tilde{C}_{\text{PS}_{1,8}}(\mu), \\
\Omega_{q,1}(\mu) &\equiv g_s^2(\mu)\,C_{4q_1}(\mu), \\
\Omega_{q,8}(\mu) &\equiv g_s^2(\mu)\,C_{4q_8}(\mu),
\end{aligned} \tag{4.65}$$

for which we find

$$\begin{aligned}
\begin{pmatrix}\tilde{\Sigma}_1\,(M_{\text{QCD}})\\ \tilde{\Sigma}_8\,(M_{\text{QCD}})\end{pmatrix} &= \begin{pmatrix}-0.64\\ 0.064\end{pmatrix}\times\left[\frac{m_d v}{M_H^2}\text{Im}\,Y'^u(1\,\text{TeV}) + \frac{m_u v}{M_H^2}\text{Im}\,Y'^d(1\,\text{TeV})\right], \\
\begin{pmatrix}\Omega_{q,1}\,(M_{\text{QCD}})\\ \Omega_{q,8}\,(M_{\text{QCD}})\end{pmatrix} &= \begin{pmatrix}-1.3\\ 0.13\end{pmatrix}\times\frac{m_q v}{M_H^2}\text{Im}\,Y'^q\,(1\,\text{TeV})\,.
\end{aligned} \tag{4.66}$$

These results indicate that the color-singlet operators with couplings $\tilde{\Sigma}_1$ and Ω_{q_1} are larger by an order of magnitude than their color-octet counterparts $\tilde{\Sigma}_8$ and Ω_{q_8}. Thus, at low

energies, it is sufficient to consider only the color-singlet operators which are of the same order as $\mathrm{Im}\,\Sigma_{1,8}$ and $\mathrm{Im}\,\Xi_{LR_{1,8}}$.

To summarize this section we write the $\not{P}\not{T}$ Lagrangian at the scale $M_{\rm QCD}$, in the case that the dominant dimension-six operators at the electroweak scale are the Higgs-quark interactions in Eq. (4.51). Neglecting, as discussed above, the quark (C)EDMs and the $\tilde{\Sigma}_8$ and $\Omega_{q,8}$ four-quark operators, the Lagrangian at $M_{\rm QCD}$ is given by

$$\begin{aligned}
\mathcal{L}_{6,\mathrm{set}\,2} &= i\frac{\mathrm{Im}\,\Sigma_1}{2}(\bar{u}u\,\bar{d}\gamma_5 d + \bar{u}\gamma_5 u\,\bar{d}d - \bar{d}u\,\bar{u}\gamma_5 d - \bar{d}\gamma_5 u\,\bar{u}d) \\
&\quad + i\frac{\mathrm{Im}\,\Sigma_8}{2}(\bar{u}t^a u\,\bar{d}\gamma_5 t^a d + \bar{u}\gamma_5 t^a u\,\bar{d}t^a d - \bar{d}t^a u\,\bar{u}\gamma_5 t^a d - \bar{d}\gamma_5 t^a u\,\bar{u}t^a d) \\
&\quad + i\,\mathrm{Im}\,\Xi_{LR_1}\left(\bar{u}_R\gamma^\mu d_R\,\bar{d}_L\gamma_\mu u_L - \bar{d}_R\gamma^\mu u_R\,\bar{u}_L\gamma_\mu d_L\right) \\
&\quad + i\,\mathrm{Im}\,\Xi_{LR_8}\left(\bar{u}_R\gamma^\mu t^a d_R\,\bar{d}_L\gamma_\mu t^a u_L - \bar{d}_R\gamma^\mu t^a u_R\,\bar{u}_L\gamma_\mu t^a d_L\right) \\
&\quad + i\frac{\tilde{\Sigma}_1}{2}(\bar{u}u\,\bar{d}\gamma_5 d + \bar{u}\gamma_5 u\,\bar{d}d + \bar{d}u\,\bar{u}\gamma_5 d + \bar{d}\gamma_5 u\,\bar{u}d) \\
&\quad + i\,\Omega_{u,1}(\bar{u}\gamma^5 u\,\bar{u}u) + i\,\Omega_{d,1}(\bar{d}\gamma^5 d\,\bar{d}d),
\end{aligned} \tag{4.67}$$

where the coupling constants are all evaluated at $M_{\rm QCD}$ and their values in terms of the coupling constants in Eq. (4.51) are given in Eqs. (4.64) and (4.66). All coupling constants in Eq. (4.67) scale as $(m_q/v)(1/M_{\not{T}}^2)$ and, in general, are much smaller than the constants appearing in Eq. (4.44). We stress again that the new four-quark operators appearing in this section are only important in specific scenarios involving additional symmetries and/or fine-tuning. In the scenario sketched here there are seven relevant $\not{P}\not{T}$ four-quark operators around $M_{\rm QCD}$ with only two independent coupling constants.

We now move on to discuss the last group of operators, namely the suppressed operators involving heavy gauge fields.

4.3.2 α_w suppressed operators involving heavy gauge bosons

In this section we deal with the remaining operators in section 3.1 which contain heavy $W^\pm$, Z, and Higgs-boson fields. These operators will no longer exist in the effective theory below the electroweak scale, where the heavy gauge fields are integrated out, but they will contribute to operators containing light fields only. The operators in this section only give rise to low-energy PT violation via electroweak one-loop diagrams, such that their effects will scale as $\sim \alpha_w/M_{\not{T}}^2$. The operators studied are the weak dipole moments of the quarks in Eqs. (3.5) and (3.7) and the interactions among electroweak gauge and Higgs bosons in Eqs. (3.17), (3.19), and (3.20).

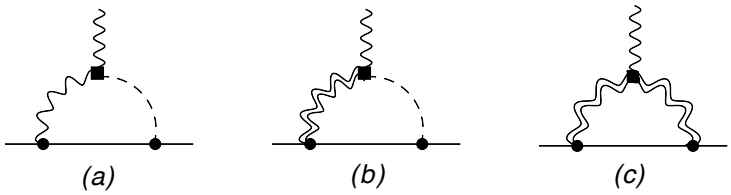

Figure 4.7: One-loop diagrams contributing to the quark electric moment. The double wavy lines denote the propagation of $W^{\pm}$ and Z bosons. The black square denotes a vertex from one of the operators in Eq. (4.68). The other notation is as in Figs. 4.3 and 4.4. For simplicity only one possible ordering is shown here.

We begin by defining the relevant operators above M_W,

$$\begin{aligned}
O_B &= e^2\varepsilon^{\mu\nu\alpha\beta}\left(F_{\mu\nu}F_{\alpha\beta} - 2\frac{s_w}{c_w}F_{\mu\nu}Z_{\alpha\beta}\right) vh + \ldots,\\
O_W &= e^2\varepsilon^{\mu\nu\alpha\beta}\left(F_{\mu\nu}F_{\alpha\beta} + 2\frac{c_w}{s_w}F_{\mu\nu}Z_{\alpha\beta}\right) vh + \ldots,\\
O_{WB} &= e^2v^2\varepsilon^{\mu\nu\alpha\beta}\left\{\left[F_{\mu\nu}F_{\alpha\beta} + \left(\frac{c_w}{s_w} - \frac{s_w}{c_w}\right)F_{\mu\nu}Z_{\alpha\beta}\right]\frac{h}{v} - i\frac{g}{s_w}W^+_\mu W^-_\nu F_{\alpha\beta}\right\} + \ldots,\\
O_{d_W} &= i\varepsilon^{\mu\nu\alpha\beta}W^{+\,\rho}_\beta W^-_{\rho\alpha}F_{\mu\nu} + \ldots,\\
O_{Wu} &= -\frac{g}{\sqrt{2}}m_u\left[(\bar{d}_L i\sigma^{\mu\nu}u_R)\,W^-_{\mu\nu} - i\frac{g}{\sqrt{2}}(\bar{u}i\sigma^{\mu\nu}\gamma_5 u)\,W^+_\mu W^-_\nu + \text{h.c.}\right],\\
O_{Wd} &= -\frac{g}{\sqrt{2}}m_d\left[(\bar{u}_L i\sigma^{\mu\nu}d_R)\,W^+_{\mu\nu} + i\frac{g}{\sqrt{2}}(\bar{d}i\sigma^{\mu\nu}\gamma_5 d)\,W^+_\mu W^-_\nu + \text{h.c.}\right],\\
O_{Zq} &= -\frac{g}{2}m_q\,\bar{q}i\sigma^{\mu\nu}\gamma_5 q\,Z_{\mu\nu},
\end{aligned} \tag{4.68}$$

where the dots denote terms which are not relevant at $\mathcal{O}(\alpha_w)$. The coupling constants at the scale $M_{\not T}$ are

$$\begin{aligned}
C_B(M_{\not T}) &= \theta'_B(M_{\not T}), & C_W(M_{\not T}) &= \theta'_W(M_{\not T}),\\
C_{WB}(M_{\not T}) &= \theta'_{WB}(M_{\not T}), & C_{d_W}(M_{\not T}) &= -s_w d_w(M_{\not T}),\\
C_{Wq}(M_{\not T}) &= w_q(M_{\not T}), & C_{Zq}(M_{\not T}) &= z_q(M_{\not T}).
\end{aligned} \tag{4.69}$$

These operators contribute to quark (C)EDMs through various diagrams, however, in all cases the contributions are suppressed by electroweak coupling constants in the typical combination $\alpha_w = e^2/4\pi$. The quark (C)EDMs are generated when the effective operators are evolved from $M_{\not T}$ to $M_{\rm EW}$. Below $M_{\rm EW}$ the heavy bosons can be integrated out and the running of the quark (C)EDMs to $M_{\rm QCD}$ can simply be obtained from the results in section 4.2. There is one operator discussed in this section which does not contribute to the quark (C)EDMs through the running, namely, O_{d_W} of Eq. (3.17). The first contribution of this operator appears through the finite part of a one loop diagram. Therefore, in this case we consider the finite part, which otherwise could have been neglected, in order to obtain a contribution to the q(C)EDMs.

Table 4.6: The anomalous dimensions of the various heavy-boson operators. Here T_q^3 stands for the third component of weak isospin of the external quark, *i.e.* $1/2$ $(-1/2)$ for the up (down) quark.

	$\gamma_{13}^{(1)}$	$\gamma_{23}^{(1)}$	γ_H
O_B	$-16\left(1-\frac{T_q^3/2-s_w^2Q_q}{Q_qc_w^2}\right)$	0	0
O_W	$-16\left(1+\frac{T_q^3/2-s_w^2Q_q}{Q_qs_w^2}\right)$	0	0
O_{WB}	$-4\frac{1}{s_w^2}\left(2T_q^3V_{ud}^2\frac{1}{Q_q}+4s_w^2+\frac{T_q^3-2s_w^2Q_q}{Q_qc_w^2}\cos 2\theta_w\right)$	0	0
O_{d_W}	0	0	0
O_{Wq}	$\frac{1}{s_w^2}\left[V_{ud}\left(5-9\frac{Q_{q'}}{Q_q}\right)-6\left(1-\frac{Q_{q'}}{Q_q}\right)\right]$	$\frac{4}{s_w^2}V_{ud}$	$8C_2(N)$
O_{Zq}	$-4\frac{T_q^3-2Q_qs_w^2}{c_ws_w^2}$	$4\frac{T_q^3-2Q_qs_w^2}{c_ws_w^2}$	$8C_2(N)$

To calculate the running of the operators we will treat the $\mathcal{O}(\alpha_w)$ contributions as a perturbation to the QCD RGE. We only consider the electroweak corrections which induce a quark (C)EDM. That is, we do not consider the electroweak running of α_w itself, nor that of the operators involving the heavy bosons. These effects would give rise to $\mathcal{O}(\alpha_w^2)$ corrections to the induced quark (C)EDMs. We write the relevant couplings as

$$\vec{C} = (C_q, \tilde{C}_q, C_H)^T, \tag{4.70}$$

where C_H stands for the coupling constant of one of the heavy-boson operators. These will be treated one at a time because their mixing can be neglected at the order we consider. We write $\vec{C} = \vec{C}^{(0)} + \vec{C}^{(1)}$ and $\gamma = \gamma^{(0)} + \gamma^{(1)}$, where the superscript 0 (1) denotes terms of $\mathcal{O}(\alpha_w^0)$ $(\mathcal{O}(\alpha_w^1))$. Up to $\mathcal{O}(\alpha_w^1)$, Eq. (4.70) splits into two equations

$$\frac{\partial\vec{C}^{(0)}}{\partial\ln\mu} = \gamma^{(0)}\,\vec{C}^{(0)}, \qquad \frac{\partial\vec{C}^{(1)}}{\partial\ln\mu} = \gamma^{(0)}\,\vec{C}^{(1)} + \gamma^{(1)}\,\vec{C}^{(0)}, \tag{4.71}$$

where $\gamma^{(0)}$ describes the effects of QCD corrections, while $\gamma^{(1)}$ describes the mixing of the operators due to electroweak corrections. The LO matrix can, for our purposes, be written as

$$\gamma^{(0)} = \frac{\alpha_s}{4\pi}\begin{pmatrix}\gamma_e & \gamma_{qe} & 0\\ 0 & \gamma_q & 0\\ 0 & 0 & \gamma_H\end{pmatrix}, \tag{4.72}$$

where $\gamma_{e,q,qe}$ can be read off from Eq. (4.22) ($\gamma_e = -\gamma_{qe} = 8C_2(N)$ and $\gamma_q = 16C_2(N) - 4N$) while γ_H and the matrix $\gamma^{(1)}$ depend on the heavy-boson operator under investigation. The electroweak effects can, at this order, be described by

$$\gamma^{(1)} = \frac{\alpha_w}{4\pi}\begin{pmatrix}0 & 0 & \gamma_{13}^{(1)}\\ 0 & 0 & \gamma_{23}^{(1)}\\ 0 & 0 & 0\end{pmatrix}. \tag{4.73}$$

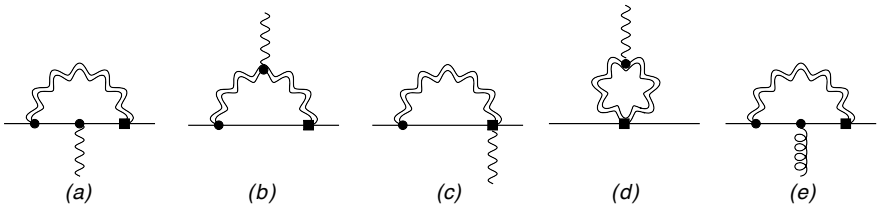

Figure 4.8: One-loop diagrams contributing to the quark electric and chromo-electric dipole moments. The notation is as in Fig. 4.7. For simplicity only one possible ordering is shown.

What remains is the calculation of the unknown entries γ_H, $\gamma_{13}^{(1)}$, and $\gamma_{23}^{(1)}$ for each operator. The results for the anomalous dimensions for the heavy boson operators are collected in Table 4.6. The electroweak loops for O_{WB}, O_{d_W}, O_{Zq}, and O_{Wq} were evaluated in Ref. [39] in a different regularization scheme. However, for O_{Wq} not all diagrams were taken into account.

The operators O_B, O_W, O_{WB}, and O_{d_W} induce a quark EDM through the diagrams in Fig. 4.7. The first two operators contribute through diagrams 4.7(a,b) and O_{d_W} through diagram 4.7(c), while O_{WB} contributes via all diagrams. None of these operators induces a quark CEDM at the one-loop level. As can be seen from Table 4.6, the anomalous dimensions of O_{d_W} vanish. The reason is that for this operator diagram 4.7(c) is finite in dimensional regularization. However, the diagram does have a finite part which was evaluated in several regularization schemes in Ref. [82], where it was found to be scheme dependent. We will use the result found in dimensional regularization, which was shown to give the correct answer in Ref. [83]. In our notation the operator O_{d_W} induces the quark EDM [82]

$$C_{u,d}(M_W^-) = \pm \frac{g^2}{32\pi^2} \frac{1}{eQ_{u,d}} C_{d_W}, \tag{4.74}$$

where the plus (minus) sign is for the up (down) quark EDM.

The weak dipole moments, O_{Zq} and O_{Wq}, contribute to four-quark operators at tree level. However, this necessarily involves one power of the exchanged momentum because of the derivative acting on the gauge fields. The coupling constants of these effective dimension-seven operators then scale as $m_q M_W^{-2} M_{\mathcal{T}}^{-2}$ and are heavily suppressed. The same holds for one-loop contributions to four-quark operators. Larger effects come from one-loop diagrams shown in Fig. 4.8(a-d) and 4.8(e) contributing to, respectively, light-quark EDMs and CEDMs. The weak dipole moments are the only operators in this section which produce a quark CEDM. Furthermore, they are the only operators which are affected by QCD corrections and, hence, have a nonzero γ_H.

Employing all the anomalous dimensions, the finite contribution from O_{d_W}, and using

$$\alpha_w(M_W) \simeq \frac{1}{128}, \qquad s_w^2(M_W) \simeq 0.23, \tag{4.75}$$

we calculate the induced quark (C)EDMs at M_W. The results for $M_{\mathcal{T}} = 1,\, 10\,\text{TeV}$ are given in Table 4.7. The quark EDM entries for C_B, C_W, and C_{WB} for $M_{\mathcal{T}} = 10\,\text{TeV}$ are almost twice as large as those for $M_{\mathcal{T}} = 1\,\text{TeV}$. This can be understood from the logarithmic

Table 4.7: The contributions of the various heavy boson operators at $M_{\not T}$ to the q(C)EDMs at M_W in units of 10^{-2}. A "–" indicates that there is no contribution at this order.

	$C_B\,(1\,\text{TeV})$	$C_W\,(1\,\text{TeV})$	$C_{WB}\,(1\,\text{TeV})$	$C_{d_W}\,(1\,\text{TeV})$	$C_{Wq}(1\,\text{TeV})$	$C_{Zq}(1\,\text{TeV})$
$C_{u,\,d}$	$\{1.8,\,0.73\}$	$\{3.6,\,7.3\}$	$\{6.2,\,11\}$	$\{0.65,\,1.3\}$	$\{-13,\,-15\}$	$\{-2.4,\,4.3\}$
$\tilde{C}_{u,\,d}$	–	–	–	–	$\{-2.2,-2.2\}$	$\{-0.49,\,0.88\}$
	$C_B\,(10\,\text{TeV})$	$C_W\,(10\,\text{TeV})$	$C_{WB}\,(10\,\text{TeV})$	$C_{d_W}\,(10\,\text{TeV})$	$C_{Wq}(10\,\text{TeV})$	$C_{Zq}(10\,\text{TeV})$
$C_{u,\,d}$	$\{3.2,\,1.3\}$	$\{6.4,\,13\}$	$\{11,\,19\}$	$\{0.65,\,1.3\}$	$\{-25,\,-29\}$	$\{-4.9,\,8.8\}$
$\tilde{C}_{u,\,d}$	–	–	–	–	$\{-3.6,-3.6\}$	$\{-0.81,\,1.5\}$

dependence on $M_{\not T}$, while, simultaneously, QCD corrections suppress the contributions. The same holds for the quark CEDM entries for C_{W_q} and C_{Z_q}. The quark EDM entries in the last two columns are more complicated because they get additional contributions when the induced quark CEDM is evolved to lower energies. It should be noted that although our main goal is to obtain the contribution of the heavy gauge operators to hadronic EDMs, some of them appear in a number of other observables. For instance, the operators O_W, O_B and O_{WB} have recently been under investigation as they can modify the $h \to \gamma\gamma$ rate [84, 76, 85]. In addition, the same three operators as well as O_{d_W} can also contribute to the electron EDM [85]. We will come back to these considerations when discussing the bounds coming from the neutron EDM in the next chapter.

The above concludes the running of the heavy gauge operators from $M_{\not T}$ to M_W. The remainder of the running down to M_{QCD} can be obtained straightforwardly by employing the results for the quark (C)EDMs of section 4.2. Thus, the combination of results of this section and those of section 4.2 complete the evolution of the heavy gauge operators, and thereby the evolution of both sets of operators.

4.4 Summary

In order to study the effects of the dimension-six operators on low-energy observables, such as EDMs, it is necessary to evolve the operators to these lower-energy scales. In the process heavy SM particles decouple and must be integrated out. Simultaneously, it is necessary to include the effects of QCD and, in some cases, electroweak renormalization-group running. Qualitatively, the most important effect of the running is that it allows for mixing between the different operators. As a result, a single operator at high energies can give rise to several interactions at lower energies. Therefore, the relation between the operators at high and low energies is not simply one-to-one, and requires the calculation of the RGE evolution.

In order to do so, it turns out to be convenient to divide the dimension-six operators at $M_{\not T}$ into two sets. The division is based on the size of the induced low-energy $\not P\not T$ operators. The first set contains the dimension-six operators which induce low-energy operators that also scale as $M_{\not T}^{-2}$. That is, the operators obtain no additional suppression when evolved to lower energies apart from minor suppressions due to QCD corrections.

The second set contains the remaining operators which are suppressed, either by small Yukawa couplings or α_w, when run to $M_{\rm QCD}$. Of course, the first set is expected to give the dominant contribution to first generation $\not{P}\not{T}$ observables.

Set 1: Operators in the first set have been discussed in section 4.2. This set contains operators which consist of only light fields such as the gluon CEDM and the FQPS operators. The form of these operators stays the same all the way from $M_{\not{T}}$ to $M_{\rm QCD}$ and, apart from QCD corrections, their scalings are not altered. Other operators in the first set are the quark EDMs and CEDMs. At high energies these operators couple to a Higgs field, but these can be replaced by their vev and there are no suppression factors at low energies. The next operator describes a derivative interaction among right-handed quarks and two Higgs fields (see Eq. (3.12)). When the Higgs field takes on its vev, an interaction among right-handed quarks and a W boson remains. Integrating out the W boson induces an additional $\not{P}\not{T}$ four-quark operator (the FQLR operator) [52]. The W exchange suppresses the operator by M_W^{-2}, but this is compensated by the two powers of v appearing in the operator. Finally, the first set contains $\not{P}\not{T}$ quark-Higgs and gluon-Higgs interactions. When the Higgs field takes its vev, the resulting terms renormalize, respectively, the SM Yukawa couplings and the $\bar{\theta}$ term. Via loop diagrams the quark-Higgs [77] and gluon-Higgs interactions induces contributions to the quark (C)EDM. The associated loop suppressions are not very stringent and we therefore keep these operators in the first set.

The low-energy form of the operators in the first set has been derived in section 4.2.1. Around $M_{\rm QCD}$ there are seven relevant $\not{P}\not{T}$ operators among light quarks, gluons, and photons. They consist of the quark EDM, the quark and gluon CEDM, and four four-quark operators. The first three of these operators have been extensively considered in the literature. The four-quark operators are less often taken into account, possibly due to the belief that they should be proportional to the quark masses and are therefore effectively higher-dimensional operators in disguise. Although this arguments holds for some four-quark operators it does not hold for the FQPS and FQLR operators which genuinely scale as $M_{\not{T}}^{-2}$ and are in general not suppressed compared to the dipole operators. It should be noted that there exist six additional four-quark operators which one would expect to arise if one does not take $SU(2)_L$ gauge invariance into account. Here, we find these operators to be suppressed, such that they only appear in the second set. Therefore, model-independent studies of hadronic and nuclear EDMs due to the dominant beyond-the-SM physics should use the seven operators at $M_{\rm QCD}$ as a starting point. Only using model-dependent statements can one favor the operators in the second set over those in set 1.

Set 2: The second set of dimension-six operators at $M_{\not{T}}$ consists of the remaining operators which do suffer from additional suppression when evolved to lower energies. We first discuss $\not{P}\not{T}$ quark-Higgs interactions which already appeared in the first set because they induced relatively large corrections to the quark CEDM via loops. At tree level these quark-Higgs couplings induce $\not{P}\not{T}$ four-quark operators which are different from the FQPS and FQLR operators. However, the couplings of these operators scale as $(m_q/v)M_{\not{T}}^{-2}$, and they are thus additionally suppressed by the ratio of the light-quark mass to the Higgs

vev. It is interesting that when the quark-Higgs operators are evolved to energies around $M_{\rm QCD}$, all ten possible $\not{P}\not{T}$ four-quark operators among up and down quarks are induced, albeit with only two independent couplings (C_{uH} and C_{dH}, see Eq. (4.57)) and the coefficients of three operators are an order of magnitude smaller than the others. The QCD evolution of these operators was studied in a different basis in Refs. [47, 48]. These ten four-quark operators involve the FPQS and FQLR operators but also six new structures. However, because the quark-Higgs operators induce a larger contribution to the quark CEDM, the additional six four-quark operators can in general be neglected.

The other dimension-six operators in the second set describe $\not{P}\not{T}$ interactions involving electroweak gauge and/or Higgs bosons. The operators consist of the quark weak dipole moments and $\not{P}\not{T}$ interactions among three gauge bosons and/or two gauge bosons and a Higgs boson. The quark weak dipole moments are similar to the quark EDM but the photon is replaced by a W or Z boson. In fact, as seen from Eqs. (3.4), (3.6), and (3.8) these operators are related by gauge symmetry. The purely bosonic interactions originate in four independent gauge-invariant operators [37]. All of these operators contain at least one heavy field which decouples below the electroweak scale generating contributions to the quark EDMs and CEDMs via electroweak one-loop diagrams [39]. These contributions are suppressed by loop factors, typically $\sim \alpha_w/4\pi$. At the one-loop level there are no dimension-six four-quark operators generated. The induced quark (C)EDMs, which make up the low-energy effective Lagrangian in this case, were calculated in section 4.3.2.

To conclude, in this chapter we have evolved the parity- and time-reversal violating operators of dimension six from $M_{\not{T}}$ down to the electroweak scale and subsequently to hadronic scales. This evolution allowed for the derivation of the set of operators which is expected to dominate hadronic and nuclear EDMs due to physics beyond the SM. In addition, it allowed us to express these low-energy operators in terms of the original dimension-six operators at the high-energy scale. Thus, the results of this chapter allow one to translate bounds on the low-energy couplings into constraints on the couplings at high energies. In order to make use of these results, we will make the connection to experimental observables in the next chapter. Among other things, we will employ the limit on the neutron EDM in order to bound the couplings at high energies by using the results of this chapter. The limits that can be derived from the neutron EDM in this way will also play a role in later chapters, when considering specific models, such as the left-right model.

Appendix 4.A An example RGE calculation

As an example of an explicit calculation of anomalous dimensions, we will consider the running of the quark EDM and color EDM in this appendix. We define the operators themselves as in Eq. (4.17),

$$O_q = -\frac{i}{2} e m_q Q_q \bar{q} \sigma^{\mu\nu} \gamma_5 q \, F_{\mu\nu}, \qquad \tilde{O}_q = -\frac{i}{2} g_s m_q \, \bar{q} \sigma^{\mu\nu} \gamma_5 t_a q \, G^a_{\mu\nu}. \tag{4.76}$$

The running of their couplings is then described by the RGEs,

$$\frac{dC_i(\mu)}{d\ln\mu} = \gamma_{ij} C_j(\mu), \tag{4.77}$$

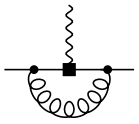

Figure 4.9: Diagram that adds to the anomalous dimension of the qEDM. Quarks are denoted by straight solid lines, photons by wavy lines, and gluons by curly lines. The black square represents an insertion of a $\not{P}\not{T}$ interaction, in this case the quark EDM. Other vertices denote SM PT invariant interactions.

where $C_i = (C_q, \tilde{C}_q)$. Here the anomalous dimensions are determined by loop diagrams that contribute to O_q or $\tilde{O}_q$. Starting with the qEDM, the only diagram up to $\mathcal{O}(\alpha_s)$ which involves a O_q insertion and renormalizes this operator is shown in Fig. 4.9. This diagram, however, is convergent and so does not contribute to γ_{11}. From Eq. (4.9), one finds

$$\gamma_{11} = \frac{\partial}{\partial \ln \mu}\delta_q - \gamma_m = 8\frac{\alpha_s}{4\pi}C_2(N), \tag{4.78}$$

where we used the well-known results for the field renormalization and anomalous dimension of the quark mass in the $\overline{MS}$ scheme, see e.g. [86],

$$\delta_q \;=\; -\frac{\alpha_s}{4\pi}C_2(N)L, \qquad \delta_G = \frac{\alpha_s}{4\pi}\left[\frac{5}{3}C_2(G) - \frac{4}{3}n_f C(N)\right]L, \qquad \gamma_m = -6\frac{\alpha_s}{4\pi}C_2(N),$$

with $L \equiv \left(\frac{2}{4-d} - \gamma_E + \ln 4\pi - \ln \mu^2\right)$, and $C_2(N) = \frac{N^2-1}{2N}$, $C_2(G) = N$, $C(N) = 1/2$.

The renormalization of the qCEDM takes slightly more work. The diagrams involving $\tilde{O}_q$ which contribute to the qCEDM are depicted in Fig. 4.10. The divergent pieces of these diagrams give

$$\sum_{i=a\ldots e} \text{Diagram } 4.10(i)\Big|_{\text{div}} = \frac{\alpha_s}{4\pi}\left(\sum_{i=a\ldots e} A_i\right)\left(\frac{2}{4-d} - \gamma_E + \ln 4\pi\right) F_G^{\mu,\,a}(q), \tag{4.79}$$

where $F_G^{\mu,\,a}(q) = -ig_s m_q t^a \sigma^{\mu\nu}\gamma^5 q_\nu$ is the Feynman rule for the qCEDM operator for a gluon with incoming momentum q, Lorentz index μ and color index a. The coefficients of the poles can be calculated as

$$\begin{aligned} A_a = 0, \qquad A_b = -4\left[C_2(N) - \tfrac{1}{2}C_2(G)\right], \qquad A_c = -\tfrac{1}{2}C_2(G), \\ A_d = 3C_2(G), \qquad A_e = -\tfrac{3}{2}C_2(G). \end{aligned} \tag{4.80}$$

Thus, the counterterm needed to cancel these divergences, in the $\overline{MS}$ scheme, is given by $\delta_{22} = -\frac{\alpha_s}{4\pi}\left(\sum_{i=a\ldots e} A_i\right)L$. In this case, the expression for the anomalous dimension, Eq. (4.9), becomes

$$\gamma_{22} \;=\; -\gamma_m - \frac{\beta}{g_s} + \mu\frac{\partial}{\partial\mu}(\delta_q + \frac{1}{2}\delta_G - \delta_{22}) = \frac{\alpha_s}{4\pi}\left[16C_2(N) - 4N\right]. \tag{4.81}$$

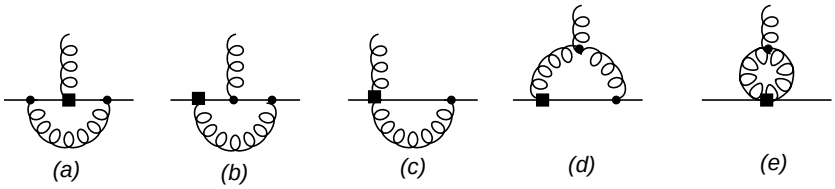

Figure 4.10: Diagrams that adds to the anomalous dimension of the quark chromo-electric dipole moment. Notation is as in Fig. 4.9. Only one ordering per diagram is shown.

This leaves only the off-diagonal elements of γ, i.e. the mixing between the two operators. Under QCD renormalization the qEDM does not contribute to the qCEDM, which implies that $\gamma_{21} = -\frac{\partial}{\partial \ln \mu}\delta_{12} = 0$. On the other hand, the reverse is possible: The qCEDM does contribute to the qEDM through diagram 4.10(b) with the emitted gluon replaced by a photon. The divergent piece is similar to the diagram with a gluon, only the color factor is different: One effectively replaces $t^a t^b t^a \to -t^a t^a$, where the additional sign comes from the chosen definition of e, namely, $e > 0$. The result is

$$\text{Diagram } 4.10(b)(g \to \gamma)\Big|_{\text{div}} = 4C_2(N)\frac{\alpha_s}{4\pi}\left(\frac{2}{4-d} - \gamma_E + \ln 4\pi\right) F_\gamma^\mu(q), \tag{4.82}$$

where $F_\gamma^\mu(q) = -ieQ_q m_q \sigma^{\mu\nu}\gamma^5 q_\nu$ is the Feynman rule for O_q. Thus, the required counterterm and anomalous dimension are given by

$$\delta_{21} = -4C_2(N)\frac{\alpha_s}{4\pi}L, \qquad \gamma_{12} = -\frac{\partial}{\partial \ln \mu}\delta_{12} = -8C_2(N)\frac{\alpha_s}{4\pi}. \tag{4.83}$$

Having calculated the anomalous-dimension matrix, all that is left is to solve the RGEs, Eq. (4.77). This can be done by the method outlined in section 4.1.1. One first diagonalizes the anomalous-dimension matrix after which the decoupled equations can be solved. Defining $\eta = \frac{\alpha_s(\mu_2)}{\alpha_s(\mu_1)}$, $\gamma_{ij} = \frac{\alpha_s}{4\pi}\gamma^0_{ij}$, and $\kappa_{ij} = \gamma^0_{ij}/2\beta_0$, the couplings at a scale μ_1 can be written in terms of those at a scale μ_2 as

$$C_i(\mu_1) = U_{ij}(\mu_1, \mu_2)C_j(\mu_2), \qquad U = \begin{pmatrix} \eta^{\kappa_{11}} & \frac{\gamma_{12}}{\gamma_{11}-\gamma_{22}}(\eta^{\kappa_{11}} - \eta^{\kappa_{22}}) \\ 0 & \eta^{\kappa_{22}} \end{pmatrix}. \tag{4.84}$$

For instance, if we would like to express the couplings at $\mu = M_{\text{QCD}}$ in terms of those at, say, $\mu = M_W$, we obtain

$$\vec{C}^{(3)}(M_{\text{QCD}}) = U^{(3)}(M_{\text{QCD}}, m_c)U^{(4)}(m_c, m_b)U^{(5)}(m_b, M_W)\vec{C}^{(5)}(M_W). \tag{4.85}$$

Here we took into account the thresholds of the bottom and charm quarks, integrating these quarks out in the process. The superscripts indicate the number of flavors that should be used. The above equation implicitly uses the matching conditions, which, at this level, are given by $\vec{C}^{(5)}(m_b) = \vec{C}^{(4)}(m_b)$ and $\vec{C}^{(4)}(m_c) = \vec{C}^{(3)}(m_c)$. Thus, the matrix $U^{(5)}(m_b, M_W)$ takes the couplings from $\mu = M_W$ to $\mu = m_b$, while $U^{(4)}(m_c, m_b)$ takes them from $\mu = m_b$ to $\mu = m_c$, etc. Using the input of Eqs. (4.32), (4.33) and (4.41), we obtain

$$C_q(M_{\text{QCD}}) = 0.48\, C_q(M_W) + 0.37\, \tilde{C}_q(M_W), \qquad \tilde{C}_q(M_{\text{QCD}}) = 0.53\, \tilde{C}_q(M_W), \tag{4.86}$$

as in Table 4.3.

Chapter 5

Phenomenology of CP-violating new physics

The main goal of considering the CP-violating dimension-six sources is to see how they are constrained experimentally, in this case, by the search for electric dipole moments (EDMs), in particular hadronic EDMs. In order to do so we will employ the χPT and NDA techniques discussed in chapter 3, and the results of chapter 4. After connecting the dimension-six operators to hadronic EDMs in this way, we will be able to use the experimental limits on these systems to constrain the new sources of CP violation. These limits are the result of numerous efforts to measure EDMs of leptons, hadrons, nuclei, atoms, and molecules (for an overview, see Ref. [87]). At the moment the strongest existing limits have been obtained for the neutron EDM [18], the EDM of the diamagnetic ^{199}Hg atom [88], and the electron EDM (which can be inferred from measurements on the polar molecules ThO [89] and YbF [90, 91]). In addition there are plans to measure the EDMs of charged spin-carrying particles, besides the electron, in storage rings [92, 93, 94, 95]. The spin precession of a particle trapped in such a ring is affected by its EDM and it has been proposed that this method can be used to measure the EDMs of the proton and deuteron with a precision of $10^{-29}\,e\,\text{cm}$, three orders of magnitude better than the current neutron EDM limit, $|d_n| \leq 2.9 \cdot 10^{-26} e\,\text{cm}$ (90% C.L.). EDMs of other light ions, such as the helion (^{3}He nucleus) and triton (^{3}H nucleus) are candidates as well.

At present the most stringent limits on the BSM sources will therefore derive from the bound on the neutron EDM[1]. However, apart from setting bounds on the dimension-six sources, we will also consider how EDM measurements can be used to distinguish between the sources of BSM CP violation. Although only a single measurement is needed in order to constrain the BSM sources, multiple measurements would be needed to trace the fundamental origin of CP violation. After discussing the bounds from the neutron EDM limit we will consider which of the dimension-six operators could be disentangled in this way. Of course, in actual models of BSM physics such operators do not appear on their own, but will most likely appear in combinations. Thus, one might wonder whether being able to distinguish single operators from one another also allows one to distinguish

[1]The limit on the proton EDM, $d_p \lesssim 10^{-24} e\,\text{cm}$ [96, 88], derives from the limit on the ^{199}Hg atom and is roughly two orders of magnitude weaker than that on the neutron EDM and involves large theoretical uncertainties. The EDMs of light nuclei have not been measured.

more realistic models of new physics. It turns out the EDMs of the deuteron and helion could play an important role in disentangling such models of BSM CP violation from one another. We leave a detailed discussion of this question to chapters 8 and 9.

In addition to the study of the EDMs of nucleons and light nuclei we will also briefly discuss the EDMs of the paramagnetic atoms/molecules ^{205}Tl, YbF, and ThO, which depend on the electron EDM, and the EDM of the diamagnetic ^{199}Hg atom. There are strong constraints on the EDMs of these systems, however, atomic and nuclear theory is required to relate the experimental constraints to the underlying mechanism of CP violation. These nuclear-theory calculations lead to large uncertainties, especially for the ^{199}Hg atom. Nonetheless, a measurement of the electron EDM could serve as another way to distinguish the CP-violating sources, discussed in chapter 3, from one another.

Finally, in order to prepare for the next chapter we will also look at the phenomenology of other processes, namely, that of meson mixing and nuclear β decay. The reason for this is that, in the upcoming chapters, we will turn from the model-independent EFT approach followed so far to a specific extension of the SM, namely, the left-right model. As already mentioned in the introduction, the constraints in a specific model could be more stringent than those suggested by the EFT approach, as the BSM interactions will no longer be independent. As a result, different observables can become connected in a way one would not immediately expect from the bottom-up approach. Thus, by considering multiple observables one can often strongly constrain specific models. In left-right models stringent constraints arise from the B and K meson-mixing observables mentioned earlier, which will play an important role in the upcoming chapters.

The outline of this chapter is as follows. We will start with a quick review of electric dipole moments, before moving on to express the nucleon EDMs in terms of the couplings of dimension-six operators. It is here that we will also derive the constraints on the CP-violating sources of BSM physics. After considering the constraints we will discuss possible ways in which these sources can be disentangled, either through the EDMs of light nuclei or the EDMs of other systems. Lastly, in preparation for chapters 6 and 7, we will briefly review neutron β decay and B and K mixing.

5.1 Electric dipole moments

As was mentioned in earlier chapters, for rotationally symmetric systems, electric dipole moments represent an interaction between the spin of a particle and an external electromagnetic field. This interaction appears in the matrix element of the electromagnetic current J_μ, which can be decomposed into tensor structures as

$$\begin{aligned}\langle f(p')|J^\mu(0)|f(p)\rangle &= \bar{u}(p')\big[F_1(q^2)\gamma^\mu + \frac{F_2(q^2)}{2m_f}i\sigma^{\mu\nu}q_\nu + \frac{F_3(q^2)}{2m_f}i\sigma^{\mu\nu}\gamma_5 q_\nu \\ &\quad + F_A(q^2)(\gamma^\mu\gamma_5 q^2 - 2m_f q^\mu\gamma_5)\big]u(p), \end{aligned} \tag{5.1}$$

where $q = p' - p$. Here the Dirac and Pauli form factors, F_1 and F_2, at $q^2 = 0$, represent the usual electromagnetic charge and the anomalous magnetic moment of the fermion, while F_A represents the anapole moment. In the SM only F_1 appears at tree level while

the remaining form factors are generated at loop level. The form factor we are interested in is F_3 which can be related to the electric dipole moment as

$$d_f = -\frac{eF_3(0)}{2m_f}. \tag{5.2}$$

This form factor corresponds to the dimension-five operator

$$\mathcal{L} = -d_f \frac{i}{2}\overline{\psi}_f \sigma^{\mu\nu}\gamma_5 \psi_f F_{\mu\nu}. \tag{5.3}$$

Although the above interaction representing the EDM has dimension five, operators of this form only arise from dimension-six operators in the EFT framework discussed in chapter 3. The fact that no true dimension-five operators of this form are allowed is due to the fact that one needs to include the Higgs field in order to construct a $SU(2)_L$-invariant term, raising the dimensionality by one. The normalization in Eq. (5.3) is such that the operator reduces to $\mathcal{L} = d_f \boldsymbol{\sigma}\cdot\boldsymbol{E}$ in the nonrelativistic limit, where $\boldsymbol{\sigma}$ is the spin and $\boldsymbol{E}$ the electric field. As the spin changes its sign under T, while the electric field remains the same, this term is T-odd. It is in fact $\not{P}$ and $\not{T}$, so that, by the CPT theorem, it is also CP violating.

The EDMs we have considered in chapter 3 have been the EDMs of fundamental fermions, namely, those of the quarks. However, in order to connect these operators, as well as the SM and BSM CP-violating sources, to experiment, we will require their contributions to the EDMs of composite systems. In the next section we employ the results from χPT and NDA techniques in order to estimate the contributions from the SM and BSM sources of CP violation to the EDMs of the nucleons and light nuclei.

5.1.1 Contributions to the low-energy constants

As was already discussed in chapter 3, the interactions in the χPT Lagrangian which give rise to the EDMs of the nucleons and light nuclei can, for our purposes, be written as [58, 74, 56]

$$\begin{aligned}\mathcal{L}_{\not{P}\not{T}} &= -2\,\bar{N}\left(\bar{d}_0 + \bar{d}_1\tau_3\right) S^\mu N\, v^\nu F_{\mu\nu} \\ &\quad + \bar{g}_0 \bar{N}\boldsymbol{\pi}\cdot\boldsymbol{\tau}N + \bar{g}_1\bar{N}\pi_3 N.\end{aligned} \tag{5.4}$$

Here $\bar{d}_{0,1}$ represent the isoscalar and isovector nucleon EDMs, in the heavy-baryon formalism, while $\bar{g}_0$ (g_1) is a CP-odd isoscalar (isovector) pion-nucleon coupling. See section 3.2 for the remaining definitions and conventions.

It should be noted that the above Lagrangian is in general not complete. In principle, there are additional nucleon-nucleon couplings as well as a three-pion vertex which, although of little importance for the nucleon and deuteron EDMs, do play a role in the tri-nucleon EDMs [56]. These additional interactions could become important when trying to establish more precisely how the different EDMs are related. We will consider such relations in specific BSM scenarios in chapters 8 and 9, where we will comment on these interactions in more detail. For now, we will stick to Eq. (5.4) for simpler estimates of the relative sizes of the EDMs.

In order to relate the fundamental sources of CP-violation to the EDMs of the nucleons and light nuclei, these EDMs will have to be expressed in terms of the LECs of Eq. (5.4), which, in turn, should be expressed in the couplings of the CP-violating operators. Thus after expressing the EDMs in terms of $\bar{d}_{0,1}$ and $\bar{g}_{0,1}$ we will be able to evaluate the contributions of the fundamental sources to the hadronic EDMs. We will turn to this in the upcoming sections. First, however, we will employ NDA estimates for the contributions of the CP-violating operators to the low-energy constants (LECs). These LECs will in principle receive contributions from SM as well as BSM operators. Both types of contributions are collected in Table 5.1. We start by considering the contributions in the SM.

Contributions of the $\bar{\theta}$-term

As discussed in chapter 3, there are two fundamental sources of CP violation in the SM. These are the QCD $\bar{\theta}$ angle and the phase in the CKM matrix. The contributions of the former can be read off from Table 5.1. Here, the contributions to $\bar{d}_{0,1}$ are the NDA estimates. These contributions involve a factor of $\frac{e}{4\pi}$ as they require the coupling of a photon. Instead, the listed contributions to $\bar{g}_{0,1}$ are exceptions in the sense that they result from χPT arguments, which allow one to link these terms to those induced by strong isospin breaking [97, 98, 99]. The argument for the $\bar{g}_0$ contribution was explained in section 3.2, and allowed one to relate the $\bar{\theta}$-induced $\bar{g}_0$ to the neutron-proton mass difference induced by the strong interaction, $(m_n - m_p)^{\text{strong}} = (2.6 \pm 0.85)\,\text{GeV}$ [63, 64]. Similar arguments allow one to derive the $\bar{\theta}$ contribution to $\bar{g}_1$. In this case the contribution to $\bar{g}_1$ can be related to a shift in the neutral-pion mass induced by the strong interaction, $(\delta m_\pi^2)^{\text{strong}} \simeq (\varepsilon m_\pi^2)^2/(4(m_K^2 - m_\pi^2))$ [100]. Here $c_1 = (-1.0 \pm 0.3)\,\text{GeV}^{-1}$ [101] is related to the quark mass contribution to the nucleon mass. As we will see later, the contributions from $\bar{d}_{0,1}$ and $\bar{g}_{0,1}$ to the neutron EDM are of similar size in the case of $\bar{\theta}$.

Contributions of the CKM phase

In contrast to the $\bar{\theta}$ term, the CP-violating phase in the CKM matrix does not directly induce any of the LECs. Instead, after integrating out the $W^\pm$ boson, the CKM phase induces CP-violating operators such as the quark EDMs and the Weinberg operator. The first SM contributions to these operators appear at three loops (for the electron EDM, no less than four loops are necessary [19, 20]) and are approximately given by [102, 103, 42],

$$\begin{aligned}
d_u &\simeq -\frac{2}{9}\frac{1}{M_W^2}\left(\frac{\alpha_{em}}{4\pi s_w^2}\right)^2 \frac{\alpha_s}{4\pi}\frac{m_s^2}{M_W^2}\ln^2\frac{m_b^2}{m_s^2}\ln\frac{M_W^2}{m_b^2}J, \\
d_d &\simeq -\frac{8}{9}\frac{1}{M_W^2}\left(\frac{\alpha_{em}}{4\pi s_w^2}\right)^2 \frac{\alpha_s}{4\pi}\frac{m_c^2}{M_W^2}\ln^2\frac{m_b^2}{m_c^2}\ln\frac{M_W^2}{m_b^2}J, \\
d_W &\simeq \frac{1}{M_W^2}\left(\frac{\alpha_{em}}{4\pi s_w^2}\right)^2 \frac{g_s^3}{64\pi^2}\frac{m_b^2 m_c^2 m_s^2}{M_W^6}\ln\frac{m_b^2}{m_s^2}\ln\frac{M_W^2}{m_b^2}J,
\end{aligned} \tag{5.5}$$

where $J \equiv \text{Im}\, V_{11}V_{22}V_{12}^*V_{21}^*$ is the Jarlskog invariant in terms of CKM matrix elements. Although these contributions do not scale with M_T^{-2} they are suppressed by loop factors,

Table 5.1: Contributions from the $\bar{\theta}$ term and dimension-six operators to the LECs in Eq. (5.4) [56, 62]. All of the entries are NDA estimates, with exception of the $\bar{\theta}$ contributions to $\bar{g}_{0,1}$ which derive from chiral symmetry arguments. A dash denotes the corresponding operator cannot contribute directly to the LEC. See section 5.1.1 for more details.

	$\bar{\theta}$	d_q	$\tilde{d}_q$	d_W	$\mathrm{Im}\,\Sigma_{1,8}$	$\mathrm{Im}\,\Xi_{1,8}$
$\bar{d}_{0,1}$	$\frac{e\bar{m}}{M_{\rm QCD}^2}$	em_qQ_q	$\frac{e}{4\pi}m_q$	$\frac{eM_{\rm QCD}}{4\pi}$	$\frac{eM_{\rm QCD}}{(4\pi)^2}$	$\frac{eM_{\rm QCD}}{(4\pi)^2}$
$\bar{g}_0$	$\frac{(m_n-m_p)^{\rm strong}(1-\varepsilon^2)}{4\varepsilon F_\pi}$	$\frac{\alpha_{em}}{\pi}$	$m_qM_{\rm QCD}$	$\bar{m}M_{\rm QCD}$	$\frac{\bar{m}M_{\rm QCD}}{4\pi}$	–
$\bar{g}_1$	$\frac{2c_1(\delta m_\pi^2)^{\rm strong}(1-\varepsilon^2)}{\varepsilon F_\pi}$	$\frac{\alpha_{em}}{\pi}$	$m_qM_{\rm QCD}$	$\varepsilon\bar{m}M_{\rm QCD}$	$\frac{\varepsilon\bar{m}M_{\rm QCD}}{4\pi}$	$\frac{M_{\rm QCD}^2}{4\pi}$

small mass fractions, and the Jarlskog invariant. Numerically, the contributions to the quark EDMs are roughly given by $d_q \simeq 10^{-18}\,\mathrm{GeV}^{-2}$ [102], while the Weinberg operator is roughly $d_W \simeq 10^{-27}\,\mathrm{GeV}^{-2}$ [103]. These small contributions clearly allow possible contributions from BSM physics to be dominant. If we assume these operators to be generated at the one-loop level in a BSM scenario, $d_{u,d} \simeq \frac{g_{\rm BSM}^2}{(4\pi)^2}M_{\not T}^{-2} \simeq 10^{-3}M_{\not T}^{-2}$, the scale of new physics can be rather high before the SM contributions start to dominate. Indeed, it is only at a scale of $M_{\not T} \simeq 10^4\,\mathrm{TeV}$ that the BSM contribution would become as small as that of the SM (for the Weinberg operator, using the same assumptions, this scale is even higher). Although this argument shows BSM physics could dominate the SM contribution to the quark EDMs even if it arises at a high scale, this is not necessarily true for the neutron EDM. In fact, in the SM larger contributions to the nucleon EDMs, of the order of $10^{-32}e\,\mathrm{cm}$, are induced through a four-quark operator induced by the CKM phase [104, 105, 106, 42]. Nevertheless, as we will see when considering the nucleon EDMs, even taking this contribution into account there is plenty of room for contributions from BSM physics. The actual contributions of the quark EDMs and Weinberg operator to Eq. (5.4) can be read off from Table 5.1 and will be discussed next.

Contributions of the dimension-six operators

Moving on to the dimension-six operators, we will consider the contributions from the unsuppressed operators in Eq. (4.44), starting with the quark EDMs.

The quark EDMs contribute mainly to the LECs $\bar{d}_{0,1}$, because the non-electromagnetic pion-nucleon interaction is suppressed by the necessity of integrating out the photon appearing in the quark EDM operator. Since $\bar{d}_0$ and $\bar{d}_1$ are isoscalar and isovector quantities respectively, $\bar{g}_0$ is proportional to the summed contributions, $e(Q_um_ud_u + Q_dm_dd_d)$, while $\bar{g}_1$ is induced by the difference, $e(Q_um_ud_u - Q_dm_dd_d)$. These NDA result are consistent with results obtained in quark models [107].

In contrast, the quark CEDM operators induce both $\bar{g}_{0,1}$ and, by including P- and T-even electromagnetic effects, $\bar{d}_{0,1}$. The contributions of these LECs to the neutron EDM, see Eq. (5.6) of the next section, appear formally at the same order (one expects, *a priori*, no cancellation among them) but the chiral logarithm, $\log(m_\pi^2/m_N^2) \simeq -4$, somewhat enhances the $\bar{g}_0$ contribution. Again, due to isospin considerations, $\bar{g}_0$ is induced by

$m_u\tilde{d}_u + m_d\tilde{d}_d$, while the induced $\bar{g}_1$ is proportional to $m_u\tilde{d}_u - m_d\tilde{d}_d$. The contributions to $\bar{d}_{0,1}$ do not necessarily appear in these combinations as the required electromagnetic interaction already breaks isospin. The NDA results for $\bar{g}_{0,1}$ in Table 5.1 are consistent with a calculation using QCD sum rules [108].

The gluon CEDM, d_W, conserves chiral symmetry and, as a consequence, its contribution to $\bar{g}_0$ and $\bar{g}_1$ (the LECs of chiral-symmetry-breaking interactions) require the insertion of the average quark mass $\bar{m}$ and quark mass difference $\varepsilon\bar{m}$ respectively [109, 56]. Due to this requirement, the induced $\bar{d}_{0,1}$ will turn out to give the main contributions to the neutron EDM. The estimates of these LECs is approximately twice as large as a calculation based on QCD sum rules [109] which reflects the intrinsic uncertainty in these kind of estimations.

Next are the FQPS operators with coupling constants $\mathrm{Im}\,\Sigma_{1,8}$. As pointed out in Refs. [74, 56], these operators conserve, just as the gluon CEDM, chiral symmetry such that for these sources $\bar{g}_{0,1}$ again require the insertion of quark masses. This again implies the dominant contribution to the neutron EDM of the FQPS will derive from the induced $\bar{d}_{0,1}$.

Finally, the FQLR operators, with couplings $\Xi_{LR_{1,8}}$, break chiral symmetry and, similar to the quark CEDM, the neutron EDM is determined by both the $\bar{d}_{0,1}$ and $\bar{g}_{0,1}$ contributions. However, for this dimension-six source $\bar{g}_0$ is smaller than one would expect from NDA alone. This is due to the fact that the FQLR is isospin breaking and is therefore unable to contribute to the isospin-conserving LEC $\bar{g}_0$ directly. There is an indirect contribution, which is left behind after eliminating tadpole terms in the χPT Lagrangian [56]. Nevertheless, this contribution is small, due to the proton-neutron mass difference, for details, see Ref. [56]. In contrast, $\bar{g}_1$ can be induced directly, leading to a large $\frac{\bar{g}_1}{\bar{g}_0}$ ratio. As a result of the above the main contribution to the neutron EDM of the FQLR will again derive from the induced $\bar{d}_{0,1}$.

Having discussed the contributions from both SM sources and the dimension-six operators to the χPT Lagrangian, we now move on to discuss the consequences of the interactions in Eq. (5.4) in the nucleon EDMs.

5.1.2 The EDMs of the neutron and proton

The contributions of the LECs in Eq. (5.4) to the neutron and proton EDMs were already briefly mentioned in chapter 3. In summary, the $\bar{d}_{0,1}$ terms give tree-level contributions to the neutron and proton EDMs, $d_{p,n} = \bar{d}_0 \pm \bar{d}_1$, while the remaining interactions contribute to $\bar{d}_{0,1}$ through loop diagrams. The next-to-leading order results are [57, 58, 59]

$$\begin{aligned} d_n &= \bar{d}_0 - \bar{d}_1 + \frac{eg_A\bar{g}_0}{8\pi^2 F_\pi}\left(\ln\frac{m_\pi^2}{m_N^2} - \frac{\pi m_\pi}{2m_N}\right), \\ d_p &= \bar{d}_0 + \bar{d}_1 - \frac{eg_A}{8\pi^2 F_\pi}\left[\bar{g}_0\left(\ln\frac{m_\pi^2}{m_N^2} - \frac{2\pi m_\pi}{m_N}\right) - \bar{g}_1\frac{\pi m_\pi}{2m_N}\right], \end{aligned} \tag{5.6}$$

where the loop divergences have been absorbed in the counterterms of $\bar{d}_{0,1}$.

From the above expression and the contributions listed in Table 5.1, it can be seen that the measurements of the neutron and proton EDMs alone are not very useful to identify

Table 5.2: Bounds on the coupling constants of various dimension-six operators at $M_{\rm QCD}$ and M_W in units of $(100\,\text{TeV})^{-2}$.

	$\mu = M_{\rm QCD}$	$\mu = M_W$
$d_{u,\,d}\,(\mu)$	$\leq \{7.1,\, 6.8\}$	$\leq \{15,\, 14\}$
$\tilde{d}_{u,\,d}\,(\mu)$	$\leq \{17,\, 8.0\}$	$\leq \{18,\, 8.7\}$
$d_W\,(\mu)$	≤ 0.19	≤ 0.42
$\text{Im}\,\Sigma_1\,(\mu)$	≤ 2.3	≤ 0.51
$\text{Im}\,\Sigma_8\,(\mu)$	≤ 2.3	≤ 2.8
$\text{Im}\,\Xi_{LR_1}\,(\mu)$	≤ 2.3	≤ 1.7
$\text{Im}\,\Xi_{LR_8}\,(\mu)$	≤ 2.3	≤ 0.85

the fundamental CP-violating source. In fact, for all the sources in Table 5.1 the neutron and proton EDMs are expected to be of similar size. This estimate, in combination with the significant uncertainties related to it, makes disentangling the different sources difficult using only the nucleon EDMs. On the other hand, the stringent limit on the neutron EDM, $|d_n| \leq 2.9 \cdot 10^{-13}\, e\,\text{fm}$ (90% C.L.) [18], does allow one to constrain the sources. We will do so in the next section.

5.1.3 Bounds from the neutron EDM

Standard Model sources

In principle both the SM sources and the dimension-six operators can be constrained by the neutron EDM limit. However, for the CKM contribution the neutron EDM is too small to be probed by current experiments. As mentioned, the dominant contribution of the CKM phase appears through a flavor-changing four-quark operator induced by the CKM phase. The induced neutron EDM was estimated to be [104, 105, 106]

$$d_n^{\rm CKM} \simeq 10^{-32} e\,\text{cm}, \tag{5.7}$$

which is significantly larger than the contributions induced through the quark EDMs and Weinberg operators. Nevertheless, it is roughly six orders of magnitude below the current experimental sensitivity, thereby leaving room for larger BSM contributions. For example, if we again assume BSM physics generates quark EDMs which scale as $d_{u,d} \simeq \frac{g^2_{\rm BSM}}{(4\pi)^2} M_{\not T}^{-2} \simeq 10^{-3} M_{\not T}^{-2}$, a similar sized EDM could be induced if $M_{\not T} \simeq 10^3\,\text{TeV}$.

On the other hand, the $\bar{\theta}$-term can be constrained by the neutron EDM limit. Combining the estimates in Table 5.1 and Eq. (5.6) one finds $\bar{\theta} \lesssim 10^{-10}$ [28, 110]. In the following we will focus on the dimension-six operators arising from BSM physics, and tacitly assume the possible $\bar{\theta}$ contribution to vanish (or at least, not to cancel the BSM contributions).

Table 5.3: Bounds on the coupling constants of various dimension-six operators. All entries are dimensionless.

	$M_{\not T} = 1\,\text{TeV}$	$M_{\not T} = 10\,\text{TeV}$
$(M_{\not T}^2) d_{u,\,d}\left(M_{\not T}\right)$	$\leq \{1.8,\, 1.8\} \cdot 10^{-3}$	$\leq \{2.1,\, 2.1\} \cdot 10^{-1}$
$(M_{\not T}^2) \tilde{d}_{u,\,d}\left(M_{\not T}\right)$	$\leq \{1.9,\, 0.91\} \cdot 10^{-3}$	$\leq \{1.7,\, 0.94\} \cdot 10^{-1}$
$(M_{\not T}^2) d_W\left(M_{\not T}\right)$	$\leq 5.6 \cdot 10^{-5}$	$\leq 7.0 \cdot 10^{-3}$
$(M_{\not T}^2) \text{Im}\,\Sigma_1\left(M_{\not T}\right)$	$\leq 3.2 \cdot 10^{-5}$	$\leq 2.3 \cdot 10^{-3}$
$(M_{\not T}^2) \text{Im}\,\Sigma_8\left(M_{\not T}\right)$	$\leq 3.3 \cdot 10^{-4}$	$\leq 2.4 \cdot 10^{-2}$
$(M_{\not T}^2) \text{Im}\,\Xi\left(M_{\not T}\right)$	$\leq 1.7 \cdot 10^{-4}$	$\leq 1.7 \cdot 10^{-2}$
$(M_{\not T}^2) \text{Im}\, Y'^{u,\,d}\left(M_{\not T}\right)$	$\leq \{8.9,\, 8.9\} \cdot 10^{-5}$	$\leq \{7.9,\, 7.9\} \cdot 10^{-3}$
$(M_{\not T}^2) \theta'\left(M_{\not T}\right)$	$\leq 2.4 \cdot 10^{-3}$	$\leq 1.5 \cdot 10^{-1}$

Unsuppressed beyond the Standard Model sources

Of the dimension-six operators, the unsuppressed set will generally be more stringently constrained than the suppressed operators. We start by discussing the bounds on the operators which give rise to the unsuppressed contributions to the neutron EDM, i.e. the operators in Eq. (4.44). For the necessary input values we use $g_A \simeq 1.27$, $m_\pi \simeq 137\,\text{MeV}$, $m_N \simeq 938\,\text{MeV}$ [110] and for the quark masses at $\mu = M_{\text{QCD}}$, $m_u(M_{\text{QCD}}) = 3.1\,\text{MeV}$ and $m_d(M_{\text{QCD}}) = 6.5\,\text{MeV}$ [65]. The bounds on these dimension-six coupling constants are shown in table 5.2 for the scales $\mu = M_{\text{QCD}}$ and $\mu = M_W$, giving some insight into the effect of the running between M_{QCD} and M_W on the derived limits.

For the bounds at $\mu > M_{\text{QCD}}$, certain operators contribute to the neutron EDM in different ways. For example, a quark CEDM at M_W induces both a quark EDM and CEDM at M_{QCD} which both contribute to the neutron EDM. In these cases we present the strongest bound and do not take into account possible cancellations between different contributions. The limits in table 5.2 involve order of magnitude estimates from NDA, and thereby contain significant uncertainties. As such, the number of significant digits is not a reflection of the precision involved. All bounds are of order $(100\,\text{TeV})^{-2}$ apart from the bounds on the quark (C)EDMs which are approximately an order of magnitude weaker because they scale with the small quark mass. The running from the electroweak scale to low energies does not affect the bounds by a large amount. For most operators less than a factor two, the exception being the color-singlet FQPS operator whose bound is strengthened by a factor 5. The QCD corrections are thus not very significant, especially not in the light of the order of magnitude NDA estimates involved[2].

It is also possible to set bounds on the couplings in Eq. (4.44) at energies above the electroweak scale. These are the energy scales where one would expect these couplings to arise, bounds the couplings at these scales thus limit the CP-violating sources at

[2]The NDA estimate for the FQLR contribution to the neutron EDM is about an order of magnitude smaller than the result obtained in Ref. [47]. A possible explanation for this discrepancy was already given in Ref. [56], while a more recent analysis indicates the result of Ref. [47] may have been an overestimate [111].

Table 5.4: Bounds on the couplings of various $\not{P}\not{T}$ operators involving heavy bosons. All entries are dimensionless.

	$M_{\not{T}} = 1\,\text{TeV}$	$M_{\not{T}} = 10\,\text{TeV}$
$(M_{\not{T}}^2) C_B\,(M_{\not{T}})$	$\leq 8.1 \cdot 10^{-2}$	≤ 4.6
$(M_{\not{T}}^2) C_W\,(M_{\not{T}})$	$\leq 1.9 \cdot 10^{-2}$	≤ 1.1
$(M_{\not{T}}^2) C_{WB}\,(M_{\not{T}})$	$\leq 1.3 \cdot 10^{-2}$	≤ 0.74
$(M_{\not{T}}^2) C_{d_W}\,(M_{\not{T}})$	≤ 0.11	≤ 11
$(M_{\not{T}}^2) C_{Wu,\,d}\,(M_{\not{T}})$	$\leq \{1.0,\, 0.84\} \cdot 10^{-2}$	$\leq \{0.53,\, 0.45\}$
$(M_{\not{T}}^2) C_{Zu,\,d}\,(M_{\not{T}})$	$\leq \{5.3,\, 2.8\} \cdot 10^{-2}$	$\leq \{2.7,\, 1.4\}$

the scale they are generated. However, this depends on the particular value of $M_{\not{T}}$ in two ways. First, the coupling constants are expected to scale as $\sim M_{\not{T}}^{-2}$. We therefore present bounds on the dimensionless combination $M_{\not{T}}^2 C_i(M_{\not{T}})$ where C_i denotes the various coupling constants. Second, the QCD corrections depend on the particular value of $M_{\not{T}}$ as well. In the first two columns of table 5.3 we present bounds for two values of $M_{\not{T}}$. The last three rows contain couplings which did not appear in table 5.2 because the corresponding operators decoupled from the EFT below the electroweak scale. Although the gluon-Higgs operator only contributes to the qCEDM via a one-loop diagram, the bounds on θ' and $\tilde{d}_q$ are (accidentally) equally strong.

Additionally suppressed beyond the Standard Model sources

Having discussed the bounds on the unsuppressed operators, we now move on to consider the limits on the suppressed operators of Eq. (4.68). Following the results of section 4.3.2 and using the same procedure as employed above, we obtain the results in Table 5.4. The limits on the different operators are all of similar size apart from those on C_{d_W} which are somewhat weaker. A comparison with table 5.3 shows that the bounds on the heavy-boson operators are approximately an order of magnitude weaker than the bounds on the quark (C)EDMs, while they are a factor of $\mathcal{O}(10^2\text{-}10^3)$ weaker than the limits on $\text{Im}\, Y'^q$, $\text{Im}\, \Xi$, and $\text{Im}\, \Sigma_{1,8}$.

It must be stressed that none of the bounds obtained here can simply be used to set bounds on the scale of BSM CP violation, $M_{\not{T}}$. The reason is that the relation between the effective couplings, constrained in Tables 5.3 and 5.4, and $M_{\not{T}}$ depends on the specific scenario of BSM CP violation under consideration. For example, dimension-six operators that are induced by tree-level exchange of new BSM particles will receive a coupling of order, $C \sim g_{BSM}^2 / M_{\not{T}}^2$, where g_{BSM} is a coupling constant and, in this case, $M_{\not{T}}$ stands for the mass of the exchanged particle. Instead, for operators generated by loop diagrams involving BSM particles one expects $C \sim \frac{g_{BSM}^2}{(4\pi)^2} M_{\not{T}}^{-2}$. Therefore, the couplings of the dimension-six operators generally depend on dimensionless factors appearing in the high-energy theory and possibly on factors of 4π arising from integrating out the heavy fields through loop diagrams.

In fact, if the dimension-six operators originate from a weakly-coupled BSM gauge

theory, the couplings $d_{u,d}$ $\tilde{d}_{u,d}$, d_W, θ', and those of the suppressed operators can only be generated at the loop level[3] [113]. In this scenario these couplings will thus be associated with a loop factor $\sim 1/(4\pi)^2 \simeq 10^{-2}$, while compensation factors might arise if the fundamental theory is strongly coupled. In case of such loop factors, the bounds on the quark (C)EDMs are less stringent than one would naively conclude from Table 5.3, corresponding to $M_{\not T} \gtrsim 1\,\text{TeV}$. The couplings $\Sigma_{1,8}$, Ξ, and $Y'^{u,d}$ can be generated at tree level, even when they arise from a weakly-coupled BSM gauge theory. Nevertheless, they might still be suppressed by small couplings or phases. For example, in the minimal left-right symmetric model, $Y'^{u,d}$ is suppressed by the SM light-quark Yukawa couplings [79].

5.1.4 EDMs of light nuclei

The EDMs of the deuteron

The EDM of the lightest bound nucleus, the deuteron, has been investigated in many papers in recent years [114, 99, 115, 116, 117, 74, 98, 118, 119]. From a theoretical point of view, the deuteron is particularly interesting. Not only because its EDM can be described relatively accurately, but also because its spin-isospin properties ensure that the deuteron EDM has rather distinctive properties. In particular, the deuteron EDM depends, already at tree level, on $\bar{g}_1$, while the contribution from $\bar{g}_0$ is suppressed. Moreover, while the $\not P\not T$ pion-nucleon vertices only contribute to the nucleon EDM at the one-loop level, which brings in a loop suppression and counterterms, light-nuclear EDMs depend already at tree-level on the pion-nucleon vertices and counterterms only appear at subleading orders.

At leading order in the EFT, the deuteron EDM obtains two contributions. The first one is simply the contribution from the constituent-nucleon EDMs, which is trivially evaluated as $d_n + d_p$. The second contribution is due to the exchange of a single pion between the nucleons involving a $\not P\not T$ pion-nucleon vertex (i.e., $\bar{g}_0$ or $\bar{g}_1$) and the coupling of the external photon to the proton charge. All calculations are consistent and here we quote the central value and uncertainty of the chiral EFT result [119, 120]:

$$d_D = d_n + d_p + \big[(0.18 \pm 0.023)\,\bar{g}_1 + (0.0028 \pm 0.0003)\,\bar{g}_0\big]\, e\,\text{fm}\,, \tag{5.8}$$

which is almost independent of $\bar{g}_0$.

Employing NDA estimates of Table 5.1 we can now estimate the relative sizes of the deuteron and nucleon EDMs. As the nucleon EDMs depend only very weakly on $\bar{g}_1$ while its contribution to the deuteron EDM is significant, there is a possibility of a hierarchy between the different EDMs. Indeed, this is the case for the sources which induced a large $\bar{g}_1$, namely, the four-quark left-right operator and the quark CEDM. For these two sources the induced deuteron EDM is expected to be roughly an order of magnitude larger than the nucleon EDMs, as can be seen in Table 5.5. For the remaining sources no such hierarchy exists and the deuteron EDM is of roughly the same size as $d_n + d_p$.

[3]The distinction between tree-level and loop-level induced operators is not quite this clear-cut. For instance, when the dimension-six operators originate from a BSM theory which is itself an EFT, these couplings could be induced at tree level [112].

Table 5.5: Predicted ratios for the light nuclei-to-nucleon EDMs, when originating from the $\bar{\theta}$ term or one of the dimension-six operators [74, 62].

	$\bar{\theta}$	d_q	$\tilde{d}_q$	d_W	$\mathrm{Im}\,\Sigma_{1,8}$	$\mathrm{Im}\,\Xi_{1,8}$
$d_D/(d_n+d_p)$	$\mathcal{O}(1)$	$\mathcal{O}(1)$	$\mathcal{O}(\frac{M^2_{\rm QCD}}{m_\pi^2})$	$\mathcal{O}(1)$	$\mathcal{O}(1)$	$\mathcal{O}(\frac{M^2_{\rm QCD}}{m_\pi^2})$
$d_{^3\mathrm{He}}/(d_n+d_p)$	$\mathcal{O}(\frac{M^2_{\rm QCD}}{m_\pi^2})$	$\mathcal{O}(1)$	$\mathcal{O}(\frac{M^2_{\rm QCD}}{m_\pi^2})$	$\mathcal{O}(1)$	$\mathcal{O}(1)$	$\mathcal{O}(\frac{M^2_{\rm QCD}}{m_\pi^2})$
$d_{^3\mathrm{H}}/(d_n+d_p)$	$\mathcal{O}(\frac{M^2_{\rm QCD}}{m_\pi^2})$	$\mathcal{O}(1)$	$\mathcal{O}(\frac{M^2_{\rm QCD}}{m_\pi^2})$	$\mathcal{O}(1)$	$\mathcal{O}(1)$	$\mathcal{O}(\frac{M^2_{\rm QCD}}{m_\pi^2})$

The EDMs of the helion and triton

The experimental EDM storage-ring program not only allows the possible measurement of the proton and deuteron EDMs, but also those of other light nuclei. In particular, measurements on the tri-nucleon EDMs are interesting from the theoretical point of view. The number of nucleons in these systems is small enough in order to be accurately described within chiral effective theory, with nuclear uncertainties which are small compared to the hadronic uncertainties in the LECs. In addition, the tri-nucleon EDMs are complementary to the deuteron EDM, mainly due to their much larger dependence on $\bar{g}_0$.

The ^{3}He and ^{3}H EDMs have been investigated a number of times over the years [121, 122, 74, 118, 119, 120]. Here we quote the results of [119, 120],

$$\begin{aligned} d_{^3\mathrm{He}} &= (0.89\pm0.01)\,d_n - (0.039\pm0.01)\,d_p \\ &\quad +\big[(0.099\pm0.026)\,\bar{g}_0 + (0.14\pm0.028)\,\bar{g}_1\big]\,e\,\mathrm{fm}\ , \\ d_{^3\mathrm{H}} &= -(0.051\pm0.01)\,d_n + (0.87\pm0.01)\,d_p \\ &\quad -\big[(0.098\pm0.024)\,\bar{g}_0 - (0.14\pm0.028)\,\bar{g}_1\big]\,e\,\mathrm{fm}\,. \end{aligned} \tag{5.9}$$

Due to the larger $\bar{g}_0$ dependence with respect to the nucleon or deuteron EDMs, there is again a possibility of a hierarchy between these EDMs and the nucleon EDMs. For ^{3}He and ^{3}H this will be the case for the sources which induce a large $\bar{g}_0$. As can be seen from Table 5.5 this is generally the case, apart from the quark EDMs, the Weinberg and the FQPS operators. These operators induce a small $\bar{g}_0$ either because of the need to integrate out a photon (the quark EDM) or because the operators in question were chiral invariants (the FQPS and Weinberg operators).

In summary, although the nucleon EDMs does not pinpoint the fundamental sources that induce them, the EDMs of light nuclei can give a hint as to their origins, as was pointed out in Ref. [74]. For example, as can be seen from Table 5.5, a deuteron EDM significantly larger than the sum of the neutron and the proton EDM would point towards a quark CEDM or the FQLR operators [99, 74]. Therefore, a measurement of the nucleon and deuteron EDMs could point to, or falsify, the quark CEDMs and the FQLR as the dominant source of CP violation. In addition, Eqs. (5.8) and (5.9) seem to allow for more precise tests. For instance, the relation $d_D - d_n - d_p \simeq 0.18\,\bar{g}_1\,e\,\mathrm{fm}$ implies the measurements of the nucleon and deuteron EDMs would allow for the extraction of $\bar{g}_1$. In turn, Eq. (5.9) would then allow for a prediction of $d_{^3\mathrm{He}}$, if the $\bar{g}_0$ contribution can

be neglected. This would be the case if the FQLR is dominant, as this operator does not generate $\bar{g}_0$ directly, and predicts $\bar{g}_0/\bar{g}_1 \ll 1$. The measurement of $d_{^3\mathrm{He}}$ would then provide a test of the scenario where the FQLR is dominant[4].

There are a number ways in which such an argument could be invalidated. Firstly, in principle, we would like to be able to test the predictions of models of BSM physics, which will generally contain multiple sources of CP violation instead of a single operator. The appearance of multiple operators could alter the test mentioned above. Secondly, there are the additional nucleon-nucleon interactions and the three-pion vertex mentioned earlier which could appear in Eq. (5.4). Whether these interactions are generated by the CP-violating sources depends on the specific model of BSM physics under consideration. Therefore, in order to see whether the EDMs of light nuclei can be used to test models of BSM physics and distinguish between them, a more careful analysis is needed. We will come back to this in chapters 8 and 9, where we will consider exactly such tests in specific models of new physics.

Having discussed the EDMs of light nuclei we will move on to briefly discuss the EDMs of other systems.

5.1.5 EDMs of other systems

In this section we briefly discuss EDMs of other systems which are not the main focus of this thesis. In particular we consider $\not{P}\not{T}$ effects in the paramagnetic atom/molecules ^{205}Tl, YbF, and ThO, which depend on the electron EDM (eEDM) and semi-leptonic four-fermion operators. We also discuss the EDM of the diamagnetic ^{199}Hg atom. There exist strong experimental limits on these EDMs, but atomic and nuclear theory is required to relate the existing experimental bounds on T-violating effects in these complicated systems to an underlying mechanism of CP violation.

The EDMs of paramagnetic systems

So far we have focused on hadronic EDMs, but the electron EDM is, of course, an important observable as well. In general, eEDM measurements are complementary to hadronic EDM measurements because they probe different fundamental parameters. The current strongest bound on the eEDM comes from the limit on a T-violating effect in the molecule ThO [89], leading to $|d_e| \leq 8.7 \cdot 10^{-29} e\,\mathrm{cm}$ (90% C.L.). Strong limits are obtained from the molecule YbF [90, 91] and the paramagnetic atom ^{205}Tl [123] as well.

As in the case of the neutron EDM, the SM contribution to the electron EDM is very small. In fact, it is even smaller than the neutron EDM as it appears only at the four-loop level and should be below $d_e < 10^{-38} e\,\mathrm{cm}$ [19, 124, 20] (assuming no additional CP violation in the neutrino sector, see section 2.4). Another difference with respect to the neutron EDM is that the $\bar{\theta}$ contribution is much smaller in this case. Given the current bound on $\bar{\theta}$ from d_n, this contribution is $d_e(\bar{\theta}) \lesssim 10^{-38} e\,\mathrm{cm}$ [125]. Contributions from $\not{P}\not{T}$ semi-leptonic interactions to T-violating effects in atoms and molecules might be larger

[4]Here we do not consider measurements of the EDM of ^{3}H since, due to its radioactive nature, it is not likely to be measured in a storage-ring experiment.

than those from the eEDM, but also they are strongly suppressed [126]. As a result the SM leaves considerable room for contributions from BSM CP violation.

At first sight, one might not expect the dimension-six operators we have been discussing so far to contribute to either the electron EDM or the semi-leptonic operators, as we have been focusing on hadronic CP violation so far. Indeed, most of the contributions of the dimension-six operators to either the electron EDM or the semi-leptonic operators are suppressed, as usually additional loops are needed to generate either of these operators. Nevertheless, there are some operators which can contribute. Firstly, the quark-Higgs couplings discussed in section 4.2 can induce the semi-leptonic operators discussed above. However, these operators are suppressed by small Yukawa couplings. This suppression implies that the induced EDM of ^{205}Tl or the T-violating effects searched for in YbF and ThO are very suppressed with respect to the generated neutron EDM. This suppression should be of the same order as the suppression of the four-quark interactions discussed in 4.3 compared to the contribution that arise through a two-loop diagram in section 4.2. Likewise, for most of the other operators discussed in previous sections one would also expect the EDMs of paramagnetic systems to be suppressed with respect to the neutron EDM.

However, there is one group of operators which contributes at the same level to the electron EDM as the neutron EDM. This group consists out of the loop-suppressed operators describing purely bosonic interactions, i.e. the operators, O_{W,B,WB,d_W}, which were constrained using the neutron EDM in Table 5.4 (for their definitions, see Eq. (4.68)). These operators induce an electron EDM through the same loop diagrams that induce the quark EDMs, discussed in section 4.3. Some of these operators have been under recent investigation as they can modify the $h \to \gamma\gamma$ rate [84, 76, 85]. In this context, Ref. [85] employed the electron EDM limit to set bounds on O_W, O_B, O_{WB}, and O_{d_W}[5]. Presently, the resulting constraints are approximately two orders of magnitude stronger than those derived in section 5.1.3. The main difference between the eEDM and neutron EDM constraints is due to the fact that the electron EDM limit is roughly 300 times stronger than the neutron EDM limit, although this effect is softened slightly by the smallness of the electron mass with respect to the light-quark mass. Furthermore, the electron EDM is not subject to QCD corrections which suppress the quark EDMs by a small amount when they are evolved to lower energies.

In summary, the electron and neutron EDM searches are complementary because they are sensitive to different $\not{P}\not{T}$ sources. For example, if the dominant $\not{P}\not{T}$ source is the operator O_W, the electron and neutron EDM would be of approximately the same size, whereas if, say, the gluon CEDM is the dominant source, the neutron EDM is expected to be much larger. This illustrates that measurements on different systems are needed to disentangle the fundamental $\not{P}\not{T}$ mechanism, and that the eEDM can provide useful information even when considering CP-violating sources mainly important for hadronic EDMs.

[5]The limits that can be obtained from EDMs are, for all four operators, stronger than limits obtained from accelerator-based experiments [127].

The ^{199}Hg EDM

Schiff's theorem [128] states that in the non-relativistic limit point-like constituents of an atomic system, which interact only electrostatically, completely screen each other's EDMs. This would imply the total EDM of an atomic system is zero. However, in real atoms the necessary conditions for Schiff's theorem to apply are violated. For example, in case of ^{199}Hg, a diamagnetic atom, the largest contribution to the atomic EDM stems from the finite size of the nucleus and is induced by the so-called nuclear Schiff moment $S_{\mathrm{H}g}$.[6] For ^{199}Hg, the relation between the atomic EDM, d_{Hg}, and S_{Hg} is given by [129, 130, 131, 132]

$$d_{\mathrm{Hg}} = (2.8 \pm 0.6) \cdot 10^{-4}\, S_{\mathrm{Hg}}\, \mathrm{fm}^{-2} \ , \tag{5.10}$$

with an uncertainty estimate based on Ref. [133]. While the atomic calculation is rather well under control, the main uncertainties arise from the nuclear-theory calculation of S_{Hg}. Typically it is calculated as a function of the pion-nucleon couplings, cf. Eq. (5.4), and the nucleon EDMs. However, at present there exists no EFT for nuclei with this many nucleons. It is therefore not clear whether or not there will be important contributions from other $\not{P}\not{T}$ hadronic interactions such as the contact interactions in Eq. (8.18). In addition, corrections to leading terms cannot be systematically calculated which means that the uncertainties are difficult to quantify. If we assume that S_{Hg} is dominated by pion-nucleon interactions, the estimated uncertainties are large [134, 135, 129],

$$S_{\mathrm{Hg}} = [(0.37 \pm 0.3)\bar{g}_0 + (0.40 \pm 0.8)\bar{g}_1]\ e\,\mathrm{fm}^3 \ . \tag{5.11}$$

In contrast to the results for the EDMs of light nuclei, here the nuclear uncertainty is dominant and might be difficult to reduce. This implies that the constraints that follow from the limit on the ^{199}Hg atom, $|d_{\mathrm{Hg}}| \leq 3.1 \cdot 10^{-29} e\,\mathrm{cm}$ (95% C.L.) [88] involve large uncertainties. In addition, if a nonzero EDM is measured for ^{199}Hg, these uncertainties would make it difficult to use it as a test for specific scenarios of BSM physics.

Now that we have discussed the EDM searches and what we could learn from them, we will move on to discuss other observables in the next section.

5.2 Other constraints on CP violation

When considering a specific model the BSM interactions will tend to become interdependent, this implies different observables can become linked to one another as well. As a result, some models of new physics can be best constrained by combining measurements of multiple observables. As we will be discussing the left-right model in the upcoming chapters, as preparation it will be useful to consider a number of observables. In particular, we will consider kaon mixing and decays, $\overline{B}_{d,s}$-$B_{d,s}$ mixing, and neutron β decay, and the way these observables can be affected by BSM physics.

[6] The mercury EDM also receives contributions from the electron EDM and $\not{P}\not{T}$ semi-leptonic interactions. However, if we assume all semi-leptonic operators to be of similar size, the measurements in paramagnetic ThO have a greater sensitivity to these interactions, which are thereby better probed in the paramagnetic systems discussed in the previous section [129]. We therefore do not discuss the (semi-)leptonic contributions here.

5.2.1 Meson-mixing observables

The left-right models to be discussed in the upcoming chapter will be tightly constrained by the meson mixing observables considered in this section. The most stringent bounds are obtained when combining the limits from the kaon and B-meson sectors. Here we will start by introducing CP violation in mixing and decays in the kaon sector, after which we will turn to the B-meson sector.

Kaon mixing and decays

In the systems of neutral mesons CP violation can occur indirectly, through mixing, as well as directly in decays. The former process is caused by a misalignment of the CP and mass eigenstates of the mesons. We will write the flavor eigenstates of the kaons as $|K^0\rangle$ and $|\bar{K}^0\rangle$ ($K^0 = (\bar{s}d)$, $\bar{K}^0 = (\bar{d}s)$). The transformation rules under CP are

$$CP|K^0\rangle = -|\bar{K}^0\rangle, \qquad CP|\bar{K}^0\rangle = -|K^0\rangle, \tag{5.12}$$

where we follow the conventions of [136]. Thus, the CP eigenstates will be the linear combinations, $K_{1,2} = 1/\sqrt{2}(K^0 \mp \bar{K}^0)$, such that K_1 (K_2) is even (odd) under CP. The evolution of the mesons is described by the Hamiltonian

$$i\frac{d}{dt}\begin{pmatrix} K^0 \\ \bar{K}^0 \end{pmatrix} = H\begin{pmatrix} K^0 \\ \bar{K}^0 \end{pmatrix}, \qquad H = M - \frac{i}{2}\Gamma, \tag{5.13}$$

where M and Γ are 2×2 hermitian matrices describing the dispersive and absorptive parts of the matrix elements, respectively. In addition, CPT invariance demands $M_{11} = M_{22}$ and $\Gamma_{11} = \Gamma_{22}$. In the SM these matrix elements are determined by box diagrams such as the one depicted in Fig. 5.1.

The above Hamiltonian can be diagonalized by moving to the mass eigenstates. However, these mass eigenstates do not coincide with the CP eigenstates, instead we have,

$$\begin{pmatrix} K_S \\ K_L \end{pmatrix} = \frac{1}{\sqrt{1+|\bar{\varepsilon}|^2}}\begin{pmatrix} 1 & \bar{\varepsilon} \\ \bar{\varepsilon} & 1 \end{pmatrix}\begin{pmatrix} K_1 \\ K_2 \end{pmatrix}, \tag{5.14}$$

thus, for $\bar{\varepsilon} \neq 0$ the mass eigenstates are not CP eigenstates. If we now move to the mass basis, where the Hamiltonian is diagonal, we can deduce that

$$\begin{aligned} M_{L,S} &= M \pm \mathrm{Re}\sqrt{(M_{12} - i/2\Gamma_{12})(M_{12}^* - i/2\Gamma_{12}^*)}, \\ \Gamma_{L,S} &= \Gamma \mp 2\mathrm{Im}\sqrt{(M_{12} - i/2\Gamma_{12})(M_{12}^* - i/2\Gamma_{12}^*)}, \\ \left(\frac{1-\bar{\varepsilon}}{1+\bar{\varepsilon}}\right)^2 &= \frac{M_{12}^* - i/2\Gamma_{12}^*}{M_{12} - i/2\Gamma_{12}}, \end{aligned} \tag{5.15}$$

where $M_{L,S}$ and $\Gamma_{L,S}$ are the masses and decay widths of the mass eigenstates, i.e. $M_{L,S} - i/2\Gamma_{L,S}$ are the eigenvalues of H. It turns out that for both kaon and B-meson mixing the mass difference between the two mass eigenstates is well approximated by $\Delta M = 2|M_{12}|$ [136, 137].

Now turning to the CP violation in the mixing, the parameter used to quantify this is defined through the CP-violating decay parameter [136]

$$\varepsilon = \frac{\langle(\pi\pi)_{I=0}|H|K_L\rangle}{\langle(\pi\pi)_{I=0}|H|K_S\rangle}, \tag{5.16}$$

where $(\pi\pi)_{I=0}$ indicates the two-pion final state has zero strong isospin. This is called indirect CP violation as it occurs through the mixing between the two CP eigenstates. In fact, ε can be related to the mixing parameter $\bar{\varepsilon}$ by plugging in Eq. (5.14)

$$\varepsilon = \bar{\varepsilon} + i\frac{\mathrm{Im}\, A_0}{\mathrm{Re}\, A_0}, \tag{5.17}$$

where A_0 is the amplitude corresponding to the $I = 0$ final state, and we assumed $\mathrm{Im}\, A_0/\mathrm{Re}\, A_0 \ll 1$.

BSM contributions to kaon mixing can then be parametrized by the combinations [138, 139]

$$h_K = \frac{\mathrm{Re}\,\langle\bar{K}^0|\mathcal{H}_{BSM}|K^0\rangle}{\mathrm{Re}\,\langle\bar{K}^0|\mathcal{H}_{SM}|K^0\rangle}, \qquad h_\varepsilon = \frac{\mathrm{Im}\,\langle\bar{K}^0|\mathcal{H}_{BSM}|K^0\rangle}{\mathrm{Im}\,\langle\bar{K}^0|\mathcal{H}_{SM}|K^0\rangle}, \tag{5.18}$$

where $\mathcal{H}_{SM}$ and $\mathcal{H}_{BSM}$ are the effective Hamiltonians describing the SM and BSM interactions responsible for $\bar{K}^0 - K^0$ mixing, respectively. Furthermore, the BSM contribution to the mass difference h_K has been normalized to the experimental value due to the uncertain long-distance parts of the SM contribution. The experimental values of ε and ΔM can then be expressed in terms of the SM contribution and the above parameters as

$$\Delta M = (\Delta M)_{SM}(1 + h_K), \qquad \varepsilon = \varepsilon_{SM}(1 + h_\varepsilon). \tag{5.19}$$

In contrast to ε, the parameter ε' indicates direct CP violation. It is a measure of the CP violation in the decay $K_L \to \pi\pi$, which does not proceed through the mixing between CP eigenstates. As the strong interactions conserve isospin to a good approximation, the relevant matrix elements for these decays can be written as

$$\begin{aligned} \langle\pi^0\pi^0|H|K^0\rangle &= \sqrt{\frac{2}{3}}A_0 e^{i\delta_0} - 2\sqrt{\frac{1}{3}}A_2 e^{i\delta_2}, \\ \langle\pi^+\pi^-|H|K^0\rangle &= \sqrt{\frac{2}{3}}A_0 e^{i\delta_0} + \sqrt{\frac{1}{3}}A_2 e^{i\delta_2}. \end{aligned} \tag{5.20}$$

Here $A_{0,2}$ are again the amplitudes corresponding to the $I = 0, 2$ final states ($\Delta I = 1/2,\ 3/2$ transitions), while $\delta_{0,2}$ are phases induced by the strong interaction. Thus $A_{0,2}$ only contain phases generated by the weak interaction. With these definitions, the measure of direct CP violation can be written as

$$\varepsilon' = \frac{i}{\sqrt{2}}e^{i(\delta_2 - \delta_0)}\mathrm{Im}\,\frac{A_2}{A_0}, \tag{5.21}$$

where the strong phases are determined to be $\delta_2 - \delta_0 \simeq -\pi/4$ [136]. Thus, ε' measures the phase difference between the $I = 0$ and $I = 2$ transitions. We will discuss the contributions from BSM physics, specifically the LR model, in chapter 6.

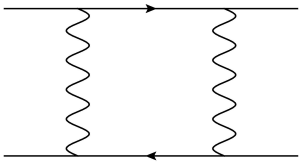

Figure 5.1: The figure shows a typical contribution to meson mixing. The wavy lines represent $W^{\pm}$ bosons, while the external fermions lines are the quarks in the mesons.

Both ε and ε' can be determined from the following decay ratios

$$\eta_{00} = \frac{\langle \pi^0\pi^0|H|K_L\rangle}{\langle \pi^0\pi^0|H|K_S\rangle}, \qquad \eta_{+-} = \frac{\langle \pi^-\pi^+|H|K_L\rangle}{\langle \pi^-\pi^+|H|K_S\rangle}. \tag{5.22}$$

Indeed, if we assume ε and ε' are small and use the fact that $\Delta I = 1/2$ transitions are preferred over $\Delta I = 3/2$ transition, i.e. $\mathrm{Re}\, A_2/\mathrm{Re}\, A_0 \ll 1$, one obtains [136]

$$\eta_{00} = \varepsilon - 2\varepsilon', \qquad \eta_{+-} = \varepsilon + \varepsilon'. \tag{5.23}$$

Experimentally, ε and ε', are currently determined to be [65]

$$|\varepsilon| = (2.228 \pm 0.011)\cdot 10^{-3}, \qquad \mathrm{Re}\,(\varepsilon'/\varepsilon) = (1.65 \pm 0.26)\cdot 10^{-3}. \tag{5.24}$$

We leave a discussion of the contributions in LRMs to the upcoming chapters, and focus on B-meson mixing observables in the next section instead.

$\overline{B}_{d,s} - B_{d,s}$ mixing

$\overline{B}_{d,s} - B_{d,s}$ mixing is described in much the same way as it is in the kaon sector. For example, Eq. (5.15) holds in this case as well, such that the magnitude of M_{12}^q is again related to the mass difference, $\Delta M_{B_q} = 2|M_{12}|$ between the mesons. However, in this case we can, to good approximation, write the combination describing the CP violation in the mixing as follows

$$\frac{1-\bar{\varepsilon}}{1+\bar{\varepsilon}} \simeq -\frac{M_{12}^*}{|M_{12}|}, \tag{5.25}$$

using the notation of the previous section. This is due to the fact that for B mesons, $\Delta\Gamma_{B_q} \ll \Delta M_{B_q}$, their fraction is of the order of $\frac{\Delta\Gamma_{Bq}}{\Delta M_{B_q}} \lesssim \mathcal{O}(1\%)$ in either case [140]. As a result, the phase parametrizes CP violation $B_{d,s}$-meson mixing is

$$\phi_q = \mathrm{Arg} M_{12}^q. \tag{5.26}$$

In the SM M_{12}^q is determined by box diagrams involving $W_L^{\pm}$ bosons, depicted in Fig. 5.1, while in models of BSM physics, such as the LRM, additional contributions can appear. Separating the SM and BSM contributions, $M_{12} = M_{12}^{\mathrm{SM}} + M_{12}^{\mathrm{LR}}$ the new contributions can be parametrized by the quantities

$$M_{12}^q = M_{12}^{\mathrm{SM}}(1+h_q), \qquad h_q \equiv \frac{M_{12}^{\mathrm{BSM}}}{M_{12}^{\mathrm{SM}}}, \qquad h_q = |h_q|e^{i\sigma_q}. \tag{5.27}$$

Thus, the magnitude of $1 + h_q$ can be constrained by the mass differences, while CP violation in B_q mixing as measured by $\phi_{d,s}$ is sensitive to its phase. The BSM contributions to these angles can be written as

$$\phi_q^{\rm BSM} = {\rm Arg}(1 + |h_q| e^{i\sigma_q}), \tag{5.28}$$

The phases ϕ_d and ϕ_s appear in asymmetries of $B_{d,s}$ decays. Currently the averages of experimental measurements give the values [140]

$$-\mathcal{A}_{CP}^{\rm mix}(B_d \to f) = \sin\phi_d = 0.68 \pm 0.02 \quad (68\%\,{\rm CL}), \tag{5.29}$$
$$\mathcal{A}_{CP}^{\rm mix}(B_s \to f') = \sin\phi_s = 0.00 \pm 0.07 \quad (68\%\,{\rm CL}), \tag{5.30}$$

where $f = (J/\psi\, K_S,\, J/\psi\, K_L, \dots)$ and $f' = (J/\psi\,\phi,\, J/\psi\, f_0(980), \dots)$ are all final states involving $\bar{c}c\bar{s}d$ and $\bar{c}c\bar{s}s$ valence quarks, respectively. Currently the value for $\sin\phi_d$ is still compatible with its SM prediction, $\sin\phi_d^{\rm SM} \sim 0.83$ [141], within (theoretical) errors, but is approaching a 3σ level deviation [142]. The SM prediction for $\sin\phi_s^{\rm SM} \sim 0.036$ is also still consistent with the experimental value [141]. The precision of these measurements is expected to improve of course. In the long run, the error in the ϕ_d (ϕ_s) measurements should decrease by roughly a factor 3 (10), while the determination of the mass differences is not expected to improve significantly. This assumes 50 fb^{-1} LHCb and 50 ab^{-1} Belle II data, which may be achieved by the mid 2020's at the earliest [143].

It should be clear that none of the BSM sources of CP violation discussed so far can contribute directly to K or $B_{d,s}$ mixing, as none of them contain strange or bottom quarks. Of course, this is mainly due to our focus on operators which contribute to hadronic EDMs so far. Nevertheless, LRMs do generally give rise to operators which can induce such contributions. Implications of the $\phi_{d,s}$ measurements in terms of bounds for left-right models will be discussed in chapters 6 and 7.

5.2.2 Neutron β decay

Unlike the B-meson mixing processes described above, neutron β decay does receive a contribution from one of the dimension-six operators in the CP-violating EFT. The operator responsible is the right-handed weak current in Eq. (3.12). With regard to the upcoming chapters this interaction is especially interesting as it will play a role in LRMs as well. This interaction can contribute to neutron β decay as it does not only give rise to the FQLR operator, but also to $\not{T}$ semi-leptonic interactions by coupling the $W^\pm$ boson to the left-handed lepton current. The operator produced in this way does not contribute to hadronic EDMs but, instead, contributes to the $\not{T}$ triple correlation $\sim D\,\vec{J}\cdot(\vec{p}_e \times \vec{p}_\nu)$ in nuclear β-decay [52]. Explicitly, this contribution takes the form

$$D \simeq \frac{4 g_V g_A}{g_V^2 + 3 g_A^2} {\rm Im}\left(\frac{\Xi}{2\sqrt{2} V_{ud} G_F}\right), \tag{5.31}$$

where $\langle p|\bar{u}\gamma^\mu d|n\rangle = g_V \bar{p}\gamma^\mu n$ and $\langle p|\bar{u}\gamma^\mu\gamma_5 d|n\rangle = g_A \bar{p}\gamma^\mu\gamma_5 n$.

Both the FQLR operator and its semi-leptonic cousin arise from the same dimension-six operator and depend on the parameter ${\rm Im}\,\Xi(M_T)$. In Ref. [52] it is argued that the best

limit on $\mathrm{Im}\,\Xi(M_T)$ comes from the limit on the neutron EDM. Furthermore, the authors of Ref. [52] used the neutron EDM limit to set a strong constraint on the coefficient D. However, QCD corrections were neglected and one might wonder whether their effect is significant. The semi-leptonic operator does not run under QCD RGE which makes it sufficient to consider only the running of the FQLR operator. The running of the color-singlet FQLR gives an enhancement of 10% which does not alter the results of Ref. [52] in a significant way. In fact, the limit set by the most recent D measurement [144, 145] gives

$$\mathrm{Im}\,\Xi(M_T) \lesssim 3.8 \times 10^{-3}\mathrm{TeV}^{-2}, \tag{5.32}$$

which is indeed weaker, by roughly one to two orders of magnitude, than the bound from the neutron EDM listed in Table 5.3. However, the fact that at low energies not only the color-singlet but also the color-octet operator is present, with a larger coefficient, may be more important. It is difficult to say how this affects the bound obtained in Ref. [52] since this depends on nonperturbative physics linking the FQLR operators to the neutron EDM. In the event of a partial cancellation between the neutron EDM contributions from the color-singlet and color-octet FQLR operators, the bound on the D coefficient would be weakened. In any case, a measurement of D could, in principle, provide additional information which may be used to trace back the fundamental source of CP violation. In the scenario that a nonzero neutron EDM is measured, a measurement of the triple coefficient D could point to, or rule out, the right-handed $W^{\pm}$ current as a dominant source of CP violation. However, seeing the relative strengths of the bounds from the D coefficient and the neutron EDM this would clearly require a significant improved experimental sensitivity. In addition, this would require disentangling the true T-odd effects from electromagnetic final-state interactions, which can mimic these effects and contribute to D at the $\mathcal{O}(10^{-5})$ level [146].

Similar to the link between β decay and EDMs, there also exists a connection between T violation in *radiative* β decay and the neutron EDM. In radiative β decay it is possible to construct a T-odd correlation, $\sim \boldsymbol{p}_\gamma \cdot (\boldsymbol{p}_e \times \boldsymbol{p}_\nu)$ [147, 148, 149], for which the SM background is small [150], such that it might be used as a probe for BSM CP violation. The dimension-six operators which could contribute to this correlation are O_{WB}, O_{W_R} and O_{Wq}, which, as discussed in this thesis, also contribute to hadronic EDMs. In fact, in case the CP-violating BSM physics can be described by dimension-six operators, the analysis of Ref. [151] shows that the EDM searches are far more sensitive to these operators than radiative β-decay experiments. Thus, unless the contributions of these operators to the EDM cancel to a very high degree, possible future radiative β-decay experiments would not be able to constrain the dimension-six operators significantly.

5.3 Summary

A measurement of a nonzero EDM in any of the upcoming experiments would be a major breakthrough. Within the SM, a non-zero hadronic or nuclear EDM at the current experimental accuracies can only originate from the $\bar{\theta}$ term because P and T violation from the quark-mixing matrix is simply too small. Therefore, the severe suppression of

the CKM phase and the non-observation of the $\bar{\theta}$ term leave room for physics beyond the SM. This BSM physics can be parametrized by the dimension-six operators which were discussed in previous chapters. In this chapter we considered their effects on a number of observables, in particular the EDMs of the nucleons and light nuclei.

In section 5.1.3 we have used the neutron EDM limit to set bounds on the seven operators at $M_{\rm QCD}$ using χPT calculations [58, 56]. In order to do so, first their contributions to the interactions in the χPT Lagrangian, Eq. (5.4), was considered, from which the nucleon EDMs and the EDMs of light nuclei could be calculated. By use of the results in chapter 4 these limits were translated into bounds, valid at energies around $M_{\not T}$, on all dimension-six operators that were not additionally suppressed by loop factors or Yukawa couplings.

In addition, we considered the various dimension-six operators which did suffer from additional (loop) suppression. All these operators contain at least one heavy field which decouples below the electroweak scale, generating contributions to the quark EDMs and CEDMs via electroweak one-loop diagrams [39]. These contributions are typically suppressed by $\alpha_w/4\pi$. In section 5.1.3 we have used the neutron EDM limit to set bounds on these dimension-six operators. As one might expect, these bounds are weaker than the bounds on the operators in the first set, but by how much depends on the particular operator.

The calculation of these bounds on the operators with and without additional suppression, concludes the analysis carried out over several chapters, in which the operators were evolved from the scale of new physics down to $M_{\rm QCD}$. Such a comprehensive analysis encompassing all dimension-six operators relevant for hadronic EDMs and their QCD RGE effects was absent from the literature until Ref. [152]. These results make it possible to quickly obtain restrictions imposed by the neutron EDM on specific high-energy models. After performing a matching calculation between the high-energy model and the effective dimension-six operators, these restrictions can be read off immediately. Because the effective Lagrangian is model independent, this framework is useful for any model of new physics. Therefore, we will employ this framework in chapters 8 and 9, where we will consider specific scenarios of BSM physics.

Apart from using the neutron EDM to set bounds section 5.1.4 looked into the possibility of tracing the fundamental source of CP violation, by use of the EDMs of light nuclei. There are interesting proposals to measure these EDMs in storage rings with high accuracy [92, 153, 94, 95]. Such an experimental program could give important complementary information on the dominant $\not P\not T$ mechanism. In Refs. [58, 74] (see also [56, 98]) a strategy has been proposed to (partially) disentangle the $\not P\not T$ sources at the energy scale $M_{\rm QCD}$. For example, as discussed in section 5.1.4, a deuteron EDM significantly larger than the sum of the neutron and the proton EDM would point towards a quark CEDM or the FQLR operators [99, 74]. On the other hand, if the quark EDM is dominant one would expect the deuteron EDM to be close to the sum of the nucleon EDMs [58], also see Table 5.5. Although this strategy is useful for disentangling scenarios where a single source is dominant, it is in principle not clear one could do the same for actual models of BSM physics, where one would expect multiple sources to appear simultaneously. To see whether one could disentangle several models of BSM physics requires a more careful analysis than was adopted in this chapter. We will go into this possibility in more detail

in chapters 8 and 9.

In addition to the EDMs of light nuclei, the EDMs of paramagnetic systems, such as ^{205}Tl, YbF, and ThO, which depend on the electron EDM, could also help to shed light on the fundamental source of CP violation. In fact, some of the dimension-six operators induce, apart from quark EDMs, also contributions to the electron EDM [85] via very similar diagrams. The operators in question are the loop-suppressed operators (O_W, O_B, O_{WB}, O_{d_W}) involving purely bosonic interactions. The limits obtained from the electron EDM on these interactions are stronger than those from the neutron EDM, which is due to the more stringent limit on the electron EDM (both limits are stronger than those from accelerator experiments [85, 127]). What is interesting is that the bosonic operators induce an electron and neutron EDM of similar size, while the remaining dimension-six operators induce a significantly larger neutron EDM. Observation of such a pattern in future experiments could provide a hint towards the fundamental source of P and T violation.

Finally, in preparation for the upcoming chapters, we have considered observables besides EDMs in section 5.2, namely, those connected to meson mixing and neutron β decay. As was already mentioned in the introduction, the constraints in a specific model can be more stringent than those suggested by the EFT approach, as the BSM interactions will be no longer be independent. Therefore, by considering multiple observables one can often strongly constrain specific models. As we will see in the next chapter, strong constraints arise from the B and K meson-mixing observables in the LR model. It is for this reason that we briefly reviewed these mixing processes in section 5.2.1. In addition, we also discussed the T-odd triple correlation, D, in neutron β decay. Apart from the fact that this observable is generated at tree level in the LR model, it also has an interesting connection to the neutron EDM [52]. Although the neutron EDM generally gives stronger constraints than measurements of the D coefficient, the latter could in principle help distinguish between different sources of CP violation, if a nonzero neutron EDM is measured. Similarly, we briefly discussed the link between the neutron EDM and a T-odd correlation in radiative β decay. This T-odd correlation can be induced by a number of the operators discussed in this thesis, namely, O_{WB}, O_{W_R} and O_{Wq}. However, as was shown in Ref. [151], due to the constraints from the neutron EDM, future radiative β decay experiments are unlikely to provide new information on these dimension-six operators.

Chapter 6

Features of minimal left-right models

After the model-independent approach discussed in the previous chapters, we will now turn to a specific model, namely the left-right model (LRM). As mentioned before, in specific models interactions tend to become related to one another, which can lead to links between different observables. As a result, such models can often be strongly constrained by taking multiple observables into account. In the upcoming two chapters we will see to what degree this is the case in LRMs, as well as discuss the fine-tuning present in these models.

Left-right models have been studied extensively as possible physics beyond the SM [11, 12, 13, 154, 155]. LRMs extend the standard model gauge-group to $SU(3)_c \times SU(2)_L \times SU(2)_R \times U(1)_{B-L}$ and possess several attractive features. They offer an interpretation of the $U(1)$ generator in terms of baryon and lepton number and naturally allow for neutrino masses through the see-saw mechanism [156, 157]. Furthermore, the gauge group of the LRM can appear in grand unified theories (GUTs), such as $SO(10)$ and E_6, as an intermediate step [158], while avoiding the $SU(5)$ group which does not always satisfy the proton-decay bounds. But perhaps their most appealing feature is the possibility (but not necessity) of having a symmetry between left- and right-handed particles at high energies, a so-called LR symmetry. LR models employing such a symmetry, LR symmetric models (LRSMs), restore parity (P) and/or charge conjugation (C) invariance at high energies, such that P and/or C violation appear as a low-energy effects. Thus, in these theories the spontaneous breaking of P and/or C accounts for the P and/or C violation in the SM.

From a theoretical standpoint, the most attractive LRSMs might be the more symmetric LRMs. For this reason, we will turn to these C and/or P models in the next chapter, where we will consider how these LRSMs can be constrained by the observables discussed in the previous chapter. In addition to the LRMs with a P and/or C symmetry we will also discuss a LRM which is not necessarily P- or C-symmetric, but is symmetric under a CP transformation. A difference between this CP-symmetric case and the C and/or P models is that the CP is not a LR symmetry; it does not relate left- and right-handed particles. Finally, we will be considering the Higgs sectors of these models, and, in particular, the fine-tuning required within them.

In order to prepare for these discussions we will focus on the LRM in a more general form (the minimal LRM) and its most important features in the current chapter. We start

by introducing the LR model and the possible P and C symmetries it could incorporate. After this we will derive the Higgs potentials for the P, C, and CP symmetric cases. We will discuss these potentials and the fine-tuning they require in chapter 7. Finally, we will consider the way LRMs affect the observables considered in the previous chapter, namely, meson mixing and low-energy observables, such as beta decay and EDMs. The constraints imposed by these observables in the more symmetric versions of the LRM will be discussed in more detail in the next chapter.

6.1 Minimal left-right models

In this section we will discuss minimal left-right models and highlight some of their features. We will start with the basic ingredients of the model, namely, its field content.

6.1.1 Particle content

The gauge group of left-right (LR) models is given by $SU(2)_L \times SU(2)_R \times U(1)_{B-L}$ [11, 12, 13, 154, 155]. While $U(1)_{B-L}$ was a global symmetry in the standard model (SM) it is promoted to a gauge symmetry in the LR model, replacing the role hypercharge ($U(1)_Y$) played in the SM by baryon minus lepton number ($U(1)_{B-L}$) at high energies. As in the SM the left-handed fermions form doublets under $SU(2)_L$. New, with respect to the SM, is that the right-handed fermions now form doublets under the added gauge group, $SU(2)_R$. In order to build these doublets right-handed neutrinos have to be introduced. In short, the fermions are assigned to representations of the above gauge group as follows,

$$\begin{aligned} Q_L &= \begin{pmatrix} u_L \\ d_L \end{pmatrix} \in (2,1,1/3), \qquad Q_R = \begin{pmatrix} u_R \\ d_R \end{pmatrix} \in (1,2,1/3), \\ L_L &= \begin{pmatrix} \nu_L \\ l_L \end{pmatrix} \in (2,1,-1), \qquad L_R = \begin{pmatrix} \nu_R \\ l_R \end{pmatrix} \in (1,2,-1). \end{aligned} \tag{6.1}$$

With the fermions in the above representations a scalar, $\phi \in (2, 2^*, 0)$, is required in order to produce fermion masses. Furthermore, additional scalar fields are introduced to facilitate the breakdown of the LR gauge group to that of the SM. In the LR model under discussion here, which has been often considered e.g. [156, 159, 155, 79], these are two triplets $\Delta_{L,R}$ assigned to $(3,1,2)$ and $(1,3,2)$, respectively. These fields can be written as

$$\phi = \begin{pmatrix} \phi_1^0 & \phi_1^+ \\ \phi_2^- & \phi_2^0 \end{pmatrix}, \qquad \Delta_{L,R} = \begin{pmatrix} \delta_{L,R}^+/\sqrt{2} & \delta_{L,R}^{++} \\ \delta_{L,R}^0 & -\delta_{L,R}^+/\sqrt{2} \end{pmatrix}. \tag{6.2}$$

We will refer to LR models with such a Higgs sector as *minimal* LRMs. Symmetry breaking is realized through the vacuum expectation values (vevs) of the scalar fields,

$$\begin{aligned} \langle \phi \rangle &= \sqrt{1/2} \begin{pmatrix} \kappa & 0 \\ 0 & \kappa' e^{i\alpha} \end{pmatrix}, \\ \langle \Delta_L \rangle = \sqrt{1/2} \begin{pmatrix} 0 & 0 \\ v_L e^{i\theta_L} & 0 \end{pmatrix}, &\qquad \langle \Delta_R \rangle = \sqrt{1/2} \begin{pmatrix} 0 & 0 \\ v_R & 0 \end{pmatrix}, \end{aligned} \tag{6.3}$$

where all parameters are real after gauge transformations have been used to eliminate two of the possible phases [155]. In the first step of symmetry breaking the vev of the right-handed triplet, v_R, breaks the $SU(2)_L \times SU(2)_R \times U(1)_{B-L}$ group down to $SU(2)_L \times U(1)_Y$. This vev also defines the high scale of the model, and gives the main contribution to the masses of the additional gauge bosons, $W_R^\pm$ and Z_R belonging to $SU(2)_R$. At the electroweak scale the vevs of the bidoublet, κ and $\kappa' e^{i\alpha}$, then break $SU(2)_L \times U(1)_Y$ to $U(1)_{\rm EM}$. In turn, these vevs dictate the masses of the $W_L^\pm$ and Z_L bosons, which belong to $SU(2)_L$, while α is the parameter can induce spontaneous CP violation. This implies these vevs are of the electroweak scale,

$$\kappa_+ = v \simeq 246\,\text{GeV}, \tag{6.4}$$

where $\kappa_\pm^2 \equiv \kappa^2 \pm \kappa'^2$. Finally, while the Dirac masses of the fermions are generated by the vevs of ϕ, the vevs of the triplets generate Majorana masses for the neutrinos. As a result, the light neutrinos obtain their masses through both a type-I and a type-II see-saw mechanism. Here type-I refers to the generation of light neutrino masses through the addition of heavy right-handed neutrinos, while the type-II see-saw mechanism refers to the contribution from a triplet scalar field. In the mLRM both of these contributions are present and the light-neutrino mass matrix takes the form

$$m_\nu = M_L - M_{\nu_D}^T M_R^{-1} M_{\nu_D}, \tag{6.5}$$

where $M_{L,R}$ are the Majorana mass matrices for the left- and right-handed neutrinos and M_{ν_D} is the neutrino Dirac mass matrix. All these mass matrices are determined by the couplings of the scalars to the neutrinos and their vevs. In particular, the Majorana masses are generated by the triplet vevs, $M_{L,R} = y_{L,R} v_{L,R}$, while the Dirac mass matrix is generated by the vevs of the bidoublet, $\kappa^{(\prime)}$, such that we schematically have, $M_{\nu_D} = y_D \kappa$, and

$$m_\nu = \mathcal{O}(y_L v_L) - \mathcal{O}\Big(\frac{y_D^2 \kappa^2}{y_R v_R}\Big). \tag{6.6}$$

Because the neutrino masses are no larger than $\mathcal{O}(1\,\text{eV})$, one would expect the terms above not to exceed this scale by much. For for $y_R v_R$ in the TeV range, the type-I see-saw contribution (the second term) can satisfy this constraint only if the neutrino Dirac Yukawa couplings are of similar size as that of the electron.

For the type-II see-saw contribution one would naturally expect[1] that $y_L = \mathcal{O}(1)$ and $v_L \lesssim \mathcal{O}(1\,\text{eV})$. A (much) less stringent upper bound without theoretical prejudice can be derived from the ρ_0 parameter, $\rho_0 \equiv \frac{M_W^2}{M_Z^2 c_W^2}$, defined such that it is 1 to all orders in the SM. Since v_L breaks the global symmetry $(SU(2)_L \times SU(2)_R$, not related to the local gauge symmetries of the LRM) which guarantees $\frac{M_W^2}{c_W^2 M_Z^2} = 1$ at tree level in the SM, it contributes to $\rho_0 - 1$. From a global fit of ρ_0 [65] one can then deduce that $v_L \lesssim 5\,\text{GeV}$.

[1] One could also take y_L to be small. However, in models with a left-right symmetry y_L and y_R are related. In this case, a smaller y_L would decrease the type-II see-saw contribution, but increase the size of the type-I see-saw contributions.

As for the Higgs fields themselves, there are two neutral and two singly-charged would-be-Goldstone bosons. The remaining fields are physical and make up six neutral, two singly-charged, and two doubly charged fields. For approximate expressions of the mass eigenstates and their masses, see e.g. [79, 159, 160]. One of the mass eigenstates plays the part of a SM-like scalar whose mass should be 125 GeV. The non-SM neutral fields arising from the bidoublets are required to be heavy, > 10 TeV in LRMs [161, 138], because they give rise to stringently constrained flavor-changing neutral currents, see section 7.1.1 of chapter 7. The scalars arising from the triplet fields are not as well constrained and can still be relatively light while keeping the flavor-changing scalars heavy [162]. In fact, the doubly charged scalars can still have masses ~ 450 GeV, while in the future, at $\sqrt{s} = 14$ TeV with 300 fb^{-1}, the LHC is expected to probe masses up to 600 GeV [162, 163].

6.1.2 LR symmetries

One of the main motivations for LRMs is the possibility of explaining the broken symmetry between left and right in the SM as a low-energy phenomenon. In LR models it is possible to restore this symmetry at high energies, which is then spontaneously broken at lower energies by the vevs of the scalar fields. There are two possible transformations which qualify as symmetries between left and right[2]

$$\begin{aligned} P: &\qquad Q_L \longleftrightarrow V_P\, Q_R, &&\qquad \phi \longleftrightarrow e^{i\varphi_P}\phi^\dagger, &&\qquad \Delta_L \longleftrightarrow e^{i\phi_P}\Delta_R, \\ C: &\qquad Q_L \longleftrightarrow V_C\, (Q_R)^c, &&\qquad \phi \longleftrightarrow e^{i\varphi_C}\phi^T, &&\qquad \Delta_L \longleftrightarrow e^{i\phi_C}\Delta_R^*, \end{aligned} \tag{6.7}$$

where the superscript c indicates charge conjugation as defined in section 2.3. In the general case $V_{P,C}$ are arbitrary unitary matrices and $\varphi_{C,P}$ and $\phi_{C,P}$ arbitrary phases. However, one can usually pick the basis in which the transformations are simple, $V_{C,P} = \mathbf{1}$, $\varphi_{C,P} = \phi_{C,P} = 0$, the exception is the case where both C and P are imposed.

A LR model with a P or C symmetry is called left-right symmetric. Note that the transformation, CP, obtained by applying C and P in Eq. (6.7) does not interchange left- and right-handed fields and so is not a LR symmetry. Both LR symmetries require the $SU(2)_{L,R}$ gauge couplings to be equal, $g_L = g_R$, at the LR scale, although a difference between the two could be induced when they are evolved down to the electroweak scale. In the past, the case of a P-symmetric LR model was mainly studied [11, 12, 79]. However, recently there has been renewed interest in the C-symmetric case as well [164, 138]. In either case these symmetries impose important restrictions, as we will see later.

6.1.3 Charged gauge-bosons

Perhaps the most characteristic way in which LR models affect observables is through the right-handed charged-current interaction of the $W_R^\pm$ boson. For the quarks it is given by (in the quark-mass basis)

$$\mathcal{L}^{\mathrm{CC}} = \frac{g_L}{\sqrt{2}}\overline{U}_L\gamma^\mu V_L D_L W_{L\mu}^+ + \frac{g_R}{\sqrt{2}}\overline{U}_R\gamma^\mu V_R D_R W_{R\mu}^+ + \mathrm{h.c.}\,, \tag{6.8}$$

[2]There are two other possible transformations on the ϕ fields which would qualify as a left-right symmetry, namely, $\phi \to \tilde{\phi}^\dagger$ and $\phi \to \tilde{\phi}^T$, where $\tilde{\phi} = \tau_2\phi^*\tau_2$. However, as observed in [164] these lead to unrealistic quark mass matrices, $M_u = M_d^\dagger$ in the former case and $\mathrm{Tr}(M_u M_u^\dagger) = \mathrm{Tr}(M_d M_d^\dagger)$ in the latter.

where V_L and V_R are the SM CKM matrix and its right-handed equivalent. However, the gauge fields $W^{\pm}_{L,R}$ are not quite mass eigenstates. The two charged gauge-bosons mix because both of them couple to the bidoublet ϕ which is charged under both $SU(2)$ groups. The mass terms for the charged gauge-bosons are given by

$$\mathcal{L}^{W_{\text{mass}}} = \begin{pmatrix} W^-_{L\mu} & W^-_{R\mu} \end{pmatrix} \begin{pmatrix} \frac{g_L^2}{4}(\kappa^2 + \kappa'^2 + 2v_L^2) & -\frac{1}{2}g_L g_R \kappa\kappa' e^{-i\alpha} \\ -\frac{1}{2}g_L g_R \kappa\kappa' e^{i\alpha} & \frac{g_R^2}{4}(\kappa^2 + \kappa'^2 + 2v_R^2) \end{pmatrix} \begin{pmatrix} W_L^{+\mu} \\ W_R^{+\mu} \end{pmatrix}, \tag{6.9}$$

where $g_{L,R}$ are the coupling constants of $SU(2)_{L,R}$. These gauge couplings will be equal in both the P- and C-symmetric case. The gauge eigenstates are related to the mass eigenstates by

$$\begin{pmatrix} W_L^{+\mu} \\ W_R^{+\mu} \end{pmatrix} = \begin{pmatrix} \cos\zeta & -\sin\zeta e^{-i\alpha} \\ \sin\zeta e^{i\alpha} & \cos\zeta \end{pmatrix} \begin{pmatrix} W_1^{+\mu} \\ W_2^{+\mu} \end{pmatrix}, \qquad \tan\zeta \simeq \frac{g_L}{g_R}\frac{\kappa\kappa'}{v_R^2}, \tag{6.10}$$

where $W^{\pm}_{1,2}$ refer to the mass eigenstates of the charged gauge-bosons. Clearly, after performing the rotation of Eq. (6.10) the lightest $W_1^{\pm}$ boson acquires a right-handed interactions, while the heavy fields obtains a left-handed interactions. The masses themselves are approximately given by

$$M_1^2 \simeq \frac{g_L^2 \kappa_+^2}{4}, \qquad M_2^2 \simeq \frac{g_R^2 v_R^2}{2}. \tag{6.11}$$

Direct searches at the LHC set a lower limit of 2 TeV (95% CL) on the mass of the right-handed $W_R^{\pm}$ from the $W_R^+ \to t\bar{b}$ channel [165]. More stringent limits have been obtained in leptonic decays which rely on certain assumptions about right-handed neutrinos. These limits extend to $M_2 \geq 2.5-3$ TeV [166, 167, 168] for a range of values for the right-handed neutrino mass, M_N. Although these bounds on M_2 depend on M_N the two masses become correlated in some LRSMs after applying constraints from low-energy precision experiments in muon decay, thereby considerably reducing the allowed region in parameter space [169]. The mentioned collider bounds from both types of channels assume the right-handed couplings to be the same as the left-handed couplings, e.g. for the $W_R^+ \to t\bar{b}$ channel $g_L|V_L^{tb}| = g_R|V_R^{tb}|$. Thus, the strength of the above bounds is in part determined by whether or not the model is LR symmetric. If we do not assume any LR symmetry these bounds can be weakened and even be evaded in some cases.

6.1.4 Yukawa couplings

In turn, the masses for the quarks are generated by the interactions of the bidoublet with the quarks. The most general form of the Yukawa interactions respecting the gauge symmetries in the weak basis is

$$-\mathcal{L}_Y = \bar{Q}_L\big(\Gamma\phi + \tilde{\Gamma}\tilde{\phi}\big)Q_R + \text{h.c.} \quad , \tag{6.12}$$

where Γ and $\tilde{\Gamma}$ are complex 3×3 matrices and $\tilde{\phi} \equiv \tau_2\phi^*\tau_2$. After the Higgs fields acquire their vevs this leads to the mass matrices for the quarks

$$M_u = \sqrt{1/2}(\kappa\Gamma + \kappa' e^{-i\alpha}\tilde{\Gamma}), \qquad M_d = \sqrt{1/2}(\kappa' e^{i\alpha}\Gamma + \kappa\tilde{\Gamma}). \tag{6.13}$$

The implications of the possible LR symmetries on the Yukawa sector are the following[3]

$$P: \quad \Gamma = \Gamma^\dagger, \quad \tilde{\Gamma} = \tilde{\Gamma}^\dagger, \tag{6.14}$$

$$C: \quad \Gamma = \Gamma^T, \quad \tilde{\Gamma} = \tilde{\Gamma}^T. \tag{6.15}$$

For the P-symmetric case this means that if α were zero the mass matrices would be hermitian as well. In this limit there is a relation between the left- and right-handed CKM matrices, namely,

$$V_R = S_u V_L S_d, \tag{6.16}$$

where $S_{u,d}$ are diagonal matrices of signs. In general $\alpha \neq 0$ and the above relation will not be satisfied. Nonetheless, in the P-symmetric case, in order to reproduce the observed quark masses, the combination $\kappa'/\kappa \sin\alpha$ should be small [164]. Thus, the quark masses will be nearly hermitian, implying that Eq. (6.16) is approximately correct and the right and left mixing angles should be nearly equal. This was already shown numerically in Refs. [170, 164] and was recently confirmed by an explicit solution of V_R [171].

In the C-symmetric case the mass matrices will be symmetric which implies the following relation between the two CKM matrices [172]

$$V_R = K_u V_L^* K_d, \tag{6.17}$$

where $K_u = \mathrm{diag}(e^{i\theta_u}, e^{i\theta_c}, e^{i\theta_t})$ and $K_d = \mathrm{diag}(e^{i\theta_d}, e^{i\theta_s}, e^{i\theta_b})$ are diagonal matrices of phases, of which one combination can be set to zero, while the rest remains unconstrained. This relation holds irrespective of the value of α. As a result, the mixing angles in both matrices will be equal.

Two more specific (albeit not necessarily minimal) LR models, often discussed in the literature, are the *manifest* and *pseudomanifest* LR models. The former refers to a LR model with P-symmetric Higgs-quark interactions, i.e. P-symmetric Yukawa couplings, and the additional assumption of a vanishing spontaneous phase, $\alpha = 0$ [173, 174]. The manifest LRM thus implies $V_R = S_u V_L S_d$,. A pseudomanifest LR model on the other hand assumes C- and P-symmetric Yukawa couplings, while P and C do not necessarily hold for the rest of the Lagrangian [175, 174]. A pseudomanifest LRM therefore predicts, $V_R = K_u V_L^* K_d$ due to the C symmetry, in addition, as a result of the P symmetry all the phases in the CKM matrices can be expressed in terms of r and α in this case.

Which relation between the left- and right-handed CKM matrices applies has implications for the bounds that can be set on these models. We will come back to this issue when discussing the C and P-symmetric case ($C+P$), the P- or C-symmetric LR models, as well as the (pseudo)manifest cases, in more detail in chapter 7.

In addition to the right-handed CKM the C and P symmetries also have an impact on the Higgs potential, as we will discuss in the next section. Whether the Yukawa couplings and the Higgs potential adhere to the same symmetries depends on the scenario under

[3]Here we considered the case, $V_{C,P} = \mathbf{1}$, $\varphi_{C,P} = \phi_{C,P} = 0$, thereby implicitly taking the basis in which the C or P transformations take a simple form. It not always possible to find a basis in which both transformations take these simple forms, as we will see when discussing the C and P symmetric case in section 7.1.

investigation. We will take the $C+P$-, P-, C-, and CP-symmetric cases, that will be discussed in the next chapter, to mean that the complete Lagrangian is invariant under the corresponding symmetry. Instead, the (pseudo)manifest case also implies a P ($C+P$) symmetry in the Yukawa sector, but not necessarily a P ($C+P$) symmetry in the Higgs potential. Therefore, when discussing the (pseudo)manifest case we will not demand P ($C+P$) invariance of the complete Lagrangian.

6.1.5 The Higgs potential

The final part of the Lagrangian to be discussed is the Higgs potential. Since we intend to discuss the potential for the LR symmetries, P and C as well as the CP-symmetric case, we will give the potentials for these three cases, while relegating the derivations of these, and the general Higgs potential, to appendix 6.A.

The potential invariant under the gauge group and the P symmetry is given by [155]

$$\begin{aligned}
V_H^P \;=\; & -\mu_1^2\,\mathrm{Tr}(\phi^\dagger\phi) - \mu_2^2\big[\mathrm{Tr}(\tilde\phi^\dagger\phi) + \mathrm{Tr}(\phi^\dagger\tilde\phi)\big] - \mu_3^2\big[\mathrm{Tr}(\Delta_L\Delta_L^\dagger) + \mathrm{Tr}(\Delta_R\Delta_R^\dagger)\big] \\
& +\lambda_1\left[\mathrm{Tr}(\phi^\dagger\phi)\right]^2 + \lambda_2\Big(\left[\mathrm{Tr}(\tilde\phi^\dagger\phi)\right]^2 + \left[\mathrm{Tr}(\phi^\dagger\tilde\phi)\right]^2\Big) + \lambda_3\,\mathrm{Tr}(\tilde\phi^\dagger\phi)\,\mathrm{Tr}(\phi^\dagger\tilde\phi) \\
& +\lambda_4\,\mathrm{Tr}(\phi^\dagger\phi)\big[\mathrm{Tr}(\tilde\phi^\dagger\phi) + \mathrm{Tr}(\phi^\dagger\tilde\phi)\big] \\
& +\rho_1\Big(\left[\mathrm{Tr}(\Delta_L\Delta_L^\dagger)\right]^2 + \left[\mathrm{Tr}(\Delta_R\Delta_R^\dagger)\right]^2\Big) \\
& +\rho_2\big[\mathrm{Tr}(\Delta_L\Delta_L)\mathrm{Tr}(\Delta_L^\dagger\Delta_L^\dagger) + \mathrm{Tr}(\Delta_R\Delta_R)\mathrm{Tr}(\Delta_R^\dagger\Delta_R^\dagger)\big] + \rho_3\mathrm{Tr}(\Delta_L\Delta_L^\dagger)\mathrm{Tr}(\Delta_R\Delta_R^\dagger) \\
& +\rho_4\big[\mathrm{Tr}(\Delta_L\Delta_L)\mathrm{Tr}(\Delta_R^\dagger\Delta_R^\dagger) + \mathrm{Tr}(\Delta_R\Delta_R)\mathrm{Tr}(\Delta_L^\dagger\Delta_L^\dagger)\big] \\
& +\alpha_1\,\mathrm{Tr}(\phi^\dagger\phi)\big[\mathrm{Tr}(\Delta_L\Delta_L^\dagger) + \mathrm{Tr}(\Delta_R\Delta_R^\dagger)\big] \\
& +\alpha_2\Big(e^{i\delta_2}\big[\mathrm{Tr}(\tilde\phi^\dagger\phi)\mathrm{Tr}(\Delta_R\Delta_R^\dagger) + \mathrm{Tr}(\phi^\dagger\tilde\phi)\mathrm{Tr}(\Delta_L\Delta_L^\dagger)\big] + \mathrm{h.c.}\Big) \\
& +\alpha_3\big[\mathrm{Tr}(\phi\phi^\dagger\Delta_L\Delta_L^\dagger) + \mathrm{Tr}(\phi^\dagger\phi\Delta_R\Delta_R^\dagger)\big] \\
& +\beta_1\big[\mathrm{Tr}(\phi\Delta_R\phi^\dagger\Delta_L^\dagger) + \mathrm{Tr}(\phi^\dagger\Delta_L\phi\Delta_R^\dagger)\big] \\
& +\beta_2\big[\mathrm{Tr}(\tilde\phi\Delta_R\phi^\dagger\Delta_L^\dagger) + \mathrm{Tr}(\tilde\phi^\dagger\Delta_L\phi\Delta_R^\dagger)\big] \\
& +\beta_3\big[\mathrm{Tr}(\phi\Delta_R\tilde\phi^\dagger\Delta_L^\dagger) + \mathrm{Tr}(\phi^\dagger\Delta_L\tilde\phi\Delta_R^\dagger)\big], \qquad (6.18)
\end{aligned}$$

while the potential in the case of an unbroken C symmetry at high energies is given by

$$\begin{aligned}
V_H^C \;=\;& -\mu_1^2\,\mathrm{Tr}(\phi^\dagger\phi) - \mu_2^2\big[e^{i\delta_{\mu_2}}\mathrm{Tr}(\tilde\phi\phi^\dagger) + \text{h.c.}\big] - \mu_3^2\big[\mathrm{Tr}(\Delta_L\Delta_L^\dagger) + \mathrm{Tr}(\Delta_R\Delta_R^\dagger)\big] \\
&+\lambda_1\left[\mathrm{Tr}(\phi^\dagger\phi)\right]^2 + \lambda_2\Big(e^{i\delta_{\lambda_2}}\left[\mathrm{Tr}(\tilde\phi\phi^\dagger)\right]^2 + \text{h.c.}\Big) + \lambda_3\,\mathrm{Tr}(\tilde\phi^\dagger\phi)\,\mathrm{Tr}(\phi^\dagger\tilde\phi) \\
&+\lambda_4\,\mathrm{Tr}(\phi^\dagger\phi)\big[e^{i\delta_{\lambda_4}}\mathrm{Tr}(\tilde\phi\phi^\dagger) + \text{h.c.}\big] \\
&+\rho_1\Big(\big[\mathrm{Tr}(\Delta_L\Delta_L^\dagger)\big]^2 + \big[\mathrm{Tr}(\Delta_R\Delta_R^\dagger)\big]^2\Big) \\
&+\rho_2\big[\mathrm{Tr}(\Delta_L\Delta_L)\mathrm{Tr}(\Delta_L^\dagger\Delta_L^\dagger) + \mathrm{Tr}(\Delta_R\Delta_R)\mathrm{Tr}(\Delta_R^\dagger\Delta_R^\dagger)\big] + \rho_3\mathrm{Tr}(\Delta_L\Delta_L^\dagger)\mathrm{Tr}(\Delta_R\Delta_R^\dagger) \\
&+\rho_4\big[e^{-i\delta_{\rho_4}}\mathrm{Tr}(\Delta_L\Delta_L)\mathrm{Tr}(\Delta_R^\dagger\Delta_R^\dagger) + e^{i\delta_{\rho_4}}\mathrm{Tr}(\Delta_R\Delta_R)\mathrm{Tr}(\Delta_L^\dagger\Delta_L^\dagger)\big] \\
&+\alpha_1\,\mathrm{Tr}(\phi^\dagger\phi)\big[\mathrm{Tr}(\Delta_L\Delta_L^\dagger) + \mathrm{Tr}(\Delta_R\Delta_R^\dagger)\big] \\
&+\alpha_2\big[e^{i\delta_{\alpha_2}}\mathrm{Tr}(\tilde\phi^\dagger\phi) + \text{h.c.}\big]\big[\mathrm{Tr}(\Delta_L\Delta_L^\dagger) + \mathrm{Tr}(\Delta_R\Delta_R^\dagger)\big] \\
&+\alpha_3\big[\mathrm{Tr}(\phi\phi^\dagger\Delta_L\Delta_L^\dagger) + \mathrm{Tr}(\phi^\dagger\phi\Delta_R\Delta_R^\dagger)\big] \\
&+\beta_1\big[e^{i\delta_{\beta_1}}\mathrm{Tr}(\phi\Delta_R\phi^\dagger\Delta_L^\dagger) + e^{-i\delta_{\beta_1}}\mathrm{Tr}(\phi^\dagger\Delta_L\phi\Delta_R^\dagger)\big] \\
&+\beta_2\big[e^{i\delta_{\beta_2}}\mathrm{Tr}(\tilde\phi\Delta_R\phi^\dagger\Delta_L^\dagger) + e^{-i\delta_{\beta_2}}\mathrm{Tr}(\tilde\phi^\dagger\Delta_L\phi\Delta_R^\dagger)\big] \\
&+\beta_3\big[e^{i\delta_{\beta_3}}\mathrm{Tr}(\phi\Delta_R\tilde\phi^\dagger\Delta_L^\dagger) + e^{-i\delta_{\beta_3}}\mathrm{Tr}(\phi^\dagger\Delta_L\tilde\phi\Delta_R^\dagger)\big]. \qquad (6.19)
\end{aligned}$$

Finally, the CP-symmetric, but not necessarily C- or P-symmetric, potential is given by

$$\begin{aligned}
V_H^{CP} \;=\;& -\mu_1^2\,\mathrm{Tr}(\phi^\dagger\phi) - \mu_2^2\big[\mathrm{Tr}(\tilde\phi^\dagger\phi) + \mathrm{Tr}(\phi^\dagger\tilde\phi)\big] - \mu_{3L}^2\mathrm{Tr}(\Delta_L\Delta_L^\dagger) - \mu_{3R}^2\mathrm{Tr}(\Delta_R\Delta_R^\dagger) \\
&+\lambda_1\left[\mathrm{Tr}(\phi^\dagger\phi)\right]^2 + \lambda_2\Big(\big[\mathrm{Tr}(\tilde\phi^\dagger\phi)\big]^2 + \big[\mathrm{Tr}(\phi^\dagger\tilde\phi)\big]^2\Big) \\
&+\lambda_3\,\mathrm{Tr}(\tilde\phi^\dagger\phi)\,\mathrm{Tr}(\phi^\dagger\tilde\phi) + \lambda_4\,\mathrm{Tr}(\phi^\dagger\phi)\big[\mathrm{Tr}(\tilde\phi^\dagger\phi) + \mathrm{Tr}(\phi^\dagger\tilde\phi)\big] \\
&+\rho_{1L}\big[\mathrm{Tr}(\Delta_L\Delta_L^\dagger)\big]^2 + \rho_{1R}\big[\mathrm{Tr}(\Delta_R\Delta_R^\dagger)\big]^2 \\
&+\rho_{2L}\mathrm{Tr}(\Delta_L\Delta_L)\mathrm{Tr}(\Delta_L^\dagger\Delta_L^\dagger) + \rho_{2R}\mathrm{Tr}(\Delta_R\Delta_R)\mathrm{Tr}(\Delta_R^\dagger\Delta_R^\dagger) \\
&+\rho_3\mathrm{Tr}(\Delta_L\Delta_L^\dagger)\mathrm{Tr}(\Delta_R\Delta_R^\dagger) \\
&+\rho_4\big[\mathrm{Tr}(\Delta_L\Delta_L)\mathrm{Tr}(\Delta_R^\dagger\Delta_R^\dagger) + \mathrm{Tr}(\Delta_R\Delta_R)\mathrm{Tr}(\Delta_L^\dagger\Delta_L^\dagger)\big] \\
&+\alpha_{1L}\,\mathrm{Tr}(\phi^\dagger\phi)\mathrm{Tr}(\Delta_L\Delta_L^\dagger) + \alpha_{1R}\,\mathrm{Tr}(\phi^\dagger\phi)\mathrm{Tr}(\Delta_R\Delta_R^\dagger) \\
&+\big[\mathrm{Tr}(\tilde\phi^\dagger\phi) + \mathrm{Tr}(\phi^\dagger\tilde\phi)\big]\big[\alpha_{2L}\mathrm{Tr}(\Delta_L\Delta_L^\dagger) + \alpha_{2R}\mathrm{Tr}(\Delta_R\Delta_R^\dagger)\big] \\
&+\alpha_{3L}\mathrm{Tr}(\phi\phi^\dagger\Delta_L\Delta_L^\dagger) + \alpha_{3R}\mathrm{Tr}(\phi^\dagger\phi\Delta_R\Delta_R^\dagger) + \beta_1\big[\mathrm{Tr}(\phi\Delta_R\phi^\dagger\Delta_L^\dagger) + \mathrm{Tr}(\phi^\dagger\Delta_L\phi\Delta_R^\dagger)\big] \\
&+\beta_2\big[\mathrm{Tr}(\tilde\phi\Delta_R\phi^\dagger\Delta_L^\dagger) + \mathrm{Tr}(\tilde\phi^\dagger\Delta_L\phi\Delta_R^\dagger)\big] + \beta_3\big[\mathrm{Tr}(\phi\Delta_R\tilde\phi^\dagger\Delta_L^\dagger) + \mathrm{Tr}(\phi^\dagger\Delta_L\tilde\phi\Delta_R^\dagger)\big]. \qquad (6.20)
\end{aligned}$$

In all cases all parameters are real, the P-symmetric potential contains 18 parameters while in the C- and CP-symmetric cases there are 25 and 23 parameters, respectively. This implies that the P-symmetry is the most constraining when it comes to the Higgs potential. However, as we will see in section 7.2 these potentials are all closely related. Furthermore, in general the potential can exhibit explicit CP (or P or C) violation, such as the CP-violating phase of the α_2 terms in the C- and P-symmetric potentials. In addition, the potential will determine the allowed minima, and thereby the vevs of the scalar fields. These vevs in turn determine whether CP (as well as P or C) is spontaneously broken or not. In principle, these two types of breaking could be unrelated, however, as we will

see in the next chapter, the spontaneous CP violation is often related to the terms that explicitly break CP.

6.2 Experimental constraints on CP violation

In this section we will discuss a number of experimental constraints on CP violation in LRMs, namely those from kaon mixing and decays, $\overline{B}_{d,s}$-$B_{d,s}$ mixing, electric dipole moments and neutron β decay. We will discuss the impact of these bounds in specific LRSMs in more detail in the subsequent chapter.

6.2.1 Kaon mixing and decays

As discussed in section 5.2.1, the indirect and direct CP-violating parameters in the kaon sector, ε and ε', can obtain contributions from BSM physics. In LRMs there are additional contributions to ε compared to the SM from box diagrams involving $W_R^\pm$ bosons and tree-level diagrams involving flavor-changing Higgs bosons as depicted in Fig. 6.1 [176]. Furthermore, LR contributions to ε' enter through diagrams in which the kaon decay through a $W_R^\pm$ instead of the SM $W_L^\pm$ boson.

These additional diagrams result in the following contributions [177, 138],

$$\begin{aligned}
\varepsilon'_{LR} &\simeq 2.73\,|\zeta|\big[\sin(\alpha-\theta_u-\theta_d)+\sin(\alpha-\theta_u-\theta_s)\big] \\
&\quad + 0.008\,|\zeta|\big[\sin(\alpha-\theta_c-\theta_d)+\sin(\alpha-\theta_c-\theta_s)\big] + 0.03\,\frac{M_1^2}{M_2^2}\sin(\theta_d-\theta_s), \\
h_\varepsilon^C &\simeq \mathrm{Im}\left[e^{i(\theta_d-\theta_s)}(A_{cc}+A_{ct}\cos(\theta_c-\theta_t+\phi)\right], \\
h_\varepsilon^P &\simeq \mathrm{Im}\left[e^{i(\theta_d-\theta_s)}(A_{cc}+e^{i\phi}A_{ct}\cos(\theta_c-\theta_t)\right],
\end{aligned} \tag{6.21}$$

where $h_\varepsilon^{C,P}$ is defined as in section 5.2.1, while ε'_{LR} is the LR contribution to ε'. Furthermore, A_{cc} (A_{ct}) is related to the LR amplitude for the loop diagram involving two charm quarks (a charm and a top quark) in the intermediate state and $\phi = \mathrm{Arg}\,V_{td}$. Both A_{cc} and A_{ct} depend on M_2 and M_H, numerically A_{cc} is roughly twice as large as A_{ct} [138]. Depending on the particular realization of the LR symmetry, these parameters can lead to strong constraints on the phases in the matrix $K_{u,d}$ relating the left and right CKM matrices [178, 179, 177, 138].

For example, the ε bound, together with the SM prediction, translates into a bound on h_ε. The uncertainty in the SM prediction is of the order of 10% [180], which implies $h_\varepsilon^{P,C} \lesssim 0.1$. As the amplitude A_{cc} is of order $A_{cc} = \mathcal{O}(90)$ for M_2 in the TeV range, and roughly twice as large as A_{ct}, Eq. (6.21) implies that $\theta_d - \theta_s$ should be close to zero or π in the C-symmetric case. As a result, the first term in the LR contribution to ε' will be dominant for relatively large r. The limit on ε' can then be satisfied for small values of r or if the same phase difference is close to π, $|\theta_d - \theta_s| \simeq \pi$.

6.2.2 $\overline{B}_{d,s}$-$B_{d,s}$ mixing

The additional contributions appearing in kaon mixing are analogous to those that appear in B-meson mixing which will be discussed in the next section. The $\overline{B}_{d,s}$-$B_{d,s}$ mixing is

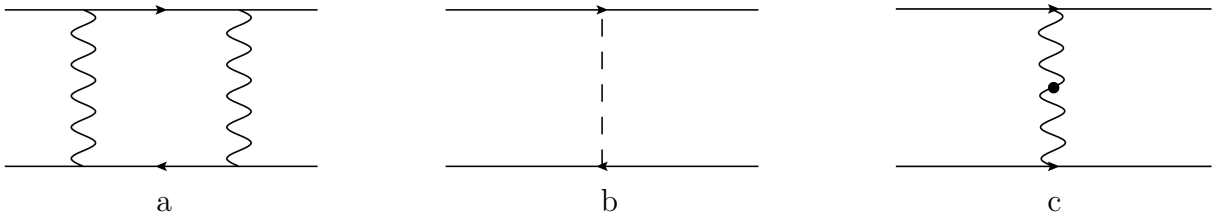

Figure 6.1: Figure a and b show some of the LR contributions to meson mixing. The wavy and dashed lines represent $W^{\pm}_{L,R}$-bosons and flavor-changing Higgs bosons, respectively. The external fermions lines are the quarks in the mesons. The fermion lines now represent up and down quarks while one line represents e and ν in case of β decay and the dot denotes W_L-W_R mixing. Figure c shows the dominant diagram contributing to the neutron EDM and CP violation in neutron β decay (assuming $\bar{\theta} = 0$).

described by the off-diagonal matrix element $M^q_{12} = \langle B_q|\mathcal{H}|\overline{B}_q\rangle/2M_{B_q}$. In the SM M^q_{12} is determined by box diagrams involving $W^{\pm}_L$ bosons. In LRMs there are additional contributions from box diagrams involving $W^{\pm}_R$ bosons and tree-level diagrams involving flavor-changing Higgs bosons. Separating the SM and LRM contributions, $M_{12} = M^{\rm SM}_{12} + M^{\rm LR}_{12}$ as in section 5.2.1 the new contributions are parametrized by

$$M^q_{12} = M^{\rm SM}_{12}(1 + h_q), \qquad h_q \equiv \frac{M^{\rm LR}_{12}}{M^{\rm SM}_{12}}, \qquad h_q = |h_q|e^{i\sigma_q}. \tag{6.22}$$

The above led to the expressions for $\phi_{d,s}$

$$\phi^{\rm LR}_q = {\rm Arg}(1 + |h_q|e^{i\sigma_q}), \qquad \sigma_q \simeq {\rm Arg}\bigg(- \frac{V^{tb}_R V^{tq\,*}_R}{V^{tb}_L V^{tq\,*}_L}\bigg). \tag{6.23}$$

The expressions for h_q can be found in Refs. [178, 179, 138]. Clearly, this contribution depends on the phases present in the CKM matrices. This in turn depends on the choice of LR symmetry. When the phases in V_R are free they can be tuned so as to satisfy the bounds from the CP-violating observables, $\phi_{d,s}$, such these experimental constraints do not necessarily result in a limit on M_2. However, in the more constrained LRSMs these constraints will result in limits on the LR scale.

Implications of these measurements in terms of bounds for the specific $C + P$, P, C, and CP symmetric LRSMs will be discussed in sections 7.1.1, 7.2.1,7.2.2, and 7.2.3, respectively, of chapter 7.

6.2.3 Electric dipole moments

As mentioned before, LR models introduce a number of additional CP-violating sources. At low energies these will generally contribute to EDMs. In the lepton sector this leads to a nonzero electron EDM, while CP-violating interactions in the quark sector EDMs can induce the EDMs of the neutron, proton and light nuclei. In the following we discuss the resulting bounds.

Hadronic EDMs

Hadronic EDMs receive contributions from the CP-violating phases in the CKM matrices and α as well as the QCD-theta term, $\bar{\theta}$. In a general LRM the latter is a free parameter. We will first discuss the case where $\bar{\theta} = 0$, simply assuming this has been achieved through the implementation of a Peccei-Quinn mechanism or in some other way.

When $\bar{\theta} = 0$ hadronic EDMs are dominated by a single interaction which appears at tree level while other contributions only appear at the loop level [80, 47]. At the scale of ~ 1 GeV the operator responsible is the FQLR of chapters 4 and 3,

$$\begin{aligned} \mathcal{L}_{LR} &= -i\,\mathrm{Im}\left(V_L^{ud*}\Xi_1(M_T)\right)\left[\eta_1\left(\bar{u}_R\gamma^\mu d_R\,\bar{d}_L\gamma_\mu u_L - \bar{d}_R\gamma^\mu u_R\,\bar{u}_L\gamma_\mu d_L\right)\right. \\ &\quad \left.+\eta_8\left(\bar{u}_R\gamma^\mu t_a d_R\,\bar{d}_L\gamma_\mu t_a u_L - \bar{d}_R\gamma^\mu t_a u_R\,\bar{u}_L\gamma_\mu t_a d_L\right)\right], \\ \Xi_1(M_T) &= \frac{2}{v^2}\frac{g_R}{g_L}\sin\zeta\; e^{i\alpha}\,V_R^{ud}, \end{aligned} \tag{6.24}$$

where $\eta_1 = 1.1$ and $\eta_8 = 1.4$ are the QCD RGE factors discussed in section 4.2.1. In the LRM this operator is induced by tree-level exchange of $W_L^\pm$-$W_R^\pm$ bosons, see Fig. 6.1c. The large uncertainty related to nonperturbative QCD effects was already pointed out in early studies of the neutron EDM in left-right models [181, 182]. Similar uncertainties still plague the FQLR contribution to the neutron EDM. Nonetheless, if we employ NDA in combination with the upper limit on the neutron EDM, $d_n \leq 2.9 \times 10^{-26}\,e$ cm [18] the bounds of section 5.1.3 translate into

$$\left|\frac{g_R}{g_L}\sin\zeta\,\mathrm{Im}\left(V_L^{ud*}V_R^{ud}e^{i\alpha}\right)\right| \leq 4\cdot 10^{-6}, \tag{6.25}$$

with a considerable theoretical uncertainty. This is about a factor 40 weaker than the upper bound found in Ref. [79]. This is due to the same discrepancy between the NDA estimate and the result of Ref. [47] that was discussed in section 5.1.3.

It is also interesting to consider, in LR models, the EDMs of the proton, deuteron, and helion (^{3}He), due to the plans for measurements in storage rings [92, 93, 94, 95], which were already mentioned in the previous chapter. As discussed in section 5.1.4 one would expect, using NDA estimates, the proton and neutron EDMs to be of similar size, while the deuteron and ^{3}He EDMs are enhanced by about one order of magnitude [56]. This implies the deuteron and ^{3}He EDMs are more sensitive probes of LRMs than the neutron and proton EDMs.

Furthermore, although the lack of knowledge of the nonperturbative physics does not allow for a prediction of the absolute size of these EDMs, it is possible to relate them. This is due to the fact that the dominant contributions come from a single operator whose chiral symmetry properties imply these EDMs are not independent. Thus, the measurements of the EDMs of light nuclei would provide a test of LR models, as was already alluded to in chapter 5. We will discuss this relation between the different EDMs in more detail in chapter 8.

The above no longer applies when $\bar{\theta}$ is not forced to zero by a Peccei Quinn symmetry or by some other mechanism. In this case, when $\bar{\theta}$ is a free parameter, it becomes hard to say something in general about hadronic EDMs. A (partial) cancellation between the $\bar{\theta}$ contribution and that of the operator in Eq. (6.24) can weaken the bound of Eq. (6.25),

or it can even be evaded. However, in the P-symmetric case without a mechanism to enforce $\bar{\theta} = 0$, the $\bar{\theta}$ term is not a free parameter. This is because the P symmetry of the Lagrangian forbids θ (the $G\tilde{G}$ term in the Lagrangian). The leading contribution to $\bar{\theta}$ is then obtained after rotating to the mass basis by a chiral transformation; $\bar{\theta} =$ Arg Det $M_u M_d$, which in this scenario is approximately $\bar{\theta} =$ Arg Det V_R. As a result, $\bar{\theta}$ then becomes calculable in terms of $r \sin\alpha$ and Yukawa couplings [183]. For the P-symmetric case this means that instead of the operator in Eq. (6.24) $\bar{\theta}$ gives the dominant contribution to the neutron EDM by far. The result is a very strong bound on $r \sin\alpha \lesssim \frac{m_b}{m_t} \cdot 10^{-10}$, which in turn implies (through ε) a strong bound on $M_2 \gtrsim 20\,\text{TeV}$ [183]. When considering the P-symmetric case *with* a mechanism to enforce $\bar{\theta} = 0$, there is no $\bar{\theta}$ contribution to the neutron EDM and the constraint resulting from the neutron EDM is that of Eq. (6.25).

In some scenarios this bound on α also has consequences for the leptonic Yukawa couplings as they contribute to α at loop level. Assuming the Dirac Yukawa couplings for the quarks and leptons are similar, a natural leptonic Dirac phase is constrained in this way to be $\lesssim 10^{-3}$ [184]. Such a bound would suppress CP violation in neutrino oscillations beyond the reach of upcoming experiments, making a discussion of α relevant for the lepton sector as well. In return, CP-violating observables in the lepton sector can have implications for α, as we will see in the next subsection.

However, it is possible to suppress $\bar{\theta}$ and thereby the contribution to the nEDM, for example, by implementation of the Peccei-Quinn mechanism. The strong bounds on α and M_2 then no longer apply, the bounds that can be derived instead will be discussed in section 7.2.1.

Returning to the $\bar{\theta} = 0$ case, from the comparison of Eqs. (6.25) and (6.23) it is clear that the neutron EDM and the phases $\phi_{d,s}$ probe different combinations of CP-violating phases. The B-mixing observables, $\phi_{d,s}$, depend on the phases in $V_{L,R}$, while the neutron EDM is also sensitive to α. Furthermore, the neutron EDM only receives contributions from W_L-W_R mixing (Fig. 6.1c) and thus depends on ζ. The best model-independent bound on ζ allows a maximal value of 0.02 [185].[4] Barring cancellations between α and the phases in the right and left CKM matrices, $\zeta \sim 0.01$ will require $\sin\alpha \lesssim 10^{-4}$, but if ζ is smaller, $\sin\alpha$ is of course allowed to be larger. Instead, $\sin\phi_{d,s}$ receive contributions from box diagrams and flavor-changing Higgs exchange (diagrams a and b of Fig. 6.1), resulting in an M_2 and M_H dependence. The CP violation in kaon mixing ε is similar to $\phi_{d,s}$ concerning the dependence on the model parameters while ε' is also sensitive to α. This emphasizes the importance of the different measurements of CP violation, e.g. EDM experiments and the measurements at B factories and LHCb, in order to probe all aspects of CP violation in LR models.

[4] To be precise this bound holds for the combination $\text{Re}\big[\tan\zeta e^{i\alpha}\frac{g_R V_R^{ud}}{g_L V_L^{ud}}\big] \leq 0.02$. Limits of this order of magnitude were already derived in Ref. [186] using hyperon decays, while more stringent limits $\mathcal{O}(10^{-3})$ can be derived if one is willing to make certain assumptions about the CKM matrices [185].

The electron EDM

Measurements of the electron EDM (eEDM) have recently improved considerably and also lead to a strong bound, at present $d_e \leq 8.7 \cdot 10^{-29} e\,\mathrm{cm}$ [89][5]. However, the eEDM is sensitive to other parameters than the hadronic EDMs, in this case the phases of the neutrino mixing matrix enter. Thus, the eEDM and hadronic EDMs are complementary observables. Furthermore, in principle the coupling of the right-handed bosons in the lepton sector may differ from those in the quark sector. Upon demanding anomaly cancellation one can relate the couplings from one sector to the other, but this could be altered by an as yet undiscovered fourth generation.

Another difference is that for the eEDM there are no contributions from a leptonic equivalent of the four-quark operators in Eq. (6.24). This means that there are no tree-level contributions and the eEDM is generated at loop level. The generated eEDM is given by [187, 188]

$$d_e \simeq -\frac{e^3}{16\pi^2 M_W^2}\frac{g_R}{g_L}\sin\zeta\,\mathrm{Im}\big(e^{-i\alpha}(M_{\nu_D})_{ee}\big), \tag{6.26}$$

where $(M_{\nu_D})_{ee}$ is the ee element of the neutrino Dirac-mass-matrix. It is in general not possible to compare the electron EDM to the neutron EDM as the two involve different phases. Nonetheless, we can still try to estimate their relative sizes. Taking the different phases to be of the same order and assuming $|(M_{\nu_D})_{ee}| \simeq m_e$ one finds $d_e/d_n \sim 10^{-4}$ (assuming the LR contributions to be dominant and $\bar{\theta} = 0$).

6.2.4 Neutron β decay

Bounds on LR models can also be obtained from neutron β decay (nβd). In fact, Ref. [189] even claims that current measurements already provide evidence against the *manifest* LRSM [173]. Although not statistically significant, their result does show that especially the correlation between the neutrino direction and the neutron spin, in particular, the asymmetry $\alpha_\nu = 2[N(\theta_\nu < \pi/2) - N(\theta_\nu > \pi/2)]/[N(\theta_\nu < \pi/2) + N(\theta_\nu > \pi/2)]$, is very sensitive to the mass M_2. Here θ_ν is the angle between the neutrino direction and the polarization direction of the neutron. The analysis of [173] assumes that the right-handed current couples equally to leptons and quarks, which is an implicit assumption on the existence and mass of the right-handed neutrinos, namely that the decay to right-handed neutrinos is kinematically allowed. This requires that they should be light ($m_{\nu_R} \leq m_N$), which is not in accordance with a see-saw mechanism as implemented in the minimal LR models under discussion here.

Neutron β decay is sensitive to the CP-violating phase of the mixing between the W_1 and W_2 bosons in a similar but not completely identical way as the neutron EDM. As described in section 5.2.2 the right-handed $W^\pm$-current operator can contribute to both

[5] As already mentioned in section 5.1.5, these experiments actually probe a combination of the eEDM and semi-leptonic four-fermion interactions. In the LRM semi-leptonic interactions originate from tree-level diagrams which involve non-SM Higgs fields and thereby small Yukawa couplings. This, together with the fact that these Higgs fields should be heavy, of order > 10 TeV for LRSMs, see section 7.1.1, implies that d_e will generally dominate.

these observables [52]. In the LRM the lightest $W_1^\pm$ boson indeed obtains right-handed interactions after the rotation of Eq. (6.10) (for the matching of the LRM onto this operator, see chapter 8). Thus, as in section 5.2.2, one would expect the nEDM bound to give the stronger constraint. Indeed, the best current limit from nβd is not as strong as that of the neutron EDM. Assuming $\bar{\theta} = 0$ and heavy right-handed neutrinos, the best bound from nβd is[6]

$$\mathrm{Im}\left(\tan\zeta e^{i\alpha}\frac{g_R}{g_L}\frac{V_R^{ud}}{V_L^{ud}}\right) = (1.0 \pm 2.4)\cdot 10^{-4} \quad (68\%\,\mathrm{CL}), \tag{6.27}$$

which results from employing Eqs. (6.24) and (5.31). For LRSMs and small mixing angles translates into

$$\frac{\kappa\kappa'}{v_R^2}\sin(\alpha+\theta_u+\theta_d) = (1.0 \pm 2.4)\cdot 10^{-4}. \tag{6.28}$$

This bound is obtained from Ref. [185] by using updated experimental results [144, 145], and a lattice determination of $g_A/g_V = 1.20(6)(4)$ [190] to avoid the LR contributions which affect experimental determinations. For LRSMs the neutron EDM bounds the same quantity (also assuming $\bar{\theta} = 0$) and is much stronger, see Eq. (6.25), thus for LRSMs this bound is superseded by the nEDM constraint. However, for more general LRMs a comparison of the two observables would be sensitive to a deviation from $|V_L^{ud}| = |V_R^{ud}|$. Another way to detect deviations from the LR symmetric case is proposed in Ref. [191] which shows that a study using b-tags at the LHC would be sensitive to deviations of $|V_R^{tb}|$ from $|V_L^{tb}|$.

6.3 Summary

In this chapter we have introduced the minimal left-right model and some of its general features. This model has certain theoretically attractive aspects, such as the automatic implementation of the type-I and type-II neutrino see-saw mechanisms, and the possibility of a symmetry between left- and right-handed particles at high energy and spontaneous CP violation at low energy. In addition, we presented the Higgs potentials for the LRMs with a C, P, or CP symmetry (and derived them in appendix 6.A), as, to our knowledge the C- and CP-symmetric potentials were absent from the literature. Furthermore, the contributions to a number of observables were discussed.

In particular, we discussed the LR contributions to CP violation in $B_{d,s}$ and kaon mixing, the neutron and electron EDMs as well as CP violation in neutron β decay. The contributions to meson mixing observables are generally complementary to the other CP-violating observables. This is because the meson-mixing observables depend on the phases in the CKM matrices while the remaining observables also contain an α dependence. Only in special cases, such as the P-symmetric case where V_R can be expressed in terms of r and α, can these observables become related. Similarly, the electron and neutron EDM generally probe different parameters of the LRM; the electron EDM depends on the

[6]This bound is altered if we assume the right-handed neutrinos to be light. Again, this is not what one would expect in a LRM using the scalar triplets of Eq. (6.2), however, this can be achieved in a LRM using doublets instead [154].

phases in the neutrino Dirac-mass-matrix, while the neutron EDM depends on the CKM matrices. In contrast, the neutron EDM and the CP-violating D coefficient in neutron β decay do depend on very similar parameters. For LRSMs these experiments probe the same quantities and the constraint from the neutron EDM sets a much stronger limit.

These general considerations will be of use when we move on to more symmetric LRMs which have an unbroken discrete symmetry, P, C, and/or CP at high energies in the next chapter. As already mentioned, the C and/or P symmetries of these models will have an effect on the contributions of these models to the observables discussed in this chapter. As we have seen in section 6.2, many observables, especially those characterizing CP violation in meson mixing, depend on elements of the right-handed CKM matrix. In the general minimal LRM this right-handed CKM matrix as well as the gauge coupling, g_R are free parameters, however, in models with an additional left-right symmetry this is no longer the case. Indeed, as was discussed in section 6.1.4, in these cases, as well as in the manifest and pseudomanifest LRMs, there is a relation between the left- and right-handed CKM matrices. Therefore, in addition to being attractive theoretically, the more symmetric LRMs are more predictive than general LRMs. For these reasons we will consider LR models with a C, P, or CP symmetry and the (pseudo)manifest LRM in the upcoming chapter.

Appendix 6.A The Higgs potential

The goal of this appendix is to derive the Higgs potentials discussed in section 6.1.5. In order to do so we will derive the most general Higgs potential invariant under $SU(2)_L \times SU(2)_R \times U(1)_{B-L}$, with the field content of the minimal LRM, after which we will apply the additional constraints required for C, P, or CP invariance.

6.A.1 The general Higgs potential

In minimal LRMs the Higgs fields transform according to the following representations of $SU(2)_L \times SU(2)_R \times U_{B-L}$,

$$\phi \sim (1/2, 1/2^*, 0), \quad \tilde{\phi} \equiv \tau_2 \phi^* \tau_2, \qquad \delta_L \sim (1, 0, 2), \qquad \delta_R \sim (0, 1, 2). \tag{6.29}$$

Explicitly, the transformation rules under $SU(2)_{L,R}$ are

$$\phi_{ij} \to (1 + i\alpha_L^i \tau^i/2)_{ik} \phi_{kl} (1 - i\alpha_R^i \tau^i/2)_{lj}, \qquad \delta_{L,R}^i \to (1 - \alpha_{L,R}^j \epsilon_{ijk}) \delta_{L,R}^k. \tag{6.30}$$

Here the $\delta_{L,R}$ fields are in the adjoint representations of $SU(2)_{L,R}$, while the $\Delta_{L,R}$ fields, composed out of $\delta_{L,R}$, transform as

$$\Delta_{L,R} \to (1 + i\alpha_{L,R}^i \tau^i/2) \Delta_{L,R} (1 - i\alpha_{L,R}^i \tau^i/2). \tag{6.31}$$

The δ and Δ both describe the same set of scalar triplet fields. We will find it convenient to employ the δ fields throughout this appendix, while the Δ are commonly used in the literature to represent the scalar triplet fields. In order to see how the δ and Δ fields are related we can use the fact that

$$Q = \frac{B - L}{2} + T_{3L} + T_{3R}, \tag{6.32}$$

from which one can deduce that the combination $\delta^0 \equiv (\delta_1 + i\delta_2)/\sqrt{2}$ is neutral, $\delta^+ \equiv \delta_3$ is singly charged, and $\delta^{++} \equiv (\delta_1 - i\delta_2)/\sqrt{2}$ is doubly charged, where we suppressed the L, R subscripts for brevity. For the ϕ fields we find two neutral scalars, $\phi_1^0 \equiv \phi_{11}$ and $\phi_2^0 \equiv \phi_{22}$, and two singly-charged scalars, $\phi_1^+ \equiv \phi_{12}$ and $\phi_2^- \equiv \phi_{21}$. We can then write these fields as

$$\Delta \equiv \tau \cdot \delta/\sqrt{2} = \begin{pmatrix} \delta^+/\sqrt{2} & \delta^{++} \\ \delta^0 & -\delta^+/\sqrt{2} \end{pmatrix}, \qquad \phi = \begin{pmatrix} \phi_1^0 & \phi_1^+ \\ \phi_2^- & \phi_2^0 \end{pmatrix}, \tag{6.33}$$

such that Δ transforms as expected,

$$\Delta \to (1 + i\alpha^i \tau^i/2) \Delta (1 - i\alpha^i \tau^i/2). \tag{6.34}$$

This particular combination of fields has the following property $\tilde{\Delta} \equiv \tau_2 \Delta^* \tau_2 = -\Delta^\dagger$.

In order to build to most general Higgs potential, we will have to find all possible combinations of the above fields which form singlets under $SU(2)_L \times SU(2)_R \times U(1)_{B-L}$. To create such singlets it is clear we need an equal number of Δ and Δ^* fields due to their $B - L$ charge. We will also need an even number of ϕ fields as it is not possible to construct a singlet with an odd number of doublets. This already implies there are no invariant dimension-one or dimension-three terms. We therefore start by considering the possible dimension-two terms.

Dimension-two terms

- *Terms involving two ϕ fields*

There is just one way to combine two doublets to form a singlet under $SU(2)$. Therefore if we want to combine two ϕ fields, which we will denote as $\phi_1 \in \{\phi, \tilde{\phi}\}$ and $\phi_2 \in \{\phi, \tilde{\phi}\}$, there is just one way to do this,

$$\phi_1^{ij}\epsilon_{ik}\epsilon_{jl}\phi_2^{kl} = \mathrm{Tr}(\phi_1\tilde{\phi}_2^\dagger), \tag{6.35}$$

where the left (right) indices of the ϕ fields are $SU(2)_L$ ($SU(2)_R$) indices. Considering all the possible combinations for $\phi_{1,2}$, we obtain three invariant terms,

$$A_1 = \mathrm{Tr}(\phi\phi^\dagger) = \mathrm{Tr}(\tilde{\phi}\tilde{\phi}^\dagger), \qquad A_2 = \mathrm{Tr}(\phi\tilde{\phi}^\dagger), \qquad A_3 = \mathrm{Tr}(\tilde{\phi}\phi^\dagger) = A_2^*. \tag{6.36}$$

- *Terms involving two δ fields*

Similarly, there is one way to build a singlet from two triplets, namely, $\delta \cdot \delta$. Thus, if we want to combine two δ fields, $\delta_1 \in \{\delta, \delta^*\}$ and $\delta_2 \in \{\delta, \delta^*\}$ (δ can be either δ_L or δ_R), we have the following $SU(2)$-invariant term,

$$\delta_1 \cdot \delta_2 = \mathrm{Tr}(\Delta_1\Delta_2) \tag{6.37}$$

where $\Delta_{1,2} \in \{\Delta, \Delta^\dagger\}$. Note that δ and δ^* transform in the same way as these fields are in a real representation.

In this case, not all the possible combinations of $\delta_{1,2}$ give rise to invariant terms. Clearly the two fields need to have the same handedness in order to be $SU(2)_{L,R}$ invariant and $B - L$ requires equal number of Δ and Δ^* fields. We therefore have two options

$$A_{L,R} = \mathrm{Tr}(\Delta_{L,R}\Delta_{L,R}^\dagger) \tag{6.38}$$

Due to the fact that an even number of ϕ and δ fields are needed in order to build an invariant, this concludes the dimension-two invariants.

Dimension-four terms

- *Terms involving four ϕ fields*

To start with, all possible combinations of $A_{1,2,3}$ invariants we found previously fall in this category.

Additionally, we have combinations of four doublets. The decomposition of $1/2 \otimes 1/2 \otimes 1/2 \otimes 1/2$ gives two ways to construct singlets. For four doublets a, b, c, d, we can build a singlet by combining pairs of fields into singlets, $(ab)^0(cd)^0$, or by combining pairs into triplets whose combination gives a singlet, $(ab)^1(cd)^1$ (plus possible permutations). However, the latter combination can be rewritten, $(ab)^1(cd)^1 \sim 2(ad)^0(bc)^0 - (ab)^0(cd)^0$. Therefore, we only have to consider the first way to construct singlets, $(ab)^0 = a_i\epsilon_{ij}b_j$. As we have both $SU(2)_L$ and $SU(2)_R$ invariance to deal with, we need to find all ways to contract the indices of

$$\phi_1^{ij}\phi_2^{kl}\phi_3^{mn}\phi_4^{op} \tag{6.39}$$

using epsilon tensors. Here $\phi_{3,4}$ are defined similarly to $\phi_{1,2}$. Choosing to contract the $SU(2)_L$ indices of the ϕ_1 and ϕ_2 fields, and thereby ϕ_3 with ϕ_4, we are left with two options; we can connect the $SU(2)_R$ indices in the same way or contract ϕ_1 with ϕ_4 and ϕ_2 with ϕ_3 instead (the 1-3 and 2-4 option is simply a relabeling of this term).

The first option gives rise to terms in which the four ϕ fields are split up into pairs which are singlets under both $SU(2)_L$ and $SU(2)_R$ by themselves. These terms are therefore made up out of combinations of the $A_{1,2,3}$ invariants found earlier.

Instead, the second option gives

$$\mathrm{Tr}(\tilde{\phi}_1^\dagger \phi_2 \tilde{\phi}_3^\dagger \phi_4), \tag{6.40}$$

again letting $\phi_i \in \{\phi, \tilde{\phi}\}$ we have sixteen possibilities. However, these terms are not all independent. By writing the ϕ fields as combinations of Pauli matrices one can derive

$$\begin{aligned} \tilde{\phi}^\dagger\phi &= \frac{1}{2}\mathrm{Tr}(\tilde{\phi}^\dagger\phi)\mathbf{1}, \qquad \tilde{\phi}\phi^\dagger = \frac{1}{2}\mathrm{Tr}(\phi^\dagger\tilde{\phi})\mathbf{1}, \\ \phi^\dagger\phi + \tilde{\phi}^\dagger\tilde{\phi} &= \mathrm{Tr}(\phi^\dagger\phi)\mathbf{1}, \qquad \phi\phi^\dagger + \tilde{\phi}\tilde{\phi}^\dagger = \mathrm{Tr}(\phi^\dagger\phi)\mathbf{1}. \end{aligned} \tag{6.41}$$

With these relations one can show that all the sixteen options can be written in terms of $A_{1,2,3}$. In fact, changing notation slightly for the moment, $\phi_i = (\phi, \tilde{\phi})$, $i = 1, 2$, the sixteen options,

$$Z_{ijkl} = \mathrm{Tr}(\tilde{\phi}_i^\dagger \phi_j \tilde{\phi}_k^\dagger \phi_l), \tag{6.42}$$

are given by

$$\begin{aligned} Z_{1111} &= 1/2A_2^2, \qquad Z_{2222} = 1/2A_3^2, \\ Z_{1112} &= Z_{1121} = Z_{1211} = Z_{2111} = 1/2A_2A_1, \\ Z_{1122} &= Z_{2211} = Z_{1221} = Z_{2112} = 1/2A_2A_3, \\ Z_{1222} &= Z_{2122} = Z_{2212} = Z_{2221} = 1/2A_1A_3, \\ Z_{1212} &= Z_{2121} = A_1^2 - 1/2A_2A_3. \end{aligned} \tag{6.43}$$

- *Terms involving four δ fields*

Similar to the previous category, combinations of $A_{L,R}$ fall in this category as well.

In the case of four δ fields we either need two left- and two right-handed fields or four fields of the same handedness (any other possibility would require a single δ_L or δ_R field to appear). The first option has to be built up out of singlets of the form of Eq. (6.37). However, there are now additional ways to satisfy $B - L$ invariance. This gives two new options,

$$B_{LR} = \mathrm{Tr}(\Delta_L\Delta_L)\mathrm{Tr}(\Delta_R^\dagger\Delta_R^\dagger), \qquad B_{RL} = \mathrm{Tr}(\Delta_R\Delta_R)\mathrm{Tr}(\Delta_L^\dagger\Delta_L^\dagger). \tag{6.44}$$

For the second possibility we have the combination of four triplets, $1 \otimes 1 \otimes 1 \otimes 1$ the decomposition of which gives rise to three ways to construct a singlet. However, these are equivalent, for triplets, a, b, c, d we have

$$\begin{aligned} (ab)^1(cd)^1 &\sim (ac)^0(bd)^0 - (ad)^0(bc)^0, \\ (ab)^2(cd)^2 &\sim (ac)^0(bd)^0 + (ad)^0(bc)^0 - \frac{2}{3}(ab)^0(cd)^0. \end{aligned} \tag{6.45}$$

Thus, we simply have to use the combination Eq. (6.37) in all possible ways. Again there are additional ways to construct a term with zero $B-L$ number, namely,

$$B_{LL} = \mathrm{Tr}(\Delta_L\Delta_L)\mathrm{Tr}(\Delta_L^\dagger\Delta_L^\dagger), \qquad B_{RR} = \mathrm{Tr}(\Delta_R\Delta_R)\mathrm{Tr}(\Delta_R^\dagger\Delta_R^\dagger). \tag{6.46}$$

- *Terms involving two ϕ and two δ fields*

(i) δ fields of the same handedness

The combination of two doublets and two triplets, $1/2 \otimes 1/2 \otimes 1 \otimes 1$ allows for two ways to build singlets. The first is schematically of the form

$$(\phi_1\phi_2)^0(\delta_1\delta_2)^0, \tag{6.47}$$

clearly both brackets are invariants by themselves, therefore the first will be given by $A_{1,2,3}$ while the second is given by $A_{L,R}$. Thus, these terms are combinations of $A_{1,2,3}$ and $A_{L,R}$.

The second way to build an invariant is

$$(\phi_1\phi_2)^1(\delta_1\delta_2)^1, \tag{6.48}$$

where the superscript of $(\phi_1\phi_2)^1$ corresponds to the representation of the $SU(2)$ group under which the δ fields are charged. Thus, under the $SU(2)$ group under which the δ fields are singlets the ϕ's in the first bracket should form a singlet. Furthermore, one of the $\delta_{1,2}$ fields should be the charge-conjugated field in order to preserve $B-L$. With these considerations the above term can then be written as (for left-handed δ fields)

$$\begin{aligned} \mathrm{Tr}(\phi_1^\dagger\tau^k\phi_2)\delta_L^i\epsilon_{ijk}\delta_L^{j*} &= -i\,\mathrm{Tr}(\phi_1^\dagger\left[\Delta_L,\,\Delta_L^\dagger\right]\phi_2) \\ &= 2\,\mathrm{Tr}(\phi_1^\dagger\Delta_L\Delta_L^\dagger\phi_2) - \mathrm{Tr}(\phi_1^\dagger\phi_2)\mathrm{Tr}(\Delta_L\Delta_L^\dagger), \end{aligned} \tag{6.49}$$

where we used the (anti)commutation relations of the Pauli matrices. The last term is a combination of $A_{1,2,3}$ and $A_{L,R}$ and therefore nothing new. Again letting $\phi_{1,2}$ to be $\phi, \tilde{\phi}$ we have four new options, which are again not independent,

$$\begin{aligned} \mathrm{Tr}(\phi^\dagger\Delta_L\Delta_L^\dagger\phi) &\equiv C_L, \\ \mathrm{Tr}(\tilde{\phi}^\dagger\Delta_L\Delta_L^\dagger\phi) &= \mathrm{Tr}(\phi^\dagger\Delta_L\Delta_L^\dagger\tilde{\phi})^* = 1/2A_2A_L, \\ \mathrm{Tr}(\tilde{\phi}^\dagger\Delta_L\Delta_L^\dagger\tilde{\phi}) &= -C_L + A_1A_L. \end{aligned} \tag{6.50}$$

Thus, there is just one new independent combination. The case for right-handed δ fields is analogous and gives

$$C_R = \mathrm{Tr}(\phi\Delta_R\Delta_R^\dagger\phi^\dagger). \tag{6.51}$$

(ii) δ fields of different handedness

In this case we have, for both $SU(2)_L$ and $SU(2)_R$, $1/2 \otimes 1/2 \otimes 1$ which allows just one way to build a singlet, namely,

$$(\phi_1\phi_2)^1\delta. \tag{6.52}$$

Taking both $SU(2)$ groups and triplets into account this takes the form

$$\mathrm{Tr}(\phi_1^\dagger \tau^i \phi_2 \tau^j)\delta_{1L}^i \delta_{2R}^j. \tag{6.53}$$

Letting $\delta_{1L,2R} \in (\delta_{L,R}, \delta_{L,R}^*)$ and $\phi_{1,2} \in (\tilde{\phi}, \phi)$ there are eight possibilities (after taking into account the $B-L$ constraint) of which six are independent,

$$\begin{aligned} D_1 &= \mathrm{Tr}(\phi^\dagger \Delta_L \phi \Delta_R^\dagger), & D_1^* &= \mathrm{Tr}(\phi^\dagger \Delta_L^\dagger \phi \Delta_R)^*, \\ D_2 &= \mathrm{Tr}(\phi^\dagger \Delta_L \tilde{\phi} \Delta_R^\dagger), & D_2^* &= \mathrm{Tr}(\tilde{\phi}^\dagger \Delta_L^\dagger \phi \Delta_R)^*, \\ D_3 &= \mathrm{Tr}(\tilde{\phi}^\dagger \Delta_L \phi \Delta_R^\dagger), & D_3^* &= \mathrm{Tr}(\phi^\dagger \Delta_L^\dagger \tilde{\phi} \Delta_R)^*, \\ \mathrm{Tr}(\tilde{\phi}^\dagger \Delta_L \tilde{\phi} \Delta_R^\dagger) &= \mathrm{Tr}(\phi^\dagger \Delta_L^\dagger \phi \Delta_R)^* = D_1. \end{aligned} \tag{6.54}$$

Summary of possible terms

In total we then have 32 terms, of which five are dimension-two terms,

$$\begin{aligned} A_1 = \mathrm{Tr}(\phi\phi^\dagger), \qquad A_2 = \mathrm{Tr}(\phi\tilde{\phi}^\dagger), \qquad A_3 = \mathrm{Tr}(\tilde{\phi}\phi^\dagger) = A_2^*, \\ A_{L,R} = \mathrm{Tr}(\Delta_{L,R}\Delta_{L,R}^\dagger). \end{aligned} \tag{6.55}$$

For the dimension-four terms we have the fifteen possible combinations of the $A_{1,2,3,L,R}$ terms. Additionally,

$$\begin{aligned} B_{LL} &= \mathrm{Tr}(\Delta_L\Delta_L)\mathrm{Tr}(\Delta_L^\dagger\Delta_L^\dagger), & B_{RR} &= \mathrm{Tr}(\Delta_R\Delta_R)\mathrm{Tr}(\Delta_R^\dagger\Delta_R^\dagger), \\ B_{LR} &= \mathrm{Tr}(\Delta_L\Delta_L)\mathrm{Tr}(\Delta_R^\dagger\Delta_R^\dagger), & B_{RL} &= \mathrm{Tr}(\Delta_R\Delta_R)\mathrm{Tr}(\Delta_L^\dagger\Delta_L^\dagger), \\ C_L &= \mathrm{Tr}(\phi^\dagger\Delta_L\Delta_L^\dagger\phi), & C_R &= \mathrm{Tr}(\phi\Delta_R\Delta_R^\dagger\phi^\dagger), \\ D_1 &= \mathrm{Tr}(\phi^\dagger\Delta_L\phi\Delta_R^\dagger), & D_1^* &= \mathrm{Tr}(\phi^\dagger\Delta_L^\dagger\phi\Delta_R)^*, \\ D_2 &= \mathrm{Tr}(\phi^\dagger\Delta_L\tilde{\phi}\Delta_R^\dagger), & D_2^* &= \mathrm{Tr}(\tilde{\phi}^\dagger\Delta_L^\dagger\phi\Delta_R)^*, \\ D_3 &= \mathrm{Tr}(\tilde{\phi}^\dagger\Delta_L\phi\Delta_R^\dagger), & D_3^* &= \mathrm{Tr}(\phi^\dagger\Delta_L^\dagger\tilde{\phi}\Delta_R)^*, \end{aligned} \tag{6.56}$$

where $B_{RL} = B_{LR}^*$ while A_1, $A_{L,R}$, $B_{LL,RR}$ and $C_{L,R}$ are real. By imposing additional constraints on these terms will forbid some (combinations of) terms, reducing the number of independent parameters in the potential. We will now consider the result of imposing a C, P or CP symmetry on the potential.

6.A.2 The P-symmetric case

Under the P transformation,

$$\phi \to \phi^\dagger, \qquad \Delta_{L,R} \to \Delta_{R,L}, \tag{6.57}$$

the invariant terms transform as

$$A_2 \leftrightarrow A_3, \qquad A_L \leftrightarrow A_R, \qquad B_{LL} \leftrightarrow B_{RR}, \qquad B_{LR} \leftrightarrow B_{RL}, \tag{6.58}$$

$$C_L \leftrightarrow C_R, \qquad D_i \leftrightarrow D_i^*. \tag{6.59}$$

The above allows for the following terms in the Higgs potential,

$$\begin{aligned} V_H^P &= -\mu_1^2 A_1 - \mu_2^2(A_2+A_3) - \mu_3^2(A_L+A_R) \\ &\quad +\lambda_1 A_1^2 + \lambda_2(A_2^2+A_3^2) + \lambda_3 A_2 A_3 + \lambda_4 A_1(A_2+A_3) \\ &\quad +\rho_1(A_L^2+A_R^2) + \rho_2(B_{LL}+B_{RR}) + \rho_3 A_L A_R + \rho_4(B_{LR}+B_{RL}) \\ &\quad +\alpha_1 A_1(A_L+A_R) + \alpha_2(e^{i\delta_2}(A_2A_R+A_3A_L) + e^{-i\delta_2}(A_2A_L+A_3A_R)) \\ &\quad +\alpha_3(C_L+C_R) + \beta_1(D_1+D_1^*) + \beta_2(D_3+D_3^*) + \beta_3(D_2+D_2^*), \end{aligned} \tag{6.60}$$

which has 18 parameters.

(i) The CP_1-invariant case

Now considering the CP_1 transformation, which will be discussed as a possible CP symmetry in chapter 7, in addition to the P symmetry,

$$\phi \to \pm\phi^*, \qquad \Delta_{L,R} \to e^{i\phi_{L,R}}\Delta_{L,R}^*. \tag{6.61}$$

Among the $SU(2)_L \times SU(2)_R$-invariant terms several transform under Eq. (6.61) as

$$A_2 \leftrightarrow A_3, \qquad B_{LR} \leftrightarrow e^{i2(\phi_L-\phi_R)}B_{RL}, \qquad D_{1,2,3} \leftrightarrow e^{i(\phi_L-\phi_R)}D_{1,2,3}^*. \tag{6.62}$$

When $e^{i(\phi_L-\phi_R)} = 1$ we only have one further constraint[7], namely, $\alpha_2 e^{i\delta_2} = \alpha_2 e^{-i\delta_2}$, resulting in 17 independent parameters.

(ii) The CP_2-invariant case

The CP_2 transformation,

$$\phi \to \pm i\phi^*, \qquad \Delta_{L,R} \to e^{i\phi_{L,R}}\Delta_{L,R}^*, \tag{6.63}$$

transforms the following terms,

$$\begin{aligned} A_2 \leftrightarrow -A_3, \qquad & B_{LR} \leftrightarrow e^{i2(\phi_L-\phi_R)}B_{RL} \\ D_1 \leftrightarrow e^{i(\phi_L-\phi_R)}D_1^*, \qquad & D_{2,3} \leftrightarrow -e^{i(\phi_L-\phi_R)}D_{2,3}^*. \end{aligned} \tag{6.64}$$

From the above transformation rules, it follows that CP_2 invariance requires,

$$\mu_2^2 = \lambda_4 = 0, \qquad \alpha_2 e^{i\delta_2} = -\alpha_2 e^{-i\delta_2}, \tag{6.65}$$

$$\rho_4(1-e^{2i(\phi_L-\phi_R)}) = \beta_1(1-e^{i(\phi_L-\phi_R)}) = \beta_{2,3}(1+e^{i(\phi_L-\phi_R)}) = 0, \tag{6.66}$$

again taking $e^{i(\phi_L-\phi_R)} = 1$ this results in a potential with a total of 13 parameters.

[7]This is perhaps the most natural choice for $\phi_L - \phi_R$ as it does not alter the terms responsible for the Majorana masses for the neutrinos, $\sim \bar{L}\Delta\tau_2 L^c$.

6.A.3 The C-symmetric case

Instead, if we consider the C transformation,

$$\phi \to \phi^T, \qquad \Delta_{L,R} \to \Delta^*_{R,L}, \tag{6.67}$$

which transforms the following terms,

$$A_L \leftrightarrow A_R, \qquad B_{LL} \leftrightarrow B_{RR}, \qquad C_L \leftrightarrow C_R. \tag{6.68}$$

The most general potential is then given by,

$$\begin{aligned} V_H^C \;=\; & -\mu_1^2 A_1 - \mu_2^2(e^{-i\delta_{\mu_2}} A_2 + e^{i\delta_{\mu_2}} A_3) - \mu_3^2(A_L + A_R) + \lambda_1 A_1^2 \\ & + \lambda_2(e^{-i\delta_{\lambda_2}} A_2^2 + e^{i\delta_{\lambda_2}} A_3^2) + \lambda_3 A_2 A_3 + \lambda_4 A_1(e^{-i\delta_{\lambda_4}} A_2 + e^{i\delta_{\lambda_4}} A_3) + \rho_1(A_L^2 + A_R^2) \\ & + \rho_2(B_{LL} + B_{RR}) + \rho_3 A_L A_R + \rho_4(e^{-i\delta_{\rho_4}} B_{LR} + e^{i\delta_{\rho_4}} B_{RL}) + \alpha_1 A_1(A_L + A_R) \\ & + \alpha_2(e^{i\delta_{\alpha_2}} A_2 + e^{-i\delta_{\alpha_2}} A_3)(A_L + A_R) + \alpha_3(C_L + C_R) + \beta_1(e^{-i\delta_{\beta_1}} D_1 + e^{i\delta_{\beta_1}} D_1^*) \\ & + \beta_2(e^{-i\delta_{\beta_2}} D_3 + e^{i\delta_{\beta_2}} D_3^*) + \beta_3(e^{-i\delta_{\beta_3}} D_2 + e^{i\delta_{\beta_3}} D_2^*), \end{aligned} \tag{6.69}$$

which has 25 parameters.

6.A.4 The CP-symmetric case

Finally, considering the CP invariant case, we have the transformation

$$\phi \to \phi^*, \qquad \Delta_{L,R} \to \Delta^*_{L,R}, \tag{6.70}$$

under which the following terms transform,

$$A_2 \leftrightarrow A_3, \qquad B_{LR} \leftrightarrow B_{RL}, \qquad D_{1,2,3} \leftrightarrow D^*_{1,2,3}. \tag{6.71}$$

This gives rise to the potential

$$\begin{aligned} V_H^{CP} \;=\; & -\mu_1^2 A_1 - \mu_2^2(A_2 + A_3) - \mu_{3L}^2 A_L - \mu_{3R}^2 A_R \\ & + \lambda_1 A_1^2 + \lambda_2(A_2^2 + A_3^2) + \lambda_3 A_2 A_3 + \lambda_4 A_1(A_2 + A_3) \\ & + \rho_{1L} A_L^2 + \rho_{1R} A_R^2 + \rho_{2L} B_{LL} + \rho_{2R} B_{RR} + \rho_3 A_L A_R + \rho_4(B_{LR} + B_{RL}) \\ & + \alpha_{1L} A_1 A_L + \alpha_{1R} A_1 A_R + \alpha_{2L}(A_2 + A_3) A_L + \alpha_{2R}(A_2 + A_3) A_R \\ & + \alpha_{3L} C_L + \alpha_{3R} C_R + \beta_1(D_1 + D_1^*) + \beta_2(D_3 + D_3^*) + \beta_3(D_2 + D_2^*), \end{aligned} \tag{6.72}$$

which has 23 terms.

Chapter 7

Constraints and fine-tuning in left-right symmetric models

One of the most attractive features of the LRM is the possibility of a C or P symmetry of the Lagrangian. In fact, from a theoretical standpoint, the most attractive LRMs might be those which exhibit both P and C symmetries, and thereby CP symmetry, at high energies. Such models *in principle* can explain the observed CP violation as resulting from spontaneous CP violation in contrast to the explicit CP violation of the SM. However, the LR symmetries of such "$C + P$" models strongly constrain the left and right CKM matrices, dictating the amount and pattern of CP and flavor violation. For the minimal LRSMs, those with a minimally extended Higgs sector as discussed in chapter 6, these constraints turn out to be already incompatible with measurements of kaon and B-meson mixing, as will be discussed. Therefore, minimal LRSMs require explicit P or C violation in order to be viable still. In this chapter we will assess the viability of the remaining minimal LRMs with a C, P, or CP symmetry. Here we will review the available results in the literature and where necessary extend these in order to arrive at clear conclusions about which models are ruled out by current experimental constraints. Apart from minimal LRMs with a "$C + P$", P or C symmetry, we also will consider a LRM that is CP symmetric, but not necessarily P and C symmetric. Since this option does not correspond to a LR symmetry, it does not interchange left- and right-handed fields; it is not a left-right *symmetric* model.

For all these models we consider the quark and Higgs sectors, review the relations between the left- and right-handed CKM matrices, consider the possible vacua and calculate a measure of the fine-tuning in the Higgs potential in each case. Furthermore, we give an overview of the relevant experimental constraints on the different LRMs, considering bounds from direct searches at the LHC as well as the observables discussed in the previous chapter.

As mentioned, in the "$C + P$" models current constraints, from the LHCb and Belle experiments, are sufficiently strong to exclude them. For the other options future measurements, in particular on CP violation by LHCb will be able to considerably limit the options further and may also be able to differentiate between the C-symmetric and P-symmetric LRMs. Measurements on EDMs for the neutron, but also for the proton, other

light nuclei[1] and the electron would offer additional tests of LRMs. Currently, the LR scale as given by the mass of the right-handed W boson, commonly referred to as W' boson, is required to be at least 2 TeV by direct searches and in the case of P or C-symmetric LRSMs 3 TeV by indirect kaon and B-meson constraints [138]. In the coming decade the latter bound could be extended to 8 TeV or higher. As this scale gets pushed upwards, the already considerable, if not huge, fine-tuning required in the models will increase further, making the models increasingly less likely scenarios. These bounds and perhaps the fine-tuning may be weakened though by considering non-minimal [192, 193] or less symmetric models [174, 194]. We will not include such models here, keeping symmetry and simplicity as main guidelines.

The large amount of fine-tuning in the LRMs models considered here is due to the fact that the Higgs potential necessarily relates the electroweak scale to the LR scale. As the LR scale has been pushed into the TeV range there is a hierarchy of scales which requires the tuning of some of the parameters in the potential. In fact, as we will see, unless some of the parameters are chosen to be zero (or exactly related) the fine-tuning becomes extreme. Although it is not clear what amount of fine-tuning should be considered acceptable, one would generally consider highly fine-tuned models to be less attractive. On the other hand, a high degree of fine-tuning might turn out to be a generic feature of theories that are highly symmetric at high energies, and involve a large hierarchy between the electroweak scale and the scale of the new physics. In order to quantify the amount of fine-tuning in LRSMs we will introduce a measure of fine-tuning often employed in studies of supersymmetric extensions of the SM [195, 196].

We start by discussing the "$C + P$" LRSMs in detail in section 7.1. Although these models turn out not to be viable, they have many features in common with the LRSMs with a single LR symmetry to be discussed in section 7.2. We summarize and conclude in section 7.3.

7.1 P- and CP-symmetric left-right models

A LR model with both discrete symmetries has the appealing feature that P, C, and CP violation are explained as low-energy phenomena. However, there is no unique LR theory with both a C and a P symmetry, because there are several ways of implementing both LR symmetries in Eq. (6.7). This is due to the fact that the P and C transformations need not be aligned in flavor space. In what follows we will briefly discuss all possible ways of implementing both the P and C symmetries of Eq. (6.7), we relegate a more detailed discussion to appendix 7.A, see also Refs. [181, 178].

Whenever the C and P symmetries are not aligned the transformation rules for P or C will not both have the simple form discussed in section 6.1.2. We will select the basis in which the P transformation takes its simplest form, i.e. $V_P = \mathbf{1}$ and $\phi_P = \varphi_P = 0$ in Eq. (6.7), while the C transformation may be different. The implications in Eq. (6.15) for the P symmetry are then unchanged so that the Yukawa matrices Γ and $\tilde{\Gamma}$ will be hermitian. Following Ref. [197] we next demand invariance under CP symmetry.

[1] Tests of the LRM involving the EDMs of light nuclei are detailed in chapter 8.

The most general CP transformation can be written as follows

$$Q_{L,R} \to U_{L,R}\, Q^c_{L,R}, \qquad \Phi \to H\Phi^*, \qquad \Delta_{L,R} \to e^{i\phi_{L,R}} \Delta^*_{L,R}, \tag{7.1}$$

where $U_{L,R}$ are unitary 3×3 matrices, $\Phi \equiv (\phi, \tilde{\phi})^T$, and H is a unitary 2×2 matrix. As ϕ and $\tilde{\phi}$ are not independent fields this implies a relation between the elements of H. Taking this and the unitarity of H into account there are two possible forms of H,

$$H_1 = \begin{pmatrix} 0 & \pm 1 \\ \pm 1 & 0 \end{pmatrix}, \qquad H_2 = \begin{pmatrix} e^{i\varphi} & 0 \\ 0 & e^{-i\varphi} \end{pmatrix}, \tag{7.2}$$

where φ is a real number. These possibilities for H and $U_{L,R}$ give rise to a number of possible CP transformations, which in principle lead to different models. To simplify the discussion, and without loss of generality, we work in the basis where Γ is diagonal. The possible transformation rules and the consequences of the resulting models are summarized in Fig. 7.1. For a more detailed discussion see appendix 7.A and Refs. [181, 178]. In short, only the option $H = H_2$ with $e^{4i\varphi} = 1$ remains as a possible CP transformation for the Φ fields, while the other possibilities are unable to reproduce the quark masses or their mixing. Thus, there are two CP transformations which cannot be excluded on the basis of yielding unrealistic quark masses, namely [197]

$$\begin{aligned} &\text{Type I} \quad CP_1: && H = \pm\mathbf{1}, && U_L = \mathbf{1}, && U_R = \pm\mathbf{1}, \\ &\text{Type II} \quad CP_2: && H = \pm i\sigma_3, && U_L = \mathbf{1}, && U_R = \mp i\mathbf{1}. \end{aligned} \tag{7.3}$$

We now discuss these two possibilities in more detail.

7.1.1 Type I CP-symmetric LR models

Mass and mixing matrices

The CP_1 case is the more widely studied possibility, see for instance Refs. [197, 178, 198, 161]. At first sight, this model is able to produce phenomenologically viable mass and mixing angles for the quarks. However, as we will discuss, the model is unable to produce the observed CP violation due to the CP_1 symmetry, which constrains the Yukawa interactions as

$$\Gamma = \Gamma^T = \Gamma^*, \qquad \tilde{\Gamma} = \tilde{\Gamma}^T = \tilde{\Gamma}^*. \tag{7.4}$$

The symmetric Yukawa couplings imply $V_R = K_u V_L^* K_d$ [172] for the CKM matrices, as in Eq. (6.17). In general there are seven phases present in the CKM matrices, these are parametrized by the usual SM phase in the left-handed CKM matrix and six additional phases in the right-handed CKM matrix. However, the hermiticity of the Yukawa couplings implies additional relations which allow all phases in the CKM matrices to be solved in terms of known mixing angles, quark masses, and the parameters α and $r \equiv \kappa'/\kappa$ [199, 178]. This solution allows for the prediction of CP-violating observables in terms of the combination $r \sin\alpha$. However, the relations following from C and P invariance only admit a solution for a certain range of $r \sin\alpha$. As a result, the model is consistent,

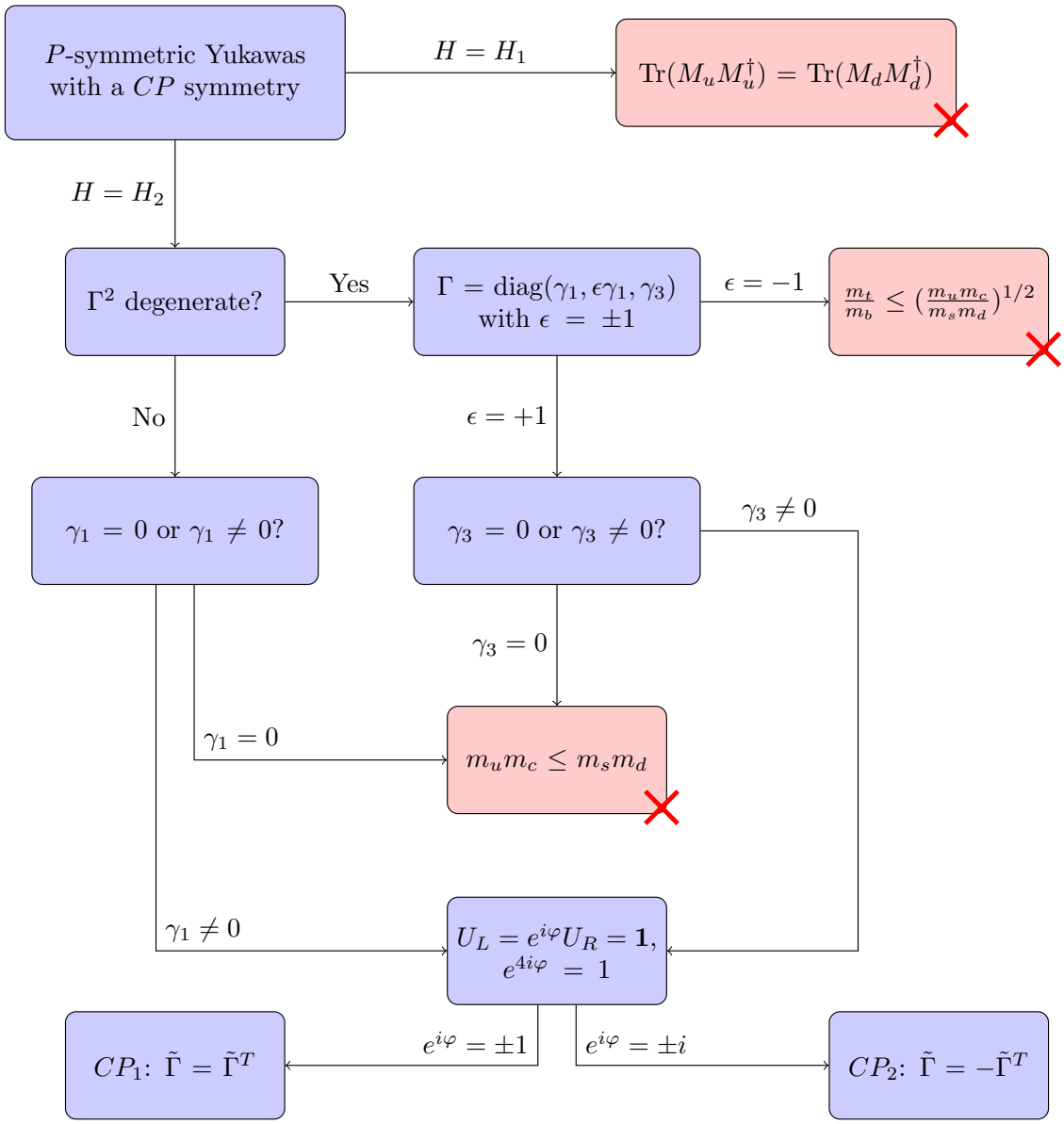

Figure 7.1: Flowchart for a P- and CP-symmetric Yukawa sector, depicting the possible choices for the CP transformation, Eq. (7.1), and their consequences. We work in a basis where $\Gamma = \mathrm{diag}(\gamma_1, \gamma_2, \gamma_3)$ is diagonal. See appendix 7.A and Refs. [181, 178] for a detailed discussion.

meaning that the above solution exists, only for relatively small amounts of CP violation, namely [198, 161]

$$\frac{r \sin\alpha}{1 - r^2} \lesssim \frac{m_b}{m_t}. \tag{7.5}$$

The SM CKM phase δ can be expressed in terms of the above combination, this bound then requires δ to be rather small, $\delta < 0.25$ [161]. In contrast, the SM CKM fit requires δ to be rather large, $\delta \simeq 1.2$ [65]. This means that the CP_1 LR model does not reproduce

the CP violation of the SM in the decoupling limit, $v_R \to \infty$, implying that M_2 can not be infinitely heavy [161].

The above observations have further implications. Since the decoupling limit does not reproduce the SM there is not necessarily a range in parameter space where the CP_1 LR model reproduces the SM. In fact, from recent measurements of the CP violation in B-$\bar{B}$ mixing the predictions of the model can be shown to be too small. After taking into account constraints from CP-violating parameters in the kaon sector, ε and ε', the model predicts (for any value of M_2 and M_H) [200, 198],

$$|\sin\phi_d| < 0.1, \qquad \sin\phi_s < -0.1. \tag{7.6}$$

Clearly, this is incompatible, at more than the 5σ level, with the measured value [140] discussed in section 5.2, Eq. (5.29). Thus, although the model can reproduce the observed quark masses and mixing angles, it is untenable when discussing CP-violating observables. Since the Yukawa couplings of the pseudomanifest LRM coincide with that of the P- and CP_1-symmetric LRM under discussion here, we conclude that the *minimal* pseudomanifest LRM can be excluded in the same way.

The Higgs potential

Further problems arise when considering the Higgs sector of the CP_1 model. Although the above considerations may be considered to rule out the model we will nevertheless review some of these problems as they are exemplary of what will be encountered in other versions of LR symmetric models. Our discussion will largely follow that of Refs. [155, 201].

In this case the Higgs potential takes the form of Eq. (6.18) with the additional constraint from the CP_1 transformation that there is no explicit CP violation (see appendix 6.A.2):

$$\delta_2 = 0. \tag{7.7}$$

Note that if the phases $\phi_{L,R}$ are introduced in the CP transformation of the $\Delta_{L,R}$ fields, Eq. (7.1), additional constraints, $\beta_i = \rho_4 = 0$, are acquired. However, due to the fact that the potential Eq. (6.18) is $(B-L)$-symmetric no such constraints appear when $e^{i(\phi_L-\phi_R)} = 1$. Making another choice for $\phi_L - \phi_R$ would alter the terms responsible for the Majorana masses for the neutrinos, $\sim \bar{L}\Delta\tau_2 L^c$, forcing them to zero. As such, we will adopt the CP transformation with $e^{i(\phi_L-\phi_R)} = 1$, throughout most of the upcoming discussions, and comment on the possibility of making other choices where this leads to different results.

This P-symmetric Higgs potential with $\delta_2 = 0$ has been widely studied in the literature [202, 203, 155, 201, 160]. From the requirement that the potential is minimized one can obtain for the dimensionful parameters of the potential [201]

$$\begin{aligned}
\frac{\mu_1^2}{v_R^2} &= \frac{\alpha_1}{2} - \frac{\kappa'^2}{2\kappa_-^2}\alpha_3 + \frac{\kappa_+^2}{v_R^2}\lambda_1 + 2\frac{\kappa\kappa'}{v_R^2}\lambda_4\cos\alpha, \\
\frac{\mu_2^2}{v_R^2} &= \frac{\alpha_2}{2} + \frac{\kappa\kappa'}{4\kappa_-^2\cos\alpha}\alpha_3 + \frac{\kappa_+^2}{2v_R^2}\lambda_4 + \frac{\kappa\kappa'}{v_R^2\cos\alpha}(\lambda_3 + 2\lambda_2\cos 2\alpha), \\
\frac{\mu_3^2}{v_R^2} &= \rho_1 + \frac{\kappa_+^2}{2v_R^2}\alpha_1 + \frac{2\kappa\kappa'\cos\alpha}{v_R^2}\alpha_2 + \frac{\kappa'^2}{2v_R^2}\alpha_3,
\end{aligned} \tag{7.8}$$

where we neglected terms of order v_L/v_R and v_L^2/v_R^2. Substituting the exact expressions for μ_i^2, including terms which are higher order in v_L/v_R, in the three remaining minimum equations we obtain

$$2\rho_1 - \rho_3 = \frac{\beta_1\kappa\kappa'\cos(\alpha-\theta_L) + \beta_2\kappa^2\cos\theta_L + \beta_3\kappa'^2\cos(2\alpha-\theta_L)}{v_R v_L}, \tag{7.9}$$

$$\begin{aligned} 0 = {} & \kappa\kappa'\big[\alpha_3(1+\frac{v_L^2}{v_R^2}) + \frac{\kappa_-^2}{v_R^2}(4\lambda_3 - 8\lambda_2)\big]\sin\alpha \\ & + \frac{v_L}{v_R}\big[\beta_1\big(\kappa^2\sin\theta_L + \kappa'^2\sin(\theta_L - 2\alpha)\big) \\ & + 2(\beta_2+\beta_3)\kappa\kappa'\sin(\theta_L-\alpha)\big], \end{aligned} \tag{7.10}$$

$$0 = \beta_1\kappa\kappa'\sin(\alpha-\theta_L) - \beta_2\kappa^2\sin\theta_L + \beta_3\kappa'^2\sin(2\alpha-\theta_L). \tag{7.11}$$

These equations were obtained by minimizing with respect to v_L, α, and θ_L, respectively. From Eq. (7.10) we approximately have (for $v_R \gg \kappa_+ \gg v_L$)

$$\alpha_3\sin\alpha = \mathcal{O}(\beta_i\, v_L/v_R). \tag{7.12}$$

Requiring the hierarchy $v_R \gg v_L$ implies that $\alpha_3\sin\alpha$ must be small in order for β_1 to be in the perturbative regime. In the extreme cases we could have a small spontaneous phase, i.e. $\alpha = \mathcal{O}(v_L/v_R)$, while α_3 can be of order one, or α_3 is small with a sizeable α, thus, $\alpha_3 = \mathcal{O}(v_L/v_R)$ with $\alpha = \mathcal{O}(1)$. It turns out that in both extremes, as well as in all intermediate cases, some of the additional Higgs fields become too light, such that their effects should have been detected experimentally already [201, 155]. Approximate expressions for the masses of the scalars are given in appendix 7.B. In one extreme, $\alpha = \mathcal{O}(v_L/v_R)$ and $\alpha_3 = \mathcal{O}(1)$, Eqs. (7.9) and (7.11) imply $2\rho_1 - \rho_3 = \mathcal{O}(\kappa_+^2/v_R^2)$, which in turn implies that the left-handed triplet fields become light, $\mathcal{O}(\kappa_+)$ (see appendix 7.B). Explicit calculation shows that they are even lighter, namely of order $\mathcal{O}(v_L)$. As these fields couple to the electroweak gauge bosons such light fields should already have been discovered at LEP-I [201].

For the other extreme, whenever α_3 is small $\mathcal{O}(\kappa_+^2/v_R^2)$, there are problems with flavour-changing neutral-currents (FCNCs). In the minimal LR model these FCNCs are generated by the neutral scalars of the bidoublet. FCNCs are stringently constrained by kaon- and B-mixing, in fact, the mass of such a scalar should be of the order of > 10 TeV [161, 138] in LRSMs. An analysis of the masses of the physical Higgs fields [201] shows that whenever α_3 is small, $\mathcal{O}(\kappa_+^2/v_R^2)$, the Higgs fields with the FCNC couplings remain light and the FCNC bounds cannot be evaded.

The remaining scenarios interpolate between the two extremes. Here one finds three light neutral states, which are now mixtures of the neutral triplet field, δ_L^0, and the flavor-changing neutral Higgs field [201].

Thus, whenever $\sin\alpha \neq 0$ the potential Eq. (6.18) cannot reproduce the SM Higgs spectrum. The addition of extra scalar fields could solve this, simultaneously allowing for a SM-like Higgs spectrum and spontaneous CP violation in the CP_1 potential [204, 161]. Such a non-minimal option will not be discussed any further here. Another possibility is to have a potential without spontaneous CP violation, $\alpha = \theta_L = 0$. In this case all the non-SM scalars can obtain a large mass and decouple, thereby allowing for a SM-like Higgs

spectrum. Even in this case, however, there is a price to pay in the form of fine-tuning as we will discuss next.

Fine-tuning

The fact that there should be a hierarchy between the vevs, $v_R \gg \kappa$, $\kappa' \gg v_L$, induces fine-tuning in the potential. This occurs because the minimum equations relate the different scales to one another. For the parameters of the potential to be in the perturbative range this requires a certain amount of fine-tuning. Similar to the Higgs potential itself it is useful to review the fine-tuning in the CP_1-invariant potential, as it will turn out to be exemplary of the cases we will study in the following sections.

One of the dominant sources of fine-tuning appears in Eq. (7.9), schematically we have,

$$2\rho_1 - \rho_3 \sim \frac{\kappa\kappa'}{v_L v_R}\beta_i, \tag{7.13}$$

which has been called the vev see-saw relation [155]. If we insist on the desired hierarchy, one may make the following estimates for the vevs, $v_R \sim 10$ TeV, $\kappa, \kappa' \sim 100$ GeV, and $v_L \sim 1$ eV, which would imply the fraction in Eq. (7.13) to be huge $\sim 10^9$. Thus, in order for the ρ parameters to be of order one, the β_i parameters should cancel to a precision of $\sim 10^{-9}$, implying a very fine-tuned potential. There are two ways to avoid this fine-tuning. One can either accept a very high scale for the LR model, $v_R \sim 10^{13}$ GeV, making the additional gauge fields, Z_R and $W_R^\pm$ unobservable, or eliminate the vev see-saw relation. The latter option can be achieved by setting v_L and β_i to zero. In this case Eq. (7.9) vanishes and is no longer a source for fine-tuning. This option was concluded to be the only viable CP_1-invariant option leading to observable effects in Ref. [155]. However, even in this case there is still a considerable amount of fine-tuning. Looking, for instance, at the third equation in Eq. (7.8) we see that the ρ_1 and μ_3^2 terms should cancel to $\mathcal{O}(\frac{\kappa_+^2}{v_R^2})$ in order for α_1 to be of order one. Similarly, from the first equation in Eq. (7.8) the $\alpha_{1,3}$ and μ_1^2 terms should cancel to $\mathcal{O}(\frac{\kappa_+^2}{v_R^2})$ in order for λ_i to be of order one. Combining the two, we see that cancellations to a precision of order $\mathcal{O}(\frac{\kappa_+^4}{v_R^4})$, i.e. $\mathcal{O}(10^{-7})$ for the above selected values, are needed. Some of this fine-tuning may be avoided if we set some of the parameters to be small by hand or by introducing an additional mechanism [160].

As we will discuss in more detail in the upcoming sections, this type of fine-tuning tends to occur in more general scenarios as well. Before moving on to these LR models, however, we will first review the second $P + CP$-symmetric case.

7.1.2 Type II CP-symmetric LR models

This case has received somewhat less attention than the CP_1 possibility [197, 204]. Although the Yukawa sector is distinct from the CP_1 case, which is relevant for the amount of CP violation allowed, we will see that the Higgs potential is very similar.

Mass and mixing matrices

As in the previous case, the Yukawa interactions are constrained by the P and CP transformations. For the Yukawa interactions the P and CP_2 transformations have the implications

$$\Gamma = \Gamma^T = \Gamma^*, \qquad \tilde{\Gamma} = -\tilde{\Gamma}^T = -\tilde{\Gamma}^*. \tag{7.14}$$

The fact that $\tilde{\Gamma}$ is antisymmetric means that in this case the mass matrices will not be symmetric. Thus, there is, in general, no simple relation between the left and right-handed CKM matrices. However, the Higgs potential is more constrained in this case.

The Higgs potential

The CP_2-invariant Higgs potential is that of Eq. (6.18) with the additional constraints,

$$\begin{gathered} \mu_2 = \lambda_4 = 0, \qquad \delta_{\alpha_2} = \pm\pi/2, \\ \beta_1(1 - e^{i(\phi_L - \phi_R)}) = 0, \qquad \beta_{2,3}(1 + e^{i(\phi_L - \phi_R)}) = 0, \qquad \rho_4(1 - e^{2i(\phi_L - \phi_R)}) = 0. \end{gathered} \tag{7.15}$$

Thus, we have $\beta_1 = 0$ and/or $\beta_{2,3} = 0$ (and possibly $\rho_4 = 0$) depending on $\phi_L - \phi_R$.

As was already noted in Ref. [204], barring fine-tuning, there will be very little CP violation in this scenario. Neglecting subleading terms in the potential, one finds $\alpha = \pm\pi/2$, which in this case is a CP conserving minimum, as, after an $SU(2)_{L,R}$ gauge-transformation, the vevs of the bidoublet can then be written as

$$\langle\phi\rangle = e^{\pm i\pi/4} \begin{pmatrix} \kappa & 0 \\ 0 & \kappa' \end{pmatrix}, \tag{7.16}$$

which is invariant under the CP_2 transformation.

The feature that without fine-tuning the spontaneous CP violation will be small is reminiscent of the CP_1 case. In fact, we observe that the CP_2-symmetric potential is very similar to a special case of the CP_1-symmetric potential. This can be seen by use of a field redefinition. In case we take $e^{i(\phi_L - \phi_R)} = 1$, and thereby $\beta_{2,3} = 0$, we can apply the redefinition

$$\phi \to e^{\mp i\pi/4}\phi, \tag{7.17}$$

the resulting potential is then, after an $SU(2)_{L,R}$ transformation, nearly equal to the CP_1 case with the identifications

$$\begin{aligned} &\mu_2^{CP_1} = \lambda_4^{CP_1} = \beta_{2,3}^{CP_1} = 0, \qquad \lambda_2^{CP_1} = -\lambda_2^{CP_2}, \\ &\alpha^{CP_1} = \alpha^{CP_2} \pm \pi/2, \qquad \theta_L^{CP_1} = \theta_L^{CP_2} \pm \pi/2. \end{aligned} \tag{7.18}$$

The only remaining difference comes from the α_2 terms involving $\mathrm{Tr}(\Delta_L\Delta_L^\dagger)$. Clearly, these terms are suppressed with respect to their right-handed equivalent, due to the hierarchy $v_R \gg \kappa, \kappa' \gg v_L$, meaning that to good approximation the two potentials are equivalent. Thus, in this case the minimum equations correspond to those of Eqs. (7.8)

and (7.9)-(7.11) to $\mathcal{O}(\kappa_+^2/v_R^2)$, with the identifications of Eq. (7.18). A similar redefinition can be made for the case $e^{i(\phi_L-\phi_R)}=-1$.

Thus, the CP_2 potential is, to good approximation, equal to a special case of the CP_1 invariant potential. This also implies that the conclusions about the CP_1-symmetric potential carry over. The case with spontaneous CP violation implies a non-SM-like Higgs spectrum whereas the case without spontaneous CP violation has no CP violation at all. Therefore, we conclude that also the CP_2-symmetric case is not viable.

In the following sections we will study minimal LR models with fewer discrete symmetries. We will see that although there may be important differences between the Yukawa sectors of these models, their Higgs potentials will tend to be very similar, like for the CP_1 and CP_2 cases.

7.2 P-, C-, or CP- symmetric left-right models

7.2.1 P-symmetric LR models

P-symmetric LRMs have been studied quite extensively in the literature, e.g. [11, 12, 160, 79, 138]. In this case there is an approximate relation between the mixing matrices,

$$V_L \simeq K_u V_R K_d, \tag{7.19}$$

where $K_{u,d}$ are diagonal matrices of phases. As was already mentioned, this is due to the fact that the combination $r\sin\alpha$ should be small in order to be able to reproduce the small ratio m_b/m_t [164]. In fact, the same bound (7.5) as in the CP_1 case applies here too. In order to satisfy this bound and simultaneously the experimental constraints on CP violation, one can arrive at constraints on the phases in $K_{u,d}$ and on M_2. In other words, even though CP violation can arise in this type of model, the pattern of CP violation in kaon and B-meson mixing and the nEDM may not be reproducible unless M_2 has some minimum value. We will briefly summarize this point.

At the moment we do not know the value of r, but if it is small ($r \ll m_b/m_t$) one can use the analytical expressions for the phases in $K_{u,d}$ derived in terms of $r\sin\alpha$ [79, 205], which have recently been generalized to general r values [171]. For M_2 in the TeV range, the measurements of indirect CP violation in kaon mixing, ϵ, then drives a combination of the phases in $K_{u,d}$ to a nonzero value, $|\theta_d-\theta_s| \simeq 0.17$. As in this case all the phases are functions of $r\sin\alpha$, this requires a nonzero value for this combination. Both the neutron EDM as well as ε' then set a strong bound on $\zeta\sin\alpha$. The data on ε' and the neutron EDM can then only be reconciled with ε for large values of $M_2 \gtrsim 10\,\text{TeV}$ [79, 206, 138].

On the other hand, if r is large ($r \gtrsim m_b/m_t$) the phases in $K_{u,d}$ can be sizable and tuned to satisfy the CP violation constraints. This leads to $\theta_c - \theta_t \simeq \pi/2$ from ε and $\theta_d-\theta_s \simeq \pi$ from ε'. In addition, for the CP violation in B-meson mixing (see Eq. (6.23)) we have

$$\sigma_d \simeq \pi + \theta_b - \theta_d, \qquad \sigma_s \simeq \pi + \theta_b - \theta_s, \tag{7.20}$$

Table 7.1: The ranges taken for the parameters of the potential when generating random points in parameter space.

ρ_1	ρ_3	λ_1, ρ_2, $\alpha_{2,3}$	$\lambda_{2,3,4}$, α_1, ρ_4, $\beta_{1,2,3}$	α, δ_2, θ_L	v_L (eV)	κ (GeV)	v_R (GeV)
$[0, 5]$	$[2\rho_1, 10]$	$[0, 10]$	$[-10, 10]$	$[0, 2\pi]$	$[0, 10]$	$[0, 246]$	$[0, 5 \cdot 10^4]$

which leads to a correlation between ϕ_d and ϕ_s due to the ε' constraint, we will comment on this further below (7.26). These constraints together with the kaon and B-meson mass-differences, ΔM_K and $\Delta M_{B_{d,s}}$, require $M_2 \gtrsim 3\,\text{TeV}$ [138]. The recently derived analytical solution for ${V_R}^2$ [171] for general r would allow one to constrain, not only M_2 and M_H through meson-mixing constraints as was done in Ref. [183], but also bound r and α.

In the limit of vanishing α the quark sector of the P-symmetric LRM coincides with that of the minimal manifest LRM. In this case ε sets a strong bound on the $W_R^\pm$ mass of $M_2 \gtrsim 20$ TeV [183].

The above shows that the indirect constraints for P-symmetric LRMs are more stringent than the direct limits on M_2 and will be even more so in the future thanks to LHCb, B factories and improvements in lattice determinations of the relevant matrix elements. The increase of experimental sensitivity discussed in section 5.2.1 of chapter 5, which will take at least another 10 years to realize, is expected to push the lower bound on M_2 to roughly 8 TeV [138], which will likely allow confrontation of the P-symmetric LRMs with data, although in this case there is no upper limit on M_2, as the decoupling limit has not been excluded, in contrast to the CP_1 case.

The Higgs potential

The Higgs potential in this case is that of Eq. (6.18). As pointed out in Ref. [201], it can be mapped onto the CP_1 case to good approximation by a field redefinition, similar to that of Eq. (7.17),

$$\phi \to \phi e^{-i\varphi/2}, \qquad \varphi = \text{Arg}(\alpha_2 v_R^2/2e^{i\delta_2} - \mu_2^2). \tag{7.21}$$

After an $SU(2)_L$-gauge transformation this gives

$$\alpha^{CP_1} \to \alpha^P + \varphi, \qquad \theta_L^{CP_1} \to \theta_L^P + \varphi. \tag{7.22}$$

The remaining differences between the two potentials then are terms subleading in v_R, $\mathcal{O}(\kappa_+^2/v_R^2)$. Thus, the minimum equations of Eqs. (7.8)–(7.10) with the above replacement apply here too, to $\mathcal{O}(\kappa_+^2/v_R^2)$. The remaining minimum equations result from subleading terms and are not obtained from their CP_1 equivalents after applying the identifications Eq. (7.22). Instead they simply equal the corresponding CP_1 equations, Eqs. (7.9) and (7.11). This near-equivalence means the conclusions about CP_1 models discussed in section 7.1.1 should apply here too. Thus, again it will not be possible to obtain a SM-like

[2]Note that although this solution expresses all phases in $K_{u,d}$ in terms of $r \sin\alpha$ like in the CP_1 case, unlike the CP_1 scenario the SM phase δ cannot be expressed in terms of $r \sin\alpha$.

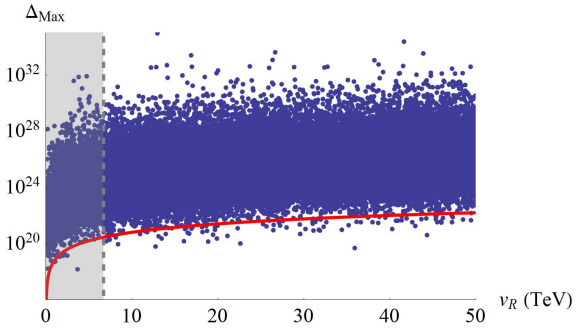

Figure 7.2: The figure shows the fine-tuning measure Δ_{Max} as a function of v_R in TeV for a P-symmetric V_H. The blue points are randomly generated points satisfying the minimum equations and the ranges in Table 7.1. Here the red line is chosen such that 0.1% of the points are found below it. It is parametrized by $6 \cdot 10^{-4} v_R^2/v_L^2$ taking an average value for v_L of 10 eV.

Higgs spectrum for arbitrary values of α. However, as mentioned in section 7.1.1 for the CP_1 case there is the possibility of a SM-like Higgs spectrum in the limit $v_R \to \infty$ for a specific value of α which now occurs very close to $\alpha = \varphi$. This is now an acceptable possibility as it still allows for spontaneous CP violation and we already allowed explicit CP violation in the Yukawa couplings. Thus, in the P-symmetric LR model it is possible to have a SM-like spectrum in the decoupling limit in combination with spontaneous CP violation. However, the amount of spontaneous CP violation then entirely results from the explicit CP violation present in the Higgs potential, as $\varphi = 0$ when $\delta_2 = 0$. In a sense this means that the CP violation is put in by hand and can be as large as allowed by the value of r. However, as discussed in the previous section, the pattern of CP violation in kaon and B-meson mixing and the neutron EDM also put stringent constraints on the model, in particular on the CP-violating phases and M_2. Moreover, there is the issue of fine-tuning.

Fine-tuning

The fact that the minimum equations relate several very different scales, namely, $v_R \gg \kappa_+ \gg v_L$ to one another means that some of the parameters in the potential will tend to be fine-tuned. This is especially true for cases where $v_L \neq 0$ [155] as was already noted in section 7.1.1. In this case one can obtain the vev see-saw relation of Eq. (7.13). This requires some parameters to be fine-tuned to a precision of order $\mathcal{O}(v_L/v_R)$. However, as we will show, more fine-tuning may be required, similar to that discussed in section 7.1.1, due to the remaining minimum equations. In fact, solving the minimum equations for $\mu_{1,2}^2$, $\beta_{1,2}$, α_2 and ρ_3 we see that the leading terms in ρ_3 are proportional to v_R^2/v_L^2. This implies that if ρ_3 is to be of order one, i.e. in the perturbative regime, these terms should cancel to a precision of v_L^2/v_R^2.

In order to study the matter quantitatively we use the minimum equations to solve for as many parameters, which we will denote by p_i, as there are equations. Subsequently we study the dependence of these p_i on the remaining parameters, p_j. More specifically, we adopt the following quantity as a measure for the fine-tuning in p_i typically used for

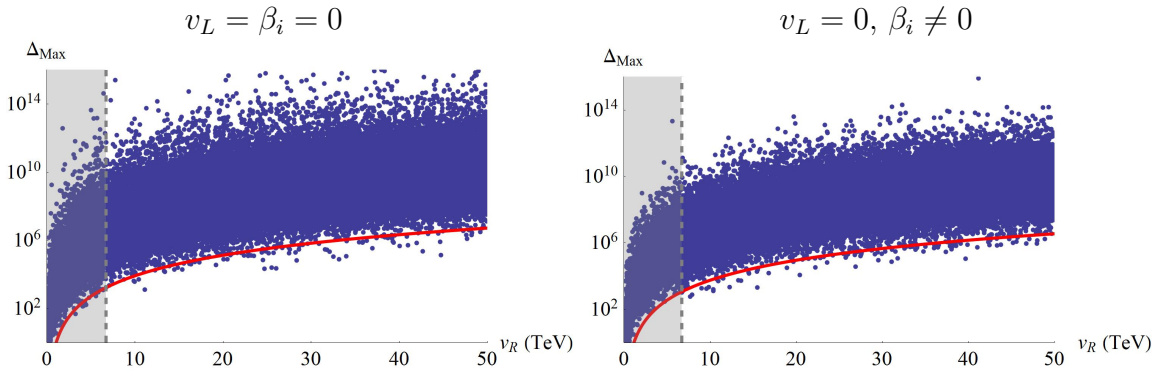

Figure 7.3: Similar plots to that of Fig. 7.2. The plot on the left shows the fine-tuning in the case where β_i and v_L are set to zero, while the figure on the right does the same in the case where only v_L is set to zero. The red lines are again chosen such that 0.1% of the points are found below it. It is parametrized by $3 \cdot 10^{-3} v_R^4/\kappa_+^4$ and $2 \cdot 10^{-3} v_R^4/\kappa_+^4$ in the left and right plots, respectively.

supersymmetric extensions of the SM [195, 196],

$$\Delta_i = \text{Max}_j \left| \frac{d \ln p_i}{d \ln p_j} \right|. \tag{7.23}$$

Our procedure is as follows, we first generate random $\mathcal{O}(1)$ values for nearly all parameters in the potential while obtaining values for the remainder through the minimum equations. The allowed ranges for the parameters are shown in Table 7.1. As the dimensionless parameters should remain in the perturbative range we conservatively constrain their values to lie in the interval $[-10, 10]$. Exceptions occur for several dimensionless parameters. These are further constrained in order for the potential to be bounded from below, in the case of λ_1 and ρ_1 and to have positive masses-squared values of the Higgs fields, like for ρ_2, $\rho_3 - 2\rho_1$, and α_3 [160]. However, the imposed constraints are actually not sufficient to keep all mass-squared values positive, but this will not affect the conclusions. In addition, we have not imposed any experimental constraints on these masses. Thus, only a subset of the generated points will be phenomenologically viable. We further take values for the vevs which adhere to their naive expectations. We make no assumptions for the μ_i^2 parameters, instead we calculate their values through the minimum equations.

We then solve the minimum equations for as many parameters as there are equations. The random points in parameter space are then used to calculate the fine-tuning measures for the solved parameters p_i. The results are shown in Fig. 7.2 where we plot the maximum value of $\Delta_{\text{Max}} \equiv \text{Max}_i \Delta_i$ against v_R.

Clearly, the degree of fine-tuning can be significantly larger than one might expect from the see-saw relation of Eq. (7.13) alone and be enhanced through the coupled minimum equations. As can be seen from the plot in Fig. 7.3 and was noted in Ref. [155] the fine-tuning may be considerably decreased by setting $v_L = \beta_i = 0$, as was done in e.g. [79]. In this case, however, still a fine-tuning of order $\Delta = \mathcal{O}(v_R^4/\kappa_+^4) \gtrsim 100$ remains. Since setting $\beta_i = 0$ may lack justification [155, 201], we observe that setting only v_L to zero

leads to the same reduction in the amount of fine-tuning. In this case the vev see-saw relation vanishes and instead we obtain two relations for the β_i parameters, namely [201],

$$\beta_1 = -2\beta_3 \frac{\kappa'}{\kappa}\cos\alpha, \qquad \beta_2 = \frac{\kappa'^2}{\kappa^2}\beta_3. \tag{7.24}$$

It remains to be seen whether these relations can be justified or not. Therefore, setting v_L and possibly β_i to zero is a simple way to greatly reduce the fine-tuning in the Higgs potential, but in both cases one may wonder whether this is justified.

7.2.2 C-symmetric LR models

C-symmetric LRMs have been less investigated in the literature so far, although recently there has been renewed interest ([164, 138]). In this case the mixing matrices are related by Eq. (6.17),

$$V_R = K_u V_L^* K_d, \tag{7.25}$$

with $K_{u,d}$ diagonal matrices of phases. The mass matrices are now less constrained than in the P-symmetric case; the Yukawa couplings are symmetric as opposed to hermitian. One of the consequences is that the combination $r\sin\alpha$ is no longer required to be small in order to reproduce the quark masses, as opposed to the P-symmetric case. Furthermore, now the phases in $K_{u,d}$ are free parameters of the model. These can be tuned in order to evade the constraints from CP-violating observables. The ε constraint can be evaded when $|\theta_d - \theta_s| \simeq n\pi$ $(n = 0, 1)$, while the ε' constraint can be satisfied when $\theta_d - \theta_s \simeq \pi$ or r is small. From the relation in Eq. (6.17) we have for the phases $\sigma_{d,s}$ (see Eq. (6.23))

$$\sigma_d = \pi + \theta_b - \theta_d + 2\phi, \qquad \sigma_s = \pi + \theta_b - \theta_s, \tag{7.26}$$

where $\phi = \mathrm{Arg}\big(V_L^{tb*} V_L^{td}\big)$. Note that σ_d and σ_s are again correlated in an M_2 and M_H dependent way through the $\varepsilon^{(\prime)}$ constraints. To be specific, for the quantities which determine the $B_{d,s}$ observables one has

$$1 + h_d \simeq 1 - |h_d| e^{i(\theta_b - \theta_d + 2\phi)}, \qquad 1 + h_s \simeq 1 - (-1)^n |h_s| e^{i(\theta_b - \theta_d)}, \tag{7.27}$$

while in the P-symmetric case, again taking into account the $\varepsilon^{(\prime)}$ constraints, one has

$$1 + h_d \simeq 1 - |h_d| e^{i(\theta_b - \theta_d)}, \qquad 1 + h_s \simeq 1 + |h_s| e^{i(\theta_b - \theta_d)}. \tag{7.28}$$

From the $B_{d,s}$-mixing observables ($\Delta M_{B_{d,s}}$ and $\phi_{d,s}$) it should in principle be possible to see which of the above patterns, Eq. (7.27) or (7.28), fits the data better (especially since $|h_d|/|h_s|$ is constant to good approximation [161, 164]). In other words, if a sign of an LRSM is found in $B_{d,s}$-mixing these observables are in principle also sensitive to the difference between the P- and C-symmetric options.

After the $\varepsilon^{(\prime)}$ constraints have been used to fix the phases, the constraints from ΔM_K and from $B_{d,s}$ mixing can again be used to put a strong limit on the $W_R^\pm$ mass. In this case the $B_{d,s}$ meson limits are competitive with the bound from kaon mixing, $M_2 \gtrsim 3\,\mathrm{TeV}$ [138], which is similar to the P-symmetric case.

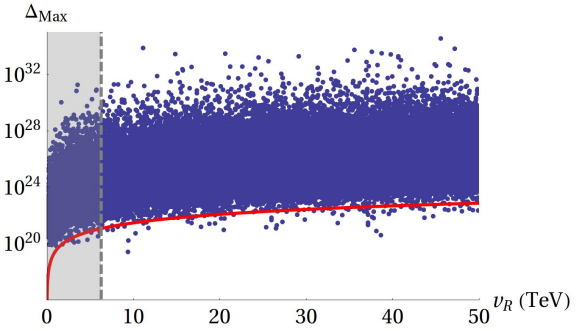

Figure 7.4: The figure shows the fine-tuning measure Δ_{Max} as a function of v_R in TeV for a C-symmetric V_H. With respect to the P-symmetric potential the C-symmetric potential has seven additional phases, for which we choose the range $[0, 2\pi]$. The red line is parametrized by $30 \cdot 10^{-4} v_R^2/v_L^2$ taking an average value for v_L of 10 eV.

The Higgs potential

The Higgs potential in this case is that of Eq. (6.19). The form of this potential is quite similar to that of the P-symmetric potential, Eq. (6.18). In this case, however, phases appear in the μ_2, $\lambda_{2,4}$, ρ_4, and β_i terms which were absent in the P-symmetric potential. Nonetheless, we find that to good approximation the potential of Eq. (6.19) can again be mapped onto the CP_1-symmetric case by a field redefinition,

$$\phi \to e^{-i\varphi'/2}\phi, \qquad \varphi' = \text{Arg}\Big(\frac{\alpha_2 v_R^2}{2} e^{i\delta_{\alpha_2}} - \mu_2^2 e^{-i\delta_{\mu_2}}\Big). \tag{7.29}$$

After an $SU(2)_L$-gauge transformation this then implies the identifications

$$\alpha^{CP_1} = \alpha^C + \varphi, \qquad \theta_L^{CP_1} = \theta_L^C + \varphi. \tag{7.30}$$

This redefinition removes the phases from the μ_2^2 and α_2 terms, but does not remove the phases related to the $\lambda_{2,4}$, ρ_4, and β_i terms. However, these terms are subleading, i.e. of order $\mathcal{O}(\kappa_+^2/v_R^2)$ and smaller. At first sight the ρ_4 term may be an exception to this, however this term only contributes to the masses of doubly charged scalars at $\mathcal{O}(v_L v_R)$ and does not appear in the minimum equations. Thus, up to terms subleading in v_R, after the redefinition Eq. (7.29) the C-symmetric potential is equal to the CP_1-symmetric potential. Indeed four of the minimum equations are again those of the CP_1 case, Eq. (7.8) and (7.10), to $\mathcal{O}(\kappa_+^2/v_R^2)$, with the above identifications. The remaining two do not follow this rule as they emerge from subleading terms in the potential. Instead they are given by

$$\begin{aligned} 2\rho_1 - \rho_3 &= \frac{\beta_1 \kappa\kappa' \cos(\delta_{\beta_1} + \alpha - \theta_L) + \beta_2 \kappa^2 \cos(\delta_{\beta_2} - \theta_L) + \beta_3 \kappa'^2 \cos(\delta_{\beta_3} + 2\alpha - \theta_L)}{v_R v_L}, \\ 0 &= \beta_1 \kappa\kappa' \sin(\delta_{\beta_1} + \alpha - \theta_L) + \beta_2 \kappa^2 \sin(\delta_{\beta_2} - \theta_L) + \beta_3 \kappa'^2 \sin(\delta_{\beta_3} + 2\alpha - \theta_L). \end{aligned} \tag{7.31}$$

Nevertheless, up to small corrections the conclusions of P- and CP_1-symmetric case, discussed in section 7.1.1, should apply once more.

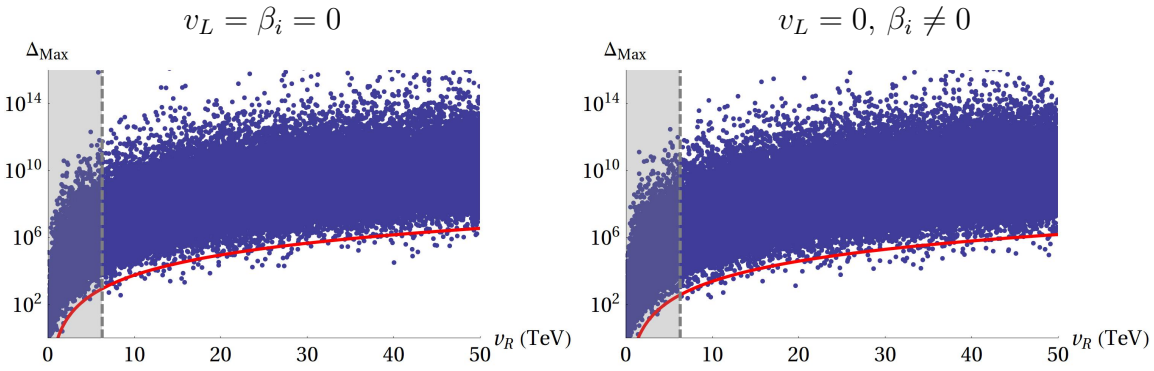

Figure 7.5: Similar plots to that of Fig. 7.4. The plot on the left shows the fine-tuning in the case where β_i and v_L are set to zero, while the figure on the right does the same in the case where only v_L is set to zero. The red lines are again chosen such that 0.1% of the points are found below it. It is parametrized by $2 \cdot 10^{-3} v_R^4/\kappa_+^4$ and $1 \cdot 10^{-3} v_R^4/\kappa_+^4$ in the left and right plots, respectively.

Thus, the conclusions for the C-symmetric potential are very much like those for the P-symmetric case. Again it will not be possible to obtain a SM-like Higgs spectrum for arbitrary values of α. Nonetheless, there is a possibility of a SM-like Higgs spectrum in the decoupling limit for a specific value of the spontaneous phase which in this case occurs for $\alpha = \varphi'$. Thus, much like for the P-symmetric potential, it is possible to have a SM-like spectrum in the decoupling limit in combination with spontaneous CP violation, however, the size of the spontaneous phase is again entirely dictated by the explicit CP violation present in the potential, through Eq. (7.29).

Fine-tuning

Not surprisingly, the fine-tuning measures in the C- and P-symmetric potentials are rather similar. If we do not eliminate the vev see-saw relation, Eq. (7.13), the potential must again be very fine-tuned, as can be seen in Fig. 7.4, which can be compared with Fig. 7.2 of the P-symmetric case.

One can again choose to eliminate the see-saw relation in order to reduce the amount of fine-tuning substantially. As before, this can be achieved by setting $v_L = 0$ and possibly $\beta_i = 0$, see Fig. 7.5. In both cases still a considerable amount of fine-tuning remains, $\Delta = \mathcal{O}(v_R^4/\kappa_+^4) \gtrsim 100$. In case of $v_L = 0$ only, one obtains again two relations for the β_i parameters, which, however, differ from the P-symmetric case, Eq. (7.24),

$$\beta_1 = r\beta_3 \frac{\sin(\delta_{\beta_2} - \delta_{\beta_3} - 2\alpha)}{\sin(\delta_{\beta_1} - \delta_{\beta_2} + \alpha)}, \qquad \beta_2 = -r\beta_1. \tag{7.32}$$

7.2.3 CP-symmetric LR models

The CP-symmetric, but not necessarily P- or C-symmetric, case has been less well-studied in the literature. In this model the CKM matrices are in principle unrelated to one another, the same is true for the gauge couplings, generally, $g_R \neq g_L$. Nevertheless,

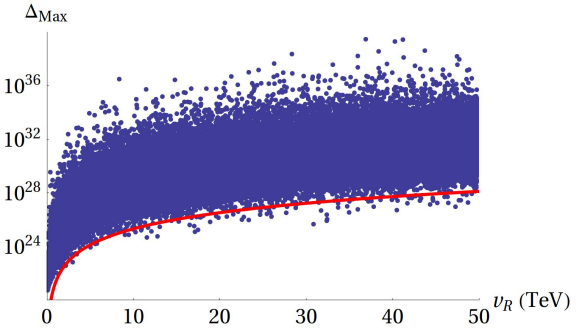

Figure 7.6: The figure shows the fine-tuning measure Δ_{Max} as a function of v_R in TeV for a CP-symmetric V_H. The red line is parametrized by $1 \cdot 10^{-2} v_R^4/\kappa_+^2 v_L^2$ taking an average value for v_L of 10 eV.

in a similar fashion to the P and CP_1 cases one may again derive the upper bound of Eq. (7.5). Despite this similarity, here it is possible to tune the right-handed gauge coupling and CKM elements in order to weaken the constraints from direct searches and B and K mixing. In fact, the study of general LRMs (without the constraints on V_R of the C and P cases) of Ref. [207] shows that for M_2 in the $2-3$ TeV range a nearly diagonal form of V_R, much like that of the SM CKM matrix, is allowed, but also regions with large off-diagonal (V_R^{cb} and V_R^{ub}) elements are possible.

The Higgs potential

The Higgs potential in this case is that of Eq. (6.20). This potential contains 5 more parameters than the P-symmetric potential. However, if we were to neglect $\text{Tr}(\Delta_L \Delta_L^\dagger)$ compared to $\text{Tr}(\Delta_R \Delta_R^\dagger)$, we would obtain a potential very similar to the P-symmetric case. Indeed, five of the minimum equations are, up to terms of $\mathcal{O}(v_L/v_R)$ given by those of the CP_1-symmetric case, Eqs. (7.8), (7.10) and (7.11), with the translations $\mu_3^2 \to \mu_{3R}^2$, $\rho_1^2 \to \rho_{1R}^2$ and $\alpha_i^2 \to \alpha_{iR}^2$. The final minimum equation, the vev see-saw relation, is also given by the corresponding CP_1 equation, Eq. (7.9), to $\mathcal{O}(\kappa_+^2/v_R^2)$, where μ_{3L}^2/v_R^2 now plays the role of ρ_1. Schematically,

$$2\frac{\mu_{3L}^2}{v_R^2} - \rho_3 \sim \frac{\kappa_+^2}{v_L v_R}\beta_i. \tag{7.33}$$

Thus, unless the β_i terms cancel to good precision, the natural value for μ_{3L}^2 is of the order of $\mathcal{O}(\frac{v_R}{v_L}\kappa_+^2)$. The μ_{3L}^2 parameter thereby is the main difference between this and the CP_1 case. Since, if $\mu_{3L}^2 = \mu_{3R}^2$ we could have identified it with μ_3^2 of the CP_1 case. Note, however, that μ_{3L} only appears in the mass terms for the left-handed triplet fields. Furthermore, the two mechanisms which led to small masses of additional Higgs fields in the CP_1 case (see section 7.1.1) are still in place here. The equivalent of Eq. (7.10) now implies $\alpha_{3R} \sin\alpha$ to be small. Choosing α_{3R} small again implies small flavor-changing Higgs masses. On the other hand, a small value of α implies, through Eqs. (7.11) and (7.9), small $2\mu_{3L}^2 - v_R^2\rho_3$ which dictates the masses of the left-handed triplet fields.

Thus, the condition that $\alpha_{3R} \sin\alpha$ be small and the lower bound on the flavor-changing Higgs masses force α to be small. As this is the only source of CP violation in the quark

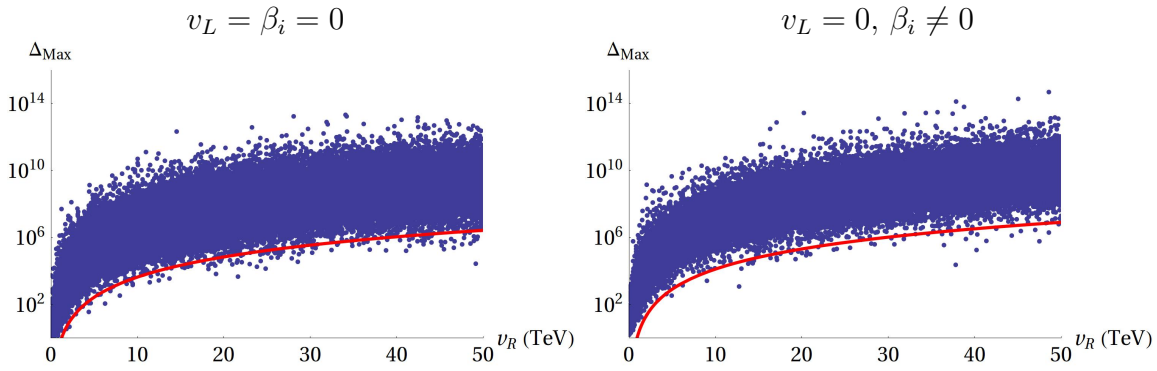

Figure 7.7: Similar plots to that of Fig. 7.6. The plot on the left shows the fine-tuning in the case where β_i and v_L are set to zero, while the figure on the right does the same in the case where only v_L is set to zero. The red lines are again chosen such that 0.1% of the points are found below it. It is parametrized by $2 \cdot 10^{-3} v_R^4/\kappa_+^4$ and $5 \cdot 10^{-3} v_R^4/\kappa_+^4$ in the left and right plots, respectively.

sector, one might expect the model to predict hardly any CP violation. This would lead one to doubt the viability of the model. However, the lower bounds on the CP-violating Higgs mass in the C and P cases assumed the relation between the CKM matrices these symmetries imply. Because there is no such relation in this case the bounds can be weakened. For example, the analysis of meson-mixing and decay data of Ref. [207] shows that points in parameters space for values of M_H as low as $M_H \sim 2.4\,\text{TeV}$ can become accessible by tuning the elements of the right-handed CKM matrix. Such values still imply a very small $\alpha = \mathcal{O}(v_L/v_R)$. However, even smaller values of M_H might be achieved at the price of additional fine-tuning of the right-handed CKM elements [207], which would allow for larger α. This fine-tuning would appear in addition to the fine-tuning in the Higgs potential.

Fine-tuning

The parameters multiplying the left-handed triplet terms do become important when discussing the fine-tuning in this potential. These terms contribute terms to the minimum equations which are smaller than those encountered in the P- and C-symmetric cases. This means these equations now relate high scales to even smaller scales, indicating more fine-tuning.

We again go through the same procedure as in the P- and C- symmetric cases, generating random points in parameter space and calculating the measure of fine-tuning. The results are shown in Figs. 7.6 and 7.7. Clearly, when $v_L \neq 0$ and $\beta_i \neq 0$ the fine-tuning measure reaches new heights, due to the vev see-saw relation and the newly added $\text{Tr}(\Delta_L \Delta_L^\dagger)^2$ terms. However, when we choose to eliminate the vev see-saw relation we obtain fine-tuning measures comparable to the C- and P-symmetric cases. This may have been expected as when $v_L = 0$ the terms which differ from the P case do not contribute to the minimum equations. We then obtain the minimum equations of the P-symmetric potential (with $\delta_2 = 0$), with the translations, $\mu_3^2 \to \mu_{3R}^2$, $\rho_1^2 \to \rho_{1R}^2$ and $\alpha_i^2 \to \alpha_{iR}^2$. Thus, as far as the fine-tuning is concerned, when $v_L = 0$ the CP-symmetric potential simplifies

to a special case of the P-symmetric potential. Therefore, the relations between the β_i parameters one then obtains are those of the P-symmetric case, Eq. (7.24).

7.3 Summary and conclusions

The most symmetric minimal LR models, the ones invariant under P, C, and CP, turn out not to be viable. There are just two possible implementations of both P and C that are able to produce the observed quark masses, yielding the CP_1 and CP_2 models. The models differ in the relation among the left and right CKM matrices. In the case of the CP_1 model this relation puts constraints on CP-violating observables from kaon and B-meson mixing that are incompatible with measurements from B factories and LHCb, in particular, the bounds on the B-mixing angle ϕ_d. As the Yukawa couplings of the minimal pseudomanifest LRM coincide with those of the CP_1 model, it follows that it is also excluded.

The CP_2 model cannot be excluded in the same way, as there is in general no simple relation between left and right CKM matrices. In this case the Higgs potential is more constraining. Here it was shown that the Higgs potentials of the CP_2 model is, to good approximation, equal to a special case of the CP_1-invariant potential. For that potential it was shown in Ref. [201] that whenever there is spontaneous CP violation, $\alpha \neq 0$, the potential cannot reproduce the SM Higgs spectrum and since the model has no explicit CP violation, the case without spontaneous CP violation has no CP violation at all. Upon field redefinitions, these conclusions carry over to the CP_2 model, which can therefore be considered excluded. In addition, both models generally require a large amount of fine-tuning. The minimum equations generally relate very different scales, κ_+, v_R and v_L, which implies that some of the parameters will have to be fine-tuned. The most extreme tuning results from the so-called vev see-saw relation Eq. (7.13) [155], which implies a huge amount of fine-tuning.

Less symmetric possibilities are the P-, C-, and CP-symmetric LRMs, the first two are LR symmetric, while the last possibility, CP, does not relate left- and right-handed fields. The most widely studied case is the P-symmetric LRM. This type of LRSM is most constrained in the limit that the ratio of vevs $r \equiv \kappa'/\kappa$ is small $\lesssim m_b/m_t$. Based on an analytical solution for the phases in the CKM matrices, which allows for strong constraints from CP-violating observables kaon and B-meson mixing and the neutron EDM, a lower bound $M_2 \gtrsim 10\,\text{TeV}$ was obtained [79]. Outside of the $r \lesssim m_b/m_t$ regime this solution for the phases does not exist and the bound is weakened, $M_2 \gtrsim 3\,\text{TeV}$ [138]. Use of a more general solution, recently derived [171], may also allow one to constrain r and α, which has so far not been done in the literature. This shows that the indirect constraints for P-symmetric LRMs are more stringent than the direct limits on M_2 for left-right symmetric models, which currently are 2 TeV if one refrains from making assumptions about right-handed neutrinos. The increase of experimental sensitivity in the coming 10 years is expected to push the lower indirect bound on M_2 to roughly 8 TeV, thereby exploring a considerable part of the still available parameter space of the P-symmetric LRMs. The minimal manifest LRSM, which is the special case of vanishing α, is more constrained, here the current bound on the $W_R^\pm$ mass is $M_2 \gtrsim 20\,\text{TeV}$ [183]. Thus, the

manifest mLRSM is viable still but beyond the reach of LHC searches.

The Higgs potential of the P-symmetric LRM has been widely studied in the literature [202, 203, 155, 201]. This potential is very similar to that of the CP_1-symmetric LRM [201], which implies that a SM-like Higgs spectrum is only possible for a specific value of the spontaneous phase. In this case, however, the spontaneous phase can be nonzero, although it is now entirely dictated by the explicit CP violation present in the potential. In a sense this means that the CP-violating phase α is put in by hand and can be as large as allowed by the value of r and the constraints from kaon and B-meson mixing and the nEDM.

Although these models are all still viable, there is the issue of fine-tuning resulting from the minimum equations. Again the most extreme tuning results from the vev see-saw relation, which implies a huge amount of fine-tuning. It is possible to avoid this by setting v_L and β_i to zero by hand as was done in Ref. [79]. As we have demonstrated, the same reduction in the amount of fine-tuning can be achieved with $v_L = 0$ only, in which case there are two relations among the β_i parameters [201]. The minimum amount of fine-tuning, assuming $\mathcal{O}(1)$ parameters, is then found to be $\Delta \sim 100$, where Δ is a measure for fine-tuning often employed in the study of supersymmetric extensions of the SM, defined in Eq. (7.23). It indicates that a change in one parameter by a factor of $\mathcal{O}(1)$ implies a change in another parameter by a factor $\mathcal{O}(100)$. This may be acceptable for a theory with such widely varying scales.

Accepting such a minimum amount of fine-tuning, the P-symmetric LRM with some constraints on its β_i parameters is still viable, but is expected to be much further constrained in the coming decade. As the lower bound on M_2 and hence on v_R increases, the amount of fine-tuning will also increase, scaling roughly with v_R^4/κ^4 as indicated by the results of this chapter.

The C-symmetric LRM has been studied less in the literature. For example the C-symmetric Higgs potential, which was derived in chapter 6, had been absent from the literature previously. Furthermore, in this case the phases in the CKM matrices are free parameters, which can be tuned to avoid constraints from CP-violating observables. Nonetheless, a lower bound similar to the P-symmetric case can be set, $M_2 \gtrsim 3\,\text{TeV}$ [138].

For the C-symmetric and P-symmetric LRMs the kaon and B observables depend on the right-handed CKM matrix elements. In turn, these elements are determined to a large extent when a P or C symmetry is enforced. As a result, the kaon and B observables are the most sensitive probes of the mass of the $W_R^\pm$ boson and the most promising way to explore the parameter space of these models. This is due to the fact that these observables are determined by the left- and right-handed CKM elements which, in the P/C-symmetric case, are constrained by the LR symmetries. Since the relation between the left and right CKM matrices is different for the C- and the P-symmetric LRMs, these two types of models predict a different pattern in $B_{d,s}$-mixing. Thus, if signs of an LRM are observed in this sector one should in principle be able to tell the difference between C- and P-symmetric LR models using $B_{d,s}$-mixing observables.

Although new complex phases arise in the Higgs sector of the C-symmetric LRM, the Higgs potential is again very similar to that of the CP_1-symmetric LRM. A SM-like Higgs spectrum is only possible for a specific value of the spontaneous phase, which is again entirely dictated by the explicit CP violation present in the potential. Perhaps

unsurprisingly, the amount of fine-tuning required in the potential is similar to the P-symmetric case. By setting $v_L = 0$ (and possibly $\beta_i = 0$) the vev see-saw relation can be eliminated and the fine-tuning dramatically reduced. Nevertheless, in this case a minimum fine-tuning of $\Delta \sim 100$ is required as well.

Finally, the CP-symmetric model, which need not be P and C symmetric separately, is considerably different from the above cases. This is due to the fact that CP is not a LR symmetry. Although, like the P case, there is a bound on $r \sin\alpha$, the CKM matrices and coupling constants are now generally unrelated to one another ($g_L \neq g_R$). This means there is more freedom in this model, such that *both* direct and indirect bounds are expected to be weakened, see, for instance, Ref. [207]. As most features of the Higgs sector again resemble the CP_1 case, a nonzero spontaneous phase again requires light Higgs fields. However, due to the additional freedom, the bounds on these fields may be weaker in this case. On the other hand, the potential generally requires more fine-tuning than the CP_1 potential, except when considering the $v_L = 0$ cases, in which the fine-tuning is similar to the P-symmetric case.

Recapitulating, LRSMs are arguably the most attractive of the possible LRMs, but also the most constrained. The LR scale of these models is currently constrained to be in the TeV range, $M_2 \gtrsim 3\,\text{TeV}$. Instead, CP-symmetric LRMs seem less constrained, allowing for more freedom in the right-handed CKM matrix. In the Higgs sector the potentials of the LRSMs all turn out to be quite similar. The CP-symmetric case allows some more freedom in the masses of the left-handed triplet fields, but is otherwise similar as well. The Higgs potentials of all three models require a considerable amount of fine-tuning, which poses the biggest challenge to their viability.

In the next chapter we will move on to see how the EFT approach of chapters 4-5 can be applied to the LRMs discussed in this and the previous chapter. In particular, we will consider the possibility to test the CP-violating scenario of the minimal LRM by use of the EDMs of light nuclei. Assuming the planned experiments for measurements of these EDMs do indeed find a nonzero value, we will explore to what extent they could be used as a test of the LRM in the next chapter.

Appendix 7.A $P + CP$ symmetric case

The goal of this appendix is to derive the possible $C + P$-symmetric LRMs. In doing so we will closely follow Refs. [181, 178], and work our way through Fig. 7.1 in more detail, starting from its top-left corner.

- $H = H_1$

  After enforcing invariance of the Yukawa interactions of Eq. (6.12) under the CP transformation of Eq. (7.1), the following relations can be obtained

  $$\Gamma = e^{i\varphi} U_L^T \tilde{\Gamma}^T U_R^*, \qquad \tilde{\Gamma} = e^{-i\varphi} U_L^T \Gamma^T U_R^*. \tag{7.34}$$

  Through Eq. (6.13), this implies

  $$\mathrm{Tr}(M_u M_u^\dagger) = \mathrm{Tr}(M_d M_d^\dagger), \tag{7.35}$$

  which is clearly excluded. Thus, only H_2 may still be an acceptable form of H.

- $H = H_2$

  Applying the CP transformation on the Yukawa interactions in this case gives the relations

  $$\Gamma = e^{-i\varphi} U_L^T \Gamma^T U_R^*, \qquad \tilde{\Gamma} = e^{i\varphi} U_L^T \tilde{\Gamma}^T U_R^*. \tag{7.36}$$

  Unlike the H_1 possibility the above relations do not allow us to immediately exclude the model, nonetheless they do constrain the Yukawa matrices. For the remaining discussion it will be useful to move to the basis where Γ is diagonal by use of a rotation in flavor-space. This does not affect the parity transformation in Eq. (6.7), furthermore, in this basis Γ and $\tilde{\Gamma}$ will still be hermitian and the relations in Eq. (7.36) will still hold. Eq. (7.36) then implies

  $$\left[U_{L,R},\, \Gamma^2\right] = 0. \tag{7.37}$$

  Clearly, if Γ^2 is non-degenerate the $U_{L,R}$ matrices are diagonal. Without loss of generality we can assume $\tilde{\Gamma}^2$ to be at least as degenerate as Γ^2. The case where Γ^2 is threefold degenerate is excluded as it would not allow for any mixing between the quarks. Thus, we are left with two possibilities: Γ^2 is either non-degenerate or has a twofold degeneracy. We start with the case where Γ^2 is non-degenerate.

  - Γ^2 non-degenerate

    In this case both U_L and U_R have to be diagonal. Furthermore, we can always choose a basis such that $U_L = \mathbf{1}$, this change of basis leaves both Γ and the parity transformation unchanged. Eq. (7.36) then suggests that $U_R = e^{-i\varphi}\mathbf{1}$, however, this is only true whenever the elements of Γ are non-zero. As Γ is non-degenerate in this case, only one element can be zero. By ordering the eigenvalues of Γ by size we can again divide this case up into two possibilities: $\Gamma_{11} = 0$ and $\Gamma_{11} \neq 0$.

I $\Gamma_{11} \neq 0$
In this case we have $U_R = e^{-i\varphi}\mathbf{1}$. Through Eq. (7.36) one can obtain $e^{4i\varphi} = 1$. This allows for the two possible CP transformations which can not be excluded solely by considering the resulting quark masses and mixing matrices.

(a) CP_1
Choosing $e^{i\varphi} = \pm 1$ implies, through Eq. (7.36), that $\tilde{\Gamma}$ is a symmetric and hermitian matrix, $\tilde{\Gamma} = \tilde{\Gamma}^* = \tilde{\Gamma}^T$.

(b) CP_2
Choosing instead $e^{i\varphi} = \pm i$, implies, through Eq. (7.36), that $\tilde{\Gamma}$ is an anti-symmetric and hermitian matrix, $\tilde{\Gamma} = -\tilde{\Gamma}^* = -\tilde{\Gamma}^T$.

II $\Gamma_{11} = 0$
In this case we have

$$U_R = e^{-i\varphi} \begin{pmatrix} e^{i\phi} & 0 \\ 0 & \mathbf{1} \end{pmatrix}. \tag{7.38}$$

The relation for $\tilde{\Gamma}$ in Eq. (7.36) then allows one form of $\tilde{\Gamma}$ different from the previous case which could generate a non-zero Cabibbo angle, namely,

$$\tilde{\Gamma} = \begin{pmatrix} 0 & \delta \\ \delta^\dagger & 0 \end{pmatrix}, \tag{7.39}$$

where $\delta = (\delta_1, \delta_2)$. This then leads to a relation for the quark masses

$$1 \leq \frac{\mathrm{Tr}(M_u M_u^\dagger)}{\mathrm{Tr}(M_d M_d^\dagger)} \frac{|\mathrm{Det} M_d|^2}{|\mathrm{Det} M_u|^2} \approx \left(\frac{m_s m_d}{m_c m_u} \right)^2, \tag{7.40}$$

which is not realized in nature.

Thus, from the non-degenerate case two possible CP transformations arose, which imply two possible models, namely, CP_1 Ia and CP_2 Ib.

Having exhausted the possiblities in the non-degenerate Γ^2 case, we will now consider the twofold-degenerate option.

– Γ^2 twofold-degenerate
After reordering its eigenvalues, we have two possibilities for Γ, namely, $\Gamma = \mathrm{diag}(\gamma_1, \epsilon\gamma_1, \gamma_3)$, where $\epsilon = \pm 1$. In either case, the matrices $U_{L,R}$ can be written as

$$U_L = \begin{pmatrix} U_L' & 0 \\ 0 & 1 \end{pmatrix}, \qquad U_R = \begin{pmatrix} U_R' & 0 \\ 0 & e^{i\beta_R} \end{pmatrix}. \tag{7.41}$$

I $\epsilon = +1$
This case does not give a new solution. Eq. (7.36) now implies $U'_L e^{-i\varphi} = U'_R$. A basis transformation can then be performed such that $U'_L = \mathbf{1} = e^{i\varphi}U'_R$ without changing Γ. This brings us back to the non-degenerate cases. If we choose $\gamma_3 \neq 0$ we obtain $U_L = \mathbf{1} = e^{i\varphi}U_R$ and thereby case Ia or Ib, depending on the choice for $e^{i\varphi}$, with the additional constraint that Γ is twofold degenerate. If we would instead choose $\gamma_3 = 0$, we would obtain a case equivalent to II, with the added constraint that Γ be twofold degenerate.

II $\epsilon = -1$
in this case a new solution can be obtained, Eq. (7.36) now implies

$$U'_R = e^{-i\varphi}\sigma_3 U'_L \sigma_3. \tag{7.42}$$

The relation for $\tilde{\Gamma}$ in Eq. (7.36) then allows for two new possibilities, which are equal up to a basis transformation [197]. The more general solution is given by

$$\tilde{\Gamma} = \begin{pmatrix} \delta & \epsilon'\delta & d \\ \epsilon'\delta & \delta & -\epsilon' d \\ d^* & -\epsilon' d^* & 0 \end{pmatrix}, \tag{7.43}$$

where $\epsilon' = \pm 1$. This implies the following mass relation

$$1 \leq \left(\frac{|\mathrm{Det}M_u|}{|\mathrm{Det}M_d|}\right)^2 \left(\frac{\mathrm{Tr}M_d M_d^\dagger}{\mathrm{Tr}M_u M_u^\dagger}\right)^3, \tag{7.44}$$

which leads to $m_t/m_b \lesssim (m_u m_c/m_s m_d)^{1/2}$ and thereby excludes this scenario.

Appendix 7.B The physical Higgs fields

In this appendix we will give a brief overview of the mass eigenstates of the Higgs particles. As these mass eigenstates, and the corresponding masses, derive from a rather complicated potentials the exact expressions are lengthy and not very enlightening. We will therefore consider only expressions resulting from the P-symmetric potential. In addition, we will restrict to the the often considered case, $\beta_i = v_L = 0$ and provide expressions up to linear terms in the following quantities which are assumed to be small, $\kappa/v_R \ll 1$ and $\xi \equiv \kappa'/\kappa \ll 1$, and keep only terms linear in them.

In total there are 20 degrees of freedom contained within the ϕ (8 d.o.f.) and $\Delta_{L,R}$ (both have 6 d.o.f.) fields. The bidoublet gives rise to 4 real neutral scalars and 2 singly-charged scalars. The triplet fields both contain two real scalars, one singly-charged field and one doubly-charged scalar. Not all of these fields are physical, since the breaking of $SU(2)_L$ and $SU(2)_R$ leads to six would-be-Goldstone bosons. These would-be-Goldstone bosons

Table 7.2: The physical Higgs mass eigenstates and their masses for the P-symmetric potential, restricted to the $\beta_i = v_L = 0$ case. Only linear terms in κ/v_R and $\xi \equiv \kappa'/\kappa$ have been kept [159, 160, 79].

Mass eigenstate	**Mass squared**
Neutral scalars	
$h^0 = \sqrt{2}\mathrm{Re}\,(\phi_1^{0*} + \xi e^{-i\alpha}\phi_2^0)$	$\frac{1}{2}\alpha_3 v_R^2 \xi^2 + (2\lambda_1 - \frac{1}{2}\alpha_1^2/\rho_1)\kappa^2$
$H_1^0 = \sqrt{2}\mathrm{Re}\,(\phi_2^0 - \xi e^{i\alpha}\phi_1^{0*})$	$\frac{1}{2}\alpha_3 v_R^2$
$A_1^0 = \sqrt{2}\mathrm{Im}\,(\phi_2^0 - \xi e^{i\alpha}\phi_1^{0*})$	$\frac{1}{2}\alpha_3 v_R^2$
$\sqrt{2}\mathrm{Re}\,\delta_R^0$	$2\rho_1 v_R^2$
$\sqrt{2}\mathrm{Re}\,\delta_L^0$	$\frac{1}{2}(\rho_3 - 2\rho_1)v_R^2$
$\sqrt{2}\mathrm{Im}\,\delta_L^0$	$\frac{1}{2}(\rho_3 - 2\rho_1)v_R^2$
Singly-charged scalars	
$H_2^+ = \phi_1^+ + \xi e^{i\alpha}\phi_2^+ + \frac{\kappa}{\sqrt{2}v_R}\delta_R^+$	$\frac{1}{2}\alpha_3 v_R^2$
δ_L^+	$\frac{1}{2}(\rho_3 - 2\rho_1)v_R^2 + \frac{1}{4}\alpha_3\kappa^2$
Doubly-charged scalars	
δ_R^{++}	$2\rho_2 v_R^2$
δ_L^{++}	$\frac{1}{2}(\rho_3 - 2\rho_1)v_R^2 + \frac{1}{2}\alpha_3\kappa^2$

consist of two singly-charged scalars and two real neutral scalars, which are absorbed by the $W_{L,R}^{\pm}$ and $Z_{L,R}$ gauge fields, and can be written as the linear combinations

$$G_L^+ = \phi_2^+ - \xi e^{-i\alpha}\phi_1^+, \qquad G_R^{\pm} = \delta_R^+ - \frac{\kappa}{\sqrt{2}v_R}\phi_1^+,$$
$$G_Z^0 = \sqrt{2}\mathrm{Im}\,(\phi_1^{0*} + \xi e^{-i\alpha}\phi_2^0), \qquad G_{Z'}^0 = \sqrt{2}\mathrm{Im}\,\delta_R^0. \tag{7.45}$$

This leaves 6 physical neutral states, 2 singly-charged scalars, and 2 doubly-charged scalars. For $\beta_i = v_L = 0$ and up to first order in $\kappa/v_R \ll 1$ and $\xi \equiv \kappa'/\kappa$ the mass eigenstates and their masses are shown in Table 7.2. Of the neutral mass eigenstates, h^0 plays the role of the SM-like Higgs boson, while H_1 and A_1 are the scalars which obtain flavor-changing neutral currents. As was discussed in section 7.1.1, and can be verified from Table 7.2, these scalars become light, $\mathcal{O}(\kappa_+^2)$, when α_3 is small, $\mathcal{O}(\frac{\kappa_+^2}{v_R^2})$.

Chapter 8

Electric dipole moments from minimal left-right models

In the previous chapters we have mainly considered EDMs measurements as a way to constrain sources of BSM CP violation. Instead, in this chapter, we will discuss the possibility of testing models of BSM physics using EDMs, in particular the minimal left-right model (mLRM) with $\bar{\theta} = 0$, assuming a nonzero value of an EDM is found. However, a single nonzero EDM alone is not enough to provide a test, as a single EDM can be attributed to any model of CP-violating BSM physics. Nonetheless, BSM models can in principle give rise to a relation between different EDMs. BSM models which predict a definite pattern among the EDMs could be tested using EDM measurements only.

The main motivations for this chapter are the plans to measure the EDMs of charged spin-carrying particles in storage rings [92, 93, 94, 95]. It has been proposed that this method can be used to measure the EDMs of the proton and deuteron with a precision of $10^{-29}\,e\,\mathrm{cm}$, three orders of magnitude better than the current neutron EDM limit. EDMs of other light ions, such as the helion (^{3}He nucleus) and triton (^{3}H nucleus) are candidates as well. Therefore, we will consider whether such a test can be devised for the mLRM using only the EDMs of light nuclei[1]. We will expand on the possibility of testing various other scenarios of CP violation using similar techniques in chapter 9, and see whether one indeed can distinguish between scenarios.

The idea to test BSM models using the EDMs of light nuclei was already discussed in section 5.1.4 of chapter 5. Many of the results, and the techniques that led up to them, stated that in chapter will again be necessary in this chapter. In particular, deriving the impact of the mLRM on the EDMs of light nuclei requires a series of steps. Firstly, at the BSM scale the heavy particles are integrated out and the mLRM can be matched onto the CP-violating EFT of chapter 3, which can then be evolved to low energies using the results of chapter 4. Secondly, around 1 GeV the resulting Lagrangian is then matched onto the low-energy constants (LECs) of the chiral Lagrangian. Finally, the EDMs can then be expressed in terms of these LECs.

[1]Of course, there are many other observables, such as those discussed in the previous chapters, that could provide tests of mLRMs. In case of a signal of BSM physics, one would ideally combine information from all measurements, from EDM measurements to meson-mixing observables and collider searches. In this chapter, however, we will restrict ourselves to tests involving light-nuclear EDMs only.

Here we briefly repeat and expand on some of the above steps, while simply employing the results of previous chapters for others. In section 8.1, we give a somewhat more rigorous derivation of the matching than was employed in chapter 6, where the mLRM was matched directly onto the four-quark operator induced at M_W. Here, we will discuss how the operator these FQ interactions originate from is generated in the mLRM . In contrast, to this more involved derivation, we will simply use the results of chapter 4 for the running.

Subsequently, we will discuss the induced chiral Lagrangian in section 8.2. In this section we will not be satisfied with simply employing the results of chapter 5. This is due to the fact that, as was already mentioned in chapter 5, an additional three-pion vertex is induced, which was neglected previously. Here we will take this interaction into account and give a more detailed discussion of the remaining induced interactions. This discussion will lead to expressions for the EDMs in terms of the LECs generated by the mLRM .

Although the hadronic uncertainty in the sizes of these LECs themselves is sizable, the same LECs appear in several EDMs which means that the hadronic uncertainties cancel to a large degree. It is this property, in addition to the envisaged high experimental accuracy, which makes the plans to measure the EDMs of light nuclei so exciting. The combination of all of the above will lead us to conclude that estimates of the nucleon EDMs, d_n and d_p, alone are insufficient to test the mLRM in section 8.6. In fact, the predictions and estimates of the two-nucleon contribution to the EDMs of the light ions, especially of the deuteron and helion, will be crucial to test the mLRM .

8.1 Matching to the CP-violating EFT

In this section we discuss the $\not{P}\not{T}$ dimension-six operators arising in the mLRM that give the leading contributions to EDMs. From previous chapters we know that the leading contributions induced by the mLRM come from the four-quark left-right (FQLR) operators, see e.g. Eq. (6.24). Here we will derive how the right-handed $W^{\pm}$ current, which these FQ operators originate from, is generated in the mLRM. In particular we derive the operator O_{W_R} of Eq. (3.13), which gives the dominant contribution to hadronic EDMs.

As mentioned in section 6.2.3, this is not the only $\not{P}\not{T}$ operator induced at the electroweak scale. The (C)EDM operators of light quarks are also generated, but only through loop diagrams which suppresses the resulting operators with respect to the FQ operators by $\sim \alpha_w/\pi$. In addition, the light-quark EDMs and CEDMs are proportional to a small quark mass, which further suppresses their contribution to hadronic EDMs with respect to the four-quark operators arising from O_{W_R} [80, 47]. The Weinberg three-gluon operator can be produced as well, but only at the two-loop level and its contribution to EDMs is negligible [80, 47].

Finally, $\not{P}\not{T}$ four-quark operators are induced by tree-level exchange of the additional, non-SM-like Higgs particles of the model that have CP-violating couplings to quarks. However, the four-quark operators involving light quarks are suppressed by small Yukawa couplings. The operators containing heavy quarks can (partially) overcome these suppression factors. However, these operators do not contribute directly to the nucleon

EDMs. Instead, four-quark operators with two heavy quark fields induce, after integrating out the heavy quarks, dimension-seven operators of the form $(\bar{q}q)\epsilon^{\alpha\beta\mu\nu}G^a_{\alpha\beta}G^a_{\mu\nu}$ and $(\bar{q}i\gamma_5 q)G^a_{\mu\nu}G^{a\,\mu\nu}$ [208, 209], where q denotes a light quark. The size of the contributions of these operators to the nucleon EDM has been estimated in Ref. [209] and turns out to be significantly smaller than the FQLR contribution. In combination with the fact that the additional Higgs bosons giving rise to these four-quark operators should be heavy, with masses exceeding 10 TeV in order to evade FCNC constraints, see e.g. chapter 7, Ref. [79], we can neglect such four-quark operators [80, 47].

Thus, for hadronic EDMs the most important interaction is the right-handed current interaction in Eq. (3.13), which is produced after integrating out the $W_R^\pm$ boson. This operator arises from the interaction between the charged gauge bosons, $W^\pm_{L,R}$, and the bidoublet ϕ. In fact, it is the kinetic term of the bidoublet which is responsible for the mixing between the $W_L^\pm$ and $W_R^\pm$ bosons, which in turn gives rise to the operator in Eq. (3.13). We will therefore need the covariant derivative of the bidoublet,

$$\mathcal{D}_\mu\phi = \partial_\mu\phi + i\frac{g_L}{2}W^a_{L\mu}\tau^a\phi - i\frac{g_R}{2}\phi W^a_{R\mu}\tau^a. \tag{8.1}$$

The kinetic term of the bidoublet is given by

$$\mathcal{L} = \mathrm{Tr}[(\mathcal{D}_\mu\phi)^\dagger(\mathcal{D}^\mu\phi)] = \frac{ig_R}{\sqrt{2}}\mathrm{Tr}\left[\begin{pmatrix}0 & W^+_{R\mu}\\ W^-_{R\mu} & 0\end{pmatrix}\phi^\dagger\mathcal{D}^\mu\phi\right] + \text{h.c.} + \dots \tag{8.2}$$

Here we only kept terms bilinear in $W_R^\pm$. We can now integrate out $W_R^\pm$ to obtain

$$\mathcal{L}_{W_R} = \frac{ig_R^2}{2M_R^2}\mathrm{Tr}\left[\begin{pmatrix}0 & J^+_{R\mu}\\ J^-_{R\mu} & 0\end{pmatrix}\phi^\dagger D^\mu_L\phi\right] + \text{h.c.} + \dots \ , \tag{8.3}$$

with $J^-_{R\mu} = \overline{U}_R V_R\gamma_\mu D_R$ and $J^+_{R\mu} = (J^-_{R\mu})^\dagger$, where V_R is the quark-mixing matrix of the right-handed sector, and $M_R \approx g_R v_R/2$ is the mass of $W_R^\pm$. Moreover,

$$D^\mu_L\phi = \partial^\mu\phi + i\frac{g_L}{2}W^{a\mu}_L\tau^a\phi \ . \tag{8.4}$$

The form of the O_{W_R} operator is already visible in Eq. (8.3). It only remains to integrate out the heavy Higgs fields. To do so we write the bidoublet ϕ in terms of two $SU(2)_L$ doublets,

$$\phi = (\phi_1, \phi_2) \ , \qquad \phi_1 \equiv \begin{pmatrix}\phi_1^0\\ \phi_2^-\end{pmatrix} \ , \qquad \phi_2 \equiv \begin{pmatrix}\phi_1^+\\ \phi_2^0\end{pmatrix} \ .$$

The SM Higgs field, φ, is a linear combination of $\tilde{\phi}_1$ and ϕ_2[2]. The remaining linear combination, φ_H, then only involves Higgs fields that are, by assumption, heavy. To good approximation these Higgs fields are given, in terms of the fields in the mass basis, by [79]

$$\varphi = \begin{pmatrix}-G_L^+\\ (h^0 + iG_Z^0)/\sqrt{2}\end{pmatrix} \ , \qquad \varphi_H = \begin{pmatrix}H_2^+\\ (H_1^0 + iA_1^0)/\sqrt{2}\end{pmatrix}. \tag{8.5}$$

[2]This linear combination can only involve $\tilde{\phi}_1$ and not ϕ_1 itself as its hypercharge should match that of the SM doublet, φ.

Expressions for the masses of these fields were given in appendix 7.B of chapter 7. Here G_L^+ and G_Z^0 are the would-be Goldstone boson fields that get absorbed by the W_L^+ and Z_L fields, respectively, while h^0 corresponds to the SM Higgs boson. The basis transformation between the fields $\phi_{1,2}$ and those of Eq. (8.5) is given by [79],

$$\begin{pmatrix} \varphi \\ \varphi_H \end{pmatrix} = \frac{1}{\sqrt{1+\xi^2}} \begin{pmatrix} -1 & \xi e^{-i\alpha} \\ \xi e^{i\alpha} & 1 \end{pmatrix} \begin{pmatrix} \tilde{\phi}_1 \\ \phi_2 \end{pmatrix} \ , \tag{8.6}$$

where $\xi = \kappa'/\kappa$ and $\tilde{\phi} = i\tau_2\phi^*$. With the vevs given in Eq. (6.3), we can check that $\langle\varphi\rangle = \sqrt{\kappa^2+\kappa'^2}/\sqrt{2} = v/\sqrt{2}$, while $\langle\varphi_H\rangle = 0$.

We can now use Eq. (8.6) to rewrite Eq. (8.2) in terms of the fields in the mass basis. Keeping only terms containing the light fields φ, we obtain

$$\begin{aligned} \mathcal{L}_{W_R} &= \frac{ig_R^2}{2M_R^2}\frac{1}{1+\xi^2}\mathrm{Tr}\left[\begin{pmatrix} J_{R\mu}^+ \xi e^{-i\alpha}\varphi^\dagger \\ J_{R\mu}^- \tilde{\varphi}^\dagger \end{pmatrix} D^\mu(\tilde{\varphi},\, \xi e^{i\alpha}\varphi)\right] + \text{h.c.} + \dots \\ &= \frac{ig_R^2}{2M_R^2}\frac{\xi}{1+\xi^2}\left[e^{i\alpha}\tilde{\varphi}^\dagger(D^\mu\varphi)J_{R\mu}^- + e^{-i\alpha}\varphi^\dagger(D^\mu\tilde{\varphi})J_{R\mu}^+\right] + \text{h.c.} + \dots \\ &= \frac{ig_R^2}{M_R^2}\frac{\xi}{1+\xi^2}e^{i\alpha}\tilde{\varphi}^\dagger(D^\mu\varphi)J_{R\mu}^- + \text{h.c.} + \dots \ , \end{aligned} \tag{8.7}$$

where we used $\left[i\tilde{\varphi}^\dagger(D_\mu\varphi)\right]^\dagger = i\varphi^\dagger(D_\mu\tilde{\varphi})$. Finally, a comparison with Eq. (3.13) shows that

$$\Xi_1 = \frac{g_R^2}{M_R^2}\frac{\xi}{1+\xi^2}e^{i\alpha}V_R^{ud} \simeq \frac{2}{\kappa^2+\kappa'^2}\frac{\kappa\kappa'}{v_R^2}e^{i\alpha}V_R^{ud} \simeq \frac{2}{v^2}\frac{g_R}{g_L}\sin\zeta\, V_R^{ud}e^{i\alpha} \ . \tag{8.8}$$

This agrees with Eq. (6.24) at M_T as it should.

Having derived the contribution of the mLRM to the right-handed $W^\pm$ current, O_{W_R}, at the electroweak scale, we can now integrate out the $W_L^\pm$ boson and evolve the resulting operators to the QCD scale. For these steps we simply apply the results derived in chapter 4. Thus, the Lagrangian at $M_{\rm QCD}$ is

$$\mathcal{L}_{LR} = -i\,\mathrm{Im}\left(V_L^{ud*}\Xi_1(M_T)\right)\left[\eta_1\bar{u}_R\gamma^\mu d_R\,\bar{d}_L\gamma_\mu u_L + \eta_8\,\bar{u}_R\gamma^\mu t_a d_R\,\bar{d}_L\gamma_\mu t_a u_L\right] + \text{h.c.}, \tag{8.9}$$

where we have $\eta_1 = 1.1$ and $\eta_8 = 1.4$.

In the next section we will discuss the interactions these operators induce in the chiral Lagrangian.

8.2 The chiral Lagrangian

As mentioned above, an additional interaction appears in the chiral Lagrangian with respect to those discussed in section 5.1.1. The relevant interactions that are induced by the FQLR operators in Eq. (8.9) can be written as

$$\begin{aligned} \mathcal{L} &= -2\,\bar{N}\left(\bar{d}_0 + \bar{d}_1\tau_3\right)S^\mu N\, v^\nu F_{\mu\nu} \\ &\quad + \bar{g}_0\bar{N}\boldsymbol{\pi}\cdot\boldsymbol{\tau}N + \bar{g}_1\bar{N}\pi_3 N - \bar{\Delta}\frac{\pi_3\boldsymbol{\pi}^2}{2F_\pi}. \end{aligned} \tag{8.10}$$

Next, we would like to express the LECs in terms of $\eta_{1,8}\mathrm{Im}\,\Xi_1$ of Eq. (8.9). As the two four-quark interactions of Eq. (8.9) have the same chiral properties they induce hadronic interactions of identical form (although the LECs, of course, will be different). We therefore use $\mathrm{Im}\,\Xi$ to collectively denote $\eta_{1,8}\,\mathrm{Im}\big(V_{ud}^*\,\Xi_1\big)$. First of all, for the isoscalar and isovector nucleon EDMs, $\bar{d}_{0,1}$ we can still do no better than the NDA estimates of section 5.1.1, which were

$$\bar{d}_{0,1} = \mathcal{O}\left(\frac{eM_{\rm QCD}}{(4\pi)^2}\mathrm{Im}\,\Xi\right). \tag{8.11}$$

We will discuss the other LECs in more detail.

Because the FQLR violates isospin symmetry it does not contribute to $\bar{g}_0$ directly. Instead, it contributes to isospin-violating LECs in two ways. Firstly, a pion tadpole is induced, i.e. a term linear in the pion field, $\mathcal{L} \propto \pi_3$. However, due to the chiral properties of the FQLR, this tadpole term is related to a three-pion term [56] which reads

$$\mathcal{L}^{\rm LR} = \bar{\Delta} F_\pi \pi_3 \left(1 - \frac{\boldsymbol{\pi}^2}{2F_\pi^2}\right) \ . \tag{8.12}$$

In addition, the FQLR induces a direct contribution to $\bar{g}_1^{LR}$, which was already discussed in section 5.1.1. The sizes of the LECs can be estimated by NDA,

$$|\bar{\Delta}| = \mathcal{O}\left(\frac{M_{\rm QCD}^4}{(4\pi)^2}\mathrm{Im}\,\Xi\right), \qquad |\bar{g}_1| = \mathcal{O}\left(\frac{M_{\rm QCD}^2}{4\pi}\mathrm{Im}\,\Xi\right). \tag{8.13}$$

The tadpole can be removed using field redefinitions, however, this leaves a three-pion vertex (see Eq. (8.16)). Moreover, the removal of the tadpole induces an additional contribution to $\bar{g}_1$ proportional to $\bar{\Delta}$,

$$\bar{g}_1 \to \bar{g}_1 + \bar{g}_1' \ , \qquad \bar{g}_1' = -\frac{4c_1\bar{\Delta}}{F_\pi} \ . \tag{8.14}$$

Since $c_1 = \mathcal{O}(1/M_{\rm QCD})$, the additional contribution is formally of the same order as the original term. However, numerically it might be somewhat larger because $4c_1$ is bigger than expected from NDA. In addition, a first non-vanishing contribution to $\bar{g}_0'$ appears[3], also proportional to $\bar{\Delta}$:

$$\bar{g}_0' = -\frac{(m_n - m_p)^{\rm strong}\bar{\Delta}}{2m_\pi^2 F_\pi} \ . \tag{8.15}$$

In conclusion, the relevant pionic and pion-nucleon interactions are given by

$$\mathcal{L}^{\rm LR} = -\bar{\Delta}\frac{\pi_3\boldsymbol{\pi}^2}{2F_\pi} + \bar{g}_0'\bar{N}\boldsymbol{\pi}\cdot\boldsymbol{\tau}N + (\bar{g}_1 + \bar{g}_1')\bar{N}\pi_3 N \ . \tag{8.16}$$

Because $\bar{g}_0'$ and $\bar{g}_1'$ both depend on the same LEC $\bar{\Delta}$, their ratio depends only on known quantities:

$$\frac{\bar{g}_0'}{\bar{g}_1'} = \frac{(m_n - m_p)^{\rm strong}}{8c_1 m_\pi^2} = -0.02 \pm 0.01 \ . \tag{8.17}$$

[3]If the $\bar{\theta}$ term is removed by the Peccei-Quinn mechanism, this contribution to $\bar{g}_0'$ would be absent [210]. Because it is small anyway this has no consequences for our analysis.

Unless $\bar{g}_1$ and $\bar{g}_1'$ cancel to a high degree – which is not expected on any grounds – the coefficient $\bar{g}_0'$ is much smaller [56] than the combination $\bar{g}_1 + \bar{g}_1'$ which appears in observables. From now on, we relabel $\bar{g}_1 + \bar{g}_1' \to \bar{g}_1$ and $\bar{g}_0' \to \bar{g}_0$, and take $|\bar{g}_0/\bar{g}_1| \ll 1$.

Before going on, it should be mentioned that, in principle, two more interactions are induced by $\mathrm{Im}\,\Xi$. These additional two LECs, introduced in Ref. [74], are associated with $\not{P}\not{T}$ nucleon-nucleon contact interactions of the form

$$\mathcal{L}_{NN} = \bar{C}_1 \bar{N} N \, \partial_\mu (\bar{N} S^\mu N) + \bar{C}_2 \bar{N} \boldsymbol{\tau} N \cdot \partial_\mu (\bar{N} S^\mu \boldsymbol{\tau} N) \ . \tag{8.18}$$

However, for the FQLR operator discussed above these contact interactions appear at high order in the chiral Lagrangians and their effects are negligible compared to the one-pion exchange between nucleons proportional to $\bar{g}_{0,1}$ [211].

As was already mentioned in section 6.2.3 the hierarchy between $\bar{g}_0$ and $\bar{g}_1$ leads to a relation between the light-nuclear EDMs, however, this could still be spoiled by the three-pion vertex in Eq. (8.16). In the upcoming sections we will derive this relation, while leaving a discussion of the role of the three-pion interaction to section 8.4.2.

8.3 The EDMs of the neutron and proton

The contributions of the LECs to the EDMs of the neutron and proton were already mentioned in section 5.1.1 and are given by

$$\begin{aligned} d_n &= \bar{d}_0 - \bar{d}_1 - \frac{e g_A \bar{g}_0}{8\pi^2 F_\pi} \left(\ln \frac{m_\pi^2}{m_N^2} - \frac{\pi m_\pi}{2 m_N} \right) \ , \\ d_p &= \bar{d}_0 + \bar{d}_1 + \frac{e g_A}{8\pi^2 F_\pi} \left[\bar{g}_0 \left(\ln \frac{m_\pi^2}{m_N^2} - \frac{2\pi m_\pi}{m_N} \right) - \bar{g}_1 \frac{\pi m_\pi}{2 m_N} \right] , \end{aligned} \tag{8.19}$$

while contributions from the three-pion vertex $\bar{\Delta}$ in Eq. (8.16) to the nucleon EDM vanish up to two loops [56].

The dependence of the nucleon EDMs on the LECs $\bar{d}_{0,1}$ implies that considerations based on chiral symmetry alone cannot tell us the sizes of these EDMs. Even if we would have precise knowledge of the LECs $\bar{g}_0$ and $\bar{g}_1$ in terms of $\mathrm{Im}\,\Xi$, the exact dependence of d_n and d_p on $\mathrm{Im}\,\Xi$ would be unclear due to the unknown finite parts of $\bar{d}_{0,1}$. Thus, the EDM results in the nucleon case alone are of limited use to test mLRMs. Therefore, in order to devise such a test, the deuteron and tri-nucleon EDMs will be indispensable.

Nevertheless, we will estimate the size of the nucleon EDMs, so we will be able to compare them to the EDMs to be discussed in the upcoming sections. Naive dimensional analysis gives

$$|d_{n,p}| = \mathcal{O}\left(\frac{e M_{\mathrm{QCD}}}{(4\pi)^2} \mathrm{Im}\,\Xi \right) \simeq (10\,\mathrm{MeV})\, e \mathrm{Im}\,\Xi \ , \tag{8.20}$$

with an unknown sign and the usual (large) uncertainty associated with NDA.

8.4 EDMs of light nuclei

8.4.1 The EDM of the deuteron

The expression for the deuteron EDM in terms of the nucleon EDMs, $d_{n,p}$, and the pion-nucleon interactions, $\bar{g}_{0,1}$ was already discussed in section 5.1.4 and is given by [114, 99, 115, 116, 117, 74, 98, 118, 119],

$$d_D = d_n + d_p + \big[(0.18 \pm 0.023)\,\bar{g}_1 + (0.0028 \pm 0.0003)\,\bar{g}_0\big] e\,\mathrm{fm}\,. \tag{8.21}$$

Because the mLRM predicts $\bar{g}_0/\bar{g}_1 \ll 1$ (see Eq. (8.17)), we can safely ignore the $\bar{g}_0$ term in Eq. (8.21). Inserting the NDA estimates given in Eqs. (8.13) and (8.20) into the expression for the deuteron EDM, we obtain

$$|d_D| = \big|(10\,\mathrm{MeV}) \pm (100\,\mathrm{MeV})\big|\,|e\mathrm{Im}\,\Xi|\ , \tag{8.22}$$

where the first term is due to the nucleon EDMs and the second term is the two-body contribution.

These rough estimates tell us that the two-body contribution to the dEDM is about an order of magnitude larger than the sum of the nucleon EDMs. However, without detailed information on the LECs (for which input from lattice calculations is required) this statement cannot be made much more precise. Nevertheless, as we will see in the next chapter, there are differences between the ratios of deuteron-to-nucleon-EDMs for the mLRSM and other scenarios of BSM CP violation. Therefore, a deuteron EDM experiment is complementary to nucleon EDM experiments, and could give some insight in the fundamental CP-violating source.

Thus, although a measurement of the nucleon EDMs and the deuteron EDM could give a hint of BSM physics and thereby the mLRSM, they would not allow for a precise test of the mLRM. However, measurements of d_n, d_p, and d_D do allow for the extraction of $\bar{g}_1$ from the relation

$$d_D - d_n - d_p = (0.18 \pm 0.023)\bar{g}_1\, e\,\mathrm{fm}\ . \tag{8.23}$$

As we shall discuss in the next section, this extraction of $\bar{g}_1$ allows for the prediction of the ^{3}He and ^{3}H EDMs.

8.4.2 The EDMs of the helion and triton

The experimental EDM storage-ring program not only allows the possible measurement of the proton and deuteron EDMs, but also those of other light nuclei. These EDMs, in terms of $d_{n,p}$ and $\bar{g}_{0,1}$, were already discussed in section 8.4. The relevant expressions are [118, 119, 120]

$$\begin{aligned} d_{^3\mathrm{He}} &= (0.89 \pm 0.01)\, d_n - (0.039 \pm 0.01)\, d_p \\ &\quad + \big[(0.099 \pm 0.026)\,\bar{g}_0 + (0.14 \pm 0.028)\,\bar{g}_1\big]\, e\,\mathrm{fm}\ , \\ d_{^3\mathrm{H}} &= -(0.051 \pm 0.01)\, d_n + (0.87 \pm 0.01)\, d_p \\ &\quad - \big[(0.098 \pm 0.024)\,\bar{g}_0 - (0.14 \pm 0.028)\,\bar{g}_1\big]\, e\,\mathrm{fm}\,, \end{aligned} \tag{8.24}$$

with a nuclear uncertainty of the two-body contributions of approximately 25% [120, 119]. The uncertainty of the dependence on the single-nucleon EDMs is much smaller and will be neglected below. In principle, the tri-nucleon EDMs also depend on the $\not{P}\not{T}$ contact interactions of Eq. (8.18). However, as was already mentioned, these terms only appear at next-to-next-to-leading order, and can be neglected [56].

Because of the smallness of $\bar{g}_0/\bar{g}_1$, we can neglect the terms proportional to $\bar{g}_0$ in Eq. (8.24). The estimates in Eqs. (8.13) and (8.20) then tell us that the tri-nucleon EDMs are, just as the dEDM, about an order of magnitude larger than the nucleon EDMs. In particular, assuming that the nucleon EDM contribution can be neglected at leading order, the mLRM predicts

$$d_{^3\mathrm{He}} \simeq d_{^3\mathrm{H}} \simeq 0.7\, d_D \ . \tag{8.25}$$

That is, in this scenario these dipole moments have the same sign and are of the same order of magnitude.

There are two ways in which this prediction could be altered. First of all, the ratio of the two-body-to-one-body contributions has been estimated by NDA. It is possible that the nucleon EDM contributions are more important than NDA suggests. A better test then would be to extract $\bar{g}_1$ from $(d_D - d_n - d_p)$ and use this to predict $(d_{^3\mathrm{He}} - 0.89 d_n + 0.039 d_p)$ and/or $(d_{^3\mathrm{H}} + 0.051 d_n - 0.87 d_p)$.

However, even this prediction might still be altered by the possible contributions to the tri-nucleon EDMs proportional of the three-pion vertex $\bar{\Delta}$ in Eq. (8.16). If these contributions would be significant, both tests described above may fail because the tri-nucleon EDMs depend on an independent LEC which does not appear in the leading-order expressions of the nucleon and deuteron EDMs. We will discuss this issue in more detail here.

First of all, the three-pion vertex can contribute to $\bar{g}_1$ at the one-loop level. This contribution, at zero momentum transfer, is given by [56]

$$\delta\bar{g}_1 = \frac{15}{64\pi}\frac{g_A^2 m_\pi}{F_\pi^3}\bar{\Delta}. \tag{8.26}$$

Compared to Eq. (8.14) this contribution increases the effective $\bar{g}_1$ by roughly 50%. However, as this contribution only decreases the small $\bar{g}_0/\bar{g}_1$ ratio, the previous arguments are unaffected by this loop contribution.

However, unlike the case for the neutron, proton and, deuteron, in the tri-nucleon systems the three-pion vertex can contribute already at tree level. The responsible diagrams are those where each of the pions in the three-pion vertex connect to a different nucleon in the tri-nucleon system. These contributions potentially pose a more serious problem. This issue was first discussed in Refs. [119, 212], where it was shown that these contributions are smaller than expected by power-counting arguments and negligible with respect to the above loop contribution. Therefore, the main effect of the three-pion vertex is the loop diagram renormalizing $\bar{g}_1$, and the above arguments still hold.

Table 8.1: Sensitivities to the magnitudes of *CP*-violating parameters of the mLRM. The first column shows the relevant parameters, while the second column shows bounds from the current upper limit on the neutron EDM, $d_n \leq 2.9 \cdot 10^{-26} e\,\text{cm}$. The remaining columns show the values to which the *CP*-violating parameters could be probed by measurements of the proton, deuteron, and helion EDMs at the envisaged accuracy of 10^{-29} e cm.

	d_n	d_p	d_D	$d_{^3\text{He}}$
$\sin\zeta\,\text{Im}(V_L^{ud*}V_R^{ud}e^{i\alpha})$	$4 \cdot 10^{-6}$	$2 \cdot 10^{-9}$	$2 \cdot 10^{-10}$	$2 \cdot 10^{-10}$

8.5 Expected sensitivities

We will now turn to see how well the proposed EDM experiments are able to constrain the mLRM. Using the expressions in sections 8.3 and 8.4 we can the derive the bounds that would results from the proposed EDM experiments of the proton, deuteron, and helion at the envisaged accuracy [92, 93, 94, 95]. These sensitivities are shown in Table 8.1. For comparison, the bound that can be set by the current upper limit on the neutron EDM [18] is also shown.

As can be seen from Table 8.1, the current upper limit on the neutron EDM already stringently constrains the *CP*-violating parameters of the mLRM. Since the neutron and proton EDMs have a similar sensitivity to the mLRM, a measurement of the proton EDM at the proposed accuracy would greatly improve the sensitivity as compared to the current neutron EDM limit. In the LR scenario both the deuteron and helion EDMs are expected to be an order of magnitude larger than the proton EDM. This is reflected in Table 8.1, where a deuteron EDM measurement would be the best probe of the LR scenario.

8.6 Summary and conclusions

In the mLRM the dominant *CP*-violating operator contributing to hadronic EDMs is the right-handed $W^\pm$ current, O_{W_R}. This operator is generated after integrating out the $W_R^\pm$ boson at high energies. After integrating out the $W_L^\pm$ boson at the electroweak scale, O_{W_R} gives rise to a $\not{P}\not{T}$ four-quark operators, the FQLRs, with nontrivial chiral and isospin properties. Below M_{QCD} the effects of this operator are described by the induced LECs. These LECs in turn generate the EDMs of, not only the neutron and proton, but also those of the light nuclei, such as the deuteron, ^{3}He, and ^{3}H.

Dedicated storage rings might allow for measurements of EDMs of these ions. Because χPT allows for a unified description of nucleons and (light) nuclei, light-nuclear EDMs can be calculated in terms of the LECs in Eq. (8.10) and the nucleon EDMs. One reason why the storage-ring proposals are so interesting is that the nuclear EDMs already depend at tree level on the pion-nucleon interactions $\bar{g}_{0,1}$. This dependence allows one to probe nontrivial relations between these LECs that may result from a BSM model. This is in contrast to the single-nucleon EDMs, where these interactions contribute only at one-loop level and are masked by the presence of the isoscalar and isovector nucleon EDMs, $\bar{d}_0$ and $\bar{d}_1$. Since different light-nuclear EDMs depend on the same set of LECs with different

relative weight [74], the dependence on them can be isolated and the predicted hierarchy can be studied experimentally, once measurements are performed on the EDMs of different light ions.

Following the reasoning above, it is possible to test the mLRM with the measurements of the EDMs of light nuclei. Such a test is possible because of the large hierarchy between $\bar{g}_0$ and $\bar{g}_1$ predicted by the mLRM, Eq. (8.17). The absence of knowledge of the absolute sizes of these LECs still hinders precise predictions for the nuclear EDMs in terms of the model parameters. However, it is now possible to relate the different EDMs to one another due to the fact that $\bar{g}_1$ dominates over $\bar{g}_0$. This hierarchy between these two LECs results in the prediction that the single nucleon EDM should be significantly smaller than the nuclear ones. In addition, one may extract $\bar{g}_1$ from Eq. (8.21),

$$d_D - (d_n + d_p) \simeq d_D = (0.18 \pm 0.02)\, \bar{g}_1 e\,\mathrm{fm}\ . \tag{8.27}$$

This value of $\bar{g}_1$ can then be used to predict $d_{^3\mathrm{He}}$ according to Eq. (8.24),

$$d_{^3\mathrm{He}} - 0.9\, d_n \simeq d_{^3\mathrm{He}} = (0.14 \pm 0.03)\, \bar{g}_1\, e\,\mathrm{fm}\ . \tag{8.28}$$

Thus, if the EDMs for proton, neutron, deuteron, and ^{3}He were measured with high precision, highly nontrivial information could be deduced on the *CP*-violating physics responsible for their appearance.

Chapter 9

Electric dipole moments in other CP-violating scenarios

In chapters 5 and 8 we discussed the use of light nuclear EDMs to identify the fundamental source of CP violation was already mentioned in chapter 5. Because the different sources of CP violation give rise to different patterns in the EDMs of light nuclei, these observables allow one to distinguish the $\bar{\theta}$ term from the higher-dimensional BSM operators, given enough EDM measurements [99, 117, 74, 98]. This conclusion, however, relies on the assumption that one operator is dominant over the others [117, 74, 98, 56], which has the advantage of a rather clean analysis. It can be questioned, however, how realistic such a scenario is. It could very well be that the underlying microscopic theory induces contributions of similar size to several effective dimension-six operators. Furthermore, even if only one operator turns out to be dominant at high energies, this operator can induce sizable contributions to other operators when evolved to the low-energy scale where EDM experiments take place. Therefore, the assumption of a single dominant dimension-six operator at low energies might not be the most likely one in all CP-violating BSM scenarios.

In this light, it is interesting to study CP violation in full-fledged BSM models, like the minimal left-right model (mLRM) considered in chapter 8. Such studies should allow one to see whether the measurements of the EDMs of light nuclei can also distinguish more realistic scenarios from one another. In the previous chapter it was already shown that an analysis of the light nuclear EDMs can exclude the mLRM if the measured EDMs do not satisfy the relations between the light-nuclear EDMs predicted by the mLRM, Eqs. (8.27) and (8.28). Nonetheless, this analysis does not tell us whether a non-zero $\bar{\theta}$ term can be distinguished from the mLRM or other models of BSM physics, or whether such BSM scenarios can be distinguished from one another. To investigate these questions in more detail, we will consider two distinct scenarios of non-KM CP violation in this chapter. The goal of this analysis will be to see whether EDM measurements can discriminate between the scenarios considered in this chapter and the mLRM, discussed in the previous chapter. Although we will consider specific models, the methods used are in not limited to these scenarios and can be applied to other BSM models as well.

In the first scenario we assume the SM $\bar{\theta}$ term to be the dominant source. Since, with the exception of the CKM matrix, this is the only CP-violating term of dimension four

in the hadronic sector, it provides the background to which the other scenarios, which induce $\not{P}\not{T}$ operators with dimension of at least of dimension six, have to be compared. The $\bar{\theta}$ scenario has already been studied extensively in the literature (although we will include here some very recent results on light-nuclear EDMs [120, 119]) and we will mainly summarize the results in the following. For the BSM models discussed in this chapter, we assume that the $\bar{\theta}$ term is absent, for instance, due to a Peccei-Quinn symmetry [30, 213] of the Lagrangian of the respective model.

The second scenario we investigate is based on the so-called aligned two-Higgs-doublet model (a2HDM) [214]. Contrary to the $\bar{\theta}$ scenario just outlined and the mLRM, in this model, which exemplifies the generic feature of non-KM CP violation in two-Higgs doublet-models, several $\not{P}\not{T}$ operators are induced at the level of quarks and gluons which, in general, make contributions of comparable size to hadronic EDMs. The coefficients of these operators depend on different parameters of the model. The main goal of this chapter is to show that the EDMs of nucleons and light nuclei can be used to disentangle different scenarios, and we do not aim at a detailed analysis of the a2HDM. We therefore make certain assumptions [81] regarding the neutral Higgs sector such that all induced higher-dimensional BSM operators depend on the same combination of parameters. Despite this simplification, the EDMs of nucleons and light nuclei receive comparable contributions from three BSM operators, which makes the analysis more complicated and uncertain. Nevertheless, we demonstrate that the model still leads to a hierarchy of EDMs which is different from the previous scenarios.

The analyses of the EDMs of light nuclei will follow many of the same steps that were performed for the mLRM in chapter 8. For each scenario, we start at the scale where the BSM physics appears, evolve the induced sources of CP violation down to the QCD scale, and match them to the chiral Lagrangian. After this, the light nuclear EDMs can once more be expressed in terms of the scenario-specific low-energy constants (LECs).

We start by introducing the two scenarios of CP violation in sections 9.1.1 and 9.1.2. We consider the induced chiral Lagrangians in these models and the generated nucleon EDMs in section 9.2, while the EDMs of light nuclei are discussed in section 9.3. Finally, we briefly discuss the sizes of the EDMs of other systems in section 9.4, and conclude and summarize in 9.5.

9.1 Two CP-violating scenarios

9.1.1 The QCD $\bar{\theta}$ term

The QCD Lagrangian for two quark flavors is given by

$$\mathcal{L}_{\text{QCD}} = -\frac{1}{4} G^a_{\mu\nu} G^{a,\mu\nu} + \bar{q}(i\not{D} - M)q - \bar{\theta}\frac{g^2}{64\pi^2}\epsilon^{\mu\nu\alpha\beta} G^a_{\mu\nu} G^a_{\alpha\beta} \ , \tag{9.1}$$

where $q = (u\,, d)^T$ denotes the quark doublet of up and down quarks and M is the real-valued quark 2×2 mass matrix. The restriction to two quark flavors is appropriate for analyzing the EDMs of nucleons and light nuclei within the framework of χPT. In this expression, we have absorbed the complex phase of the quark mass matrix into

$\bar{\theta} = \theta + \arg\det(M)$. Due to the $U_A(1)$ anomaly, an axial $U(1)$ transformation of the quark fields can be used to remove the $\bar{\theta}$ term from the Lagrangian, assuming $\bar{\theta} \ll 1$, the QCD Lagrangian becomes [28]

$$\mathcal{L}_{QCD} = -\frac{1}{4} G^a_{\mu\nu} G^{a,\mu\nu} + \bar{q} i \not{D} q - \bar{m} \bar{q} q - \varepsilon \bar{m} \bar{q} \tau_3 q + m_* \bar{\theta} \bar{q} i \gamma^5 q \ , \tag{9.2}$$

in terms of the averaged quark mass $\bar{m} = (m_u + m_d)/2$ in the two-flavor case, the quark-mass difference $\varepsilon = (m_u - m_d)/(m_u + m_d)$, and the reduced quark mass $m_* = m_u m_d/(m_u + m_d) = \bar{m}(1-\varepsilon^2)/2$. This expression shows that $\not{P}\not{T}$ effects due to the $\bar{\theta}$ term would vanish if one of the quarks were massless. However, this is not realized in nature [215, 65]. We also give the explicit PT-even quark mass terms here because, as we will discuss later, $\not{P}\not{T}$ hadronic interactions induced by the $\bar{\theta}$ term are closely linked to PT-even isospin-breaking interactions induced by the quark mass difference.

Before continuing the analysis of the $\bar{\theta}$ term, we first discuss the a2HDM scenario considered in this chapter. In this scenario we assume that the $\bar{\theta}$ term is absent, for example, due to the Peccei-Quinn mechanism [30, 213] or by extreme fine-tuning. It should be noted that the Peccei-Quinn mechanism would, apart from removing the $\bar{\theta}$ term, also affect the dimension-six operators appearing in the other scenario [42].

9.1.2 The aligned two-Higgs-doublet model

Two-Higgs-doublet models (2HDMs) are among the simplest extensions of the SM. Among other features they provide an interesting source for non-KM CP violation, namely CP violation induced by neutral and charged Higgs boson exchange, for reviews, see, e.g., Refs. [216, 217, 218]. In these models the SM field content is extended by an additional Higgs doublet. There are thus two doublets, Φ_1 and Φ_2, both transforming under $SU(3)_c \times SU(2)_L \times U(1)_Y$ as $(1, 2, 1/2)$. The electroweak symmetry is broken by the vevs of the neutral components of Φ_1 and Φ_2. One can always choose a so-called Higgs basis (see, for instance, Ref. [218]), in which only one of the doublets acquires a vev,

$$\langle \Phi_1 \rangle = (0, v/\sqrt{2})^T \ , \qquad \langle \Phi_2 \rangle = 0 \ , \tag{9.3}$$

where $v = \sqrt{v_1^2 + v_2^2} \simeq 246\,\text{GeV}$. In this basis the would-be Goldstone boson fields G^0 and G^+ are contained in Φ_1:

$$\Phi_1 = \begin{pmatrix} G^+ \\ (v + S_1 + iG^0)/\sqrt{2} \end{pmatrix} \ , \qquad \Phi_2 = \begin{pmatrix} H^+ \\ (S_2 + iS_3)/\sqrt{2} \end{pmatrix} \ . \tag{9.4}$$

Thus, the physical spin-zero fields of the 2HDM consist of 3 neutral fields, $S_{1,2,3}$, and one charged field, H^+. The neutral fields in the mass basis, $\varphi_1^0, \varphi_2^0, \varphi_3^0$, are linear combinations of the fields S_i. The two sets of fields are related by an orthogonal 3×3 matrix R, $\varphi_i^0 = R_{ij} S_j$. In general, the Higgs potential of a 2HDM violates CP explicitly. As a consequence, the φ_i^0 do not have a definite CP parity. By assumption the lightest of the fields φ_i^0 corresponds to the 125 GeV spin-zero resonance discovered at the LHC [1, 219]. If the Higgs potential conserves CP, then two of the φ_i^0 have CP parity $+1$, while the third one has CP parity -1. In this case, the fields in the mass basis are traditionally

denoted by h, H, A, where h describes the lightest of the two scalar states. For the sake of simplicity, we shall use here the notation $(\varphi_i^0) = (h, H, A)$ also in the case of Higgs sector CP violation, when h, H, and A no longer have a definite CP parity.

The most important contributions to EDMs arise from the interactions of the spin-zero fields with fermions. The most general Yukawa Lagrangian in the quark sector that obeys the SM gauge symmetries is given by

$$-\mathcal{L}_{Y'} = \frac{\sqrt{2}}{v}\left[\bar{Q}'_L(M'_d\Phi_1 + Y'_d\Phi_2)D'_R + \bar{Q}'_L(M'_u\tilde{\Phi}_1 + Y'_u\tilde{\Phi}_2)U'_R + \text{h.c.}\right] \ . \tag{9.5}$$

Here Q'_L, U'_R, and D'_R denote the $SU(2)_L$ quark doublet and singlets, respectively, in the weak-interaction basis, $M'_{u,d}$ and $Y'_{u,d}$ are complex 3×3 matrices; $M'_{u,d}$ are the quark mass matrices to which $Y'_{u,d}$, in view of having chosen the Higgs basis, do not contribute.

So far we have discussed a general 2HDM. The requirement for restricting these models comes from the fact that in its general form the 2HDM generates tree-level flavor-changing neutral-currents (FCNCs) [216, 217, 218]. One way to make sure these tree-level FCNCs are absent is to impose a Z_2 symmetry on the model which may be softly broken by the Higgs potential [216, 217, 218]. An alternative and more general way is to assume that the matrices M'_q and Y'_q $(q = u, d)$ are, at some (high) scale, proportional to each other and can therefore be simultaneously diagonalized [214]:

$$\begin{aligned} Y_d^{(\prime)} &= \varsigma_d M_d^{(\prime)} & Y_u^{(\prime)} &= \varsigma_u^* M_u^{(\prime)} \ , \\ M_{u,d} &= U_L^{u,d} M'_{u,d} U_R^{u,d}, & Y_{u,d} &= U_L^{u,d} Y'_{u,d} U_R^{u,d}. \end{aligned} \tag{9.6}$$

where $M_{u,d}$ are the real diagonal quark mass matrices , $U_{L,R}^{u,d}$ are unitary matrices diagonalizing the mass matrices, and ς_u and ς_d are complex numbers. The model that uses this assumption is called the aligned two-Higgs doublet model (a2HDM) [214]. This is similar to the hypothesis of 'minimal flavor violation' in which the flavor violation induced by BSM physics follows the pattern of the SM and is governed by the CKM matrix. [220, 221, 222].

In the mass basis both for the quark and the Higgs fields, one obtains from Eq. (9.5), using Eq. (9.6), the Yukawa interactions of the quark and the physical Higgs fields $H^\pm$ and φ_i^0,

$$\begin{aligned} -\mathcal{L}_Y \ &= \ \frac{\sqrt{2}}{v} H^+ \bar{U}\left[\varsigma_d V M_d \mathcal{P}_R - \varsigma_u M_u V \mathcal{P}_L\right] D \\ &\quad + \frac{1}{v}\sum_{i=1}^{3}\left[y_u^i \varphi_i^0 \, \bar{U}_L M_u U_R + y_d^i \varphi_i^0 \, \bar{D}_L M_d D_R\right] + \text{h.c.} \quad , \end{aligned} \tag{9.7}$$

where V is the CKM matrix and $\mathcal{P}_{R,L} = (1 \pm \gamma_5)/2$. The reduced Yukawa couplings y_u^i and y_d^i of the neutral Higgs bosons are given in terms of the complex parameters $\varsigma_{u,d}$ and the matrix elements of the 3×3 real orthogonal Higgs mixing matrix R (see above) by [214]

$$y_u^i \ = \ R_{i1} + (R_{i2} - iR_{i3})\varsigma_u^* \ , \tag{9.8}$$

$$y_d^i \ = \ R_{i1} + (R_{i2} + iR_{i3})\varsigma_d \ . \tag{9.9}$$

The orthogonality of R implies

$$\sum_{i=1}^{3} \mathrm{Re}\, y_q^i \,\mathrm{Im}\, y_{q'}^i = r_{q'} \mathrm{Im}\,(\varsigma_q^* \varsigma_{q'}) \ , \tag{9.10}$$

where $r_u = -1$, $r_d = 1$. The Yukawa couplings to leptons are analogous to those of the down-type quarks. Resulting CP-violating effects involving leptons effects will be commented on in section 9.4 and in appendix 9.A.

The interactions in Eq. (9.7) and the couplings in Eqs. (9.8) and (9.9) exhibit several interesting features. a) The exchange of a charged Higgs boson between quarks transports, apart from the KM-phase that plays no role in the discussion below, also the CP-violating phases of $\varsigma_{u,d}$. These phases induce flavor-diagonal CP-odd four-quark operators already at tree-level of the type $(\bar{u}d)(\bar{d}i\gamma_5 u)$, where u (d) denotes any of the up-type (down-type) quarks, with operator coefficients proportional to $\mathrm{Im}(\varsigma_u^* \varsigma_d)$. b) If the Higgs potential violates CP, the neutral Higgs states are, as mentioned, no longer CP eigenstates and their exchange induces, for instance, flavor-diagonal CP-odd four-quark operators $(\bar{q}q)(\bar{q}'i\gamma_5 q')$ $(q, q' = u, d)$ at tree level, in particular the operators $(\bar{q}q)(\bar{q}i\gamma_5 q)$. c) If the (tree-level) Higgs potential of the a2HDM is CP-invariant, neutral Higgs exchange nevertheless induces CP-odd operators of the type $(\bar{u}u)(\bar{d}i\gamma_5 d)$ if $\mathrm{Im}(\varsigma_u^* \varsigma_d) \neq 0$. Features a) and c) distinguish the a2HDM from 2HDM with a Z_2 symmetry that is (softly) broken by CP-violating Higgs potential, in which $\varsigma_{u,d}$ are real, *cf.* for instance Ref. [223, 224].

As already mentioned above, the lightest neutral Higgs boson h is to be identified with the 125 GeV spin-zero boson discovered at the LHC. The experimental analysis of this resonance does not (yet) prove that it is a scalar, but the data indicate [225, 226] that a possible pseudoscalar component of this state must be smaller than the scalar one. Therefore, we make the simplifying assumptions:

$$\begin{aligned} &(i) \qquad R_{11} \to 1 \ , \qquad R_{12} \to 0 \ , \qquad R_{13} \to 0 \ , \\ &(ii) \qquad M_H \to M \ , \qquad M_A \to M \ . \end{aligned} \tag{9.11}$$

Assumption (i) amounts to assuming that the lightest Higgs boson h is a scalar[1], while with (ii) we assume that the two heavier neutral Higgs bosons H and A are (nearly) mass-degenerate. These assumptions are not meant to single out a particular phenomenologically or theoretically favored version of the a2HDM. They just serve to simplify the dependence of the quark and gluon (C)EDMs on unknown parameters of the model. In this way their sizes can be compared.

We can now construct the relevant CP-violating operators up to dimension-six that are generated at a high scale $\mu \sim$ a few hundred GeV. Details of our analysis, which essentially follows Ref. [81], are given in Appendix 9.A. With the specifications in Eq. (9.11) it turns out that the dominant operators are the EDM and CEDM of the d quark, generated by two-loop Barr-Zee diagrams [77] as shown in Fig. 9.1(a,b), and the Weinberg operator

[1]The recent papers [224, 227] analyze EDMs in a 2HDM with a Z_2 symmetry and a Higgs potential that softly breaks this symmetry and violates CP. They take into account the possibility that the 125 GeV resonance has a (small) CP-odd component.

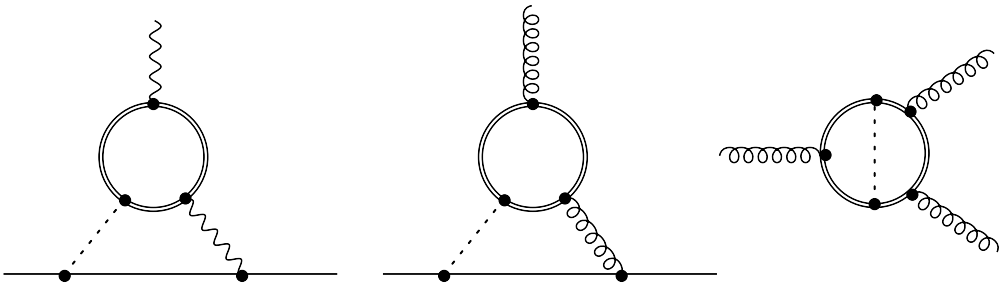

Figure 9.1: Examples of two-loop diagrams which contribute to the coefficients of the operators in Eq. (9.13). A single (double) solid lines denotes a light (heavy) quark, a dashed line corresponds to a Higgs boson, and a wavy and a curly line depicts a photon and a gluon, respectively. Diagrams (a,b) are Barr-Zee type diagrams contributing to the quark electric and chromo-electric dipole moment, while diagram (c) contributes to the Weinberg operator.

which is generated by diagrams Fig. 9.1(c) with the exchange of a charged Higgs boson. With the assumptions of Eq. (9.11) the contributions from the Barr-Zee diagrams vanish when the external quarks and the quark in the loop are both up- or down-type quarks. This implies that contributions to the u quark (C)EDM require a down-type quark in the loop. Because the Barr-Zee contributions scale roughly linearly with the mass of the internal quark, and the hierarchy between the t and b masses, the u quark (C)EDM is about two orders of magnitude smaller than that of the d quark. The resulting (C)EDM of the d quark, at $\mu = m_t$, and the gluon CEDM d_W, at $\mu = m_b$, are

$$\begin{aligned}
d_d(m_t) &= e\frac{Q_d m_d \alpha}{(4\pi)^3 v^2}\mathrm{Im}\,(\varsigma_u^*\varsigma_d)\left(\frac{32}{3}\left[f\left(\frac{m_t^2}{M^2}\right)+g\left(\frac{m_t^2}{M^2}\right)\right]+\frac{3}{s_w^2}|V_{ud}|^2|V_{tb}|^2\big[F_b-2F_t\big]\right),\\
\tilde{d}_d(m_t) &= -4m_d\frac{g_s\alpha_s}{(4\pi)^3 v^2}\mathrm{Im}\,(\varsigma_u^*\varsigma_d)\left[f\left(\frac{m_t^2}{M^2}\right)+g\left(\frac{m_t^2}{M^2}\right)\right]\ ,\\
d_W(m_b) &= \eta_W\frac{g_s\alpha_s}{(4\pi)^3 v^2}|V_{tb}|^2\mathrm{Im}\,(\varsigma_u^*\varsigma_d)\left[x_t\left(\frac{\ln x_t}{(x_t-1)^3}+\frac{x_t-3}{2(x_t-1)^2}\right)\right]\ ,
\end{aligned}\tag{9.12}$$

where x_t, f, g, and $F_{b,t}$ are (functions of) mass ratios and $\eta_W =\simeq 0.67$ is an RGE factor, for more details see appendix 9.A.

These three dipole moments depend, apart from the unknown Higgs-boson masses M and M_+ (of $H^\pm$), on the common unknown factor $\mathrm{Im}\,(\varsigma_u^*\varsigma_d)$ that signifies non-KM CP violation. Using the renormalization-group equation for these dipole interactions [71, 72, 73, 48, 152] we obtain the following $\not{P}T$ effective Lagrangian at the scale $\mu = M_{\rm QCD}$,

$$\begin{aligned}
\mathcal{L} &= -\frac{d_d(M_{\rm QCD})}{2}\bar{d}i\sigma^{\mu\nu}\gamma_5 d\,F_{\mu\nu}-\frac{\tilde{d}_d(M_{\rm QCD})}{2}\bar{d}i\sigma^{\mu\nu}\gamma_5 t_a d\,G^a_{\mu\nu}\\
&+ \frac{d_W(M_{\rm QCD})}{6}f_{abc}\varepsilon^{\mu\nu\alpha\beta}G^a_{\alpha\beta}G^b_{\mu\rho}G^{c\,\rho}_{\nu}\ .
\end{aligned}\tag{9.13}$$

For convenience, we have absorbed several factors in the definitions of the quark (C)EDMs in Eq. (9.13). With respect to previous chapters we have,

$$d_q^{\rm New} = e m_q Q_q d_q, \qquad \tilde{d}_q^{\rm New} = g_s m_q \tilde{d}_q. \tag{9.14}$$

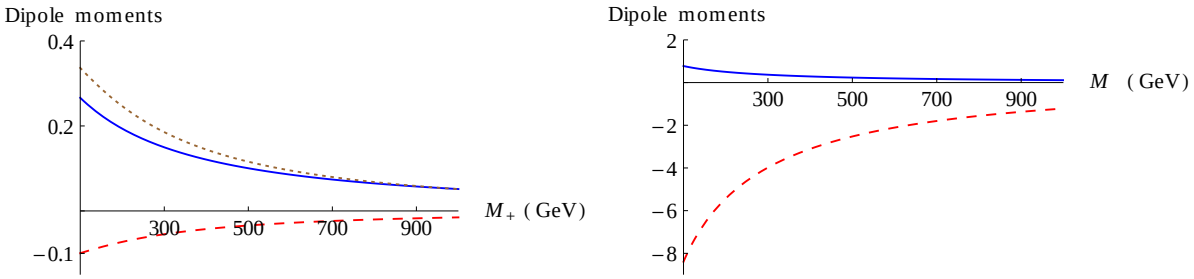

Figure 9.2: The dimensionless dipole moments δ_d, $\tilde{\delta}_d$, and δ_W, defined in Eq. (9.15), at the scale $M_{\rm QCD}$ as functions of the charged Higgs-boson mass M_+ (left plot) and of the mass M of the neutral Higgs bosons H and A. The blue (solid) and red (dashed) lines correspond to δ_d and $\tilde{\delta}_d$ (we take $g_s > 0$), respectively, and the brown (dotted) line corresponds to δ_W. For the parameter specifications in Eq. (9.11) there is no contribution to δ_W from the neutral Higgs bosons.

In order to present the sizes of these dipole moments, we define dimensionless quantities δ_d, $\tilde{\delta}_d$, and δ_W by

$$\begin{aligned} d_d(M_{\rm QCD}) &= e\delta_d \frac{\bar{m}\,{\rm Im}\,(\varsigma_u^*\varsigma_d)}{v^2}\cdot 10^{-4}\,, \quad \tilde{d}_d(M_{\rm QCD}) = \tilde{\delta}_d \frac{\bar{m}\,{\rm Im}\,(\varsigma_u^*\varsigma_d)}{v^2}\cdot 10^{-4}\,, \\ d_W(M_{\rm QCD}) &= \delta_W \frac{{\rm Im}\,(\varsigma_u^*\varsigma_d)}{v^2}\cdot 10^{-4}\,, \end{aligned} \tag{9.15}$$

where $\bar{m}(M_{\rm QCD}) = 4.8$ MeV [65]. The dimensionless moments are given as functions of the mass M_+ and of the mass M of the neutral Higgs bosons H and A in Fig. 9.2.

The plots in Fig. 9.2 show that the parameter specifications in Eq. (9.11) imply that the dominant contribution to the d-quark EDM and to the gluon CEDM d_W is due to charged Higgs-boson exchange. In contrast, the contribution of $H^\pm$ to the d-quark CEDM is induced through renormalization-group running and is very small as compared to the contribution of the Higgs bosons H and A to $\tilde{d}_d$. The neutral Higgs bosons also contribute to the d-quark EDM but not to d_W, however, the largest part of $d_d(M_{\rm QCD})$ arises when the d-quark CEDM is evolved from m_t to lower energies.

For approximately equal masses of the Higgs bosons, $M{=}M_H{\simeq}M_A{\simeq}M_+$, we find (numerically) the Higgs-mass independent relations between the dipole moments

$$\tilde{d}_d(M_{\rm QCD}) \simeq -7 d_d(M_{\rm QCD})/e \simeq -20\bar{m} d_W(M_{\rm QCD})\ . \tag{9.16}$$

Of course, these relations apply only to a very small region in the parameter space of the model, i.e. where the assumptions of Eq. (9.11) and $M \simeq M_+$ are valid. Different hierarchies could be realized. For example, if the charged Higgs boson is significantly heavier than the neutral ones, the dominance of the d-quark CEDM is reduced. However, since there is no good reason to assume $M_+ \gg M_H \approx M_A$, we will use Eq. (9.16) in what follows. Other hierarchies can be studied in similar fashion. Finally, we mention that in non-supersymmetric 2HDMs with a Z_2 symmetry and the symmetry-breaking scale set by the electroweak scale v, the masses of the Higgs bosons cannot exceed ~ 1 TeV [218].

9.2 The chiral Lagrangian

As discussed in the previous chapter the relevant interactions in the chiral Lagrangian can be written as

$$\begin{aligned}\mathcal{L} &= -2\,\bar{N}\left(\bar{d}_0+\bar{d}_1\tau_3\right)S^\mu N\,v^\nu F_{\mu\nu} \\ &\quad +\bar{g}_0\bar{N}\boldsymbol{\pi}\cdot\boldsymbol{\tau}N+\bar{g}_1\bar{N}\pi_3 N-\bar{\Delta}\frac{\pi_3\boldsymbol{\pi}^2}{2F_\pi}. \end{aligned} \tag{9.17}$$

Which of these interactions is induced will depend on the scenario under consideration. We start by discussing the induced LECs $\bar{g}_0$ and $\bar{g}_1$ in the $\bar{\theta}$ and a2HDM scenarios, before considering $\bar{d}_{0,1}$ in the context of the nucleon EDMs. Unlike the mLRM case of the previous chapter, contributions to the three-pion vertex, $\bar{\Delta}$, only appear at higher orders in $m_\pi/M_{\rm QCD}$ in either scenario [56].

The $\bar{\theta}$ scenario

As already mentioned in section 3.2, the $\bar{\theta}$-term is the isospin-conserving element of the same chiral-symmetry breaking quark-antiquark multiplet as the isospin-breaking component of the quark mass matrix – both terms are connected by an axial $SU(2)$ rotation. Therefore, in this scenario, all terms in the effective Lagrangian induced by the $\bar{\theta}$-term are linked to terms arising from the so-called *strong* isospin breaking, i.e., isospin breaking resulting from the strong interactions [110, 97]. The induced leading-order term in the pion-nucleon sector of the effective Lagrangian is proportional to the quark-mass induced part of the proton-neutron mass difference $(m_n-m_p)^{\rm strong}$ [228]. It gives the leading contribution to the coupling constant $\bar{g}_0^\theta$ [99, 97, 98],

$$\bar{g}_0^\theta=\frac{(m_n-m_p)^{\rm strong}(1-\varepsilon^2)}{4F_\pi\varepsilon}\bar{\theta}=(-0.018\pm0.007)\,\bar{\theta}\ , \tag{9.18}$$

where $(m_n-m_p)^{\rm strong}=(2.6\pm0.85)$ MeV [63, 64], $\varepsilon\equiv(m_u-m_d)/(m_u+m_d)=-0.35\pm0.10$ [65], and $F_\pi=92.2$ MeV have been used.

Because the $\bar{\theta}$ term is isospin conserving it does not directly contribute to the isospin-breaking LEC $\bar{g}_1$. The contributions to the coupling constant $\bar{g}_1^\theta$ induced by the $\bar{\theta}$-term can be traced back to the emergence of pion-tadpole terms in the pion-sector Lagrangian, which have to be removed by field redefinitions (unlike the FQLR case, this does not leave a three-pion vertex behind) [97, 98]. These field redefinitions generate the leading contribution to $\bar{g}_1^\theta$ given by [99, 97, 98]:

$$\bar{g}_1^\theta=\frac{2c_1(\delta m_\pi^2)^{\rm strong}(1-\varepsilon^2)}{F_\pi\varepsilon}\bar{\theta}=(0.003\pm0.002)\,\bar{\theta}\ , \tag{9.19}$$

where the LEC $c_1=(-1.0\pm0.3)\,{\rm GeV}^{-1}$ [101] is related to the nucleon σ-term and where $(\delta m_\pi^2)^{\rm strong}\simeq(\varepsilon m_\pi^2)^2/(4(m_K^2-m_\pi^2))$ [100] is the strong contribution to the square of the mass splitting between charged and neutral pions.

Although the isospin-conserving nature of $\bar{\theta}$ prohibits it from contributing to $\bar{g}_1$ directly, a contribution is possible at higher order in $m_\pi/M_{\rm QCD}$ by inclusion of the quark mass difference. The uncertainty in Eq. (9.19) has been increased to account for this independent

contribution to $\bar{g}_1^\theta$ [97] which arises in the next-to-next-to-leading-order pion-nucleon Lagrangian [229] with an LEC of unknown strength, which here has been conservatively bounded by its NDA estimate. In fact, a calculation based on resonance saturation predicts only one third of this estimate as an upper bound [98].

In summary, the coupling constant $\bar{g}_1^\theta$ is suppressed with respect to the coupling constant $\bar{g}_0^\theta$ by the ratio $\bar{g}_1^\theta/\bar{g}_0^\theta = -0.2 \pm 0.1$ [98]. This suppression, however, is less than the NDA prediction $|\bar{g}_1^\theta/\bar{g}_0^\theta| = \mathcal{O}(\varepsilon m_\pi^2/M_{\rm QCD}^2) \simeq 0.01$ [97]. This hierarchy is in stark contrast to the hierarchy in the mLRM $\bar{g}_0^{\rm mLRM}/\bar{g}_1^{\rm mLRM} \ll 1$, discussed in the previous chapter, which did not rely on NDA estimates. This difference has important consequences for the light-nuclear EDMs.

The a2HDM scenario

Next we discuss the hierarchy of pion-nucleon interactions which emerges in the scenario of section 9.1.2. In the a2HDM scenario we must compare the contributions from the three operators appearing in Eq. (9.13). The contributions from the qEDM to the pion-nucleon LECs are highly suppressed because of the appearance of the photon which needs to be integrated out. As a result, the qEDM contributions are suppressed by the typical factor $\alpha_{\rm em}/\pi \sim 10^{-3}$ and can be safely neglected. Because the Weinberg operator conserves chiral symmetry, it cannot directly induce the $\not{P}\not{T}$ pion-nucleon couplings which break chiral symmetry [109]. Instead, an additional insertion of the quark mass (difference) is required which implies, by NDA, that the LECs scale as $|\bar{g}_0^{\rm H}| = \mathcal{O}(\bar{m} M_{\rm QCD}\, d_W)$ and $|\bar{g}_1^{\rm H}| = \mathcal{O}(\varepsilon \bar{m} M_{\rm QCD}\, d_W)$ [58]. On the other hand, the down-quark CEDM in Eq. (9.13) can induce the pion-nucleon couplings directly such that, for this source, $|\bar{g}_{0,1}^{\rm H}| = \mathcal{O}(M_{\rm QCD}\, \tilde{d}_d)$ [58]. Together with the observation that $\bar{m}|d_W|$ is about an order of magnitude smaller than $|\tilde{d}_d|$ in the model under investigation, we conclude that the pion-nucleon couplings are dominated by the qCEDM and $\bar{g}_0^{\rm H}/\bar{g}_1^{\rm H} = \mathcal{O}(1)$.

To check whether the NDA estimate is reasonable we compare it to results obtained in Refs. [108, 42] where the pion-nucleon LECs were investigated in the framework of QCD sum rules. It was found that[2]

$$\bar{g}_1^{\rm H} = -(2^{+4}_{-1}\,{\rm GeV})\,\tilde{d}_d\ , \qquad \bar{g}_0^{\rm H} \simeq (0.5 \pm 1)\,{\rm GeV}\,\tilde{d}_d\ . \tag{9.20}$$

The coupling $\bar{g}_1^{\rm H}$ is somewhat bigger than the NDA estimate but not in disagreement. The calculation of $\bar{g}_0^{\rm H}$ has a relatively larger uncertainty (even an uncertain sign) which is also harder to quantify [108]. The size of $\bar{g}_0^{\rm H}$ is somewhat smaller than $\bar{g}_1^{\rm H}$, and it is in agreement with NDA.

Considering the large uncertainties in these estimates, from now on we will take for the a2HDM scenario that $|\bar{g}_0^{\rm H}| \simeq |\bar{g}_1^{\rm H}|$, as indicated by NDA. However, there is a significant uncertainty involved and the only way to improve the situation is, most likely, a direct

[2]These results assume a Peccei-Quinn mechanism to remove the $\bar{\theta}$ term. Although the Peccei-Quinn mechanism ordinarily results in $\bar{\theta} = 0$, in the presence the quark CEDMs operators it leads to a contribution to $\bar{\theta}$ from $\tilde{d}_q$ [42]. This effectively shifts the qCEDM contributions to pion-nucleon LECs. However, the order of magnitude stays the same. Since we use these results mainly to check the NDA estimates, this poses no real problem.

lattice calculation.

In order to get an idea of the induced LECs in terms of fundamental CP-violating parameters we summarize their sizes in the $\bar{\theta}$ and a2HDM scenarios,

$$\begin{aligned} \bar{g}_0^{\bar{\theta}} = &\quad (-0.018 \pm 0.007)\,\bar{\theta}, \qquad \bar{g}_1^{\bar{\theta}} &= (0.003 \pm 0.002)\,\bar{\theta} \\ |\bar{g}_0^{\mathrm{H}}| = &\quad \mathcal{O}\Big(10^{-7} \cdot \mathrm{Im}\,(\varsigma_u^* \varsigma_d)\Big), \qquad |\bar{g}_1^{\mathrm{H}}| &= \mathcal{O}\Big(10^{-7} \cdot \mathrm{Im}\,(\varsigma_u^* \varsigma_d)\Big), \end{aligned} \tag{9.21}$$

where we used the NDA estimates for the LECs for the a2HDM scenario, with $\tilde{\delta}_d = \mathcal{O}(1)$ as in Fig. (9.2) for $M \leq 1\,\mathrm{TeV}$. For comparison, again employing NDA estimates for the sizes of the LECs, in the mLRM scenario we have

$$|\bar{g}_1^{\mathrm{mLRM}}| \simeq 50\,|\bar{g}_0^{\mathrm{mLRM}}| \;\; = \mathcal{O}\Big(10^{-6} \cdot \sin\zeta\,\mathrm{Im}\,(V_R^{ud} V_L^{ud*} e^{i\alpha})\Big). \tag{9.22}$$

9.2.1 The EDMs of the neutron and proton

We recall that the expression for the neutron and proton EDMs in terms of the LECs in Eq. (9.17) is given by [57, 58, 59]

$$\begin{aligned} d_n &= \bar{d}_0 - \bar{d}_1 + \frac{e g_A \bar{g}_0}{8\pi^2 F_\pi}\left(\ln\frac{m_\pi^2}{m_N^2} - \frac{\pi m_\pi}{2 m_N}\right), \\ d_p &= \bar{d}_0 + \bar{d}_1 - \frac{e g_A}{8\pi^2 F_\pi}\left[\bar{g}_0\left(\ln\frac{m_\pi^2}{m_N^2} - \frac{2\pi m_\pi}{m_N}\right) - \bar{g}_1 \frac{\pi m_\pi}{2 m_N}\right]. \end{aligned} \tag{9.23}$$

We now move on to discuss how the induced LECs influence the nucleon EDMs in the specific CP-violating scenarios. We start by considering the $\bar{\theta}$ scenario.

The $\bar{\theta}$ scenario

By inserting the values of $\bar{g}_{0,1}$ from Eqs. (9.18) and (9.19) into Eq. (9.23), it is possible to evaluate the size of the loop contributions to the nucleon EDMs:

$$d_n^{\bar{\theta},\mathrm{loop}} = (-2.5 \pm 0.9) \cdot 10^{-16}\,\bar{\theta}\,e\,\mathrm{cm}\;, \qquad d_p^{\bar{\theta},\mathrm{loop}} = (2.8 \pm 0.9) \cdot 10^{-16}\,\bar{\theta}\,e\,\mathrm{cm}\;. \tag{9.24}$$

This sets the scale for the nucleon EDM but the actual numbers can change due to the LECs $\bar{d}_{0,1}$. The sizes of the LECs can be estimated by NDA. This yields

$$|\bar{d}_{0,1}^{\bar{\theta}}| = \mathcal{O}\left(e\bar{\theta}\,\frac{m_\pi^2}{M_{\mathrm{QCD}}^3}\right) \simeq 3 \cdot 10^{-16}\,\bar{\theta}\,e\,\mathrm{cm}\;, \tag{9.25}$$

which is of similar size as the loop contributions. By combining a χPT calculation with lattice QCD data, it recently became possible to compute the total nucleon EDM (loop and tree-level contributions) [29]. It was found that

$$d_n^{\bar{\theta}} = (-2.9 \pm 0.9) \cdot 10^{-16}\,\bar{\theta}\,e\,\mathrm{cm}\;, \qquad d_p^{\bar{\theta}} = (1.1 \pm 1.1) \cdot 10^{-16}\,\bar{\theta}\,e\,\mathrm{cm}\;, \tag{9.26}$$

which is the result we will use in what follows. For the deuteron EDM, an important quantity is the sum of the nucleon EDMs which is

$$d_n^{\bar{\theta}} + d_p^{\bar{\theta}} = (-1.8 \pm 1.4) \cdot 10^{-16}\, \bar{\theta}\, e\,\mathrm{cm}\ , \tag{9.27}$$

with a significant uncertainty.

The a2HDM scenario

Within the a2HDM the nucleon EDMs receive contributions from each of the three operators in Eq. (9.13). For the pion-nucleon interactions we were fortunate that one of the operators gave dominant contributions which simplified the estimates of $\bar{g}_{0,1}^{\mathrm{H}}$. For the nucleon EDM we do not have this advantage because the qEDM and Weinberg operator induce the tree-level LECs $\bar{d}_{0,1}$ without additional suppressions [58]. As a consequence, we need to study all three operators.

The results in section 9.2 tell us that the loop contributions to the nucleon EDMs are dominated by the qCEDM because the $\not{P}\not{T}$ pion-nucleon LECs are suppressed for the qEDM and Weinberg operator. Using the NDA estimate for $\bar{g}_0$ (in good agreement with the QCD sum rules result [108]) gives

$$|d_n^{\mathrm{H,\,loop}}| \simeq -|d_p^{\mathrm{H,\,loop}}| \simeq (0.7)\, e\tilde{d}_d\ , \tag{9.28}$$

in terms of the down-quark CEDM $\tilde{d}_d$. The tree-level terms $\bar{d}_{0,1}$ obtain contributions from all operators. NDA gives [58]:

$$\left|d_{n,p}^{\mathrm{H,\,tree}}\right| = \mathcal{O}\left(d_d,\ \frac{e\tilde{d}_d}{4\pi},\ F_\pi\, e d_W\right) \simeq \left(d_d,\ (0.1)\, e\tilde{d}_d,\ (0.1\,\mathrm{GeV})\, e\, d_W\right)\ , \tag{9.29}$$

which implies that the loop contributions of the qCEDM are larger than its tree-level contributions. This is due to the fact that $\bar{d}_{0,1}$ originating from the qCEDM are suppressed by $\frac{e}{4\pi}$, while this is not the case for the induced $\bar{g}_{0,1}$. The approximate hierarchy of the dipole moments $\tilde{d}_d \simeq -7\, d_d/e \simeq -20(\bar{m} d_W)$ (with $\bar{m} \simeq 5$ MeV) derived in Sect. 9.1.2, shows that the nucleon EDMs obtain contributions comparable in magnitude from all three operators, with perhaps a slight dominance of the Weinberg operator (although this is questionable, see the discussion below). Of course, these estimates are very rough and can in no way be used to make a definite statement about the exact sizes of the nucleon EDMs in the a2HDM scenario that we investigate. They only provide an order of magnitude estimate for the EDMs.

The nucleon EDM induced by the qEDM, qCEDM, and Weinberg operator has been investigated extensively in the literature (see Refs. [42, 129] for reviews). In particular, the calculation for all three operators has been performed with QCD sum rules [230, 109, 99, 42]. The authors of these references obtained, in our notation[3, 4]

$$d_n = (1 \pm 0.5)\left(1.4\, d_d - 0.55\, e\tilde{d}_d\right) \pm (0.02\,\mathrm{GeV})\, e d_W\ , \tag{9.30}$$

[3] As before, a Peccei-Quin mechanism was used to remove the $\bar{\theta}$ term.

[4] The difference between our d-quark CEDM $\tilde{d}_d$ and the one found in Refs. [230, 42] is due to an explicit factor of $g_s(M_{\mathrm{QCD}}) \simeq 2$ that appears in the definition of the qCEDM in these references.

with an unspecified sign and significant error for the coefficient of the Weinberg operator. The hierarchy between d_d, $\tilde{d}_d$, and d_W then indicates that all operators contribute at the same level to the neutron EDM. The qEDM and qCEDM results are in good agreement with the chiral-loop results and NDA. The result for the Weinberg operator is somewhat smaller (see the discussion in Ref. [109]) but, in view of the large uncertainties involved, the estimates cannot be considered to be in disagreement. The isoscalar combination $d_n + d_p$ has also been estimated with QCD sum rules [99],

$$d_n + d_p = (0.5 \pm 0.3)\, d_d - (0.2 \pm 0.1)\, e\tilde{d}_d \pm (0.02\,\mathrm{GeV})\, e d_W \ , \tag{9.31}$$

with slightly smaller coefficients in front of the qEDM and qCEDM than in the case of the neutron EDM.

To summarize, in the a2HDM scenario of Sect. 9.1.2, the nucleon EDMs receive contributions of roughly equal size from the d-quark EDM and CEDM and the Weinberg operator. The rather large uncertainties in magnitude and sign of each of these contributions make it impossible to obtain a firm prediction of the sizes of the nucleon EDMs. We conclude that we cannot do better than give a rough estimate of the combined contributions which sets the scale for the sizes of both the neutron and proton EDM:

$$|d_{n,p}| = \mathcal{O}(e\,\tilde{d}_d) \ , \tag{9.32}$$

and we do not expect the nucleon EDMs to be larger than this estimate.

9.2.2 A short intermediate summary

Before we proceed to the discussion of light-nuclear EDMs, let us briefly summarize what we found so far. We have seen that the different scenarios of sections 9.1.1 and 9.1.2, and chapter 8 predict distinct hierarchies for the $\not{P}\not{T}$ pion-nucleon interactions in Eq. (9.17). Roughly, we find $\bar{g}_1^{\bar{\theta}}/g_0^{\bar{\theta}} \simeq -0.2$ for the $\bar{\theta}$ term [98], $\bar{g}_1^{\mathrm{LR}}/\bar{g}_0^{\mathrm{LR}} \simeq -50$ for the mLRM [56], and $|\bar{g}_0^{\mathrm{H}}| \simeq |\bar{g}_1^{\mathrm{H}}|$ in the a2HDM scenario (although $|\bar{g}_1^{H}|$ might be somewhat larger than $|\bar{g}_0^{H}|$ [108]).

This information, however, does not lead to a solid prediction of the sizes of the neutron and proton EDM apart from the expectation that, in all scenarios, they are of comparable size. The lack of predictive power is mainly caused by the fact that the nucleon EDMs obtain leading-order contributions from tree-level diagrams independent of the $\not{P}\not{T}$ pion-nucleon interactions. The situation is somewhat better for the $\bar{\theta}$ term (see Ref. [29]) because of lattice data, but the uncertainties, in particular for the proton EDM, are still significant.

A signal in a single EDM measurement would, of course, not point to its origin. The above considerations imply that, at the moment, even a measurement of both the proton and neutron EDM is not enough to disentangle the various scenarios [58] (although a hint for the $\bar{\theta}$ term might be found). Additional measurements are therefore required, and in the next sections we will argue that light-nuclear EDM experiments can be used for this task.

9.3 EDMs of light nuclei

9.3.1 The EDM of the deuteron

For convenience we repeat the expression for the deuteron EDM [114, 99, 115, 116, 117, 74, 98, 118, 119], which obtains contributions from the nucleon EDMs as well as $\bar{g}_1$,

$$d_D = d_n + d_p + \big[(0.18 \pm 0.023)\,\bar{g}_1 + (0.0028 \pm 0.0003)\,\bar{g}_0\big] e\,\mathrm{fm}\,. \tag{9.33}$$

We now turn to the implications of this result for the $\bar{\theta}$ and a2HDM scenarios.

The $\bar{\theta}$ scenario

In this scenario the deuteron EDM can be given as a function of $\bar{\theta}$. It follows from Eqs. (9.18), (9.19), (9.27), and (9.33) that

$$d_D^{\bar{\theta}} = [(-1.8 \pm 1.4) + (0.55 \pm 0.36 \pm 0.054) - (0.05 \pm 0.02 \pm 0.006)] \cdot 10^{-16}\,\bar{\theta}\,e\,\mathrm{cm}\ , \tag{9.34}$$

where the first term is the contribution from the nucleon EDMs and the second and third, respectively, from the two-body contribution, resulting from pion exchange between the nucleons making up the nucleus, proportional to $\bar{g}_1^{\bar{\theta}}$ and $\bar{g}_0^{\bar{\theta}}$. The first error of the coefficients is due the hadronic uncertainty in the LECs (see Eqs. (9.18) and (9.19)), while the second error of the last two terms is due to the nuclear uncertainty, which is significantly smaller.

We can learn a few things from Eq. (9.34). First of all, the deuteron is most likely dominated by the nucleon EDMs, although the uncertainties are still too large to say this with full confidence [74]. More input from lattice calculations (in combination with χPT techniques) of $d_{n,p}$ is needed to improve the situation. Second, when measurements of d_n, d_p, and d_D will be available, the relation

$$d_D^{\bar{\theta}} - d_n^{\bar{\theta}} - d_p^{\bar{\theta}} = (5.0 \pm 3.7) \cdot 10^{-17}\,\bar{\theta}\,e\,\mathrm{cm} \tag{9.35}$$

will be a promising and relatively precise method to directly extract (or bound) the value of $\bar{\theta}$ from experiments [98]. The existence of the $\bar{\theta}$ term can then be tested in several ways. One can compare the experimental value of d_n and/or d_p to lattice results such as Eq. (9.26). A more robust test, independent of lattice results, would be the measurement of the ^{3}He or ^{3}H EDM whose dependence on $\bar{\theta}$ can be firmly predicted. We will discuss this in Sect. 9.3.2.

The a2HDM scenario

The situation for the deuteron EDM in case of a2HDM is somewhat similar to that of the mLRM. The $\bar{g}_0^{\mathrm{H}}$ term in Eq. (5.8) can be neglected since we expect $|\bar{g}_0^{\mathrm{H}}| \simeq |\bar{g}_1^{\mathrm{H}}|$, while the coefficient in front of $\bar{g}_0^{\mathrm{H}}$ is a hundred times smaller. Using the estimates from section 9.2 gives

$$d_D^{\mathrm{H}} = \pm(e\,\tilde{d}_d)\ -\ (2^{+4}_{-1})e\,\tilde{d}_d\ , \tag{9.36}$$

where the first term is due to the nucleon EDMs[5] and the second term results from the two-body contribution. The uncertainty of the two-body contribution is obtained from the QCD sum rules estimate of $\bar{g}_1^H$ [108]. The nuclear uncertainty is neglected since it is at least an order of magnitude smaller.

In the a2HDM scenario the deuteron-to-nucleon EDM ratio lies between the $\bar{\theta}$ and mLRM scenarios discussed above, in both the mLRM and the a2HDM scenarios we expect

$$\left|\frac{d_D}{d_n + d_p}\right| > 1 \ , \tag{9.37}$$

although the exact value of this ratio is uncertain. In the a2HDM, it can be expected that the deuteron EDM is a few times bigger than the sum of the nucleon EDMs. However, the nucleon EDMs obtain contributions from three different BSM operators, *cf.* Eq. (9.13). Therefore, the accumulated uncertainty is significant, in particular, the uncertainty associated with the Weinberg operator is large. As a result, the conclusion $|d_D^{\rm H}| > |d_n^{\rm H} + d_p^{\rm H}|$ might be premature. Lattice calculations of the nucleon EDMs could improve the situation. However, as the nucleon EDMs depend on the EDM and CEDM of the d quark and on the Weinberg operator in this scenario, lattice calculations of the nucleon EDM will be very difficult.

To conclude, it is likely that measurements of d_n, d_p, and d_D would allow to disentangle the $\bar{\theta}$ term from the three BSM scenarios discussed here. This already shows the potential impact of the plans to measure d_p and d_D in storage-ring experiments. Unfortunately, the three measurements are most likely not sufficient to disentangle the BSM scenarios, a problem which is mainly caused by the poor information available on the hadronic $\not{P}\not{T}$ LECs.

9.3.2 The EDMs of the helion and triton

Before discussing the tri-nucleon EDMs, we recall their expressions in terms of $d_{n,p}$ and $\bar{g}_{0,1}$ [118, 119, 120],

$$\begin{aligned} d_{^3\mathrm{He}} &= (0.89 \pm 0.01)\, d_n - (0.039 \pm 0.01)\, d_p \\ &\quad + \big[(0.099 \pm 0.026)\, \bar{g}_0 + (0.14 \pm 0.028)\, \bar{g}_1\big]\, e\,\mathrm{fm}\ , \\ d_{^3\mathrm{H}} &= -(0.051 \pm 0.01)\, d_n + (0.87 \pm 0.01)\, d_p \\ &\quad - \big[(0.098 \pm 0.024)\, \bar{g}_0 - (0.14 \pm 0.028)\, \bar{g}_1\big]\, e\,\mathrm{fm}\,. \end{aligned} \tag{9.38}$$

In principle, the tri-nucleon EDMs also depend on the $\not{P}\not{T}$ nucleon-nucleon contact interactions mentioned in chapter 8, Eq. (8.18). However, as discussed in the previous chapter, in the mLRM [56] these terms only appear at next-to-next-to-leading order, and can be neglected. The same holds for the $\bar{\theta}$ scenario [211, 98]. In the a2HDM these effects are larger because of the Weinberg operator [74], but also here their contributions turn out to be small compared to pion-exchange contributions. We discuss in this more detail after considering the contributions to the ^{3}He and ^{3}H EDMs in the $\bar{\theta}$ scenario.

[5] We most likely overestimate the nucleon EDM contribution to $d_D^{\rm H}$ since $d_n^{\rm H} + d_p^{\rm H}$ is expected to be smaller than $d_n^{\rm H}$ and $d_p^{\rm H}$ individually, see Eqs. (9.30) and (9.31).

The $\bar{\theta}$ scenario

As was the case for the dEDM, the tri-nucleon EDMs can be expressed in terms of $\bar{\theta}$ with controlled uncertainty. We insert Eqs. (9.18), (9.19), and (9.26) into Eq. (9.38) and find

$$\begin{aligned} d^{\bar{\theta}}_{^3\mathrm{He}} &= \big[(-2.6 \pm 0.80) - (1.78 \pm 0.70 \pm 0.46) + (0.42 \pm 0.28 \pm 0.08)\big] \cdot 10^{-16}\, \bar{\theta}\, e\,\mathrm{cm}\ , \\ d^{\bar{\theta}}_{^3\mathrm{H}} &= \big[\ \ (1.1 \pm 0.96) + (1.74 \pm 0.68 \pm 0.44) + (0.42 \pm 0.28 \pm 0.08)\big] \cdot 10^{-16}\, \bar{\theta}\, e\,\mathrm{cm}\ , \end{aligned} \tag{9.39}$$

where the first term in bracket denotes the nucleon EDM contribution, while the second and third term is, respectively, the two-body term due to $\bar{g}_0^{\bar{\theta}}$ and $\bar{g}_1^{\bar{\theta}}$. Just as in Eq. (9.34) the first error is the hadronic uncertainty, while the second error in the two-body contributions is the nuclear uncertainty. Despite the increase of the latter with respect to the deuteron case, the hadronic uncertainties are still dominant.

It is useful to combine the two-body terms into one expression,

$$\begin{aligned} d^{\bar{\theta}}_{^3\mathrm{He}} &= \big[(-2.6 \pm 0.80) - (1.36 \pm 0.88)\big] \cdot 10^{-16}\, \bar{\theta}\, e\,\mathrm{cm}\ , \\ d^{\bar{\theta}}_{^3\mathrm{H}} &= \big[\ \ (1.1 \pm 0.96) + (2.16 \pm 0.85)\big] \cdot 10^{-16}\, \bar{\theta}\, e\,\mathrm{cm}\ . \end{aligned} \tag{9.40}$$

Several conclusions can be drawn from these relations. First of all, both for the ^{3}He and ^{3}H EDMs the two-body contributions add constructively to the one-body contributions. Second, in both cases the two-body contributions are, within the uncertainties, of similar magnitude as the one-body contributions. Third, measurements of d_n, d_p, d_D, $d_{^3\mathrm{He}}$, and/or $d_{^3\mathrm{H}}$ allow for a relatively precise test of the relevance of the $\bar{\theta}$ term, *even without relying on any lattice results*. That is, the value of $\bar{\theta}$ can be extracted from $(d_D - d_n - d_p)$, which can then be compared with the predictions

$$\begin{aligned} d_{^3\mathrm{He}} - 0.89\, d_n + 0.039\, d_p &= -(1.36 \pm 0.88) \cdot 10^{-16}\, \bar{\theta}\, e\,\mathrm{cm}\ , \\ d_{^3\mathrm{H}} + 0.051\, d_n - 0.87\, d_p &= \ \ (2.16 \pm 0.85) \cdot 10^{-16}\, \bar{\theta}\, e\,\mathrm{cm}\ . \end{aligned} \tag{9.41}$$

Of course, using lattice data would allow for additional nontrivial tests.

The a2HDM scenario

The analysis of the tri-nucleon EDMs within the a2HDM is more complicated than in the previous two scenarios. Similar to the dEDM, the tri-nucleon EDMs are most likely larger than the nucleon EDMs by a factor of a few. However, the exact size of $d^{\mathrm{H}}_{^3\mathrm{He},^3\mathrm{H}}/d^{\mathrm{H}}_{n,p}$ is uncertain.

In addition, even with measurements of d_n, d_p, and d_D, the tri-nucleon EDMs cannot be firmly predicted. This can be understood from the $\bar{g}_0$ terms in Eq. (5.9) which are expected to be significant in the a2HDM scenario, but the size of $\bar{g}_0$ cannot be obtained from d_n, d_p, and d_D. One could then think of a negative test: measurements of d_n, d_p, and d_D allow the extraction of $\bar{g}_1$. This value, in combination with d_n and d_p, can be used to predict the tri-nucleon EDMs. If these predictions would not agree with the data, it would indicate that the tri-nucleon EDMs obtain an independent contribution, suggesting that $\bar{g}_0$ plays a role which could hint at the a2HDM or similar models.

Table 9.1: Estimates for the ratios for the light nuclei-to-neutron EDMs in each of the three scenarios [74]. The shown ratios have an undetermined sign, apart from the helion-to-nucleon EDM ration in the $\bar{\theta}$ case which has is positive.

	$\bar{\theta}$ scenario	a2HDM	mLRM
d_p/d_n	$\mathcal{O}(1)$	$\mathcal{O}(1)$	$\mathcal{O}(1)$
$d_D/(d_n+d_p)$	$\mathcal{O}(1)$	$\mathcal{O}$(few)	$\mathcal{O}(10)$
$d_{^3\mathrm{He}}/(d_n+d_p)$	$\mathcal{O}$(few)	$\mathcal{O}$(few)	$\mathcal{O}(10)$

A better method to test the a2HDM scenario then seems to be the following: from measurements of d_n, d_p, and d_D, it is possible to extract the size of $\bar{g}_1^{\mathrm{H}}$. This value, in combination with a measurement of $d_{^3\mathrm{He}}$ ($d_{^3\mathrm{H}}$), allows for the extraction of $\bar{g}_0^{\mathrm{H}}$. The value of $d_{^3\mathrm{H}}$ ($d_{^3\mathrm{He}}$) can then be predicted.

Lattice calculations could improve this scenario where five EDMs are necessary for a proper test. Because in the a2HDM, the nucleon EDMs depend on the EDM and CEDM of the d quark and on the Weinberg operator, lattice calculations of the nucleon EDM will be very difficult. Thus, in this scenario combining the measurements of light-nuclear EDMs with different experimental probes, such as collider searches, is likely needed for a definitive test. On the other hand, the $\not{P}\not{T}$ pion-nucleon LECs mainly depend on the qCEDM. If $\bar{g}_{0,1}$ can be calculated as a function of the qCEDM, the number of necessary experiments can be reduced.

Finally we turn to the $\not{P}\not{T}$ contact LECs in Eq. (8.18). As discussed in Refs. [211, 74], for most $\not{P}\not{T}$ dimension-four and -six operators these terms are very small. For the Weinberg operator, however, which appears in the a2HDM scenario, these operators could be as important as one-pion exchange between nucleons involving $\bar{g}_0$. As was argued in section 9.2, in the a2HDM the contribution from the Weinberg operator to $\bar{g}_0$ can be neglected, because of the larger contribution from the down-quark CEDM. This implies that the contributions from the interactions in Eq. (8.18) to the $\not{P}\not{T}$ NN potential can be neglected as well. In addition, Ref. [74] found that the dependence of the tri-nucleon EDMs on the $N\,N$ interactions was smaller then expected by power counting.

Tri-nucleon EDMs: an overview

The tri-nucleon EDMs are very promising probes of the $\bar{\theta}$ scenario. Because the tri-nucleon EDMs depend on $\bar{g}_0$ at leading order, the two-body contributions are a few times bigger than for the deuteron EDM, which implies that the tri-nucleon EDMs are not dominated by the constituent nucleon EDMs. The EDMs of the helion and trition are thus expected to be larger than the EDMs of the neutron and proton. Furthermore, the small nuclear uncertainties allow for a proper test of strong CP violation, once $\bar{\theta}$ has been determined from measurements of d_n, d_p, and d_D, or from lattice calculations (together with χPT techniques) in combination with a measurement of d_n and/or d_p.

In the a2HDM scenario, the tri-nucleon EDMs are in principle independent from the deuteron EDM because of the dependence on $\bar{g}_0^H$. Estimates of the nucleon EDMs and

the pion-nucleon LECs $\bar{g}^{\rm H}_{0,1}$ suggest that the two-body contributions dominate the light-nuclear EDMs – however, the uncertainties are large. A lattice calculation of the $\bar{g}^{\rm H}_{0,1}$ induced by the qCEDM could significantly improve the situation. A lattice calculation of $d_{n,p}$ would be beneficial as well, but more complicated because of its dependence on the three BSM operators in Eq. (9.13). This makes the a2HDM scenario much harder to test than the mLRM, where measurements of d_n, d_p and d_D allowed for the prediction of the tri-nucleon EDMs. Estimates for the light nuclei-to-neutron EDM ratios for each scenario are summarized in Table 9.1. These ratios can not be predicted as precisely as the relations between different EDMs in the $\bar{\theta}$ scenario, Eqs. (9.41), because the rather uncertain contributions to the nucleon EDMs do not cancel in the ratios.

In any scenario, measurements of the tri-nucleon EDMs would provide important information on the source of non-KM *CP* violation, if such a source exists. Measurements of the nucleon, deuteron, and tri-nucleon EDMs allow one to disentangle the $\bar{\theta}$ and mLRM scenarios from the a2HDM scenario considered in this chapter.

9.4 The EDMs of paramagnetic systems

In this section we briefly discuss the EDMs of systems other than light nuclei. In particular we consider, within the above scenarios, $\not{P}\not{T}$ effects in the paramagnetic atom/molecules ^{205}Tl, YbF, and ThO, which were discussed in the context of dimension-six operators in section 5.1.5. As mentioned in chapter 5, these $\not{P}\not{T}$ effects are not only induced by the electron EDM (eEDM), but also by semi-leptonic four-fermion operators.

In the SM with massless neutrinos and a nonzero $\bar{\theta}$ term, the eEDM is generated by the quark sector, namely, by the $\bar{\theta}$ term and the KM phase, and is therefore much smaller than the EDM of a nucleon [125, 124, 19], $|d_e| \lesssim 10^{-37}\, e$ cm. Contributions from $\not{P}\not{T}$ semi-leptonic interactions to T-violating effects in atoms and molecules might be larger than those from the eEDM, but also they are strongly suppressed [126]. Therefore, in the $\bar{\theta}$ scenario we do not expect a nonzero measurement of a T-violating effect in the above paramagnetic systems.

In the version of the a2HDM discussed in Sect. 9.1.2 the contribution to the eEDM is dominated by two-loop diagrams and the expressions are nearly identical to those of the d-quark EDM. Two things are altered. First of all, there is the obvious difference between the masses and charges of the d quark and the electron. More important is that the eEDM depends on a different *CP*-odd parameter, namely, $\mathrm{Im}(\varsigma_l \varsigma_u^*)$ where ς_l is defined analogously to ς_d [214], *cf.* Eq. (9.6). This means it will be hard to compare the d-quark EDM and eEDM in general. If we assume the two *CP*-violating parameters to be of the same order, the magnitudes of the two EDMs should be comparable at the electroweak scale with a minor enhancement of the d-quark EDM by a factor m_d/m_e. However, the d-quark EDM gets large contributions from the d-quark CEDM when the operators are evolved to lower energies, while there is no such mechanism for the electron EDM. Therefore, it is more interesting to look at the electron-to-neutron-EDM ratio in the a2HDM. Assuming the *CP*-violating parameters to be equal (see Eq. (9.44)) and using Eq. (9.32) we estimate $|d_e/d_n| \sim 10^{-2}$. The upper bound on the eEDM then implies a bound on the nEDM $d_n \lesssim 10^{-26}\, e\,$cm in this scenario. In view of the dependence of the eEDM and nEDM on

different parameters this bound is not very stringent.

What about the semi-leptonic operators in the a2HDM scenarios? In this scenario they are generated through tree-level exchange of a heavy Higgs boson. These operators are therefore suppressed by a factor $m_q m_e/v^2$ from the Yukawa couplings. In addition there is a factor $1/m_H^2$ from heavy Higgs-boson exchange H, where m_H denotes the mass of H. Even though in the a 2HDM the eEDM is generated at the loop level, it nevertheless dominates the contributions to the above atomic/molecular T-odd effects. The only way around this is if the CP phases that appear in d_e are tuned to be much smaller than the phases of the coefficients of the semi-leptonic operators. Barring this possibility then, in the a2HDM, the contributions from the semi-leptonic operators to the T-violating effects in ^{205}Tl, ThO, and YbF are suppressed by about two orders of magnitude with respect to those of the eEDM, see Ref. [81] for a more detailed discussion.

In summary, the size of the eEDM with respect to hadronic EDMs gives additional information to disentangle the various scenarios. Clearly, a nonzero eEDM would rule out the pure $\bar{\theta}$-scenario. Within the a2HDM, the eEDM is expected to be about two orders of magnitude smaller than the neutron EDM. Similarly, in the mLRM the electron EDM is expected to be significantly smaller than the neutron EDM, although, in this scenario, the ratio would be even smaller, $d_e/d_n \sim 10^{-4}$ (see section 6.2.3 of chapter 6). However, in these scenarios no solid predictions can be made because the eEDM and the hadronic EDMs depend, in general, on different unknown parameters.

9.5 Discussion

9.5.1 Testing strategies

Based on the results of this chapter there are several strategies to reveal nontrivial information on the $\not{P}\not{T}$ sources, once non-vanishing measurements and/or improved lattice calculations of EDMs of nucleons and light nuclei are available[6].

Since the $\not{P}\not{T}$ pion-nucleon coupling constants are known quantitatively for a non-vanishing $\bar{\theta}$-term, the most conclusive tests can be formulated for this scenario: if the QCD $\bar{\theta}$-term is assumed to be the prominent source of CP violation beyond the CKM-matrix, it follows directly from Eq. (9.39) that the value of $\bar{\theta}$ can be extracted from EDM measurements of both the neutron and ^{3}He via

$$d_{^3\mathrm{He}} - 0.9\, d_n = (-1.4 \pm 0.9) \cdot 10^{-16}\, \bar{\theta}\, e\,\mathrm{cm}\ , \tag{9.42}$$

where the uncertainties were added in quadrature and we dropped the contribution from the proton EDM whose contribution to $d_{^3\mathrm{He}}$ is strongly suppressed. A lattice calculation (in combination with χPT techniques) for d_n then allows for the first nontrivial test of the assumed scenario. Note that in this case all nonperturbative QCD effects can be controlled quantitatively. The value of $\bar{\theta}$ extracted from Eq. (9.42) can now be used to predict

$$d_D - d_n - d_p = (5 \pm 4) \cdot 10^{-17}\, \bar{\theta}\, e\,\mathrm{cm}\ , \tag{9.43}$$

[6]In this section we do not consider measurements of the EDM of ^{3}H since, due to its radioactive nature, it is not likely to be measured in a storage-ring experiment.

where the uncertainties displayed in Eq. (9.34) were again added in quadrature. This provides the second nontrivial test, if in addition also the EDM of the deuteron, d_D, and of the proton, d_p, were measured. If the same value of $\bar{\theta}$ could explain simultaneously the measured values of $d_{^3\mathrm{He}}$, d_D, as well as d_n and d_p extracted using lattice results, it would provide very strong evidence that indeed the QCD $\bar{\theta}$-term is the origin of the non-vanishing EDMs.

If the QCD $\bar{\theta}$-term would not pass this test, alternative scenarios need to be studied. In this chapter we considered the a2HDM, and, in the previous chapter, the mLRM. In these cases the absence of a quantitative knowledge of the induced LECs hinders predictions for the nuclear EDMs analogous to Eqs. (9.42) and (9.43). However, at least for the mLRM different EDMs can be related to each other, since in this scenario $\bar{g}_1$ dominates over $\bar{g}_0$. This results in the prediction that the single nucleon EDM should be significantly smaller than the nuclear ones. In addition, one may extract $\bar{g}_1^{\mathrm{LR}}$ from Eq. (9.33),

$$d_D - (d_n + d_p) \simeq d_D = (0.18 \pm 0.02)\, \bar{g}_1^{\mathrm{LR}} e\,\mathrm{fm}\ .$$

This value of $\bar{g}_1^{\mathrm{LR}}$ can then be used to predict $d_{^3\mathrm{He}}$ according to Eq. (9.38),

$$d_{^3\mathrm{He}} - 0.9\, d_n \simeq d_{^3\mathrm{He}} = (0.14 \pm 0.03)\, \bar{g}_1^{\mathrm{LR}}\, e\,\mathrm{fm}\ .$$

If the mLRM fails its test, too, the physics responsible for the *CP*-violation must come from yet another theory beyond the Standard Model, a candidate being the a2HDM. In this model $\bar{g}_0$ and $\bar{g}_1$ are expected to be similar in size and the single-nucleon as well as ^{3}He EDMs acquire additional important contributions. The appearance of an independent, non-negligible $\bar{g}_0$ complicates a possible test for the a2HDM scenario. In principle, five EDMs, those of the nucleons, the deuteron and the tri-nucleon EDMs, would be necessary for a proper test. A lattice calculation of the $\bar{g}_{0,1}^{\mathrm{H}}$ induced by the qCEDM could significantly improve this situation, possible removing the need for one of these measurements. As outlined in section 9.4 the electron EDM might provide additional information to disentangle the mLRM from the other scenarios. Of course, independent measurements, such as those at the LHC, provide additional information.

Thus, if the EDMs for proton, neutron, deuteron, and ^{3}He were measured with high precision, highly nontrivial information could be deduced on the *CP*-violating physics responsible for their appearance.

9.5.2 Expected sensitivities

So far we have focused on ways to disentangle the scenarios of *CP* violation. However, it is also interesting to see how well the current and proposed EDM experiments are able to probe non-KM *CP* violation in each of these scenarios. To this end we will discuss the sensitivities to the *CP*-violation parameters that would result from EDM measurements of the proton, deuteron, and helion at the envisaged accuracy [92, 93, 94, 95]. These sensitivities are shown in Table 9.2 for the $\bar{\theta}$ (and mLRM) scenarios and in Figure 9.3 for the a2HDM scenario. For comparison, we also show the bounds that can be set by the current upper limit on the neutron EDM [18]. The most conservative values allowed by the uncertainties of the expressions in sections 9.2 and 9.3 were used to obtain these

Table 9.2: Sensitivities to the magnitudes of CP-violating parameters of the $\bar{\theta}$ and mLRM scenarios. The first column shows the relevant parameters, while the second column shows bounds from the current upper limit on the neutron EDM, $|d_n| \leq 2.9 \cdot 10^{-26} e\,\text{cm}$. The remaining columns show the values to which the CP-violating parameters could be probed by measurements of the proton, deuteron, and helion EDMs at the envisaged accuracy: 10^{-29} e cm. The contributions of $\bar{\theta}$ to the proton and deuteron EDMs are consistent with zero within the uncertainties of Eqs. (9.26) and (9.34) and can therefore, at the moment, not be used to probe $\bar{\theta}$. If we were to take the central values of Eqs. (9.26) and (9.34), we would obtain sensitivities of $9 \cdot 10^{-14}$ and $8 \cdot 10^{-14}$ for d_p and d_D, respectively.

	d_n	d_p	d_D	$d_{^3\text{He}}$
$\bar{\theta}$	$1 \cdot 10^{-10}$	$\times$	$\times$	$4 \cdot 10^{-14}$
$\frac{g_R}{g_L} \sin\zeta\, \text{Im}(V_L^{ud*} V_R^{ud} e^{i\alpha})$	$4 \cdot 10^{-5}$	$2 \cdot 10^{-8}$	$2 \cdot 10^{-9}$	$2 \cdot 10^{-9}$

bounds and sensitivities. An uncertainty of a factor 10 was assigned to the expressions based on NDA in order to reflect the large uncertainties associated with these estimates.[7]

The current upper limit on the neutron EDM already stringently constrains the CP-violating parameters appearing in each of the three scenarios. Obviously, for all scenarios a measurement of the proton EDM at the proposed accuracy would greatly improve the sensitivity to the CP-violating parameters as compared to the current neutron EDM limit.

To what extent the deuteron and/or helion EDMs are more sensitive than the proton EDM depends on the relative sizes of the corresponding EDMs, which differ between the various scenarios. In the $\bar{\theta}$ scenario, the helion EDM should be a few times bigger than the deuteron and proton EDMs, while in the mLRM scenario both the deuteron and helion EDMs are expected to be an order of magnitude larger than the proton EDM. This is reflected in Table 9.2, where the greatest sensitivity to $\bar{\theta}$ would come from a helion EDM measurement, while a deuteron EDM measurement would be the best probe for the mLRM scenario. In the a2HDM scenario, the deuteron and helion EDMs are expected to be of similar size, both are larger than the proton EDM by a factor of a few. However, the exact size of this factor is rather uncertain and we therefore only show in Figure 9.3 the region of parameter space which could be probed by a measurement of the proton EDM at an accuracy of $10^{-29} e\,\text{cm}$.

We leave a summary of the results of this chapter to chapter 10.

[7]Such a conservative estimate of the involved uncertainties was not taken into account in previous chapters, thereby explaining the difference of a factor of 10 concerning the mLRM bounds.

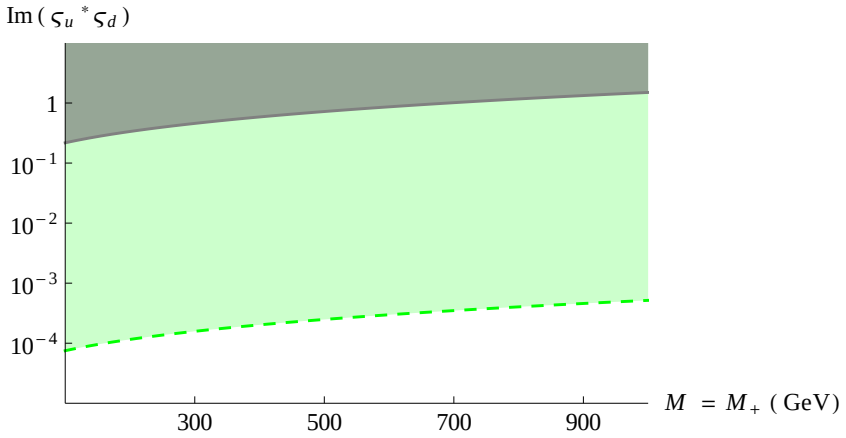

Figure 9.3: Sensitivities to the magnitude of the CP-violating parameter $\mathrm{Im}(\varsigma_u^*\varsigma_d)$ as a function of the mass of the additional Higgs fields. The region of parameter space which is excluded by the current upper limit on the neutron EDM ($d_n \leq 2.9 \cdot 10^{-26}\, e\,\mathrm{cm}$) is shown in grey and bounded by the solid line. The region that would be probed by a measurement of the proton EDM at the accuracy of 10^{-29} e cm is shown in green and bounded by the dashed line.

Appendix 9.A CP violation in the a2HDM

In this appendix we discuss how the low-energy $\not{P}\not{T}$ Lagrangian in Eq. (9.13) comes about in the a2HDM with the parameter specifications in Eq. (9.11).

9.A.1 CP-violating four-quark operators

CP-violating four-quark operators with net flavor number zero are induced, in the model with the parameters in Eq. (9.11), already at tree level by the exchange of the neutral Higgs bosons H and A and of charged Higgs bosons $H^\pm$ with Yukawa interactions in Eq. (9.7). Because we assume H and A to be (nearly) mass-degenerate, $M_H \simeq M_A \simeq M$, the relation Eq. (9.10) can be applied to the computation of the coefficients of these operators. Then, as already briefly mentioned in Sect. 9.1.2, the exchange of H and A induces operators of the type $(\bar{u}u)(\bar{d}i\gamma_5 d)$ and $(\bar{d}d)(\bar{u}i\gamma_5 u)$ with coefficients $\pm m_u m_d \mathrm{Im}(\varsigma_u^*\varsigma_d)/(v^2M^2)$, where u (d) denotes here any of the up-type (down-type) quarks. The operators that involve light quarks only are severely suppressed by the factor $m_u m_d/v^2$. The contribution of these operators to the EDM of a nucleon turns out to be, after the assumptions in Eq. (9.11), significantly smaller than the two-loop dipole contributions discussed below in the appendices 9.A.2 and 9.A.3.

The tree-level exchange of the charged Higgs bosons $H^\pm$ between quarks, with Yukawa interactions given in Eq. (9.7), induces at tree-level the $\not{P}\not{T}$ operators $(\bar{u}d)(\bar{d}i\gamma_5 u)$ and $(\bar{u}i\gamma_5 d)(\bar{d}u)$ with coefficients $2m_u m_d |V_{ud}|^2 \mathrm{Im}(\varsigma_u^*\varsigma_d)/(v^2M_+^2)$. The above statements on the size of the four-quark contributions induced by neutral Higgs boson exchanges apply also here.

The operators containing heavy quarks can (partially) overcome these suppression factors. However, these operators do not contribute directly to nucleon EDMs. Operators with two heavy quark fields can, after integrating out the heavy quarks, induce dimension-seven operators of the form $(\bar{q}q)\epsilon^{\alpha\beta\mu\nu}G^a_{\alpha\beta}G^a_{\mu\nu}$ and $(\bar{q}i\gamma_5 q)G^a_{\mu\nu}G^{a\,\mu\nu}$ [208, 209], where q de-

notes a light quark. The size of the contributions of these operators to the nucleon EDM has been estimated in Ref. [209] and also turns out to be significantly smaller than the contributions coming from the two-loop dipole diagrams to be discussed below.

These considerations justify that we neglect the contributions of four-quark operators to the low-energy effective Lagrangian in Eq. (9.13) in the a2HDM model with the parameter specifications in Eq. (9.11).

The exchange of the neutral Higgs bosons H and A between quarks and leptons ℓ induces CP-violating semileptonic four-fermion operators $(\bar{q}q)(\bar{\ell}i\gamma_5\ell)$ (and $q \leftrightarrow \ell$) with coefficients $\pm m_q m_\ell \mathrm{Im}(\varsigma_q^* \varsigma_\ell)/(v^2 M^2)$. These are of potential importance for T-violating effects in paramagnetic atoms (*cf.* Sect. 9.4). However, if

$$\mathrm{Im}(\varsigma_q^* \varsigma_\ell) = \mathcal{O}\left(\mathrm{Im}(\varsigma_u^* \varsigma_d)\right) , \tag{9.44}$$

then the electron EDM induced by two-loop Barr-Zee diagrams [77] dominates by far the contribution to the T-violating effect in the ThO molecule that was recently searched for in Ref. [89].

9.A.2 Contributions to the quark EDMs and chromo-EDMs

In general, CP-violating flavor-diagonal neutral-Higgs-boson exchanges induce the quark (C)EDMs already at one loop. Because these one-loop terms scale with the third power of the quark mass (modulo logs), $d_q^{(1l)}, \tilde{d}_q^{(1l)} \sim m_q^3/(v^2 M^2)$, they are, in the case of light quarks, suppressed as compared to the two-loop Barr-Zee contributions. Although these are nominally suppressed by an additional loop factor $\alpha/(4\pi)$, respectively $\alpha_s/(4\pi)$, where α (α_s) is the QED (QCD) coupling, they involve only one power (modulo logs) of m_q. In the a2HDM with the specifications of Eq. (9.11), the one-loop exchanges of the neutral Higgs bosons H and A cannot, in fact, generate a one-loop contribution to a quark (C)EDM. This follows from Eq. (9.10). The exchange of a charged Higgs boson does generate a one-loop contribution. For instance, the EDM of the d quark receives a contribution $d_q^{(1l)}(H^+) \sim 2 m_d m_u^2 |V_{ud}|^2 \mathrm{Im}(\varsigma_u^* \varsigma_d)/(v^2 M_+^2)$. But also these one-loop terms are subdominant compared to the two-loop terms that we now discuss and can therefore be neglected.

For the general a2HDM with the Yukawa interactions of Eq. (9.7) and the couplings in Eqs. (9.8) and (9.9) the Barr-Zee-type diagrams involving a CP-violating neutral spin-zero particle and a quark in the loop induce the following contribution to the quark EDM and CEDM, respectively [77, 231, 81, 232],

$$\begin{aligned}
d_q(\mu_H; \varphi^0, q) &= 24 e \frac{Q_q m_q \alpha}{(4\pi)^3 v^2} \sum_{q',i} Q_{q'}^2 \left[f\left(\frac{m_{q'}^2}{M_i^2}\right) \mathrm{Re}\, y_q^i \mathrm{Im}\, y_{q'}^i + g\left(\frac{m_{q'}^2}{M_i^2}\right) \mathrm{Re}\, y_{q'}^i \mathrm{Im}\, y_q^i \right], \\
\tilde{d}_q(\mu_H; \varphi^0, q) &= -4 \frac{m_q g_s \alpha_s}{(4\pi)^3 v^2} \sum_{q',i} \left[f\left(\frac{m_{q'}^2}{M_i^2}\right) \mathrm{Re}\, y_q^i \mathrm{Im}\, y_{q'}^i + g\left(\frac{m_{q'}^2}{M_i^2}\right) \mathrm{Re}\, y_{q'}^i \mathrm{Im}\, y_q^i \right],
\end{aligned} \tag{9.45}$$

where $e > 0$, $Q_u = 2/3, Q_d = -1/3$, and the label μ_H indicates that these are the quark (C)EDMs at a scale $\mu_H \sim m_t \sim M_\varphi$. The QCD coupling is understood to be evaluated

at the scale μ_H. For a neutral spin-zero particle and a $W^\pm$ boson in the loop one gets [77, 231, 81, 232],

$$d_q(\mu_H;\varphi^0,\,W^\pm) = -4eQ_q m_q \frac{\alpha}{(4\pi)^3 v^2}\sum_i \left[3f\left(\frac{M_W^2}{M_i^2}\right)+5g\left(\frac{M_W^2}{M_i^2}\right)\right]\mathrm{Im}\,\left(y_q^i R_{i1}\right)\ \ , \quad (9.46)$$

where

$$\begin{aligned} f(z) &\equiv \frac{z}{2}\int_0^1 dx \frac{1-2x(1-x)}{x(1-x)-z}\ln\frac{x(1-x)}{z}\ , \\ g(z) &\equiv \frac{z}{2}\int_0^1 dx \frac{1}{x(1-x)-z}\ln\frac{x(1-x)}{z}\ . \end{aligned} \quad (9.47)$$

When we now apply the specifications of Eq. (9.11), the contribution in Eq. (9.46) is zero, because $R_{11}=1$, $R_{21}=R_{23}=0$, and $y_q^1=1$. Eqs. (9.11) and (9.10) imply that up-type quarks in the fermion loop contribute only to the (C)EDM of a down-type quark and vice versa. Therefore, diagrams with a top quark in the loop contribute only to the (C)EDM of the d quark. Diagrams with quarks $q\neq t$ in the loop are suppressed by at least roughly two orders of magnitude as compared to the t-quark contribution, because of smaller Yukawa couplings. (This is reflected in the significantly smaller magnitudes of the respective values of the functions f and g.) Therefore, in the a2HDM with the assumptions in Eq. (9.11), the EDM and CEDM of the u quark in the low-energy effective Lagrangian can be neglected as compared to those of the d quark. There are also contributions to d_q from charged leptons in the fermion loop but, assuming that the relation in Eq. (9.44) holds, these can also be neglected as compared to the t-quark contribution to d_d.

Another set of Barr-Zee type contributions to d_q involves charged-Higgs-boson exchange [233, 81, 232]. They contribute significantly to the d-quark EDM only, while the u-quark EDM is again negligible [81, 232],

$$d_d(\mu_H;H^\pm) = m_d \frac{12M_W^2}{(4\pi v)^4}|V_{tb}|^2|V_{ud}|^2\mathrm{Im}\,(\varsigma_u^*\varsigma_d)(eQ_tF_t+eQ_bF_b)\ \ , \quad (9.48)$$

where

$$F_q = \frac{T_q(z_{H^\pm})-T_q(z_W)}{z_{H^\pm}-z_W}\ , \qquad z_i \equiv \frac{M_i^2}{m_t^2}\ \ , \quad (9.49)$$

and

$$\begin{aligned} T_t(z) &= \frac{1-3z}{z^2}\frac{\pi^2}{6}+\left(\frac{1}{z}-\frac{5}{2}\right)\ln z-\frac{1}{z}-\left(2-\frac{1}{z}\right)\left(1-\frac{1}{z}\right)\mathrm{Li}_2(1-z)\ , \\ T_b(z) &= \frac{2z-1}{z^2}\frac{\pi^2}{6}+\left(\frac{3}{2}-\frac{1}{z}\right)\ln z+\frac{1}{z}-\frac{1}{z}\left(2-\frac{1}{z}\right)\mathrm{Li}_2(1-z)\ . \end{aligned} \quad (9.50)$$

This contribution to d_d is not affected by the parameter choices in Eq. (9.11).

Additionally, there are contributions to the quark EDMs through diagrams which are similar to those that gave rise to Eq. (9.48), but where the virtual quark loop is replaced

by a loop involving the spin-zero fields [232, 224]. These diagrams are proportional to a different CP-violating parameter than the one encountered so far. Although these diagrams generate u- and d-quark EDMs of similar size, the contributions from these diagrams are smaller by a factor of a few than the ones in Eqs. (9.45), see Ref. [232]. In addition, they do not contribute to the quark CEDMs which play the dominant role in our analysis. Thus, under the assumption that the CP-violation parameters are of similar magnitude, these diagrams are expected to be less important than the CEDMs. We therefore neglect them in our analysis.

In summary, we obtain in the a2HDM with the parameter specifications in Eq. (9.11) that at a high scale μ_H the d-quark (C)EDM is significantly larger than the corresponding dipole moment of the u quark. The d-quark EDM and CEDM are given by, putting $\mu_H = m_t$:

$$d_d(m_t) = e\frac{Q_d m_d \alpha}{(4\pi)^3 v^2}\mathrm{Im}\,(\varsigma_u^*\varsigma_d)\left(\frac{32}{3}\left[f\left(\frac{m_t^2}{M^2}\right)+g\left(\frac{m_t^2}{M^2}\right)\right]+\frac{3}{s_w^2}|V_{ud}|^2|V_{tb}|^2\big[F_b-2F_t\big]\right), \tag{9.51}$$

$$\tilde{d}_d(m_t) = -4m_d\frac{g_s\alpha_s}{(4\pi)^3 v^2}\mathrm{Im}\,(\varsigma_u^*\varsigma_d)\left[f\left(\frac{m_t^2}{M^2}\right)+g\left(\frac{m_t^2}{M^2}\right)\right] . \tag{9.52}$$

They depend on a common unknown factor $\mathrm{Im}\,(\varsigma_u^*\varsigma_d)$ that signifies non-KM CP violation of the model. By renormalization-group evolution down to the scale $\mu = M_{\rm QCD}$ we obtain the d-quark (C)EDM given in Eqs. (9.13) and (9.15).

9.A.3 Contributions to the Weinberg operator

The leading-order contributions to the Weinberg operator corresponds to diagrams of the type shown in Fig. 9.1(c). From diagrams that involve CP-violating flavor-diagonal neutral Higgs boson exchange the coefficient of the Weinberg operator, i.e., the CEDM of the gluon, receives, in the 2HDM, the following contribution [38, 234, 81]:

$$d_W(m_t;\varphi^0) = -\frac{4g_s^3}{(4\pi)^4 v^2}\sum_{q,i}\mathrm{Re}\,y_q^i\mathrm{Im}\,y_q^i\,h(m_q,\,M_i) \ , \tag{9.53}$$

where

$$h(m,M) = \frac{m^4}{4}\int_0^1 dx\int_0^1 du\frac{u^3x^3(1-x)}{[m^2x(1-ux)+M^2(1-u)(1-x)]^2} \ . \tag{9.54}$$

As we restrict ourselves to the parameters of Eq. (9.11), this contribution will be proportional to $\mathrm{Im}(\varsigma_q^*\varsigma_q)$ and therefore vanishes.

The exchange of a charged Higgs boson with Yukawa couplings given in Eq. (9.13) leads to diagrams similar to Fig. 9.1(c). In this case both a bottom and top quark are present in the fermion loop. The amplitude involves two different scales, $M_+ \sim m_t$, and m_b. One may evaluate it in the EFT framework[8] by first integrating out the charged Higgs boson

[8] Alternatively, this two-loop amplitude was computed directly in Ref. [234]. This result can then by renormalization-group evolution be evaluated at a low scale.

and the top quark. This generates a one-loop contribution to the bottom quark CEDM [72, 235, 81]. At the bottom quark threshold this b-quark CEDM then induces a one-loop contribution [72] to d_W. The first step gives [235, 234, 81],

$$\tilde{d}_b(m_t;H^\pm) = -\frac{g_s(m_t)}{8\pi^2 v^2} m_b(m_t) |V_{tb}|^2 \mathrm{Im}\,(\varsigma_d \varsigma_u^*) \left[x_t \left(\frac{\ln x_t}{(x_t-1)^3} + \frac{x_t-3}{2(x_t-1)^2} \right) \right] \ , \quad (9.55)$$

where $x_t = m_t^2/M_+^2$ and $m_b(m_t)$ is the $\overline{\rm MS}$ mass of the b quark at the scale $\mu = m_t$. At $\mu = m_b$ this induces a contribution to the Weinberg operator [72],

$$d_W(m_b;H^\pm) = -\frac{g_s^2(m_b)}{32\pi^2 m_b(m_b)} \tilde{d}_b(m_b;H^\pm) \ , \quad (9.56)$$

where $m_b(m_b)$ denotes the $\overline{\rm MS}$ mass at $\mu = m_b$ and $\tilde{d}_b(m_b;H^\pm)$ is related to $\tilde{d}_b(m_t;H^\pm)$ by a renormalization-group factor: $\tilde{d}_b(m_b;H^\pm) = \eta'_W \tilde{d}_b(m_t;H^\pm)$ where we introduced the parameter $\eta'_W = \left(\frac{\alpha_s(m_t)}{\alpha_s(m_b)}\right)^{-19/46} \simeq 1.3$ [71, 72, 73, 48, 152].

In summary, we obtain in the a2HDM with the parameter set of Eq. (9.11) the CEDM d_W of the gluon at the scale $\mu = m_b$,

$$d_W(m_b) \ = \ \eta_W \frac{g_s \alpha_s}{(4\pi)^3 v^2} |V_{tb}|^2 \mathrm{Im}\,(\varsigma_u^* \varsigma_d) \left[x_t \left(\frac{\ln x_t}{(x_t-1)^3} + \frac{x_t-3}{2(x_t-1)^2} \right) \right] \ , \quad (9.57)$$

where the factors of g_s and α_s are to be evaluated at the scale $\mu = m_b$ while the parameter

$$\eta_W = \frac{g_s(m_t)}{g_s(m_b)} \frac{m_b(m_t)}{m_b(m_b)} \eta'_W = \left(\frac{\alpha_s(m_t)}{\alpha_s(m_b)}\right)^{14/23} \simeq 0.67, \quad (9.58)$$

is the resulting renormalization-group factor due to the evolution from the scale m_t to m_b. The renormalization-group evolution of Eq. (9.57) to the scale $\mu = M_{\rm QCD}$ then yields $d_W(M_{\rm QCD})$ given in Eqs. (9.13) and (9.15).

Chapter 10

Summary, conclusions, and outlook

The standard model (SM) has been tested to high precision in a large number of experiments. However, as discussed in chapters 1 and 2, it does not provide a mechanism to generate the observed matter-antimatter asymmetry of the universe and calls for CP violation beyond the standard model (BSM) [10]. This and other shortcomings of the SM, such as the inability to explain dark matter, have sparked the development of numerous models of BSM physics containing additional breaking of the discrete CP symmetry. On the experimental side, a host of experiments aiming to discover, or otherwise constrain, BSM physics have been set up. These experiments range from those at the high-energy frontier, such as CERN's LHC, to low-energy high-precision measurements like the electric-dipole-moment (EDM) searches that play an important role in this thesis.

This thesis focuses on theoretically analyzing the results of such experimental searches to constrain CP-violating BSM physics, and, if a signal is found, distinguish between different CP-violating scenarios. In order to do so, two approaches are employed: in the first, BSM physics is described in a model-independent way, while in the second a specific new-physics model is considered. Clearly, the first approach is attractive due to the fact that it is model-independent, with the downside that all possible interactions depend equally on their dimension. Instead, when considering specific models, connections between different observables can appear which are not readily apparent in the model-independent approach, so that a specific model can be more predictive and more stringently constrained.

In chapters 3-5 we take the first, model-independent, approach and focus on constraining new sources of CP violation using measurements of EDMs. The SM predictions for EDMs leave room for contributions from BSM CP violation, making them excellent probes of such sources. In order to use the experimental results of these searches to constrain BSM CP violation several steps are required. Firstly, assuming that the new physics appears at high energies, the heavy particles can be integrated out above the electroweak scale. The resulting theory is an effective field theory (EFT), which allows one to describe the leading effects of the BSM particles by effective interactions of dimension six between SM fields only. This CP-violating EFT is constructed in chapter 3, assuming the effective interactions, or operators, to be invariant under the SM gauge symmetries. In addition, we restrict ourselves to non-leptonic operators and take into account only the first generation of quarks.

Secondly, in order to connect these interactions to the low-energy EDM measurements, this effective theory has to be evolved to the low energies where EDM experiments take place. This can be done perturbatively down to the QCD scale, $M_{\rm QCD} \sim 1\,\text{GeV}$, where QCD becomes nonperturbative. To reach energies below this point we employ chiral perturbation theory (χPT), in which the connection to hadronic EDMs can be made. The χPT techniques needed to describe the effects of the dimension-six operators below $M_{\rm QCD}$, and the way in which the two effective theories can be related to one another is discussed in chapter 3. For the matching of the two EFTs, in many cases we cannot do better than an order of magnitude estimate. For this task we employ naive dimensional analysis, which has turned out to be approximately correct in many cases already.

Instead, the step in energy from the scale of new physics down to $M_{\rm QCD}$ is described in chapter 4. Here, we divide the dimension-six operators up into those which contribute to EDMs without further suppression and those which are suppressed by additional small masses $m_{u,v}/v$ or loop factors $\alpha_{em}/4\pi$. For both these sets of operators the QCD evolution is calculated, and, where necessary, electroweak loops are taken into account. This results in the effective Lagrangian at $M_{\rm QCD}$ of Eq. (4.44), which captures the dominant contributions to low-energy hadronic CP-violating observables. This Lagrangian contains seven relevant $\not{P}\not{T}$ operators among light quarks, gluons, and photons, and just four four-quark (FQ) operators. In contrast, if one does not take $SU(2)_L$ gauge symmetry into account one ends up with ten FQ operators at low energies [47, 48], which could potentially be equally important. Instead, we find that the remaining six FQ operators only appear in the set which is additionally suppressed by $m_{u,d}/v$. When the operators in the suppressed set are evolved to energies around $M_{\rm QCD}$, all ten possible $\not{P}\not{T}$ FQ operators among up and down quarks are induced, although, as we demonstrated, they depend on two couplings only. Lastly, the effects of the $\alpha_{em}/4\pi$-suppressed operators at low energies are derived.

These results allow one to translate bounds on the low-energy couplings into constraints on the couplings at high energies. In combination with results obtained using χPT techniques and the stringent experimental limit on the neutron EDM, this translation allows for the derivation of the constraints on the dimension-six operators at high energies, presented in chapter 5. These constraints can in principle be applied to any model of new physics after integrating out the heavy degrees of freedom and matching the theory to the EFT considered in this thesis. These results are subsequently used in chapters 8 and 9, where specific models of BSM physics are considered.

In addition to the neutron EDM, the EDMs of the proton and light nuclei are studied in chapter 5. It turns out that these EDMs, especially those of light nuclei, can help to distinguish between different operators. Other observables that are sensitive to CP-violating sources, and could assist in disentangling them from one another, are the electron EDM and the D coefficient, a T-odd correlation in β decay. Although the dimension-six operators we focus on are selected with hadronic EDMs in mind, some nevertheless contribute to these observables [52]. Thus, in case one of these operators is dominant one would expect a signal in both the electron EDM or the D coefficient and the neutron EDM. In addition, we consider a T-odd triple correlation in radiative β decay [148, 149]. Here the dimension-six operators contributing to this observable also induce the neutron EDM. We find that the neutron EDM sets a better limit on these operators, such that future radiative β-decay experiments are unlikely to provide new information on these

sources of CP violation [151].

Furthermore, chapter 5 covers CP-violating observables in kaon and $B_{d,s}$ mixing, namely, $\varepsilon^{(\prime)}$ and $\phi_{d,s}$, respectively. Because these mesons contain heavier quarks most of the dimension-six operators considered in chapters 3-5 do not contribute directly to these observables. Nevertheless, models of BSM physics will generally induce new contributions to them. In fact, they turn out to be excellent probes of left-right models, which are the topic of chapters 6 and 7. In turn, the ability to distinguish between the sources of CP violation is a promising feature of the electron EDM and especially the EDMs of light nuclei, which plays an important role in chapters 8 and 9.

Having discussed the model-independent approach we moved on to consider a specific model, namely, the left-right model. This model has certain theoretically attractive aspects, such as the automatic implementation of the type-I and type-II neutrino see-saw mechanisms, and the possibility of a symmetry, P or C, between left- and right-handed particles at high energy. The general features of the minimal LRM (mLRM) are introduced in chapter 6. Here we also discuss its impact on several different observables that were first introduced in chapter 5, namely, kaon and B-meson mixing observables, neutron β decay and the neutron and electron EDMs. In addition, the general Higgs potential is derived.

In chapter 7 we focus on particular mLRMs which might be more attractive theoretically, namely those with a C and P symmetry, as well as those with a C, P, or CP symmetry. These discrete symmetries influence the effects of the model on observables, and partly determine the Higgs potential. We show that the minimal LR models containing both discrete symmetries, the ones invariant under P *and* C, as well as the so-called *pseudomanifest* mLRSM [175, 174] are no longer viable. These models either cannot reproduce the CP violation that is observed in kaon and B-meson mixing by B factories and LHCb, or do not lead to a realistic Higgs mass spectrum. In the less-symmetric cases with a P *or* C symmetry, the meson-mixing constraints lead to bounds on the mass of the right-handed W boson of $M_2 \gtrsim 3\,\text{TeV}$, which is expected to be pushed to roughly 8 TeV in the coming years [138]. In addition, if a signal of new physics is found, the same meson-mixing observables should, in principle, be able to distinguish between the C- and P-symmetric scenarios. The often-considered *manifest* mLRSM [173, 174], is much more constrained, here the current bound is $M_2 \gtrsim 20\,\text{TeV}$ [183]. In contrast, we find that the CP-symmetric LRMs are less constrained, as they allow for more freedom in the right-handed CKM matrix.

All in all, future kaon- and B-meson searches by B factories and LHCb can go a long way to constrain BSM CP violation, and, in the case of a signal of BSM physics, pinpoint the source that is responsible. Hopefully, the expression derived in this thesis will be helpful in this endeavor.

For the Higgs sector, drawing on the results of chapter 6, we show that the potentials of the LRSMs are all quite similar, although the CP-symmetric case allows some more freedom in the masses of the left-handed triplet fields. Furthermore, we showed that the Higgs potentials in the C-, P-, and CP-symmetric cases all require an extreme amount of fine-tuning in general. However, as chapter 7 shows explicitly, this can be significantly decreased in specific cases, for instance by setting $v_L = 0$. Nevertheless, in all cases a

considerable amount of fine-tuning, $\mathcal{O}(100)$, remains.

Finally, in chapters 8 and 9 we consider how the EFT approach of chapters 4-5 can be applied to the LRM and two other scenarios of CP violation, namely, the SM with a nonzero $\bar{\theta}$ term and the aligned two Higgs-doublet model (a2HDM). Here we investigate how these models leave their footprint in EDMs of different systems. In each case we investigate the pertinent CP-odd sources and how they induce, at lower energies $\sim M_{\rm QCD}$, effective $\not{P}\not{T}$ operators. The resulting pattern of the EDMs of light nuclei is determined to a large extent by the hierarchy between the pion-nucleon couplings, $\bar{g}_{0,1}$, induced in the chiral Lagrangian. In turn, these interaction are determined by the effective operators at $\sim M_{\rm QCD}$ that are generated by the different scenarios. As a result, this hierarchy differs per scenario, we have $\bar{g}_1/\bar{g}_0 = \{-0.2 \pm 0.1,\, -50 \pm 25,\, 1\}$ for the $\bar{\theta}$, mLRM, and a2HDM scenario, respectively, with the largest uncertainty in the case of the a2HDM.

Despite these differences, the EDMs of the nucleons do not show distinct patterns in the different scenarios, since in all cases the nucleon EDMs obtain leading-order contributions associated with large uncertainties from the induced isoscalar and isovector nucleon EDMs [236, 57, 237, 238, 58, 59, 29]. In case of the $\bar{\theta}$ term, lattice results (in combination with χPT techniques) for the nucleon EDMs are available which provide additional information. Even so, at the moment, the uncertainties are still too large to draw firm conclusions. One reason why the storage-ring proposals to measure the EDMs of the proton, deuteron, and possibly ^{3}He and ^{3}H [92, 93, 94, 95], are so interesting is that nuclear EDMs already depend at tree level on the pion-nucleon interactions $\bar{g}_{0,1}$, leading to non-trivial relations between the different EDMs. In both the $\bar{\theta}$ and mLRM scenarios one can predict $d_{^3\rm He}$ after measuring the EDMs of the nucleons and the deuteron, even without input from lattice calculations. This is not possible in the a2HDM case, where also ^{3}H would need to be measured for a proper test, unless a more precise (lattice) determination of the $\bar{g}_1/\bar{g}_0$ ratio become available. Nonetheless, the measurements of the EDMs of light nuclei could distinguish between the three scenarios of BSM physics, and would provide non-trivial tests for two of them.

This work can be extended in several directions. As for the EFT approach, a straightforward extension would be to include the effects of heavier quarks. One would expect the contributions to hadronic EDMs of these operators to be smaller than those involving just the first generation, while the LHC is more sensitive to operators involving heavier quarks. Nevertheless, the EDM bounds on such operators can still be significant, and sometimes better than the collider limits, see e.g. [239].

An area of further study for LRMs discussed in this thesis would be the recently derived analytical solution for the right-handed CKM matrix in the P-symmetric case [171]. In principle this should allow one to constrain not only M_2 and the heavy Higgs mass M_H through meson-mixing constraints as was done in Ref. [183], but also bound the parameters r and α. In addition, similar analyses as performed in this thesis could be done for less-symmetric or non-minimal LRMs, which despite having less-attractive features are still motivated by their nontrivial embedding in grand unified theories.

Finally, the models used in the analysis of the EDMs of light nuclei were chosen to illustrate the potential as well as limitations of detailed analyses of various EDM mea-

surements. This choice is to some extent arbitrary and does by no means exhaust the possible options for physics beyond the SM. Furthermore, because the methods applied in chapters 8 and 9 are quite general, they can also be used to analyze the signatures of other models for *CP* violation. Therefore, it is certainly possible to extend the work in this thesis by performing an analysis of other well-motivated models of BSM physics in the same way.

Nederlandse Samenvatting

Het universum is bestudeerd op een groot aantal verschillende lengteschalen. Het ene extreem van deze lengteschalen wordt gegeven door de immense grootte van het waarneembare van het heelal, zo'n 10^{26} meter, terwijl onderzoek op de kleinste lengteschalen plaatsvindt op de minuscule afstanden van ongeveer 10^{-18} meter. Deze kleinste lengteschalen, die overeenkomen met de hoogste energieën, zijn het domein van de deeltjesfysica. Deze discipline houdt zich bezig met de beschrijving van de kleinste bouwstenen van de natuur, de elementaire deeltjes, en de wisselwerking tussen deze deeltjes. Ook alledaagse materie kan worden beschreven in termen van deze deeltjes. Zo zijn atomen opgebouwd uit elektronen en up en down quarks. De quarks vormen de protonen en neutronen waar de atoomkern uit is opgebouwd en de elektronen omheen bewegen. Hoewel alledaagse materie dus grotendeels kan worden beschreven in termen van slechts drie subatomaire deeltjes, zijn er door de jaren heen een groot aantal andere deeltjes ontdekt. Zo zijn er in totaal zes verschillende soorten quarks, bestaan er nog twee zwaardere versies van het elektron, en zijn er de wisselwerkingsdeeltjes zoals het foton, die de krachten tussen de deeltjes overbrengen.

Deze deeltjes en hoe ze met elkaar wisselwerken wordt beschreven in het zogenoemde standaard model (SM). Dit model levert erg precieze voorspellingen voor tal van experimenten, wat de mogelijkheid biedt om het model op een groot aantal manieren te testen. Tot nu toe heeft het SM al deze testen doorstaan, wat het tot de meest succesvolle beschrijving van de deeltjesfysica maakt die we tot onze beschikking hebben. Met de recente ontdekking van het Higgsdeeltje in de meest energetische versneller tot nu toe, de Large Hadron Collider (LHC), lijkt ook het laatste fundamentele deeltje uit het SM bevestigd. Hoewel er meer onderzoek nodig is om vast te stellen of het ontdekte deeltje zich exact zo gedraagt zoals in het SM, hebben metingen tot nu toe geen afwijking van het SM gevonden. Het SM lijkt dus ook een goede beschrijving van het gevonden Higgsdeeltje te geven.

Ondanks het grote succes van het SM zijn er ook fenomenen die het niet kan verklaren. Een van belangrijkste voorbeelden is de materie-antimaterie asymmetrie in het heelal. Deze asymmetrie duidt op de observatie dat de hoeveelheid antimaterie in het heelal veel kleiner is dan de hoeveelheid materie. Vermoedelijk zijn er dus interacties die materie verkiezen boven antimaterie, zodat tijdens de evolutie van het heelal een asymmetrie tussen materie en antimaterie kan zijn opgebouwd. Om de asymmetrie in het huidige heelal te kunnen verklaren moet aan drie condities voldaan worden, de zogenaamde Sakharov condities. Een van deze criteria is dat de interacties tussen elementaire deeltjes CP moeten schenden. CP is de combinatie van twee belangrijke discrete symmetrieën in de deeltjesfysica, namelijk pariteit (P), de omkering van ruimtelijke coördinaten ($\vec{x} \to -\vec{x}$), en

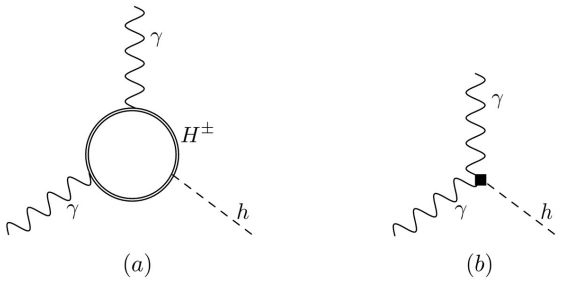

Figuur 10.1: Figuur (a) toont een interactie tussen twee fotonen γ en een Higgsdeeltje (h), via de uitwisseling van een hypothetisch deeltje uit een model van nieuwe fysica ($H^{\pm}$). Figuur (b) laat zien hoe, bij lage energie, hetzelfde proces kan worden beschreven in termen van een effectieve interactie, het zwarte blokje, in een EFT.

ladingsconjugatie (C), het verwisselen van deeltjes met hun antideeltjes. Wanneer een interactie niet verandert na het toepassen van deze twee transformaties (C en P), is deze CP behoudend, ofwel CP symmetrisch. Nu blijkt dat de interacties in het SM CP weliswaar breken, maar niet genoeg om de materie-antimaterie asymmetrie te kunnen verklaren; ze zijn te symmetrisch. Het onvermogen van het SM om de materie-antimaterie asymmetrie te verklaren lijkt dus te suggereren dat er 'nieuwe' CP-schendende fysica nodig is.

In combinatie met andere tekortkomingen van het SM heeft het bovenstaande argument geleid tot de ontwikkeling van een groot aantal theoretische modellen van nieuwe fysica, die het SM veelal uitbreiden met extra deeltjes en/of interacties. Deze modellen hebben als doel de tekortkomingen van het SM te verhelpen. Aangezien hoogstens één van deze modellen de werkelijkheid beschrijft, is een belangrijke vraag wat voor nieuwe deeltjes en interacties nog mogelijk zijn gezien de huidige experimentele resultaten. Wanneer deze metingen namelijk overeenkomen met de SM-voorspelling kunnen nieuwe-fysica effecten niet al te groot zijn, wat de mogelijkheden voor nieuwe deeltjes en interacties beperkt. Een groot deel van dit proefschrift richt zich op hoe experimentele resultaten nieuwe fysica, met name nieuwe CP-brekende interacties, limiteren.

Om nieuwe CP-brekende fysica te kunnen limiteren is het nodig de effecten hiervan op experimentele metingen te kunnen berekenen. Dit vereist echter weer een beschrijving van de nieuwe CP schending. Dit kan op meerdere manieren. Misschien de meest voor de hand liggende optie is om simpelweg een van de vele modellen van nieuwe fysica aan te nemen. In een specifiek model zijn alle nieuwe deeltjes en interacties gespecificeerd en is het, in principe, mogelijk de effecten op experimentele metingen uit te rekenen.

Een tweede mogelijkheid is een zogenaamde effectieve velden theorie, in het Engels afgekort tot EFT. Een EFT is gebaseerd op het idee dat de natuurkunde bij lage energieën niet afhangt van de details van de fysica bij hoge energieën. Doordat we weten dat het SM erg goed werkt kunnen we aannemen dat nieuwe fysica zich bij aanzienlijk hogere energieën dan het SM ophoudt (deeltjes bij hogere energieën zijn namelijk moeilijker te detecteren, wat verklaart waarom deze nog niet gezien zijn). Wanneer we deze scheiding van energieschalen aannemen zijn de effecten van nieuwe deeltjes te vangen in effectieve interacties. Een voorbeeld hiervan wordt gegeven in Figuur 10.1. In Figuur 10.1(a) zien

we hoe twee fotonen wisselwerken met een Higgsdeeltje via de uitwisseling van een nieuw deeltje ($H^{\pm}$). Bij lage energie kan ditzelfde proces worden beschreven in termen van een effectieve interactie, Figuur 10.1(b), tussen de bekende deeltjes van het SM (de fotonen en de Higgs). Het is dus mogelijk om het proces te beschrijven zonder enige kennis van het nieuwe deeltje, $H^{\pm}$. Omdat een EFT geen kennis van de nieuwe deeltjes vereist wordt het mogelijk de nieuwe fysica op een model-onafhankelijke manier te beschrijven, met als enige 'input' de energieschaal waarop nieuwe fysica zich manifesteert.

In het eerste gedeelte van dit proefschrift wordt deze EFT methode gebruikt om nieuwe fysica te beperken. De experimentele metingen die we hiervoor gebruiken zijn die van elektrische dipool momenten (EDMs). Deze EDMs geven de interactie van de spin van een deeltje met een extern elektrisch veld weer. Een belangrijke eigenschap van EDMs is dat ze CP schenden en in principe gevoelig zijn voor dezelfde fysica die verantwoordelijk is voor de materie-antimaterie asymmetrie. Hoewel het EDM van bijvoorbeeld het neutron experimenteel met grote precisie is gemeten, is er tot nu toe nog geen EDM gevonden.

In het SM zijn er twee bijdrages aan EDMs, de eerste komt van de CP schending in de zwakke wisselwerking, de tweede komt van een CP-brekende interactie in de sterke wisselwerking, de zogenoemde QCD $\bar{\theta}$ term. De eerstgenoemde bijdrage aan EDMs is zeer klein en zal in de nabije toekomst niet gemeten kunnen worden. De tweede bijdrage is in principe onbekend, maar het feit dat er tot nu toe geen EDMs gevonden zijn betekent dat deze erg klein moet zijn, $\bar{\theta} \leq 10^{-10}$. Naast de SM bijdrages kan CP-schendende nieuwe fysica ook bijdragen aan EDMs. Een gevolg hiervan is dat wanneer een EDM gevonden wordt dit ofwel door de $\bar{\theta}$ bijdrage van het SM komt, ofwel door nieuwe fysica. Verder kunnen metingen die geen EDM vinden worden gebruikt om nieuwe fysica te beperken.

Om nieuwe fysica op deze manier te beperken zijn een aantal stappen nodig. In hoofdstuk 3 stellen we de EFT van CP-schendende fysica op die de effectieve interacties bevat welke aan EDMs zouden kunnen bijdragen. We hebben echter aangenomen dat de nieuwe fysica zich manifesteert op hoge energie, terwijl EDMs worden gemeten bij lage energie. Om de bijdrages van de effectieve interacties aan EDMs te kunnen berekenen moeten we dus eerst de stap maken van hoge naar lage energie. Dit is het onderwerp van hoofdstuk 4, waar we een brug slaan tussen de effectieve interacties bij hoge en die bij lage energie. Op deze manier kunnen we de energie verlagen tot het punt waar de sterke kernkracht 'niet-perturbatief' wordt, hier wordt deze zo sterk dat de gebruikelijke benaderingen niet meer op gaan. Om toch de bijdrages van de effectieve interacties aan EDMs te kunnen uitrekenen is dan een tweede EFT nodig die de sterke interacties bij lage energieën beschrijft. Hoe de tweede EFT de nieuwe CP-schendende termen beschrijft en hoe deze uiteindelijk bijdragen aan EDMs wordt besproken in hoofdstuk 5. Hier berekenen we ook hoe sterk de EDM metingen de nieuwe CP schending beperken.

Een duidelijk voordeel van de bovengenoemde EFT methode is dat er geen specifiek model aangenomen hoeft te worden en dat in principe alle modellen van nieuwe fysica in een EFT gevangen kunnen worden. Een nadeel is echter dat het wel nodig is om alle mogelijke effectieve interacties, die onbekende sterktes hebben, mee te nemen om model onafhankelijk te kunnen werken. In vele specifieke modellen zullen echter niet al deze effectieve interacties een rol spelen, en zullen sommige interacties gerelateerd zijn. Dit zorgt ervoor dat een specifiek model relaties tussen verschillende experimentele metingen kan voorspellen die in een EFT niet meteen duidelijk zijn. Dit betekent ook dat de

limieten in een specifiek model sterker kunnen zijn dan de limieten die men afleidt in een EFT. Vandaar dat we in de hierop volgende hoofdstukken overstappen van de EFT methode op een specifiek model, namelijk, het links-rechts model (LRM).

Hoewel de symmetrie tussen links en rechts in het SM gebroken is, kan deze in links-rechts modellen op hoge energie weer hersteld worden. Concreet betekent dit dat het LRM bij hoge energie een C en/of P symmetrie toelaat, wat de asymmetrie tussen links en rechts in het SM zou kunnen verklaren als een effect wat alleen bij lage energieën optreedt. In hoofdstuk 6 bekijken we het algemene LRM, terwijl we in hoofdstuk 7 kijken naar LRMs met een P en/of C symmetrie die theoretisch gezien zijn het aantrekkelijkste zijn. Omdat de combinatie van meerdere experimentele metingen in een specifiek model tot sterkere limieten kan leiden, bekijken we in deze hoofdstukken niet alleen de effecten die het LRM heeft op EDMs, maar bijvoorbeeld ook op metingen bij de LHC. Het blijkt dat vooral metingen aan B en K mesonen, deeltjes die bestaan uit een quark en een antiquark, leiden tot sterke limieten op LRMs. Zo kunnen deze metingen de meest symmetrische modellen, namelijk diegene met zowel een P als een C symmetrie op hoge energie, al uitsluiten. Minder symmetrische modellen, de modellen met een P *of* C symmetrie, blijken nog steeds mogelijk, maar worden ook al sterk beperkt.

Behalve afwijkingen van het SM in experimenten, voorspellen LRMs ook meer dan tien extra Higgsdeeltjes. Deze Higgsdeeltjes, en de wisselwerkingen die ze met elkaar aangaan, wordt de Higgs sector genoemd. Voor elk van de LRMs die we bekijken leiden we de bijbehorende Higgs sector af, waarvan we vervolgens een maat voor de benodigde fine-tuning berekenen. Dit geeft een indicatie voor hoe precies de modelparameters (de sterktes van de interacties) moeten worden afgesteld om tot een model te komen dat nog niet is uitgesloten. Hoe preciezer deze parameters moeten worden afgesteld, hoe meer fine-tuning het bevat, des te onnatuurlijker het model. In hoofdstuk 7 laten we zien dat in LRMs de parameters over het algemeen erg precies moeten worden afgesteld, hoewel er bepaalde gevallen zijn waarbij de benodigde fine-tuning significant verminderd kan worden.

In de laatste twee hoofdstukken, 8 en 9, combineren we de EFT aanpak met specifieke modellen. Hier bekijken we wat we kunnen leren van EDM metingen in het geval dat deze EDMs zullen vinden. Met andere woorden, kunnen we met EDM metingen nieuwe fysica onderscheiden van de SM-bijdrage aan EDMs (de $\bar{\theta}$ term). Verder onderzoeken we of het op dezelfde manier mogelijk is om verschillende modellen van nieuwe fysica van elkaar te onderscheiden. Om tot een antwoord te komen, bekijken we drie CP schendende scenario's, namelijk, het SM met de $\bar{\theta}$ term, het LRM, en het zogenaamde twee Higgs-doublet model, wat het SM uitbreidt met vijf extra Higgsdeeltjes. Voor al deze scenario's berekenen we het effect dat ze hebben op de EDMs van het neutron, proton en lichte atoomkernen, namelijk die van deuterium (zwaar waterstof) en het helion. Dit doen we door, voor elk van de drie modellen de EFT uit te rekenen die het model op lage energie beschrijft. Hierna kunnen de technieken van hoofdstuk 4 en 5 gebruikt worden om de EFT naar lage energie te brengen en de bijdrages aan EDMs uit te rekenen. Op deze manier laten we in hoofdstuk 9 zien dat de drie modellen in principe te onderscheiden zijn met EDM-experimenten met lichte atoomkernen, wat betekent dat deze metingen belangrijke informatie kunnen leveren over de, toe nu toe onbekende, fundamentele bron van CP schending.

Samenvattend hebben we in dit proefschrift mogelijke nieuwe bronnen van CP schending onderzocht, zowel op een model-onafhankelijke manier als in specifieke modellen. Gebruikmakende van EFT technieken hebben we limieten gezet op nieuwe CP-schendende interacties. Aan de kant van specifieke modellen hebben we links-rechts modellen bestudeerd, waarbij niet alleen experimentele limieten zijn bekeken, maar ook hoe theoretisch aantrekkelijk deze modellen nog zijn. Tot slot is onderzocht wat gezegd kan worden over de fundamentele bron van CP schending, wanneer hier experimenteel een signaal van wordt gemeten. Uit deze analyse blijkt dat het mogelijk is om met metingen van de EDMs van lichte atoomkernen, verschillende CP-schendende scenario's te ontrafelen.

Acknowledgments

There are many people who contributed to this thesis and made my time as a PhD student more enjoyable in one way or another. I would like to start by thanking my supervisor Daniël Boer, for giving me the opportunity to work on interesting topics during both my PhD and master's projects. I enjoyed the, often lengthy, discussions we had, although we sometimes struggled to keep them from diverging. I would also like to thank you for giving me the opportunity, and encouraging me, to work on a number of different topics. I also appreciate the comments and the detailed corrections you would provide for almost anything I produced, from slightly updated versions of presentations I had already given several times, to this thesis. I am especially thankful for the effort you made to allow me to continue conducting research.

Secondly, I would like to thank my second promotor, Rob Timmermans. I first met you while writing a 'profielwerkstuk' on relativity in high school, for which you patiently answered all my questions. This was the topic that really sparked my interest in physics, so I think you are at least partly responsible for the fact that I ended up doing a PhD in particle physics. I would also like to thank you for writing a recommendation letter, and for your comments and suggestions on my applications and this thesis.

I would like to thank Diederik Roest, Robert Fleischer, and Jean-Marie Frère for agreeing to be in my reading committee, and providing me with useful comments and suggestions. In addition, I would like to thank Jean-Marie for the interesting discussions on left-right models we had during my visit to Brussels last year.

Thanks to Jan Bsaisou, Werner Bernreuther, Christoph Hanhart, Ulf-G Meißner, Andreas Nogga, and Andreas Wirzba, for a very pleasant collaboration on a rather lengthy paper. I am especially grateful to Werner Bernreuther for agreeing to write multiple recommendation letters on my behalf. In addition, I very much enjoyed working on a more recent project, together with Jordy de Vries, Emanuele Mereghetti, Yang-Ting Chien, and Vincenzo Cirigliano. I am looking forward to joining you, Yang-Ting, Emanuele, and Vincenzo, in Los Alamos.

I would like to thank Keri Vos and Jordy de Vries, whom I also collaborated with during these last four years. I enjoyed working together with both of you. I should mention Jordy in particular, not only because we collaborated on two long papers, but also because of your, often unsolicited, advice on many topics. I learned a lot from working together with you, not least of all from your strongly held opinions about football.

I would like to thank the members of the (old and new) theoretical particle physics group, Lex Dieperink, Elisabetta Pallante, and Olaf Scholten for interesting discussions and the lunch meetings we used to have. I am grateful to Eric Laenen for organizing the monthly TPP (now HPP) meetings. These meetings, as well as DRSTP schools and PhD

days, were very interesting and enjoyable, in part, due to Andrea, Daniel, Domenico, Drazen, Giuseppe, Jules, Kristof, Maarten, Michael, Natalia, Reinier, Rob, Robbert, Sander, Tom, and Wilco, thank you all for that.

I would also like to thank Elwin and Keri for agreeing to be my paranimphs.

Auke, Corine, Elwin, Geert, Hans, Jacob, Jan-Willem, Johan, Joost, Keri, Leon, Luca, Marcel, Marco, Maria, Mayerlin, Nafise, Olena, Olga, Olivier, Sophie, Sjoerd, Soumya, Stefano, Thomas, Tiago, Tom, Wendy, Wout, and Zahra, thanks for making my time as a PhD student, both at the KVI and at the Van Swinderen Insitute, that much more interesting and enjoyable. I should also thank Gerco, for effortlessly making fifteen-minute coffee breaks last for an hour. Surprisingly, however, the duration of some bike rides was shortened considerably in your presence. Thanks to Ali, Ganesh, and Keri for being such good office mates. I would include Jacob and Sophie in this list, but I am not sure you can call someone who is hardly ever in the office an 'office mate'. Thanks also to Hilde van der Meer, Amarins Petitaux, Marjan Koopmans, Annelien Blanksma, and Iris de Roo-Kwant, for helping me out and taking care of many things for me.

Finally, I would like to thank my parents and my sister, for their support, and for attempting to read (the introduction of) this thesis.

Bibliography

[1] ATLAS Collaboration, G. Aad *et al.*, Phys. Lett. B **716**, 1 (2012).

[2] F. Englert and R. Brout, Phys. Rev. Lett. **13**, 321 (1964).

[3] P. W. Higgs, Phys. Rev. Lett. **13**, 508 (1964).

[4] G. Guralnik, C. Hagen, and T. Kibble, Phys. Rev. Lett. **13**, 585 (1964).

[5] C. Wu, E. Ambler, R. Hayward, D. Hoppes, and R. Hudson, Phys. Rev. **105**, 1413 (1957).

[6] R. Garwin, L. Lederman, and M. Weinrich, Phys. Rev. **105**, 1415 (1957).

[7] J. Christenson, J. Cronin, V. Fitch, and R. Turlay, Phys. Rev. Lett. **13**, 138 (1964).

[8] A. Riotto and M. Trodden, Ann. Rev. Nucl. Part. Sci. **49**, 35 (1999).

[9] V. A. Kuzmin, M. E. Shaposhnikov, and I. I. Tkachev, Phys. Rev. D **45**, 466 (1992).

[10] M. Dine and A. Kusenko, Rev. Mod. Phys. **76**, 1 (2003).

[11] J. C. Pati and A. Salam, Phys. Rev. D **10**, 275 (1974).

[12] R. N. Mohapatra and J. C. Pati, Phys. Rev. D **11**, 566 (1975).

[13] G. Senjanović and R. N. Mohapatra, Phys. Rev. D **12**, 1502 (1975).

[14] C. Jarlskog, Z. Phys. C **29**, 491 (1985).

[15] C. Jarlskog, Phys. Rev. Lett. **55**, 1039 (1985).

[16] Particle Data Group, K. Olive *et al.*, Chin. Phys. C **38**, 090001 (2014).

[17] C.-Y. Seng, Phys. Rev. C **91**, 025502 (2015).

[18] C. A. Baker *et al.*, Phys. Rev. Lett. **97**, 131801 (2006).

[19] M. E. Pospelov and I. B. Khriplovich, Sov. J. Nucl. Phys. **53**, 638 (1991).

[20] W. Bernreuther and M. Suzuki, Rev. Mod. Phys. **63**, 313 (1991).

[21] D. Ng and J. N. Ng, Mod. Phys. Lett. A **11**, 211 (1996).

[22] J. P. Archambault, A. Czarnecki, and M. Pospelov, Phys. Rev. D **70**, 073006 (2004).

[23] S. Weinberg, The Quantum Theory of Fields, Vol. 2, Cambridge University Press (1996).

[24] A. A. Belavin, A. M. Polyakov, A. S. Schwartz, and Y. S. Tyupkin, Phys. Lett. B **59**, 85 (1975).

[25] G. 't Hooft, Phys. Rev. D **14**, 3432 (1976).

[26] G. 't Hooft, Phys. Rev. Lett. **37**, 8 (1976).

[27] K. Fujikawa, Phys. Rev. Lett. **42**, 1195 (1979).

[28] V. Baluni, Phys. Rev. D **19**, 2227 (1979).

[29] F.-K. Guo and U.-G. Meißner, JHEP **1212**, 097 (2012).

[30] R. D. Peccei and H. R. Quinn, Phys. Rev. Lett. **38**, 1440 (1977).

[31] N. V. Krasnikov, V. A. Rubakov, and V. F. Tokarev, J. Phys. A **12**, L343 (1979).

[32] A. A. Anselm and A. A. Johansen, Nucl. Phys. B **407**, 313 (1993).

[33] A. A. Anselm and A. A. Johansen, Nucl. Phys. B **412**, 553 (1994).

[34] A. Sakharov, Pisma Zh. Eksp. Teor. Fiz. **5**, 32 (1967).

[35] G. Luders, Kong. Dan. Vid. Sel. Mat. Fys. Med. **28N5**, 1 (1954).

[36] W. Pauli, in Niels Bohr and the Development of Physics (McGraw-Hill, New York) , pp30 (1955).

[37] W. Buchmüller and D. Wyler, Nucl. Phys. B **268**, 621 (1986).

[38] S. Weinberg, Phys. Rev. Lett. **63**, 2333 (1989).

[39] A. de Rujula, M. B. Gavela, O. Pene, and F. J. Vegas, Nucl. Phys. B **357**, 311 (1991).

[40] M. J. Ramsey-Musolf and S. Su, Phys. Rept. **456**, 1 (2008).

[41] B. Grzadkowski, M. Iskrzynski, M. Misiak, and J. Rosiek, JHEP **1010**, 085 (2010).

[42] M. E. Pospelov and A. Ritz, Ann. Phys. **318**, 119 (2005).

[43] H. Georgi, Ann. Rev. Nucl. Part. Sci. **43**, 209 (1993).

[44] A. V. Manohar, (1995), hep-ph/9508245.

[45] A. Pich, (1998), hep-ph/9806303.

[46] C. P. Burgess, Ann. Rev. Nucl. Part. Sci. **57**, 329 (2007).

[47] H. An, X. Ji, and F. Xu, JHEP **1002**, 043 (2010).

[48] J. Hisano, K. Tsumura, and M. J. S. Yang, Phys. Lett. B **713**, 473 (2012).

[49] R. Alonso, E. E. Jenkins, A. V. Manohar, and M. Trott, JHEP **1404**, 159 (2014).

[50] S. Weinberg, Phys. Rev. Lett. **43**, 1566 (1979).

[51] E. Braaten, C. S. Li, and T. C. Yuan, Phys. Rev. D **42**, 276 (1990).

[52] J. Ng and S. Tulin, Phys. Rev. D **85**, 033001 (2012).

[53] K. Hagiwara, R. D. Peccei, D. Zeppenfeld, and K. Hikasa, Nucl. Phys. B **282**, 253 (1987).

[54] S. Weinberg, Phys. Rev. Lett. **18**, 188 (1967).

[55] S. Weinberg, PoS CD **09**, 001 (2009).

[56] J. de Vries, E. Mereghetti, R. G. E. Timmermans, and U. L. van Kolck, Ann. Phys. **338**, 50 (2013).

[57] W. H. Hockings and U. van Kolck, Phys. Lett. B **605**, 273 (2005).

[58] J. de Vries, R. G. E. Timmermans, E. Mereghetti, and U. L. van Kolck, Phys. Lett. B **695**, 268 (2011).

[59] E. Mereghetti, J. de Vries, W. H. Hockings, C. M. Maekawa, and U. van Kolck, Phys. Lett. B **696**, 97 (2011).

[60] U. L. van Kolck, PhD thesis, Texas University (1993).

[61] U. L. van Kolck, Few Body Syst. Suppl. **9**, 444 (1995).

[62] J. de Vries, PhD thesis, University of Groningen (2012), http://irs.ub.rug.nl/ppn/350411824.

[63] J. Gasser and H. Leutwyler, Phys. Rept. **87**, 77 (1982).

[64] A. Walker-Loud, C. E. Carlson, and G. A. Miller, Phys. Rev. Lett. **108**, 232301 (2012).

[65] Particle Data Group, J. Beringer *et al.*, Phys. Rev. D **86**, 010001 (2012).

[66] A. Manohar and H. Georgi, Nucl. Phys. B **234**, 189 (1984).

[67] S. Weinberg, Phys. Lett. B **91**, 51 (1980).

[68] L. J. Hall, Nucl. Phys. B **178**, 75 (1981).

[69] B. A. Ovrut and H. J. Schnitzer, Nucl. Phys. B **179**, 381 (1981).

[70] B. A. Ovrut and H. J. Schnitzer, Nucl. Phys. B **189**, 509 (1981).

[71] F. Wilczek and A. Zee, Phys. Rev. D **15**, 2660 (1977).

[72] E. Braaten, C.-S. Li, and T.-C. Yuan, Phys. Rev. Lett. **64**, 1709 (1990).

[73] G. Degrassi, E. Franco, S. Marchetti, and L. Silvestrini, JHEP **0511**, 044 (2005).

[74] J. de Vries *et al.*, Phys. Rev. C **84**, 065501 (2011).

[75] D. B. Kaplan and A. Manohar, Nucl. Phys. B **310**, 527 (1988).

[76] C. Grojean, E. E. Jenkins, A. V. Manohar, and M. Trott, JHEP **1304**, 016 (2013).

[77] S. M. Barr and A. Zee, Phys. Rev. Lett. **65**, 21 (1990).

[78] J. M. Frère *et al.*, Phys. Lett. B **251**, 443 (1990).

[79] Y. Zhang, H. An, X. Ji, and R. N. Mohapatra, Nucl. Phys. B **802**, 247 (2008).

[80] F. Xu, H. An, and X. Ji, JHEP **1003**, 088 (2010).

[81] M. Jung and A. Pich, JHEP **1404**, 076 (2014).

[82] F. Boudjema, K. Hagiwara, C. Hamzaoui, and K. Numata, Phys. Rev. D **43**, 2223 (1991).

[83] B. Gripaios and D. Sutherland, Phys. Rev. D **89**, 076004 (2014).

[84] D. McKeen, M. Pospelov, and A. Ritz, Phys. Rev. D **86**, 113004 (2012).

[85] J. Fan and M. Reece, JHEP **1306**, 004 (2013).

[86] P. E. Peskin and D. V. Schroeder, Introduction to Quantum Field Theory, Westview Press (1995).

[87] J. L. Hewett *et al.*, (2012), arXiv:1205.2671.

[88] W. C. Griffith *et al.*, Phys. Rev. Lett. **102**, 101601 (2009).

[89] ACME Collaboration, J. Baron *et al.*, Science **343**, 269 (2014).

[90] J. J. Hudson *et al.*, Nature **473**, 493 (2011).

[91] D. M. Kara *et al.*, New J. Phys. **14**, 103051 (2012).

[92] F. J. M. Farley *et al.*, Phys. Rev. Lett. **93**, 052001 (2004).

[93] C. J. G. Onderwater, J. Phys. Conf. Ser. **295**, 012008 (2011).

[94] J. Pretz, Hyperfine Interact. **214**, 111 (2013).

[95] JEDI-collaboration, http://collaborations.fz-juelich.de/ikp/jedi/ .

[96] V. F. Dmitriev and R. A. Sen'kov, Phys. Rev. Lett. **91**, 212303 (2003).

[97] E. Mereghetti, W. H. Hockings, and U. van Kolck, Ann. Phys. **325**, 2363 (2010).

[98] J. Bsaisou *et al.*, Eur. Phys. J. A **49**, 31 (2013).

[99] O. Lebedev, K. A. Olive, M. Pospelov, and A. Ritz, Phys. Rev. D **70**, 016003 (2004).

[100] J. Gasser and H. Leutwyler, Nucl. Phys. B **250**, 465 (1985).

[101] V. Baru *et al.*, Nucl. Phys. A **872**, 69 (2011).

[102] A. Czarnecki and B. Krause, Phys. Rev. Lett. **78**, 4339 (1997).

[103] M. E. Pospelov, Phys. Lett. B **328**, 441 (1994).

[104] M. B. Gavela *et al.*, Phys. Lett. B **109**, 83 (1982).

[105] I. B. Khriplovich and A. R. Zhitnitsky, Phys. Lett. B **109**, 490 (1982).

[106] B. H. J. McKellar, S. R. Choudhury, X.-G. He, and S. Pakvasa, Phys. Lett. B **197**, 556 (1987).

[107] C. Dib *et al.*, J. Phys. G **32**, 547 (2006).

[108] M. E. Pospelov, Phys. Lett. B **530**, 123 (2002).

[109] D. A. Demir, M. E. Pospelov, and A. Ritz, Phys. Rev. D **67**, 015007 (2003).

[110] R. J. Crewther, P. Di Vecchia, G. Veneziano, and E. Witten, Phys. Lett. B **88**, 123 (1979).

[111] C.-Y. Seng, J. de Vries, E. Mereghetti, H. H. Patel, and M. Ramsey-Musolf, Phys. Lett. B **736**, 147 (2014).

[112] E. E. Jenkins, A. V. Manohar, and M. Trott, JHEP **1309**, 063 (2013).

[113] C. Arzt, M. B. Einhorn, and J. Wudka, Nucl. Phys. B **433**, 41 (1995).

[114] I. B. Khriplovich and R. A. Korkin, Nucl. Phys. A **665**, 365 (2000).

[115] C.-P. Liu and R. G. E. Timmermans, Phys. Rev. C **70**, 055501 (2004).

[116] I. R. Afnan and B. F. Gibson, Phys. Rev. C **82**, 064002 (2010).

[117] J. de Vries, E. Mereghetti, R. G. E. Timmermans, and U. L. van Kolck, Phys. Rev. Lett. **107**, 091804 (2011).

[118] Y.-H. Song, R. Lazauskas, and V. Gudkov, Phys. Rev. C **87**, 015501 (2013).

[119] J. Bsaisou *et al.*, JHEP **1503**, 104 (2015).

[120] J. Bsaisou, PhD Thesis, University of Bonn (2014).

[121] Y. Avishai and M. Fabre De La Ripelle, Phys. Rev. Lett. **56**, 2121 (1986).

[122] I. Stetcu, C.-P. Liu, J. L. Friar, A. C. Hayes, and P. Navratil, Phys. Lett. B **665**, 168 (2008).

[123] B. C. Regan, E. D. Commins, C. J. Schmidt, and D. DeMille, Phys. Rev. Lett. **88**, 071805 (2002).

[124] F. Hoogeveen, Nucl. Phys. B **341**, 322 (1990).

[125] K. Choi and J. Hong, Phys. Lett. B **259**, 340 (1991).

[126] W. Fischler, S. Paban, and S. D. Thomas, Phys. Lett. B **289**, 373 (1992).

[127] DELPHI Collaboration, J. Abdallah *et al.*, Eur. Phys. J. C **54**, 345 (2008).

[128] L. I. Schiff, Phys. Rev. **132**, 2194 (1963).

[129] J. Engel, M. J. Ramsey-Musolf, and U. L. van Kolck, Prog. Part. Nucl. Phys. **71**, 21 (2013).

[130] V. A. Dzuba, V. V. Flambaum, J. S. M. Ginges, and M. G. Kozlov, Phys. Rev. A **66**, 012111 (2002).

[131] V. A. Dzuba, V. V. Flambaum, and S. G. Porsev, Phys. Rev. A **80**, 032120 (2009).

[132] V. A. Dzuba and V. V. Flambaum, Int. J. Mod. Phys. E **21**, 1230010 (2012).

[133] V. F. Dmitriev and R. A. Sen'kov, Phys. Atom. Nucl. **66**, 1940 (2003).

[134] J. H. de Jesus and J. Engel, Phys. Rev. C **72**, 045503 (2005).

[135] S. Ban, J. Dobaczewski, J. Engel, and A. Shukla, Phys. Rev. C **82**, 015501 (2010).

[136] A. J. Buras, p. 281 (1998), hep-ph/9806471.

[137] U. Nierste, (2009), arXiv:0904.1869.

[138] S. Bertolini, A. Maiezza, and F. Nesti, Phys. Rev. D **89**, 095028 (2014).

[139] UTfit Collaboration, M. Bona *et al.*, JHEP **0803**, 049 (2008).

[140] HFAG, http://www.slac.stanford.edu/xorg/hfag/index.html .

[141] J. Charles *et al.*, Phys. Rev. D **84**, 033005 (2011).

[142] A. Lenz *et al.*, Phys. Rev. D **86**, 033008 (2012).

[143] J. Charles *et al.*, Phys. Rev. D **89**, 033016 (2014).

[144] H. P. Mumm *et al.*, Phys. Rev. Lett. **107**, 102301 (2011).

[145] T. E. Chupp *et al.*, Phys. Rev. C **86**, 035505 (2012).

[146] S.-i. Ando, J. A. McGovern, and T. Sato, Phys. Lett. B **677**, 109 (2009).

[147] V. V. Braguta, A. A. Likhoded, and A. E. Chalov, Phys. Rev. D **65**, 054038 (2002).

[148] S. Gardner and D. He, Phys. Rev. D **86**, 016003 (2012).

[149] S. Gardner and D. He, Phys. Rev. D **87**, 116012 (2013).

[150] P. Herczeg and I. B. Khriplovich, Phys. Rev. D **56**, 80 (1997).

[151] W. Dekens and K. K. Vos, (2015), arXiv:1502.04629.

[152] W. Dekens and J. de Vries, JHEP **1305**, 149 (2013).

[153] C. J. G. Onderwater, Hyperfine Interact. **211**, 9 (2012).

[154] G. Senjanović, Nucl. Phys. B **153**, 334 (1979).

[155] N. G. Deshpande, J. F. Gunion, B. Kayser, and F. I. Olness, Phys. Rev. D **44**, 837 (1991).

[156] R. N. Mohapatra and G. Senjanovic, Phys. Rev. Lett. **44**, 912 (1980).

[157] R. N. Mohapatra and G. Senjanovic, Phys. Rev. D **23**, 165 (1981).

[158] T. G. Rizzo and G. Senjanović, Phys. Rev. Lett. **46**, 1315 (1981).

[159] P. Duka, J. Gluza, and M. Zralek, Ann. Phys. **280**, 336 (2000).

[160] K. Kiers, M. Assis, and A. A. Petrov, Phys. Rev. D **71**, 115015 (2005).

[161] P. Ball, J. M. Frère, and J. Matias, Nucl. Phys. B **572**, 3 (2000).

[162] G. Bambhaniya, J. Chakrabortty, J. Gluza, M. Kordiaczyńska, and R. Szafron, JHEP **1405**, 033 (2014).

[163] G. Bambhaniya, J. Chakrabortty, J. Gluza, T. Jeliński, and M. Kordiaczynska, Phys. Rev. D **90**, 095003 (2014).

[164] A. Maiezza, M. Nemevsek, F. Nesti, and G. Senjanovic, Phys. Rev. D **82**, 055022 (2010), 1005.5160.

[165] CMS Collaboration, S. Chatrchyan *et al.*, JHEP **1405**, 108 (2014).

[166] CMS Collaboration, S. Chatrchyan *et al.*, Phys. Rev. Lett. **109**, 261802 (2012).

[167] ATLAS Collaboration, G. Aad *et al.*, Eur. Phys. J. C **72**, 2056 (2012).

[168] CMS, V. Khachatryan *et al.*, Eur. Phys. J. C **74**, 3149 (2014).

[169] J. Chakrabortty, J. Gluza, R. Sevillano, and R. Szafron, JHEP **1207**, 038 (2012).

[170] K. Kiers, J. Kolb, J. Lee, A. Soni, and G.-H. Wu, Phys. Rev. D **66**, 095002 (2002).

[171] G. Senjanović and V. Tello, Phys. Rev. Lett. **114**, 071801 (2015).

[172] G. C. Branco, J. M. Frère, and J. M. Gerard, Nucl. Phys. B **221**, 317 (1983).

[173] M. A. B. Beg, R. V. Budny, R. N. Mohapatra, and A. Sirlin, Phys. Rev. Lett. **38**, 1252 (1977).

[174] P. Langacker and S. U. Sankar, Phys. Rev. D **40**, 1569 (1989).

[175] H. Harari and M. Leurer, Nucl. Phys. B **233**, 221 (1984).

[176] G. Ecker and W. Grimus, Z. Phys. C **30**, 293 (1986).

[177] S. Bertolini, J. O. Eeg, A. Maiezza, and F. Nesti, Phys. Rev. D **86**, 095013 (2012).

[178] G. Ecker and W. Grimus, Nucl. Phys. B **258**, 328 (1985).

[179] J. Basecq, L.-F. Li, and P. B. Pal, Phys. Rev. D **32**, 175 (1985).

[180] A. J. Buras and J. Girrbach, Rept. Prog. Phys. **77**, 086201 (2014).

[181] G. Ecker, W. Grimus, and H. Neufeld, Nucl. Phys. B **229**, 421 (1983).

[182] J. M. Frère *et al.*, Phys. Rev. D **45**, 259 (1992).

[183] A. Maiezza and M. Nemevšek, Phys. Rev. D **90**, 095002 (2014).

[184] R. Kuchimanchi, Phys. Rev. D **91**, 071901 (2015).

[185] W. J. den Dunnen, PhD thesis, VU University Amsterdam (2013).

[186] I. I. Y. Bigi and J. M. Frère, Phys. Lett. B **110**, 255 (1982).

[187] J. F. Nieves, D. Chang, and P. B. Pal, Phys. Rev. D **33**, 3324 (1986).

[188] M.-C. Chen and K. T. Mahanthappa, Phys. Rev. D **75**, 015001 (2007).

[189] A. García and G. Sánchez-Colón, Phys. Rev. D **81**, 014030 (2010).

[190] RBC+UKQCD Collaboration, T. Yamazaki *et al.*, Phys. Rev. Lett. **100**, 171602 (2008).

[191] A. Fowlie and L. Marzola, Nucl. Phys. B **889**, 36 (2014).

[192] E. Ma, Phys. Rev. D **36**, 274 (1987).

[193] M. Ashry and S. Khalil, Phys. Rev. D **91**, 015009 (2015).

[194] M. Frank, A. Hayreter, and I. Turan, Phys. Rev. D **82**, 033012 (2010).

[195] J. R. Ellis, K. Enqvist, D. V. Nanopoulos, and F. Zwirner, Mod. Phys. Lett. A **1**, 57 (1986).

[196] R. Barbieri and G. F. Giudice, Nucl. Phys. B **306**, 63 (1988).

[197] G. Ecker, W. Grimus, and H. Neufeld, Nucl. Phys. B **247**, 70 (1984).

[198] J. M. Frère *et al.*, Phys. Rev. D **46**, 337 (1992).

[199] D. Chang, Nucl. Phys. B **214**, 435 (1983).

[200] P. Ball and R. Fleischer, Phys. Lett. B **475**, 111 (2000).

[201] G. Barenboim, M. Gorbahn, U. Nierste, and M. Raidal, Phys. Rev. D **65**, 095003 (2002).

[202] J. F. Gunion, J. Grifols, A. Mendez, B. Kayser, and F. I. Olness, Phys. Rev. D **40**, 1546 (1989).

[203] J. Basecq, J. Liu, J. Milutinovic, and L. Wolfenstein, Nucl. Phys. B **272**, 145 (1986).

[204] G. C. Branco and L. Lavoura, Phys. Lett. B **165**, 327 (1985).

[205] Y. Zhang, H. An, X. Ji, and R. Mohapatra, Phys. Rev. D **76**, 091301 (2007).

[206] P. Chen, H. Ke, and X. Ji, Phys. Lett. B **677**, 157 (2009).

[207] M. Blanke, A. J. Buras, K. Gemmler, and T. Heidsieck, JHEP **1203**, 024 (2012).

[208] A. A. Anselm, V. E. Bunakov, V. P. Gudkov, and N. Uraltsev, Phys. Lett. B **152**, 116 (1985).

[209] D. A. Demir, O. Lebedev, K. A. Olive, M. Pospelov, and A. Ritz, Nucl. Phys. B **680**, 339 (2004).

[210] E. Mereghetti, private communication (2014).

[211] C. M. Maekawa, E. Mereghetti, J. de Vries, and U. L. van Kolck, Nucl. Phys. A **872**, 117 (2011).

[212] J. Bsaisou, U.-G. Meißner, A. Nogga, and A. Wirzba, (2014), 1412.5471.

[213] R. D. Peccei and H. R. Quinn, Phys. Rev. D **16**, 1791 (1977).

[214] A. Pich and P. Tuzon, Phys. Rev. D **80**, 091702 (2009).

[215] M. Creutz, Phys. Rev. Lett. **92**, 162003 (2004).

[216] J. F. Gunion, H. E. Haber, G. L. Kane, and S. Dawson, The Higgs Hunter's Guide, Perseus Publishing (1990).

[217] I. I. Bigi and A. Sanda, CP violation (Second edition), Cambridge University Press (2009).

[218] G. C. Branco *et al.*, Phys. Rept. **516**, 1 (2012).

[219] CMS Collaboration, S. Chatrchyan *et al.*, Phys. Lett. B **716**, 30 (2012).

[220] G. D'Ambrosio, G. F. Giudice, G. Isidori, and A. Strumia, Nucl. Phys. B **645**, 155 (2002).

[221] A. J. Buras, P. Gambino, M. Gorbahn, S. Jager, and L. Silvestrini, Phys. Lett. B **500**, 161 (2001).

[222] A. J. Buras, G. Isidori, and P. Paradisi, Phys. Lett. B **694**, 402 (2011), 1007.5291.

[223] W. Bernreuther, T. Schroder, and T. Pham, Phys. Lett. B **279**, 389 (1992).

[224] S. Inoue, M. J. Ramsey-Musolf, and Y. Zhang, Phys. Rev. D **89**, 115023 (2014).

[225] ATLAS, CMS Collaboration, M. P. Sanders, PoS DIS **2013**, 010 (2013).

[226] CMS Collaboration, S. Meola, PoS DIS **2013**, 093 (2013).

[227] K. Cheung, J. S. Lee, E. Senaha, and P.-Y. Tseng, JHEP **1406**, 149 (2014).

[228] N. Fettes, U.-G. Meißner, and S. Steininger, Nucl. Phys. A **640**, 199 (1998).

[229] N. Fettes, U.-G. Meißner, M. Mojzis, and S. Steininger, Ann. Phys. **283**, 273 (2000).

[230] M. E. Pospelov and A. Ritz, Phys. Rev. D **63**, 073015 (2001).

[231] J. F. Gunion and D. Wyler, Phys. Lett. B **248**, 170 (1990).

[232] T. Abe, J. Hisano, T. Kitahara, and K. Tobioka, JHEP **1401**, 106 (2014).

[233] D. Bowser-Chao, D. Chang, and W.-Y. Keung, Phys. Rev. Lett. **79**, 1988 (1997).

[234] D. A. Dicus, Phys. Rev. D **41**, 999 (1990).

[235] G. Boyd, A. K. Gupta, S. P. Trivedi, and M. B. Wise, Phys. Lett. B **241**, 584 (1990).

[236] B. Borasoy, Phys. Rev. D **61**, 114017 (2000).

[237] S. Narison, Phys. Lett. B **666**, 455 (2008).

[238] K. Ottnad, B. Kubis, U.-G. Meißner, and F.-K. Guo, Phys. Lett. B **687**, 42 (2010).

[239] J. Brod, U. Haisch, and J. Zupan, JHEP **1311**, 180 (2013).